ENERGY CONSERVATION IN ACTIVE DISTRIBUTION NETWORK VIA SMART VOLT/VAR CONTROL

Thesis submitted in partial fulfilment

for the Award of Degree

Doctor of Philosophy

by

SHAILENDRA SINGH

DEPARTMENT OF ELECTRICAL ENGINEERING
INDIAN INSTITUTE OF TECHNOLOGY
(BANARAS HINDU UNIVERSITY)
VARANASI-221005

ROLL NO: 14081011 **2019**

CERTIFICATE

It is certified that the work contained in the thesis titled ***" ENERGY CONSERVATION IN ACTIVE DISTRIBUTION NETWORK VIA SMART VOLT/VAR CONTROL "*** by ***"SHAILENDRA SINGH"*** has been carried out under my supervision and that this work has not been submitted elsewhere for a degree.

It is further certified that the student has fulfilled all the requirements of Comprehensive, Candidacy and SOTA for the award of Ph.D. Degree.

Signature of Supervisor

Professor (Dr.) S. P. SINGH
Department of Electrical Engineering
Indian Institute of Technology (BHU),
Varanasi-221005, (Uttar Pradesh), India

DECLARATION BY THE CANDIDATE

I, *"SHAILENDRA SINGH"*, certify that the work embodied in this thesis is my own bonafide work and carried out by me under the supervision of *"Prof. S. P. SINGH"* from *"July 2014"* to "*November 2019*", at the *"DEPARTMENT OF ELECTRICAL ENGINEERING"*, Indian Institute of Technology (BHU), Varanasi. The matter embodied in this thesis has not been submitted for the award of any other degree/diploma. I declare that I have faithfully acknowledged and given credits to the research workers wherever their works have been cited in my work in this thesis. I further declare that I have not wilfully copied any other's work, paragraphs, text, data, results, *etc*., reported in journals, books, magazines, reports dissertations, thesis, *etc*., or available at websites and have not included them in this thesis and have not cited as my own work.

Date:

Place: VARANASI **(Shailendra Singh)**

CERTIFICATE BY THE SUPERVISOR

It is certified that the above statement made by the student is correct to the best of my knowledge.

Supervisor

Prof. (Dr.) S. P. SINGH

Department of Electrical Engineering

Indian Institute of Technology (BHU), Varanasi-221005, (Uttar Pradesh), India

Head of Department

COPYRIGHT TRANSFER CERTIFICATE

Title of the Thesis: "*ENERGY CONSERVATION IN ACTIVE DISTRIBUTION NETWORK VIA SMART VOLT/VAR CONTROL".*

Name of the Student: SHAILENDRA SINGH

Copyright Transfer

The undersigned hereby assigns to the Indian Institute of Technology (Banaras Hindu University) Varanasi all rights under copyright that may exist in and for the above thesis submitted for the award of the "DOCTOR OF PHILOSOPHY".

Date:

Place: VARANASI **(SHAILENDRA SINGH)**

Note: However, the author may reproduce or authorize others to reproduce material extracted verbatim from the thesis or derivative of the thesis for author's personal use provided that the source and the Institute's copyright notice are indicated.

DEDICATED TO MY BELOVED PARENTS,

WIFE ANCHITA

AND

LOVING SON RITUJ

ACKNOWLEDGEMENT

First and foremost, I would like to express my deep sense of gratitude and indebtedness to my respected supervisor **Prof. S. P. Singh**, Department of Electrical Engineering, IIT(BHU) Varanasi, for a valuable research opportunity, endless encouragement, and excellent supervision during my Ph.D. thesis work. I am especially, expressing my sincere gratitude to my supervisor for providing necessary support and encouragement during the period of the progress of the research work as Professor-in-change power systems complex.

I would like to express my appreciation to my thesis research progress evaluation committee (RPEC): Prof. S. Jit, Prof. D. N. Vishwakarma, and Dr. S. R. Mohanty for their valuable suggestions and guidance during the progress of the research work.

I convey my sincere gratitude to my internship mentors Dr. Murali Baggu and Dr. Santosh Veda, National Renewable Energy Laboratory (NREL), CO, USA for his kind support and guidance in various technical aspects of my work during my internship stay at Power System Engineering Centre, National Renewable Energy Laboratory, CO, USA. I am especially, expressing my gratitude to Dr. Fei Ding, Dr. Shibani Gosh, Dr. Rishabh Jain, Dr. Aadil Latif, Harsha Vardhana Padullaparti, Dr. Kalpesh Chaudhary, Dr. Himanshu Jain, Mr. Prateek Munankarmi and Mr. John Fossum from NREL for assisting me in various technical aspects of my work.

I would like to convey my sincere thanks to Indo-US Science and Technology Forum (IUSSTF) New Delhi and Department of Science & Technology, Govt. of India for awarding me prestigious Bhaskara Advance Solar Energy (BASE) Fellowship award and providing me great opportunity to carry out my research work at Power System Engineering Centre, National Renewable Energy Laboratory, CO, USA

I am thankful to all faculty members of the department, especially for their valuable suggestions. I especially, convey my gratitude to Prof. D. Singh, Prof. R.K. Mishra, Prof. M. K Verma and Dr. J. C. Pandey for their valuable guidance. I also thank all staff members of the department and library for their cooperation in the completion of this work. I express my special thanks to Mr. Sanjay Kumar Bharti, Senior Technician, Power System Laboratory, for his valuable and helpful support to carry out my research work smoothly.

I express thanks to my fellow researchers in the department for their nice company, support, and fruitful discussions during my stay in IIT(BHU) Varanasi. I am very much thankful, especially, to Mr. Vijay Babu P., Mr. Amit Kumar Thakur, Mr. Devesh Shukla, Mr. Sunil Kumar Singh, Mrs. Ekta Purwar, Ms Sri Laxmi E., Mr. Manohar Singh, Mr. Akhilesh Baranwal, Mr. Sunil Muwal, Mr. Gaurav Kumar, Mr. Tarun Maini, Dr. Satyendra Pratap Singh, Dr. Deepak Kumar Gupta, Dr. Om P. Bharti, and Dr. Munendra Singh.

I am also grateful to Dr. Saurabh Chanana, Associate Professor, Department of Electrical Engineering, National Institute of Technology, Kurukshetra for moral support and encouraging me to pursue higher education.

I express my deep sense of gratitude to my parents (Mr. Shiv Singh and Mrs. Baijanti Devi), loving brother (Mr. Bhanu Pratap Singh) and Sisters (Mrs.Vandana and Ms. Arati) to all their efforts and suffering in bringing me up to this stage.

Last but not the least, I take this opportunity to acknowledge the love, affection, support and irreplaceable time strained my wife Anchita and joyful moments with my son Rituj, that helped me in the successful completion of my thesis.

Date: (Shailendra Singh)

TABLE OF CONTENTS

LIST OF FIGURES

xxx

LIST OF TABLES

LIST OF ABBREVIATION

Abbreviation	Description about Abbreviation
ADN	Active Distribution Network
AMI	Advanced Metering Infrastructure
AVR	Automatic Voltage Regulator
ANSI	American National Standard Institute
AC	Alternating Current
BMS	Battery Management System
CES	Community Energy Storage
CVR	Conservation of Voltage Reduction
DG	Distributed Generation
DER	Distributed Energy Resources
DMS	Distributed Management System
DES	Distributed Energy Storage
DNO	Distribution Network Operator
DNP	Distributed Network Protocol
DGSA	Discrete GSA
DC	Direct current
DB	Dead Band
DMOPSO	Discrete Multi Objective Particle Swarm Optimization
DSTATCOM	Distributed Static Synchronous Compensator
EPRI	Electric Power Research Institute
EOL	End of The Line
ESS	Energy Storage System
EV	Electric Vehicle
FTSC	Fast Time Scale Control
GA	Genetic Algorithm
GSA	Gravitational Search Algorithm
IEA	International Energy Agency
LTC	Load Tap Changer
MV/LV	Medium Voltage/Low Voltage
MILP	Mixed Integer Nonlinear Programming

MW	Megawatt
MSMO	Multi-Stage Multi-Objective
MP-VVO	Model Predictive Volt/VAR Optimization
MCS	Monte-Carlo Simulation
NDS	Nondominated Solutions
N	Number of generate scenarios
N’	Number of reduced scenarios N’
OLTC	On Line Tap Changer
OpenDSS	Open Distribution System Simulator
PV	Photovoltaic
PSO	Particle Swarm Optimization
PE	Power Electronics
POC	Point of Connection
RTDS	Real Time Digital Simulator
RPS	Reactive Power Support
SG	Smart Grid
SDS	Secondary Distribution System
SOC	State of Charge
STSC	Slow Time Scale Control
SCADA	Supervisory Control and Data Acquisition
Tap	Tap Position of OLTC transformer/AVR
TCP/IP	Transmission Control Protocol/ Internet Protocol
VAR	Volt Ampere Reactive
VVO	Volt/VAR Optimization
VVC	Volt/VAR Control
V2G	Vehicle-to-Grid

LIST OF SYMBOLS

a_{tr}	Transformation ratio
ΔV_{tr}	Variation in voltage per step of OLTC/AVR which is specified by the manufacturer
Δq_{cb}^{i}	Per step variation in reactive power at i^{th} CB
Sw_{cb}^{i}	Switching step number of the i^{th} CB
Q_{cb}^{i}	Reactive power injected by an i^{th} CB
$Sw_{cb}^{i,\max}$	Maximum number of switching steps available at i^{th} CB
T	Time
P_T^{inv}	Actual real power output from inverter at time T
Q_T^{inv}	Actual reactive power output from inverter at time T
P_T	Active power generated by PV arrays at time T
Q_T	Actual reactive power output at time T
$P_{T,loss}^{Inv}$	Active power inverter loss at time T
$S_{\max}$	Maximum apparent power rating of the inverter
$Q_T^{inv,\max}$	Available maximum reactive power capacity
η_{inv}	Inverter efficiency
ZIP	Combination of constant impedance (Z), constant current (I) and constant power (P)
E_{Saving}	Energy Savings
E_{No-CVR}	Energy consumption during normal or No-CVR operation
E_{CVR}	Energy consumption during smart grid enabled CVR operation
CVR_f	CVR factor
CVR_{fE}	CVR factor in kWh
$CVR_{f(kW)}$	CVR factor in kW
$CVR_{f(kVAR)}$	CVR factor in kVAR

ΔP_{demand}	Change in power demand,
ΔP_{losses}	Change in power losses
P_{demand}	Total real power demand at substation
P_{load}	Total active power load demand
P_{loss}	Total real power losses
nl	Number of load buses (node)
V_k	Voltage at k^{th} node
V_p	Primary side voltage of OLTC/AVR
V_{tr}	Regulated voltage at secondary side of OLTC/AVR
$V_{base} or V_n$	Base voltage or nominal voltage
a,b,c	Phase(Φ) a ,b and c
$N_{tr,h}^{i}$	Total tap change of i^{th} (OLTC/AVR) device at h^{th} hour
$N_{tr,\max}^{i}$	Maximum number of daily tap change of i^{th} (OLTC/AVR) device
$N_{sw,h}^{i}$	Total switching operation of i^{th} CB device at h^{th} hour
CT_p	Primary current in Current Transformer (CT)
CT_s	Secondary current in CT
CT_{ratio}	CT ratio
$V_{LN,rated}$	Rated line to neutral voltage
KVA_{rated}^{Trf}	KVA rating of Transformer
KV_{rated}^{Trf}	Rated KV voltage of Transformer
V_{LN}	Line to neutral voltage
$N_{sw,\max}^{i}$	Maximum number of daily switching operation of i^{th} CB device
$V_{i,T}^{mon}$	Monitored line voltage at i^{th} line at time T
$Q_{i,T}^{mon}$	Monitored line reactive power flow at i^{th} line at time T
$Q_{i,T}^{\min}$	Minimum reactive power flow limit of i^{th} line at time T
$Q_{i,T}^{\max}$	Maximum reactive power flow limit of i^{th} line at time T
P_{demand}^{No-CVR}	Active power demand during No-CVR operation

E_{demand}^{No-CVR}	Energy demand during No-CVR operation
C_{cost}^{No-CVR}	Cost of power purchase during No-CVR operation
P_{demand}^{CVR}	Active power demand during CVR operation
E_{demand}^{CVR}	Energy demand during CVR operation
C_{cost}^{CVR}	Cost of power purchase during CVR operation
ΔP_{demand}	Total peak active power demand reduction, ΔE_{saving},
ΔE_{saving}	energy savings
ΔC_{saving}	Total cost savings
Cpp	Power purchase cost
$C_{Grid}(t)$	Grid electricity price at time t
CVR_{fP}	Peak kW power
CVR_{fC}	CVR factor in terms of cost
$V_{No\text{-}CVR}$	Node voltage during normal operation
V_{CVR}	Node voltage during CVR operation
ΔV	Voltage reduction
$kWh_{CES,T}^{stored}$	kWh stored value in CES
kWh_{CES}^{rated}	Rated kWh capacity
SOC	Current state of charge
SOC^{upper}	Upper limit of SOC
SOC^{lower}	Lower limit of SOC
CES^{Pout}	CES power output
C_{OMC}^{CES}	CES operating and maintenance costs
$C_{OMC,Fixed}^{CES}$	Fixed CES operating and maintenance costs
$C_{OMC,Var}^{CES}$	Variable operation and maintenance cost
$V_{i,h}$	Node voltage (p,u.) at i^{th} bus at hour h
$V_{CVR,h}$	The expected CVR voltage (p,u.) at hour, h
N	Number of the nodes
$P_{a,b,c}^{loss,h}$	Active power losses at hour, h
$Q_{a,b,c}^{loss,h}$	Reactive power losses at hour, h
N_{PV}^{k}	The switching step number at k^{th} PV system

ΔQ_{PV}^{k}	Variation in reactive power per step of switching steps at k^{th} PV system
$N_{PV}^{k,\max}$	Available maximum number of switching steps at k^{th} PV system
$V_m^{K_r}$	Velocity of each particle at K_r^{th}
$X_m^{K_r}$	Position of each particle at K_r^{th}
Tp	Prediction time horizon
Tc	Control time horizon
dt	Sampling time step
t_k	State at k^{th} time
Ω_{bus} , Ω_{br}	Set of all buses and branches respectively
Ω_{vr} , Ω_{oltc}	Branches with voltage regulators and OLTCs respectively
Ω_{CB}, Ω_{pv}	Branches with CBs and PVs respectively
Ω_{EV}	Branches with EV
α , β , γ ,π	Weighting factors

PREFACE

The faster depletion of fossil fuels and their detrimental effect on the environment, such as greenhouse gas emissions, has led to several nations to adopt the carbon emission reduction program and curtailed the electricity generation through fuel-based power plants. Though, the power generation through non- conventional sources focusing on distributed renewable energy sources has emerged as a potential solution globally but needs a lot of investment with a defined time period to achieve the goal. Another cost-effective way to achieve this goal is to enhance the energy efficiency and distribute electricity more efficiently by optimal utilization of the network assets and control devices with the help of smart technologies. In this context, energy-saving through conservation voltage reduction (CVR) has gained momentum because of its positive correlation between voltage and power demand. Moreover, the large-scale integration of distributed energy resources (DER) in the distribution network has emerged as a solution and issues for grid operation and control. Hence, there is a need for efficient, optimal, and coordinated control methodology to measure the performance of the CVR scheme, unlock the opportunity of further energy savings and to manage the voltage profiles to remain closer to the minimum limit.

The present research work focuses on the development of smart such voltage and VAR control (VVC) algorithms in the purview of CVR implementation for energy conservation in active distribution network (ADN). A closed-loop smart grid-enabled CVR method assisted through ADMS has been introduced in order to enhance the observability and energy efficiency of the system. A case study on effect of different types of load models on CVR has been performed, and simulation results validate the positive correlation between voltage-dependent loads and CVR.

Further, advanced control algorithms have been developed for optimal coordination among network devices and assets. Moreover, the proposed CVR methodology has been implemented via VVO based methods in the presence of active devices such as solar photovoltaic (PV), wind power and energy storage systems and developing controls that leverage these distributed energy resources (DERs). Besides, both the deterministic and stochastic optimization methods have been utilized to solve the centralized VVO problems. In order to maximize the benefits of CVR and distributed energy storage (DES), a coordinated, centralized deterministic VVO methodology has been proposed, and the optimal solution has been obtained using the heuristic discrete gravitation search algorithm and particle swarm optimization.

Though the centralized approach works well for a fixed time horizon interval, but it might be inflexible for fast-response events such as PV intermittency. To resolve these issues, a time horizon-based model predictive VVO methodology along with a local controller has been introduced in the smart grid framework. Moreover, increasing penetration of flexible loads such as electrical vehicle (EV) in ADN is also one of the major concerns for DNO. Therefore, in this thesis, the impact of EV charging loads with different profiles have also been considered in stochastic VVO formulation under CVR scenarios. The noteworthy application of vehicle to grid (V2G) reactive power dispatch from EV charging station for voltage regulation has also been demonstrated.

Validation of the developed methods and models has been carried out in a real-time environment. To accomplish this, a real-time event-driven predictive framework has been proposed to validate the developed VVO methods. The proposed methodology adopts the aggregated and autonomous approach for the functioning of VVO devices actively in multi time scale operation. A communication free, autonomous droop control scheme for real-time local VVC has been developed.

To check the effectiveness of the developed control algorithms and framework, a real-time co-simulation platform using the real-time digital simulator (RTDS) in distribution mode through co-simulation with models based on Python and OpenDSS (Open Distribution System Simulator) has been built. Real-time validation demonstrates that the proposed VVO methodology works well in centralized as well as local domain and also capable of controlling the voltage fluctuations during a sudden change in network behaviour and occurrence of unpredictive events.

Further, case studies carried out reveal that the proposed VVO formulation fruitfully utilized the benefits of both CVR and DER technology. Besides, higher penetration of EV charging loads having the constant power characteristics behaviour influences the CVR operation. The reduced load demand through CVR algorithms directly reduces the power generation requirement from fossil fuel-based power plants. Hence, reductions in carbon emission could be achieved as value addition in terms of cost and carbon footprint reduction.

CHAPTER 1

INTRODUCTION

1.1 Preamble

Nowadays, electricity has become the prime catalyst and indispensable power for the faster development and growth of any nation. Moreover, proliferation in smart grid technologies, green energy initiatives, and the 21st century's energy policy to improve the system efficiency have made an incredible impact on the electrical power sector. Therefore, power utilities and grid planners have to rethink in the purview of the smart grid and energy efficiency for better solutions and quality of service [1]. Further, information and communication technology-enabled smart grid solutions are offering great opportunities to resolve the distribution operational problems quickly and secured manner [2].

On the other side, a large amount of power from distributed energy resources (DER) (a major part of solar photovoltaic (PV) and wind energy) is being injected into the grid at various points of the electric power network through various initiatives and programs globally. The government of India has also planned to deploy 100 gega watts (GW) grid-connected solar power up to 2021-22 under the flagship of *National Solar Mission* [3]. The above capacity will come through grid-connected rooftop solar PV and medium & large-scale grid-connected solar power. About forty percentage, i.e., 40,000 megawatts (MW), is targeted from rooftop solar PV, which covers mainly institutional sector, commercial sector, industrial sector and housing. Rest will come (about sixty percentage, i.e., 60,000 MW) from medium and large-scale grid-connected solar power, including solar park projects and other schemes. To achieve this target for a country like India is

not an easy task. Many curious problems associated with solar PV integration have emerged in the parts of the country, such as in July-2016, the southern Indian State of Tamil Nadu, has to experience the first-ever curtailment of solar power generation [4]. It was unable to consume all the power that was produced. Though other countries such as United States, Germany also have already dealt with this issue. There are already signs that the grid's ability to absorb a large amount of unpredictable power with existing infrastructure could be a major bottleneck for higher solar PV penetrations. Distance is also a critical concern, as six states in the western and southern regions of India account for 80 percent of all of the country's presently installed solar capacity having only 38 percent of power demand. In contrast, northern states have the highest power demand. Intermittency, variability and uncertainty occurred due to the unavailability of solar irradiations, cloud transients, or cloud passage; sun eclipse and unwanted things/shedding on solar panels affect the system performance and can affect in balanced operation. Another incident, such as a critical solar eclipse occurred on 21 August 2017 in which some part of the world was completely or partially suffered blockages of solar light [5]**.** Accurate climate forecasting helped to grid managers to hand the situation and forced to shift their solar generations. In the United States, the California system operator has handled the biggest solar crass challenge. Though it was not a complete solar blockage but their 56 to 78 percent obstruction of sunlight will affect in a great manner. Thanks to their rooftops across and utility-scale power solar plants, which help a lot to manage the power shortage transient. Much more such incidents have happened across the world, to which grid operator/ electric power system operators should learn the lessons.

The integration of such large solar energy in the smart grid is an upcoming issue. The conventional transmission and distribution grids may not be able to cooperate due to their unidirectional energy flow and other limitations. However, integrating the DER from

both ends (as rooftop PV from the prosumer side and utility-scale power plants, etc.) will make the flow of energy in two way that causes the reversible power flow and voltage regulation malfunctions issues in controlling and monitoring devices during grid operations [6]. According to the various utility pilot projects and studies. in today's scenario reverse power flow and over-voltage stands as the main hurdle for the expansion of PV DER integration on a distribution grid. Another aspect is the unbalanced allocation of rooftop or in other types of PVs installation (single-phase or three phases) creates a rise in neutral current and neutral voltage in the unbalanced distribution network. This may lead to higher energy losses and may cause the detrimental impact of network devices and assets. Hence, system instability, power quality measures, deferred transmission & distribution infrastructure, and balancing demand & supply are major concerns of the grid operators for the reliable and safe operation due to the high-level PV integration.

This tends to force power utilities and grid planner to deploy the smart grid technologies with a regulatory policy which would allow both the utility and prosumers without affecting system performance. The role of smart grid in solar energy penetration is very crucial in grid modernization. Various initiatives are currently running in India and across the world for energy efficiency, peak load management and monitoring & control, etc. Some of the key attributes in smart grid solutions such as real-time system awareness, advanced Volt/VAR Control (VVC) through a smart inverter, advanced energy management system and integrated storage system that can be helpful for solar power integrations. Modern smart inverters have various attractive features such as voltage & active and reactive power control, frequency regulations, energy flow direction detection, etc. Extensive deployment of inverter also increases power loss in the distribution grid. Therefore, proper control and coordination strategies are required for optimal, efficient and mal free operation. Though the enabling of various technologies may increase the

complexity of the system and cost investment, however, with faster development in technology, this issue will not be a major concern.

1.2 Necessity of Electrical Energy Conservation

Energy conservation may be defined as **"***It is the idealistic or economic practice of reducing the use of energy by way of increasing energy efficiency and reducing the energy wastage"* [7]. In this context, the enhancement in electrical energy efficiency through energy conservation has emerged as a potential candidate. Form the economic point of view, the cost of energy creation through energy conservation is far less than the cost of energy created through the installation of power plants. The limited availability of natural energy sources, day by day continuously increasing energy demand and a rise in the level of greenhouse gases mainly due to higher carbon dioxide (CO_2) emissions. According to [8], electricity and heat are the key sources of CO_2 emissions, as can be seen in Figure 1.1. This is due to the fact that in many nations, still mainly depends upon burning fossil fuels to fulfill their electricity demand. According to International Energy Agency (IEA), in 2016, about 68% of the global electricity production came from burning coal, gas and oil, with coal accounting for about 38.3% alone, as shown in Figure 1.2 [9]. Recently, the IEA report says that, in 2018, the global electricity demand increased by 4 percent, which is nearly double of the fastest increased rate since 2010. In order to meet the increased electricity demand, the generation from coal- and gas-fired power plants have risen considerably that led to an increase in CO_2 emission from the sector by 2.5%.

In this context, the various initiatives have been floated by developed and developing countries for decarbonizing the electricity generation and implement the policies which are more envisioned towards the energy efficiency enhancement. Besides, the strategies focusing on reducing the electricity demand without negotiating the growth of nations have been encouraged widely in electric power system practices [3].

Usually, the electrical power sector has been divided mainly in the following parts: generation, transmission, distribution, and end-users [10]. In comparison to other parts of the power system, the distribution network has been given less attention in comparison to other parts of the power system.

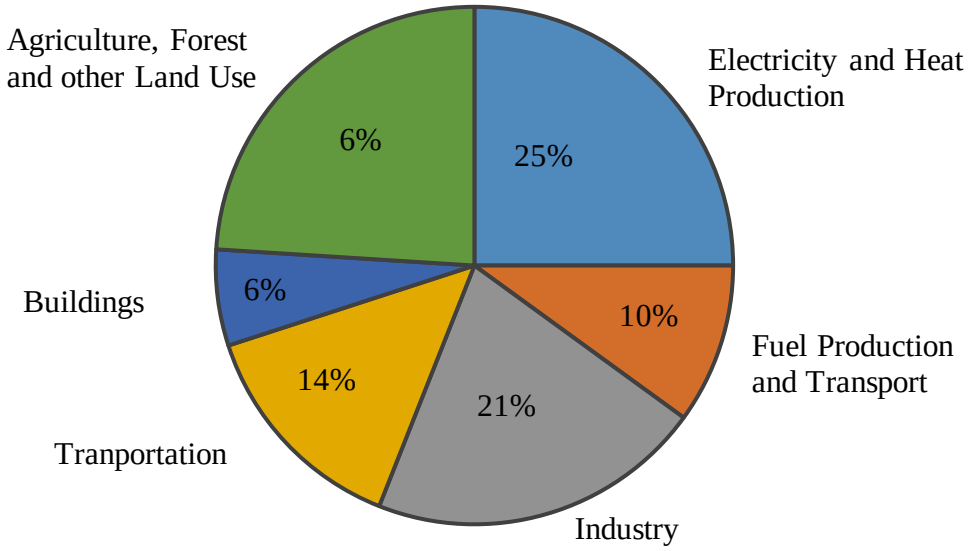

Figure 1.1 Greenhouse gas emissions by economic sectors [8]

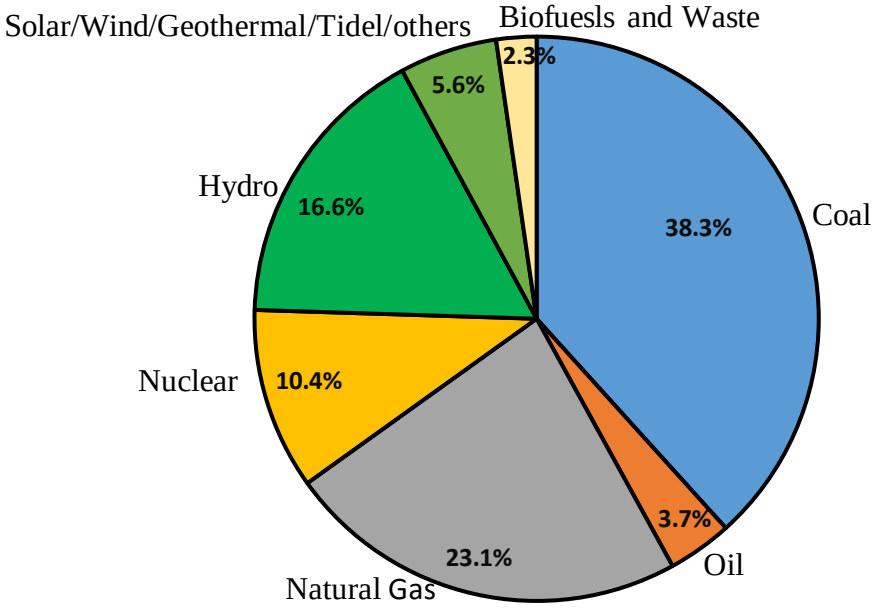

Figure 1.2 World gross electricity production by source in 2016 [9]

Indeed, it needs more attention so that energy crises and the quality of power can be improved. Besides, in the current scenario, energy conservation in the distribution network is one of the essential concerns for power engineers and researchers. Technologies such as Distributed Management System (DMS), Substation Automation, Advanced Metering Infrastructure (AMI), Conservation Voltage Reduction (CVR) and Distribution Generations (DGs) have made significant impact on distribution network operations and controls to make the system more robust, efficient, reliable and secure [10]–[16]. There are still numerous challenging problems such as high aggregate technical and commercial losses (AT&C), inefficient operation, unreliable and poor quality of services (QOS) is faced by the distribution system operator and customers. These are mainly due to the rapid increase in load growth, mismatch load demand and generation ratio, unplanned distribution network, variety of load patterns and reversible power flow due to large integration of DER [14]. In addition, energy distribution systems are significantly affected by political, social and theft hindrances in developing countries. For a complete analysis of the distribution system, it is essential to observe the distribution network at the end of the line (EOL) within the concept of the smart grid. In this context, distribution network optimization and control are one of the prime tasks for electric power utilities to deal with new smart distribution grid systems. Hence, in order to optimize such distribution grids, utilities are adopting more efficient technologies such as advanced Volt/VAR optimization (VVO) methods with multiple objectives such as CVR, loss reduction, network reconfiguration and power factor improvement[11], [12], [15], [16]. CVR technology has the ability to improve the energy efficiency at the distribution level and lower the system losses by conservation of voltage and reducing the load demand of the end-uses.

1.3 Overview of Power Distribution Network

A typical distribution network commences from the distribution substation, which is connected to one or more high-voltage and medium voltage transmission and sub-transmission lines. Each distribution substation is the combination of one or more primary distribution feeders, which feed the electricity to the consumers. Traditionally, distribution networks are designed as passive circuits where unidirectional power flows from high to low voltage levels and generally, DGs are not present at distribution feeder level. Figure 1.3 shows the passive distribution circuit with network components such as line segments, voltage regulation devices and loads mainly that have been detailed explained in later subsection. Integration of DG and/or onsite generations at both the source and load end (i.e., both high/medium voltage and low voltage terminals) of the distribution networks have totally reformed the grid operations. Consequently, the unidirectional power flow direction changed into bi-directional power flow and passive distribution circuits became active distribution circuits. Moreover, the adoption of incentive-based programs such as net metering schemes, tariff driven price mechanism and subsidies have accelerated the integration of renewable DGs around the world in order to reduce the carbon emissions [17]. Moreover, distributed solar PV systems both small scales such as household applications or building rooftop levels and large scale at utility levels, have been installed at a faster rate in both medium and low-level distribution networks.

Presently, consumer has become a "*Prosumer*" that not only consumes the power but also have the ability to feedback the power into the grid. Besides, integration of newly active devices such as DERs, distributed energy storage (DES) and electric vehicle (EV) charging stations with the capability of exchanging the power from the grid have made a passive distribution to the active distribution network (ADN) as can be seen in Figure 1.4.

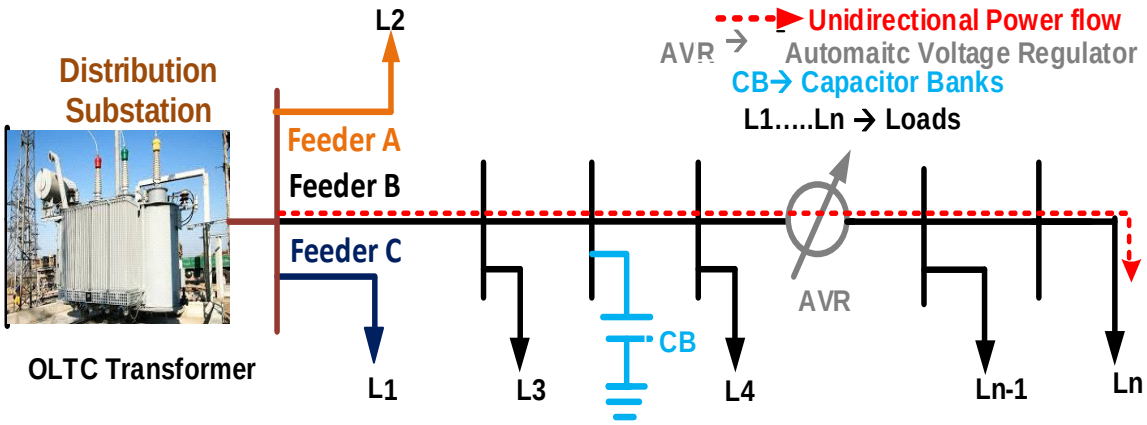

Figure 1.3 Schematics of a passive distribution network

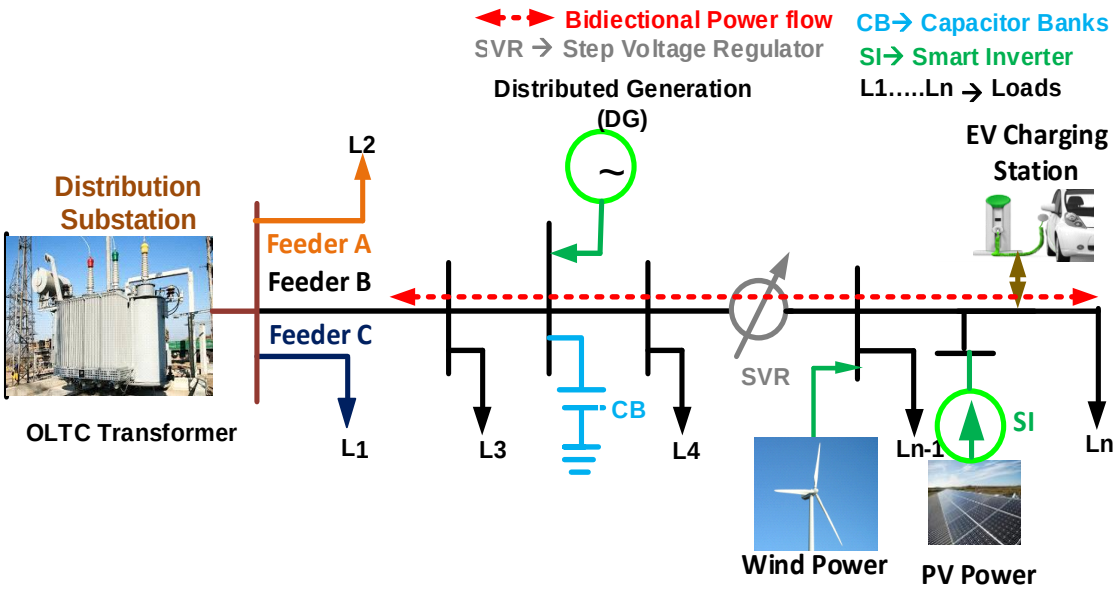

Figure 1.4 Representation of active distribution network

The new ADN not only unlock the benefits of system optimizations but also pave the way for higher-level penetration of low carbon technology. In this context, VVO schemes with high observability and voltage control capabilities fruitfully utilize the CVR benefits unlikely with traditional network operation schemes.

1.4 Description of Distribution Network Components

As earlier said, that distribution network is the combination of one or more feeders. The components of the distribution feeder can be classified as series and shunt network components. Series network components are line segments, Automatic Voltage Regulators (AVR) and transformers, whereas spot & distributed loads and Capacitor Banks (CB) are generally termed as shunt components. Accurate modeling of both series and shunt components is necessary for close observation of distribution feeder.

1.4.1 Line Segment Model

Distribution lines can be represented as exact line segment model. Voltage and current relations for exact line segment model with respect to input node 'h' and output node 'k' can be expressed as shown in Figure 1.5 and related equations are explained below [18]:

$$\left[VLG_{abc}\right]_h = [a]\cdot\left[VLG_{abc}\right]_k + [b]\cdot\left[I_{abc}\right]_k \tag{1.1}$$

where

$$[a] = [u] + \frac{1}{2}[Z_{abc}].[Y_{abc}] \tag{1.2}$$

$$[b] = [Z_{abc}] \tag{1.3}$$

and $[u]$ is identity matrix.

$$\left[VLG_{abc}\right]_k = [a]^{-1}\cdot\left(\left[VLG_{abc}\right]_h - [b]\cdot\left[I_{abc}\right]_k\right) \tag{1.4}$$

$$\left[I_{abc}\right]_h = [c]\cdot\left[VLG_{abc}\right]_k + [d]\cdot\left[I_{abc}\right]_k \tag{1.5}$$

$$[c] = [Y_{abc}] + \frac{1}{4}\cdot[Y_{abc}]\cdot[Z_{abc}]\cdot[Y_{abc}] \tag{1.6}$$

$$[d] = [u] + \frac{1}{2}[Z_{abc}].[Y_{abc}] \tag{1.7}$$

Equations (1.1) and (1.5) can be rearranged in equation (1.8) to yield:

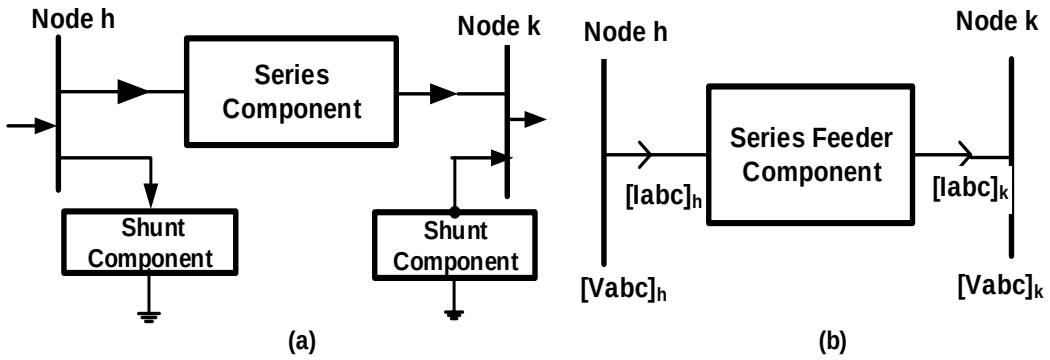

Figure 1.5 (a) Single line diagram of distribution network components (b) Series feeder component connection representation

$$\begin{bmatrix} [VLG_{abc}]_h \\ [I_{abc}]_h \end{bmatrix} = \begin{bmatrix} a & b \\ c & d \end{bmatrix} \begin{bmatrix} [VLG_{abc}]_k \\ [I_{abc}]_k \end{bmatrix} \tag{1.8}$$

where, Z_{abc}, Y_{abc} are the impedance & shunt admittance of the line segment. $[VLG_{abc}]_h$, $[VLG_{abc}]_k$ is the line to ground voltage matrix at node h and k, respectively. $[I_{abc}]_h$, $[I_{abc}]_k$ are the node current matrix at node 'h' and 'k' respectively. The value of shunt admittance is, in general, very small. Therefore, it can be neglected for simplification of the network. Similarly, voltage and current equations can be obtained for other series components. The generalized equations for series components can be written in the following equations (1.9) and (1.10):

$$[VLG_{abc}]_k = [A][VLG_{abc}]_h - [B][I_{abc}]_k \tag{1.9}$$

$$[I_{abc}]_h = [C] \cdot [VLG_{abc}]_k + [D] \cdot [I_{abc}]_k \tag{1.10}$$

The values of matrices [A], [B], [C] and [D] will change according to the series components. Detail modelling of these series and shunt components is well documented in [18].

1.4.2 *Voltage Regulation Devices*

Voltage regulating devices are widely used for not only maintaining the acceptable voltage profile throughout the network, but they also play a crucial role in the healthy

operation of the distribution grids. AVR, online tap changer (OLTC) transformers and CBs are the most commonly used voltage regulating devices. With the advancement in smart grid technologies, grid-connected power sources such as solar PV with smart inverters also provide voltage support to the system as a voltage regulating devices [19]

1.4.2.1 OLTC Transformer and AVR:

An OLTC transformer is used to vary the voltage across the network. It is generally located at the source substation side. The provision of tap changing is made towards high voltage side in off-load changing transformers, whereas the tap changing mechanism is provided towards low voltage side in on-load tap changer. It can be represented as the simple circuitry of an ideal transformer with series branch admittance as described in [19]. The OLTC transformer's tap position and its transformation ratio (a_{tr}) can be utilized to determine the voltage variation as expressed by equation (1.11).

$$a_{tr} = 1 \pm \left(\frac{\Delta V_{tr}}{100} \right) \times \text{Tap} \tag{1.11}$$

In equation (1.11), the minus/plus sign is used to denote the raise/lower in the tap position. AVR is formed by combining an autotransformer and a load tap changing mechanism. It is located at the source end and/or downstream of the feeder. It can be modeled as a tap-changing autotransformer with very small series impedance and shunt admittance. The AVR with taps in the series winding side is considered type A and that having taps on the source side is called type B [18]. Type B is widely used for downstream feeders for which the voltage regulation is governed by equation (1.11).

1.4.2.2 Capacitor Bank

Capacitor banks are a group of fixed and switchable shunt capacitors. CBs should be equipped with controllers (in the case of switchable shunt capacitors) in order to regulate

voltage and reactive power flows efficiently. Reactive power supplied by CB at each switching operation is determined using equation (1.12).

$$Q_{cb}^{i} = Sw_{cb}^{i}\ \Delta q_{cb}^{i}, \quad Sw_{cb}^{i} = \left\{0,1,2....,Sw_{cb}^{i,\max}\right\} \tag{1.12}$$

1.4.2.3 Smart Inverter

Apart from the basic inversion function, modern PV inverters have many advance attractive features. They have the capability to inject or consume the reactive power from the grid and operate as a distributed VVC device. In addition, PV inverters contribute significantly to the improvement of distribution network operation by maintaining the voltage profile and losses reduction. However, it may cause some additional loss while performing reactive power support functions.

The actual real and reactive power output from the inverter (P_T^{inv} , Q_T^{inv}) including the inverter losses are determined by following equations at given time T:

$$P_T^{inv} = P_T - P_{T,loss}^{inv} \tag{1.13}$$

$$Q_T^{inv} \approx Q_T \tag{1.14}$$

$$P_{T,loss}^{Inv} = (1-\eta_{inv}).\left(\sqrt{P_T^2+Q_T^2}\right) \tag{1.15}$$

The available $Q_T^{inv,\max}$ is dependent upon the real power generation for a period T which governed by equation (1.16) as applied in[20] [21]:

$$|Q_T^{inv,max}| = \sqrt{\left(S_{\max}\right)^2-\left(P_T\right)^2} \tag{1.16}$$

On the basis of P_T and S_{max}, $Q_T^{inv,max}$ is recalculated at every time period, T.

1.4.3 Load Models

In order to fruitful utilization and to unlock the potential benefits of VVO and CVR, an accurate and updated load modeling is essential for power flow solutions. The load model

structures typically categorized into two types namely static or time-invariant and dynamic loads. The static models such as polynomial (ZIP) load with a combination of constant impedance (Z), constant current (I) and constant power (P) and exponential load model are widely used for non-thermal cycle loads study [22]. On the other hand, loads having thermal cycles such as Heating Ventilation and Air Conditioning (HVAC) and water –heater are considered as dynamic loads and represented by Equivalent Thermal Parameter (ETP) model [23]–[25].

In the context of distribution network studies, this thesis intended to adopt the well-established ZIP and exponential load models to evaluate the CVR impact. The representation of composite ZIP load model has been shown in equations (1.17) and (1.18) respectively.

$$P_{i,t} = P_{o,i,t}\left[Z_p\left(\frac{V_{i,t}}{V_o}\right)^2 + I_p\left(\frac{V_{i,t}}{V_o}\right) + P_p\right] \quad (1.17)$$

$$Q_{i,t} = Q_{o,i,t}\left[Z_q\left(\frac{V_{i,t}}{V_o}\right)^2 + I_q\left(\frac{V_{i,t}}{V_o}\right) + P_q\right] \quad (1.18)$$

$$Z_p + I_p + P_p = 1 \quad (1.19)$$

$$Z_q + I_q + P_q = 1 \quad (1.20)$$

Where in equations (1.19) – (1.20), Z_p, I_p, P_p, and Zq, I_q, P_q are the coefficients of impedance, current, and the power for the real and reactive powers, respectively. $P_{o,i,t}$, $Q_{o,i,t}$, and $V_{i,t}$ are the rated active, reactive power and voltage at the i^{th} load node at instant t, respectively. V_o is the nominal voltage. Moreover, the constituting load models of ZIP representation have been described below [26]:

- *Constant Impedance (Z) Loads:* The relation exists between drained power and voltage is quadratic in nature. In other words, it can be defined as power is directly proportional to the square of the voltage. The resistive appliances such as hobs, electric showers or steam irons are the typical example of this type of loads.

- *Constant Current (I) Loads:* This model considers a linear relationship between power and voltage. A typical example of this type of load is a compact fluorescent lamp.
- *Constant Power (P) Loads:* This type of model drains a constant amount of power without depending upon supply voltage referred to as constant power loads. Usually, escalators and conveyor belts at 24/7 factory can be classified under this model.

Even though both the ZIP and ETP models generally show the characteristics of load to voltage sensitivity. However, most of the feeders do not have detailed load information. Therefore, it is very challenging to model the loads using the ZIP and ETP models in an explicit manner without adequate observability. Meanwhile, in order to model the loads, a method has been proposed by the Electric Power Research Institute (EPRI) [27], [28] considering the practical aspects of user-end behavior. The developed EPRI model known as a nominal linear P, Quadratic Q (feeder mix) load model, as shown in equations (1.21) - (1.22). This model is quite similar to the exponential type load model. EPRI load model uses CVR factors in place of power exponents (active and reactive) of exponential load model. Moreover, the study carried out by EPRI also reveals the impact on real and reactive load power with the variation in voltage profile using the CVR factor [28]. Therefore, apart from ZIP model, this thesis also utilizes the similar load model (feeder mix) to build a relationship among load power, voltage and CVR factor (CVR_f) with the exponential equations (1.21) -(1.22) and analyze the impact of developed CVR control schemes.

$$P_{load}^{k}(t) = P_{n}^{k}\left(\frac{V_k(t)}{V_n}\right)^{CVR_{f(\mathrm{kW})}} \tag{1.21}$$

$$Q_{load}^{k}(t) = Q_{n}^{k}\left(\frac{V_k(t)}{V_n}\right)^{CVR_{f(\mathrm{kVAR})}} \tag{1.22}$$

Where $P_{load}^{k}(t)$ and $Q_{load}^{k}(t)$ are the active and reactive power load, respectively. $CVR_{f(\mathrm{kW})}$ and $CVR_{f(\mathrm{kVAR})}$ are the CVR factors in kW and kVAR respectively.

1.5 The Need of Smart Voltage and VAR Control

Generally, a specific voltage range is defined by manufactures for the smooth operation of electrical equipment. But it is not so easy to provide the same voltage level for all end users because of the voltage drop occurs in each part of the conventional power distribution system. The larger voltage drop occurs in those consumers who have a large power demand or getting their power through larger impedance [10], [15]. This is because of the voltage drop is proportional to the magnitude of demand current and the entire impedance between the source and the consumer and unidirectional power flow. Voltage profiles along a feeder supplying residential loads in a typical passive distribution network have been shown in Figure 1.6 [10]. From Figure 1.6, it is observed that the nearest consumer to the power supply has the least voltage drop, while the last and the farthest consumer has the largest voltage drop [10]. It is achievable to maintain the required voltage level at any point along the feeder with the use of direct voltage control or controlling the flow of reactive power in the distribution system. Due to the flow of reactive power, there is a voltage drop on the inductive element of wires. Therefore, to maintain the voltage profile, voltage and reactive power flow should be considered together. This scheme is called as VVC.

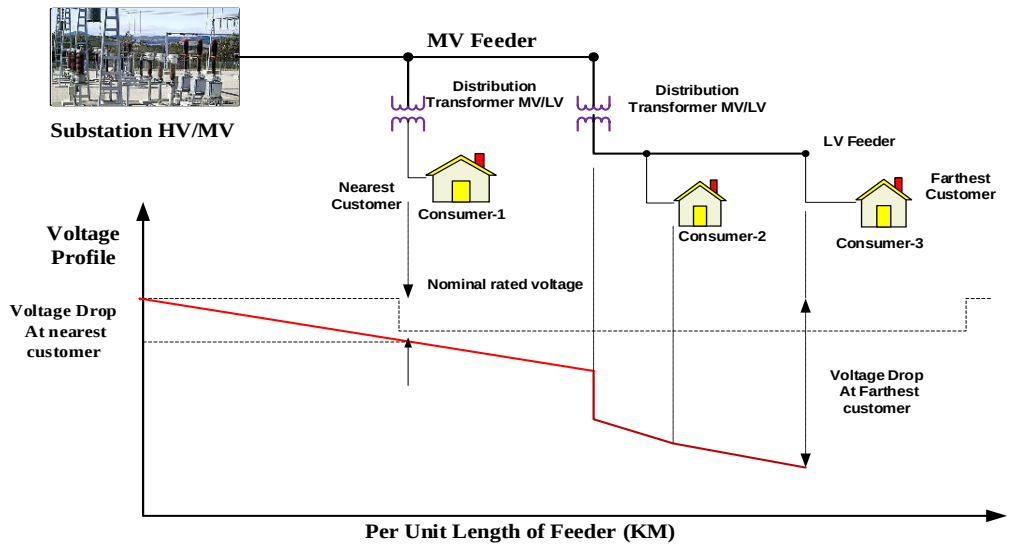

Figure.1.6 Voltage profile along a feeder supplying residential loads [10]

Equipment's such as OLTC transformers, AVR, fixed and switched shunt capacitors are used for controlling of voltage and reactive power flows and referred as slow response conventional VVC devices[11], [21]. On the other side, large scale installation of variable DERs such as solar PV and wind power has created a huge impact on grid operations. Though, the integrations of such devices are unlocking the various benefits such as lowering the carbon emission, pollution-free electricity production and enlarging the CVR energy-saving margin but also causes unwanted technical problems in distribution network operations. Moreover, traditional VVC algorithms also not work efficiently. These include feeder under/overvoltage profile and overloads in transformers, particularly those scenarios when maximum generation and minimum demand, as a result of reverse power flows [29]–[31]. Though centralized VVC with traditional devices works well for a fixed time horizon interval, it might be inflexible for fast-response events such as PV intermittency and sudden change in network behavior.

Hence, there is a need of smart VVC algorithms that coordinate the smooth operation of multiple (both slow and fast-acting) voltage regulation devices in a multi time scale in the purview of CVR implementation in ADN considering the uncertainties in power generation and loads. In this context, a smart VVC framework for ADMS applications has been introduced as shown in Figure 1.7. the proposed framework includes DER controls and coordination with other network devices and assets. Besides, the adoption of slow and fast-acting devices (such as smart inverters having the ability to respond quickly) are explored as an option to regulate the voltages closer to customers, and at the same time, provide the CVR benefits. Moreover, a time horizon based predictive control that provides coordinated management of control devices in centralized and local domains in active distribution networks will be proposed to exploit CVR benefits in cases with and without DER and EVs while catering for system constraints.

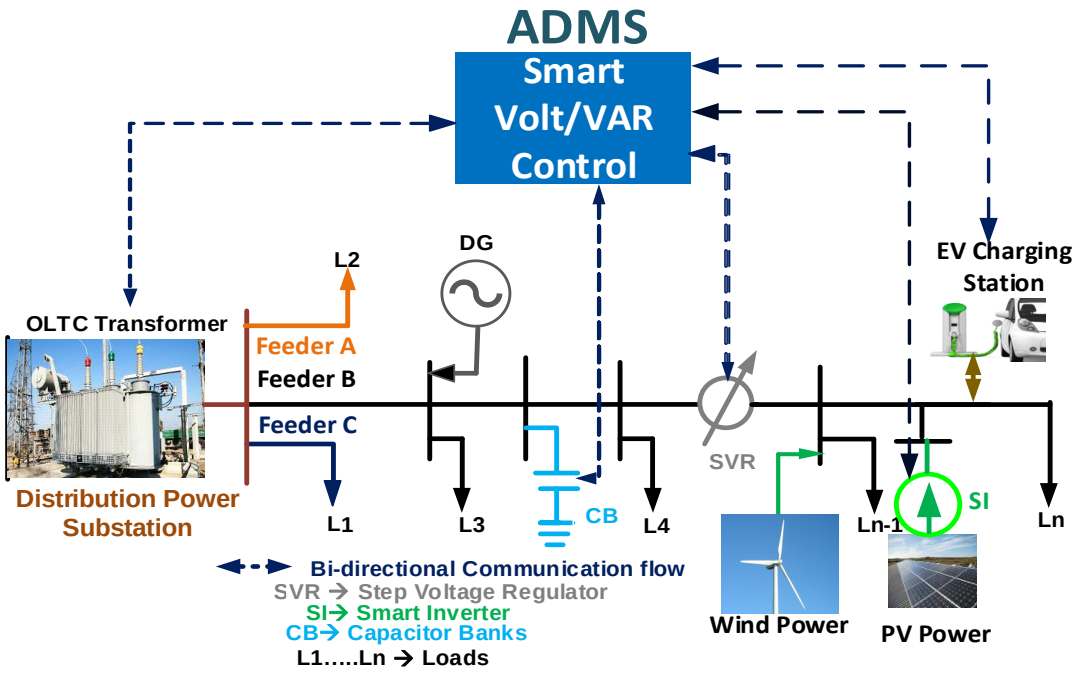

Figure 1.7 Proposed smart VVC framework for active distribution network

1.5.1 Concept of CVR

Voltage conservation produces CVR phenomena. The basic concept of CVR technology is the conservation of energy by a marginal reduction in voltage (normally 2–6% of nominal value) at user end nodes without affecting the performance of the customer's devices. In order to maintain acceptable voltage profile throughout the distribution feeder length and under various loading situations, CVR technology should follow the international Standards such as American National Standard Institute (ANSI) C84.1–2006 and Canadian Standard Association (CAN-C235-83) on voltage regulation [32]–[34]. Moreover, the ANSI C84.1–2006 standard says that the customer appliances can work smoothly on the lower half of the distributed voltage level without disturbing the device's performance. Moreover, CVR is an integral part of voltage and reactive power control. Therefore, it is enabled through the advanced functioning of the integrated VVC mechanism. A schematics of voltage distribution along the feeder length with and without CVR has been shown in Figure 1.8.

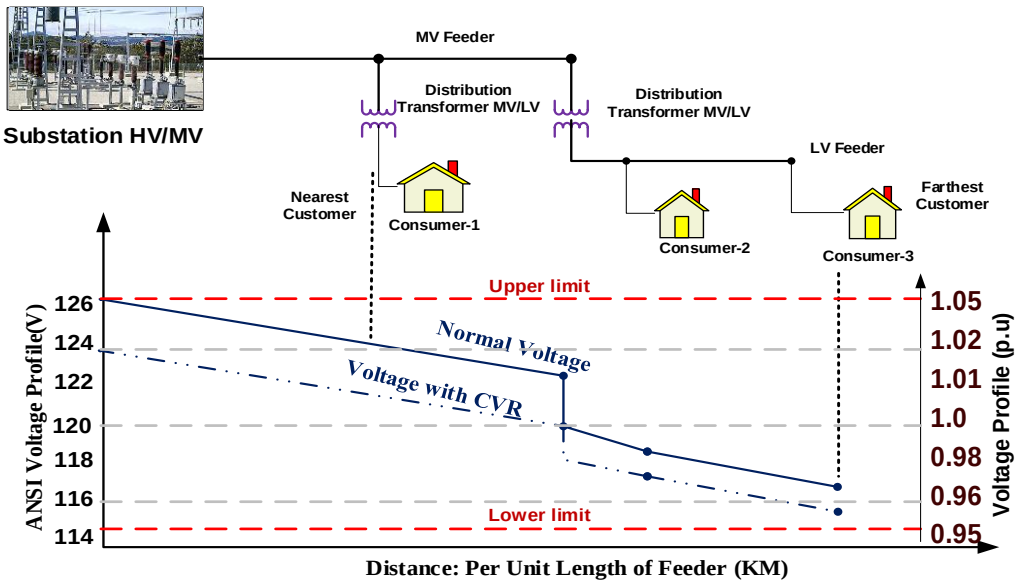

Figure 1.8 Voltage distribution along the feeder length with and without CVR

1.5.1.1 Measuring the CVR effect

Generally, CVR saving depends upon load models, loading type and network topology, etc. CVR effects can be evaluated by the CVR_f, which is defined as follows:

$$CVR_f = \frac{\Delta W}{\Delta V} \tag{1.23}$$

ΔW = % Reduction in quantity (Power, Energy and Cost) ΔV = Percentage of voltage reduction.

1.5.2 *Background of CVR Technology*

CVR is not a new technology in the area of conservation of energy; the tests have been already performed in early 1973 [32]. From Figure 1.9, it can be observed that automated VVC is a thought that has grasped the varying levels of interest over the years [11]. During the decade of 1980-90s, vertically integrated utilities have firstly examined that advanced VVC as an effective technique to reduce power demand and losses in distribution system. After the 1990's when the deregulation of power system occurred, a serious issue raised that who will be benefited from VVC saving.

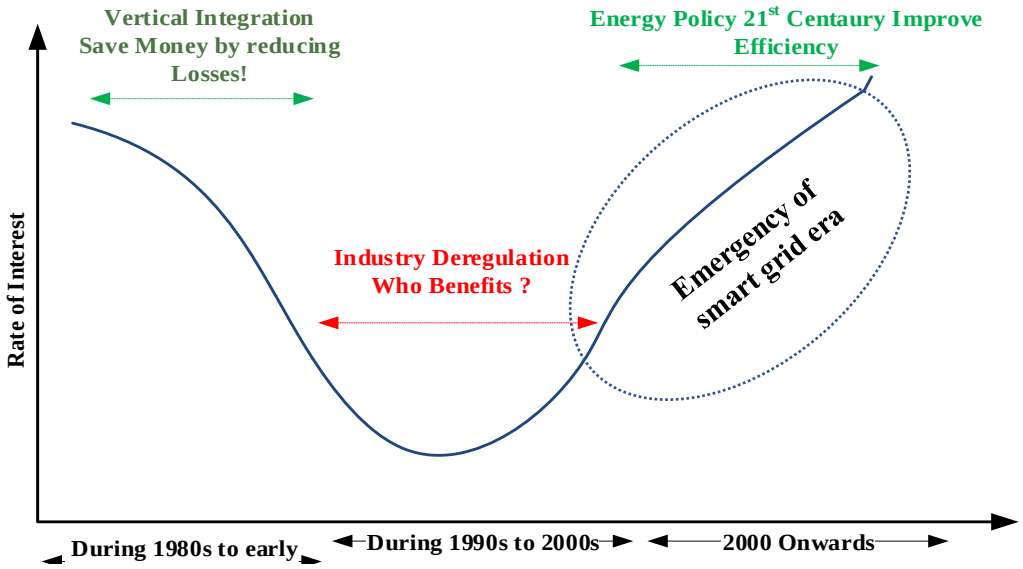

Figure.1.9 Interest cycle of CVR [11]

In many cases, utilities were not benefited from the improvement of VVC because of savings in electrical losses were delivered to customers or absorbed by suppliers and load demand balanced by several forms of generation suppliers. Consequently, during this period of time, the interest in the deployment of VVC improvements fell down dramatically [11]. In the recent scenario, the smart grid era has focused on the need for improved efficiency, energy conservation and integrated VVC techniques such as CVR and VVO to fulfill the smart grid objectives. Therefore, interest in the CVR technique is increasing drastically since 2000 onwards.

The Public Service Commission of New York and American Electric Power System (AEP) have established their first implementation of CVR in 1973 [28]. After that, various researchers [35]–[39] and utilities such as Snohomish County PUD [40], BC Hydro [41], Dominion Virginia Power [42], Southern California Edison (SCE) [43], Hydro Quebec (HQ), Northeast Utilities (NU) [33], Bonneville Power Administration (BPA) [44] and Northwest Energy Efficiency Alliance (NEEA) implemented their CVR tests and gained significant results of energy savings related to voltage reduction [31]. By reducing 1% of feeder voltage, usually 0.3% to 1% load reduction is achieved. Recently,

the United States has deployed CVR technology to all distribution feeders and obtained a 3.04% reduction in the annual national energy consumption [45]. CVR was also widely tested in other countries. Australia, Ireland has obtained 2.5% and 1.7% energy saving by a reduction of 1% of voltage, respectively [46], [47]. In twenty-one centaury, the interest rate has increased rapidly due to the implementation of energy policy structures.

1.6 Literature Review

In order to reduce the peak load demand and energy consumption, various power utilities have already applied CVR technology and quantified the achieved savings in terms of CVR factors. The outcomes of various pilot projects and studies reveal that about 1-3% of energy savings can be achieved by 1% of voltage reduction[32],[48]. However, its implementation, assessment and power quality issues pose three technical barriers such as:(i) optimal coordination among voltage and VAR regulatory devices; (ii) appropriate assessment and verification of CVR effects; and (iii) coordination between CVR and other active devices such as DER, energy storage and flexible loads etc. for the adoption of the technology at large scale deployment. In this context, the literature review on CVR has been explored, focusing on two broad categories such as i) CVR implementation strategies and ii) CVR assessment and quantifying method for current and future deployments.

1.6.1 CVR Implementation Strategies

In order to deploy the CVR technology, there are mainly two type approaches have been discussed in the existing literature. The first one is traditional or open-loop VVC schemes and second is closed-loop VVC schemes[13], [16], [32].

1.6.1.1 Traditional or open-loop VVC schemes

Traditionally**,** CVR has been applied by voltage reductions through voltage regulating devices that are as close as possible to consumers. These typical devices are OLTCs at

primary substations and line voltage regulators (in the field and/or outside the substations) to compensate for voltage drops in long MV/LV distribution feeders. The methods that are generally used to implement the CVR by the DNOs are on-load tap changer (OLTC), line drop compensation (LDC), spread voltage reduction (SVR), and home voltage reduction (HVR) [31]. The use of LDCs has been widely accepted by DNOs to improve the CVR performance [32], [49]–[55]. Though, the CVR implementation through LDC is relatively simple but poses certain limitations such as the case dependent R &X settings and cannot adapt the dynamic changes [31]. Moreover, the calculated voltage at the farthest point is an estimation only; hence, safety margins are usually considered in the voltage reductions, which limits the voltage reduction range in order to extend the CVR benefits further [31].

The additional reactive power sources such as capacitor banks and D-STATCOM have also been used in various CVR studies and trials to compensate the voltage drops occurred in heavily loaded MV feeders and boost the voltage at critical points for potential use of CVR [47] ,[53], [54], [58], [59]. Voltage reductions through open-loop CVR schemes are a convenient and cost-effective way to implement CVR. However, schemes suffer a lack of real-time information about the voltage and reactive power flows throughout the feeder length. Therefore, the configuration and settings of CVR devices may be either inefficient or ineffective. Major drawbacks of these techniques are the limited depth of voltage reduction, controlling of devices based on local data and poor dynamic adaptability.

1.6.1.2 . Online closed-loop VVC schemes

In order to improve the observability of the distribution feeders, utilities have trailed the installation of monitoring devices at critical locations in the network (typically at the end of feeders and voltage-load sensitive nodes [60]. Some of the installed devices send the

measured data directly to primary substations, while others integrate them to the control center through SCADA system, where the DNO takes the decisions (such as tap changing) based on available measurements [55],[61]. Moreover, the advent of smart grid technologies such as smart meters and ADMS have emerged as a potential solution to enhance the system's observability and performance. DNOs saw the opportunity to utilize the real-time information from primary substation feeder to end of the line and close to customers to build an advance closed-loop CVR schemes with the help of smart meters [24],[62],[63]. Moreover, an accurate and realistic load profile across any feeder can be built by using real-time measurements and sample values of voltage, power flows, current, and power factor from these measuring devices [13], [15]. In order to calculate the appropriate setting of VVC devices based on measurements such as accurate voltage profile across the feeder, climatic conditions, and time of utilization, an online adaptive real-time approach for CVR implementation has been introduced in [12],[62],[64]. In this context, centralized and decentralized control approaches are preferred by DNOs as shown in Figure 1.10 [45].

- *Centralized CVR control:* Centralized VVO/CVR control scheme collect AMI sensory data through the interfacing with the metering demand management system in the back office of multiple feeders then running CVR algorithms and sending new setting to the VVC devices in the field via SCADA system. This scheme could be work more efficient and faster if on-demand AMI sensory data available more frequently.
- *Decentralized CVR Control:* Decentralized control scheme utilized the local sensory data control related to every single feeder when CVR algorithm operates locally within each substation referred as a decentralized control scheme. The main complexity in realizing a decentralized CVR control approach is that it needs more frequent AMI data. However, these techniques do not have a direct link to access the faster AMI data.

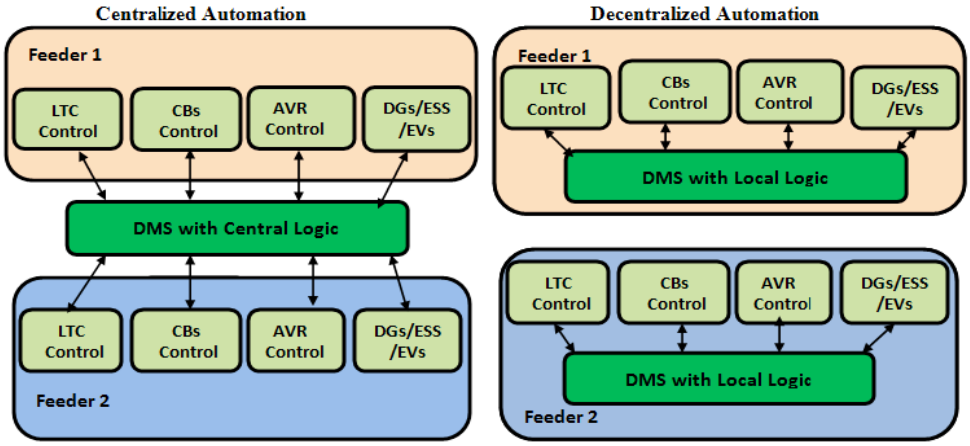

Figure 1.10 Centralized and decentralized controls

In literature, there are three main approaches for real-time VVO controls are SCADA or rule Based VVO, AMI Based VVO and DMS model-based VVO. The authors of [58] have discussed about benefits of VVO/CVR technique through implementing AMI. A real-time adaptive multi-agent system based VVO/CVR engine also based on smart metering have well discussed in [62],[64]. Moreover, the ADMS functionality based real-time VVO approach and non-intrusive energy-saving algorithm for VVC has been described in [16],[54],[65].

In summary, closed-loop techniques have extended the CVR benefits in terms of scalable voltage reduction range and higher observability. However, they also pose some limitations: (i) as these techniques work on some typical fixed local rules, therefore, cannot capable to adapt the network changes such as large load changes and feeder reconfiguration and; (ii) improper coordination among network devices and assets that result in a suboptimal operation. In order to tackle these limitations, the optimal VVC operation for CVR has also been explored and referred as optimal CVR, as delineated in the below subsection.

1.6.1.3 Volt/VAR Optimization (VVO): Optimal CVR

In order to determine the superior action of VVC and higher energy savings, the closed-loop VVC schemes have been suggested with optimal operation referred as VVO.

They offer advanced functions for VVC such as CVR and efficient coordination among VVC devices in centralized and decentralized manner. Though, the selection of optimization methods and algorithms for VVO execution is not a simple task. The main factors which generally decide the selection of right optimization methods are depending upon the nature and number of objective functions, constraints and inner behavior of the control variables. In general, the objective of VVO for CVR is to the minimize the power or energy consumption, system losses and feeder voltage deviations either separately and/or combined [12], [15], [16], [29]–[31], [52], [57], [62], [64]–[66]. As the classical VVO formulation is mixed-integer nonlinear programming (MILP) optimization, therefore, both conventional and metaheuristics optimization methods have been utilized in the literature to solve the VVO problem. Some studies have usages MILP[15], [66], and General Algebraic Modelling System (GAMS), and as solution algorithms considering both operational aspects, such as static and time-varying nature of the demand and generations[13], [20], [30], [50], [54], [59], [61], [67], [68]. Though the conventional algorithms, as suggested in [14], [15], [30], [66], work well but some time solution traps in local minima. Therefore, some researchers adopted meta heuristics optimization methods such as Non-dominated Sorting Genetic Algorithm (NSGA-II) [31], [57], [69], Genetic Algorithm (GA) [62], [64], [70] Tabu-search [71], Gray Wolf Optimization (GWO) [72] and Particle Swarm Optimization (PSO) [29], [52], [73] etc. to obtain the VVO solution. Most of these studies have performed a time-series simulation interval of 15 minutes to 1 hour and optimal control action carried out to above mentioned periods. Though the optimal centralized operation works well for fixed time horizon but in practices, during the sudden dynamic change in demand and generation and transient, these techniques suffers from some operational issues such as under/over voltage and reversible power flows.

Consequently, along with centralized optimal VVC, there is a need decentralized and local control action is required to enhanced the CVR benefits.

1.6.1.4 DER impact on CVR

As discussed in the earlier section, many nations around the globe have adopted incentives to accelerate the installation of renewable DERs generation at large scale and deploy the energy efficiency schemes to reduce carbon emissions. The successive reduction in technology costs has encouraged to DNOs to increase the distributed generation penetration in distribution networks. However, unplanned and unbalanced allocations of these DERs result in some operational issues also. On the other hand, CVR has been known as a method that can assist in accomplishing energy efficiency targets [74]. However, most of the studies performed related to CVR, where DER was not common. Hence, there is a need to better realize the interactions between DER and CVR [32],[74]. The interactions between CVR and widespread DER have been widely studied in [18]-[20],[28]-[29], [49]-[50], [65], [72]-[74]–[83],[84] for different style of distribution networks. While the studies [75], [79], [80], [86] explored the impact of CVR in the presence of various levels of DER with different range of voltages reductions with the common objectives of minimization of substation demand, energy losses and voltage deviations. In [30], [70], [83] an integrated VVO based approach has been suggested to implement the CVR and examine its impact on different load models. Optimal placement, size and integration of DG in the context of CVR application has been investigated in [51],[52],[83],[85],[87] and obtained results exposed that optimal DG allocation can boost voltages at sensitive points, therefore permitting further voltage reductions at primary substations. Moreover, the conclusive results reveal that various distribution operational issues such as under/over voltage, reversible power flow and limited hosting capacity may be resolved with combined operation of CVR and DGs.

However, most of the above-mentioned studies do not consider the effects of widespread renewable PV based where variable power generations (due to intermittency) on distribution operation. In this context, the authors of [21],[81]-[82],[84] have analyzed the CVR impact considering the various levels of PV penetrations and performed various studies such as optimal power flow [81], and rolling horizon-based time-series simulations [84]. Since these studies have mainly focused on centralized control operation with a defined time horizon; hence, there is a need of fast control actions that can compensate for quick fluctuations in PV power due to cloud transient effects.

1.6.1.5 Smart Inverter Based VVC

The large level penetrations of variable power generation such as PV, wind affect the static and dynamic performance of the distribution system. As earlier discussed, the intermittence and transient behaviors of these power sources also highly affect the operation and controls. Moreover, they also influence the impact of reactive power in voltages due to high resistance to reactance (R/X) ratio of distribution networks [20] . Though the voltage and reactive power control through traditional VVC are achieved but there is an ambiguity about the coordination and slow response of these traditional VVC devices with additional power sources during the sudden change in network behavior [32], [88]. In order to achieve a faster response of VVC, PVs equipped with smart inverter are being deployed for additional power support [82].

Distributed PV plants usually have a conventional inverter that is set to operate at maximum power point tracking to maximize output PV power, resulting in unity power factor operation. The revised IEEE 1547 (2018) [89], however, states that every DER must have reactive power support capability when requested by power system operators. Therefore, PV systems are increasingly being paired with smart inverters that can inject and absorb reactive power [19], [68], [77]. Moreover, the *Smart Inverter Working Group*

Phase 3 has recommended eight functions to be included in *California's Rule 21* as mandatory or optional for all inverter-based DER systems [90]. Accordingly, distributed PV has the capability to participate in voltage regulation (both local and centralized control) and act as a VVC device[21]. For a local VVC, a PV inverter operates in autonomous mode, and its reactive power dispatch relies on the local measurements using a predefined volt/VAR curve [20]-[21], [77], [91]-[92]. Optimal volt/VAR curve selection using a heuristics approach has been suggested in [93]. A gradient-based decentralized VVO approach under high DER penetration has been introduced in [94]. In centralized VVC, the smart inverter operates in aggregated mode, and the power factor or the reactive power dispatch is determined by the center operator using the control algorithm [72], [76], [82], [84], [91]. The authors of [20],[68] have suggested combined centralized along with local control VVO approach, but they did not include the uncertainty in the network model. Moreover, the reported methodologies have been validated using time-series simulations in offline mode; only a few strategies have been reported [64], [95], [96] for real-time VVC.

1.6.1.5 Effect of Load Models

In order to achieve a perfect solution of the VVO problem, an accurate and correct load model is required for power flow solutions. The detailed description of load models has been already explained in *subsection 1.4.2.4*. A time-series simulation of end-user loads is used for dynamic modeling. Heating Ventilation and Air Conditioning (HVAC) and Water –Heater is considered as dynamic loads with thermal cycles [25], [26]. Most of the work has considered voltage-dependent and time-invariant loads, mainly polynomial (ZIP) and exponential load for the evolution of VVO system [30]-[31], [51], [53], [68]. In [30]- [31], exponential load models have used for the analysis of VVO operation in distribution system. Moreover, [53] used CVR factors as an exponent in exponential load

models. A realization of CVR effect with field demonstration by using equivalent ZIP load models has been discussed in [53]. Authors of [14] present a framework for deploying VVO in distribution system with considering voltage dependence of loads. Effect of different load models on VVC savings have also been investigated in [70].

1.6.1.6 *Information and Communication Technology for CVR*

Information and Communication Technology (ICT)s are playing an important role in the deployment of any smart grid assets. Therefore, the study of ICT is essential for power utilities and grid planners. For distribution and substation automation, generally, IEC-61850 communication protocols are applied by smart power utilities and others [1], [64]. In order to achieve the benefits of VVO/CVR a fast, reliable and secure ICT is required. Basically, ICT links the sensors to DMS, SCADA and connect DMS/SCADA to the automatic controlling devices [97]. Most of the power utilities are applying a two-layer communications system between the ADMS and control devices. The first layer of communication consists of mainly high-speed fiber optics or microwave communication that connects DMS/SCADA to utility substations and second layer connecting substations [98]. Many communication technologies are available in the market based on their requirements. Broadband technologies are classified into two categories by broadband service providers. First one is with wire or fixed-line communication such as power line communications, hybrid/coax fiber, digital Subscriber line, home/curb fiber and another wireless Access technology as radio frequency/Microwave links, wireless fidelity (Wi-Fi), Satellite communication, cellular networks (3G and 4G), WiMAX, ZigBee etc. [1].

According to literature, most of the VVO studies have done in offline environments. Very few researchers/utilities have done their work in real-time VVO/CVR. However, most such studies are still in the early stage of considering a real-time VVO solution for the future smart grid. An intelligent agent-based distributed command and control system for

building a real-time load profile for integrated VVO/CVR engines have developed with the use of IEC-61850 communication protocols and narrow band power line communications (NB-PLC) [64]. A combined ICT and power simulation platform have realized of VVO operation in MV distribution feeder with the integration of opnet-modeller as a communication network simulator and Electromagnetic Transient Program (EMTP-RV) for system transients [99]. In [64], [100] a real-time co-simulation for the operation of the adaptive VVO engine using real-time digital simulator (RTDS) model and distributed network protocol (DNP3) protocol has been introduced. Socket based communication has been utilized in [95] to establish the connection between RTDS and external agent real-time co-simulation operation.

1.6.2 CVR Assessment and Quantifying Methods

Evaluating the CVR performance on feeder networks has always been a critical issue in the context of its implementation, selection of targeted feeder and performing the cost/benefit analyses. Generally, DNO assessed the CVR performance by determining its CVR factors according to requirements, as explained in the earlier section. In order to measure the reliably estimated energy-savings, the CVR factor still a driving force for research and deployment of CVR schemes. In this regard, Table 1.1 shows that CVR factors determined by various utilities, authors and conducted studies. However, the uncertainty regarding the achieved energy savings remains a barricade to its acceptance worldwide. The key challenge regarding the quantification of benefits can help for selecting the appropriate voltage reduction scheme, identify the networks where and when it is to enable the CVR for a defined time period. Generally, it is determined by comparing the scenarios such as normal operation or without CVR and one where CVR is applied. But doing this is no simple task because aggregate load consumption may not be exactly known or measured without and with CVR at the given time.

Table 1.1 CVR test performed by various utilities

Utilities/Authors/ Ref.	CVR Factor (CVR_f)			Published Year
	(kW)	(kVAR)	(kWh)	
American Electric Power System [101]			0.62	1973
San Diego Gas & Electric, CA [38]	0.548 -0.967		0.47-1.04	1982
Krishner & P.Giorsetto [39]			0.41-0.991	1984
American Electric Power System [37]			0.71	1986
Northeast Utilities (NU) [36]			0.57-1.35	1987
Bonneville Power Administration [44]	0.90			1990
Commonwealth Edison, California [102][40]	1.0			
Snohomish PUD, WA Northwest Utilities[40]			0.336-1.103	1991 2002
BC Hydro[41]	0.70			1995
Southern California Edison (SCE) [43]	1.0			
Tia Power[103]	0.57			
Avista utilities [104]	0.84			2005
Northwest Energy Efficiency Alliance [105]	Spring- 0.57, Summer-0.78 Fall-0.60, Winter-0.51			2007
Hydro Quebec (HQ) [106]	Summer (R, C, I) 0.67 ,0.97, 0.1 Winter (R, C, I) -0.12, 0.8, 0.1			2008
Pacific Northwest National Laboratory (PNNL)(report), U.S. [107]	With All distribution feeders 3.04% reduction in the annual national energy consumption			2010
R. Singh et. All [78]			0.67-1.33	2011
EPRI [27]	0.6-0.95	50-6.0		2011
Dominion Virginia Power [42]			0.92	
Sunderman/Utility/ EPRI [108]	0.6-1.119	3.0		2012
Australian Experience [46]			0.4	
Ireland Experience [47]	0.58-0.98	6.0 - 6. 6		
Marc Diaz-Aguiló [53]	0.50-1.0	1.5-2.0		2013
Consolidated Edison Company of NY [55]	0.54		0.55	2014
Zhaoyu Wang, et. All [109]	0.61-1.32			2014
Sacramento Municipal Utility District	0.61			2015
Korea Electric Power Corporation [110]	0.721-0.87	7.8-15.0		2016-17

According to [32], CVR effect accessing methods can be classified into four categories based on comparison, regression, synthesis and simulation studies. In this thesis, the emphasis has been given on a simulation-based approach, particularly to allow and perform detailed network and DER based generations impact in a real-time environment. Therefore, a brief discussion about the abovementioned quantifying methods has been described here. The more details about the methodologies can be found in [32], [111].

The first two techniques (i.e., comparison and regression) depend upon measurements in order to evaluate the implemented CVR schemes and latter two (synthesis and simulation-based) methodologies used to estimate the expected benefits before applying the CVR scheme in practices.

1.6.2.1 Comparison-based Method

In the comparison-based method, two basic schemes are considered; the first one is to select two similar networks (feeders) having the same configuration, characteristics and loading condition, etc. CVR scheme is implemented at one feeder while another feeder is operating in normal conditions at the same time. The second scheme is to implement the voltage reduction on a network and apply a normal voltage to the network during different time range having similar weather conditions. Then the CVR effects are determined based on the measurements such as energy consumptions, voltages from the two tests and afterward calculating the CVR factor. Utilities such as Detroit Edison and Snohomish County Public Utility District (Snohomish PUD) [40], [112] respectively have performed CVR test using this approach. Though these two methods are relatively simple to device for DNOs, but having problems as load consumption may change due to other factors such as small weather differences, measurement noises rather than voltage reduction, which can reduce the small CVR effect.

1.6.2.2 Regression-Based method

In regression-based methods, load modeling includes not only voltage level but other factors such as temperature, day type and month that can influence loading conditions. In order to calculate the more accurate CVR factor, these models used linear regression to identify the normal voltage loads and measured reduced voltage [32]. In [39], [111] a relation between network energy demand, applied voltage reduction and temperature variations for a month and day of the week has been built in order to access the CVR effect with other impacts. Authors in [49] tried to regulate the feeder-level and demand with respect to temperature; however study reveals that using measurements from an analogous network provided better regression models. Since the achieved energy savings through voltage reduction are a few percentages of load consumptions, hence it may lie in the range of regression models that limit the typical CVR using this method. Moreover, most of the authors used these linear models are known to be nonlinear functions of the exogenous variables [32]. These limitations can be handled using recently developed techniques (such as artificial neural networks and support vector regression etc.) on nonlinear regression methods.

1.6.2.3 Synthesis Based Method

This method aggregates load to voltage behaviors for a group of loads in order to estimate the corresponding CVR benefits of a network. The aggregation can be performed by synthesizing the load components and customer classes. In the component-based approach, the energy consumption of the main appliances is modeled as a function of voltage, which is obtained from laboratory tests [111]. Thus, the total load demand at network level can be estimated by aggregating the voltage-dependent load components with respect to their shares. The second method generally uses type of customer classes, which is defined as residential, commercial and industrial. Different customer classes

have a different share in the network and CVR factors [44]. Moreover, the literature survey presented in [32] clearly explained that, in general, residential and commercial feeders realize higher energy savings under CVR than industrial ones. Though, the synthesis-based approach is simple to apply and permits for fast estimation of energy savings before implementing the CVR. However, it does not provide any information about the time-varying load composition. Besides, sometimes, it is very difficult for DNOs to collect accurate load models and quantifying the participation of load demands. Thus, CVR effect assessed through synthesis methods are needed to understand before implementing in field trials.

1.6.2.4 Simulation-Based Methods

These methods are based on modeling of network, loads and execute the power flow analysis under various operating scenarios with and without considering the voltage reduction effect. The CVR benefits estimation can be calculated by comparing the results obtained from voltage reduction to normal operating conditions. In order to achieve this, estimation of load demand and appropriate modeling of loads in the function of voltage are to be carried out considering the various dominating factors such as season, solar irradiance and temperature. The main challenges of simulation methods are how to build an accurate representation of loads and their dependence on the voltage that can contribute to the major energy-saving effect. The details regarding load models have already been discussed in the previous section. Past decade literature related to simulation-based CVR studies focused on utilized aggregate power loads and average voltages to build the time-invariant load models. Moreover, few researchers have tried to develop the load models for individual appliances with appropriate rules for obtaining aggregated models based on participation factors [22],[24]-[25]. In the current scenario, the inclusion of the time-

varying loads for CVR-related studies has been introduced and demonstrated in [26],[45], [60],[109].

1.7 Objectives and Scope of the Thesis

The main objective of this thesis is to develop the smart voltage and VAR control algorithms to conserve the energy in ADN. In order to accomplish this goal, the research work further sectionalized in the following objectives

- First objective is to develop the closed-loop CVR framework with better monitoring and controllability. In order to achieve this, a closed-loop smart grid-enabled CVR method assisted through ADMS and feedback by advanced metering infrastructure data have been proposed in this work. In addition, effect of different load models on achieved savings using proposed method is to be analyzed.
- The second and foremost objective of the thesis is the development of advanced control algorithms for coordination among the network devices and network assets in an optimal manner. Therefore, optimal CVR operation using centralized VVO method has been suggested in this thesis. The impact of DERs in VVO formulation has also been incorporated. A centralized approach works well for a fixed time horizon interval, but it might be inflexible for fast-response events such as PV intermittency. Therefore, a time horizon-based model predictive VVO methodology has been proposed to resolve the deterministic VVO issues.

  Besides, the impact of EV charging loads with different profiles have been considered in stochastic VVO formulation under CVR scenarios. The noteworthy application of vehicle to grid (V2G) reactive power dispatch from EV charging station for voltage regulation has also been demonstrated.
- Third objective deals to validate the developed methods and models in real-time environment. Therefore, a real-time event-driven predictive framework has been

proposed to check the effectiveness of the developed control algorithms and framework. In addition, a coordinated three-level hierarchical dispatching structure is proposed to realize the event-driven predictive online framework. The development of a dynamic real-time droop controller for smart inverter operations has also been proposed. Besides, a real-time co-simulation platform using the RTDS in distribution mode through co-simulation with models based on Python and OpenDSS is proposed.

- Quantify the value of energy and cost savings for utilities, electricity savings for customers, and carbon emissions reduction is the fourth prime objective of the thesis. The investigation incorporates the CVR factor-driven scheme to assess the load-reduction effects via CVR using developed VVO algorithms. CVR factors in terms of power, energy, and cost have been proposed for different time durations such as peak load hours, peak day and annually. Besides, the operating costs of distributed network devices and maintenance costs of assets have been incorporated in the proposed VVO formulations. The techno-economic-environmental analysis of CVR implementation has also been carried out. Further, analyze the impact of load reductions as value addition in terms of cost and carbon footprint reduction has been analyzed.

1.8 Organization of the Thesis

The work embodied in the present thesis is organized into eight chapters. The organization of the same is as follows:

Chapter 1: Introduction

This chapter briefly introduces the necessity of electrical energy conservation, the basic concept of power distribution network and the need of smart voltage and VAR control. Besides, the basic concept of CVR has also been discussed. Further, it also presents a

comprehensive literature survey of the research carried out in Volt/VAR control, CVR implementation and assessments of its effect with and without the presence of DER. Finally, the chapter concludes with the research objective and detailed organization of the thesis.

Chapter 2: Concept of Smart Grid Enabled CVR

In this chapter, a smart grid-enabled CVR methodology has been introduced. The basic concept of the proposed methodology has also been described. Further, the proposed methodology has been implemented using traditional LDC scheme with the help of conventional VVC devices such as OLTC, AVR and capacitor banks. Besides, the effect of different load models on CVR operation has been analyzed. In addition, assessment of the CVR effect with additional reactive power support from capacitor banks has also been carried out. Finally, the proposed methodology and its effects have been demonstrated on the modified IEEE 13-node and 34-node distribution feeder test system

Chapter 3: Distributed Energy Resources Impact on CVR

This chapter describes the impact of DER on CVR energy savings and distribution grid operations. Besides, the combined effect of DER and CVR has also been analyzed using proposed smart grid-enabled CVR method. The PV smart inverter-based voltage and reactive power control of the ADN have been introduced in this chapter. In addition, the LDC approach has also been utilized to implement the proposed methodology. At last, the proposed smart PV inverter based VVC methodology has been validated on a modified IEEE 123-node unbalance distribution feeder test system. Moreover, the modeling and simulations have been carried out on OpenDSS and MATLAB platforms.

Chapter 4: Optimal CVR: Centralized Volt/VAR Optimization

In chapter 4, the implementation of optimal CVR in ADN using VVO methodology has been introduced. A centralized discrete gravitation search algorithm-driven VVO

approach has been proposed in this chapter. Further, the proposed methodology has been validated in the presence of distributed energy storage and also analyzed the combined impact of both CVR and DES technology on peak load management and energy savings. In this chapter, the community energy storage type DES has been considered and correspondingly its power flow control scheme for an unbalanced power system has also been introduced. Finally, the proposed VVO based CVR methodology has been validated on a modified IEEE 123-node unbalance distribution feeder test system.

Chapter 5: Multi-Time Multi-Objective Volt/VAR Control and Optimization

This chapter introduces a multi-time multi-objective VVC and optimization for CVR implementation. A multi-stage- multi-objective VVC methodology in a slow and fast time scale has been proposed in this chapter. In addition, for slow time scale operation, centralized VVO approach has been introduced and optimization problem has been solved using multi-objective particle swarm optimization. Further, a droop-based approach for fast time scale to control the PV DER reactive power has been introduced. In addition, the impact of cloud transients on PVs power production has also been analyzed. Besides, the economic impact of the proposed method has been described. Lastly, the proposed MSMO-VVC methodology has been validated on a modified IEEE 123-node unbalance distribution feeder test system.

Chapter 6: Time Horizon-based Model Predictive Volt/VAR Optimization in Presence of Electric Vehicle Charging Loads

This chapter investigates on the need of coordinated operation of CVR in the presence of electric vehicle penetration in the active distribution network. A time horizon-based model predictive VVO methodology has been introduced in this chapter. The developed control algorithm considers the uncertainties in load demand and PV power generation. This chapter also describes the implementation of voltage and VAR regulation through

smart inverters of PVs and EV charging stations in global as well as local domains simultaneously. In addition, a real-time Volt/VAR droop-based controller has been introduced to control the smart inverter's reactive power dispatch. Finally, the proposed model predictive VVO algorithm has been tested and validated on a modified IEEE 34 bus test system.

Chapter 7: Real-Time Event-Driven Predictive Volt/VAR optimization and Control

This chapter analyzes the impact of CVR in the presence of active devices such as solar photovoltaic (PV) and developed control algorithms in a real-time framework. An event-driven predictive framework for real-time VVO, along with a local two-level adaptive volt/VAR droop-based control algorithm for ADMS, is introduced in this chapter. Further, the proposed methodology has been validated in a real-time framework using the real-time digital simulator platform through co-simulation with models based on Python and OpenDSS.

Chapter 8: Conclusion & Future Work

Finally, this chapter summarizes the research work. The significant contributions and conclusions of the present work are drawn in this chapter. In addition, this chapter also gives the future prospects of the present work.

1.8. Conclusion

This chapter briefly describes the overview of the distribution network, its classification and working principle of different VVC devices. In addition, the concept of smart Volt/VAR control and principle of CVR has been explained. This section also discussed the required literature review. Finally, chapter one concludes with the research objectives and outline of the present thesis.

CHAPTER 2

CONCEPT OF SMART GRID ENABLED CVR

2.1 Introduction

The basic aim of CVR technology is the conservation of energy by a marginal reduction in voltage (normally 2- 6% of nominal value) at user end nodes. Thus, by setting the regulation voltage in the ANSI lower half (114-120V) range, saving in energy can be achieved. However, while reducing the voltage, CVR should meet the International Standards ANSI C84.1–2006 [33]. Application of CVR with traditional schemes has not been found much effective because of restricted voltage reduction range, inaccurate load modeling and the unavailability of end-user information. In order to overcome the above barriers, enhance the observability of the distribution network and achieve higher energy savings, a smart grid-enabled CVR approach has been proposed in this chapter. The proposed CVR scheme has been implemented using closed-loop VVC methodology. The traditional LDC approach has been utilized in order to perform the VVC operation. The proposed methodology has been validated by analyzing the effect of different load models on CVR. Besides, the impact of additional reactive power compensation through CBs has been investigated during deeper voltage reduction range. The allocation of CBs has been done based on voltage sensitivity and fulfilling the objective of loss minimization.

2.2 Smart Grid Enabled CVR

The operation of CVR through a smart VVC approach is carried out by enabling of smart grid assets (such as ADMS, AMI and smart controllers) in local as well as the global domain of the distribution network. The schematic diagram of the integrated VVC with CVR for a distribution network has been shown in Figure 2.1.

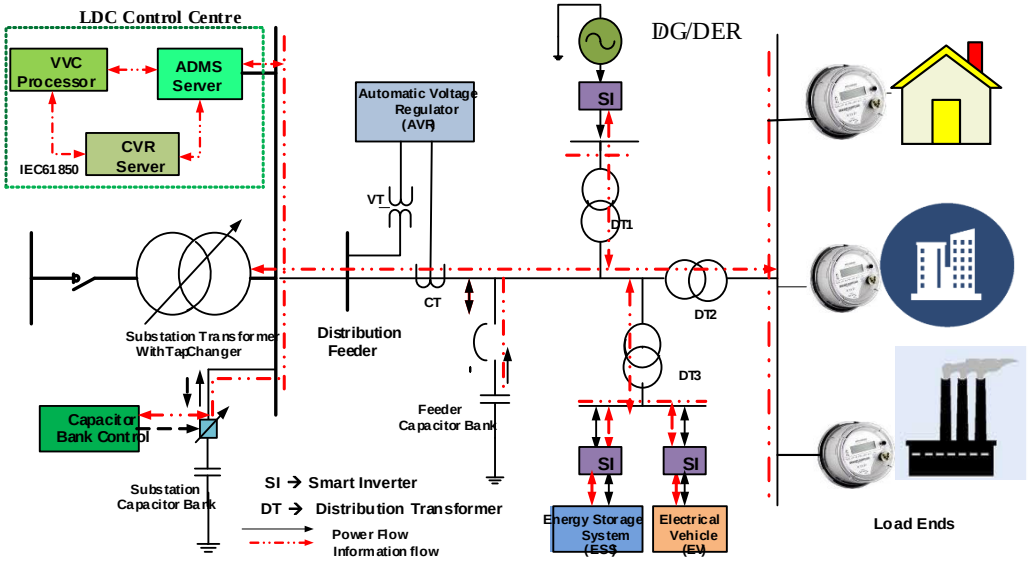

Figure 2.1. Proposed substation based Smart Grid-enabled CVR

In order to achieve the maximum energy savings, VVC processor calculates the controlled parameters of different field assets with the coordination of CVR server with ADMS. The field devices are connected to the servers through communication links. An ADMS regularly monitors and evaluates the power and voltage profile throughout the distribution network with the help of AMI and supervisory control and data acquisition (SCADA) systems. The proposed scheme first accumulates the measurements and then generates proper control signals. These control signals are transmitted through suitable communication links to VVC field devices. Accurate loads are derived through AMI data, which plays a prime role in enabling the CVR scheme in planning or in the real-time framework.

The assessment of CVR effects is judged through the CVR factor. Mathematically in terms of energy (CVR_{fE}), it is calculated as the ratio of the total E_{Saving} in percentage and amount of voltage reduction (ΔV) over a time horizon in percentage as articulated in equations (2.1) and (2.2).

$$E_{Saving} = \left(\frac{E_{No\text{-}CVR} - E_{CVR}}{E_{No\text{-}CVR}} \right) \quad (2.1)$$

$$CVR_{fE} = \frac{(E_{saving})\%}{\Delta V\%} \quad (2.2)$$

2.3 Implementation of Proposed Methodology Using Traditional Approach

The proposed CVR scheme is implemented through controlling the voltage and reactive power flow in the network, which is governed by regulating the VVC devices such as OLTC/regulator and CB bank. The functional control schemes of these devices are described below subsection.

2.3.1 OLTC/Regulator Control

The traditional LDC scheme has been adopted in this investigation to control the OLTC/regulator. The control circuitry of AVR is governed by LDC to regulate the tap position of OLTC. Figure 2.2 shows the schematic diagram of the LDC model, which consists of a compensation circuit, voltage relay, and OLTC movement mechanism.

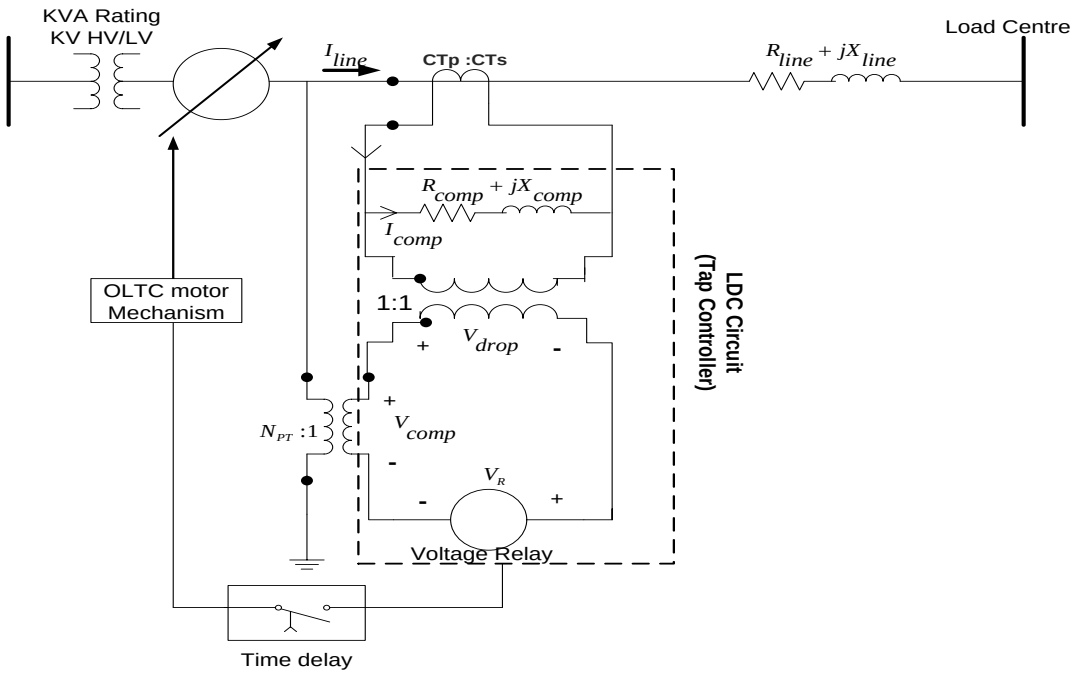

Figure 2.2 Schematics of LDC mechanism

The compensation circuit has a current transformer (CT), potential transformer (PT) and impedance matching transformer with R &X setting. These settings of compensation circuit are very critical for voltage regulation because it reveals when tap change is required. In this work, the R and X settings are referred as R_{comp}, X_{comp} which represent the equivalent impedance from the regulator location to the regulation point. The detailed explanations regarding tap calculation can be found in [18], [52].

To calculate the required tap following steps are executed by LDC algorithms:

- Determine the R_{comp}, X_{comp} value in ohm and volts using following equations (2.3) and (2.4) respectively.

$$R_{comp} + jX_{comp} = \left(R_{line} + jX_{line}\right) \cdot \frac{CT_p}{N_{PT}.CT_s} \tag{2.3}$$

$$R_{comp} + jX_{comp} = \left(R_{line} + jX_{line}\right) \cdot \frac{CT_p}{N_{PT}} \tag{2.4}$$

where, R_{line}, X_{line} are the resistance & reactance of the line respectively and N_{PT} is PT ratio determined by equation (2.5).

$$N_{PT} = \frac{V_{LN,rated}}{V_{Base}} \tag{2.5}$$

- Calculate the actual (feeder) line current (I_{line}) with the help of equation (2.6).

$$I_{line} = \left(\frac{KVA_{rated}^{Trf}}{\sqrt{3}\, KV_{rated}^{Trf}} \right) \tag{2.6}$$

- Find the compensator current (I_{comp}) through equation (2.7).

$$I_{comp} = \left(\frac{I_{line}}{CT_{ratio}} \right) \tag{2.7}$$

- Compute input voltage to the compensator circuit or compensator voltage (V_{comp}) by equation (2.8).

$$V_{comp} = \left(\frac{V_{LN}}{N_{PT}} \right) \tag{2.8}$$

Voltage drop (V_{drop}) in compensation circuit is determined through equation (2.9).

$$V_{drop} = \left(R_{comp} + jX_{comp} \right) \times I_{comp} \tag{2.9}$$

- Calculate the voltage across the voltage relay (V_R) using equation (2.10) which represents the voltage at regulation point.

$$V_R = V_{comp} - V_{drop} \tag{2.10}$$

- If V_R is outside the bandwidth of regulator then required tap change is calculated by equation (2.11). Otherwise, there is no need to change the tap position.

$$\text{Tap} = \frac{\left(V_{reg} \pm 1 - V_R \right)}{(\Delta V_r \times V_{base})} \tag{2.11}$$

V_{reg} is regulation voltage at regulating position (set point),where, $[V_{reg} \pm 1]$ is the acceptable range of V_{reg} of the distribution feeder.

- After calculating tap value, voltage relay sends the signal to the OLTC motor mechanism to change the tap position.

2.3.2 Capacitor Bank Control

CB control is very helpful to maintain the feeder voltage profile and reduce the system losses. This controller is supplemented with monitoring devices such as CTs, PTs and local decision processors with connector/discounter situated at the load side of the bus as shown in Figure 2.3. The controller device takes samples of voltage and current through CTs and PTs at the monitored location. After that, a decision is taken regarding the amount of compensation required based on control criteria such as kVAR and voltage at monitored points/devices.

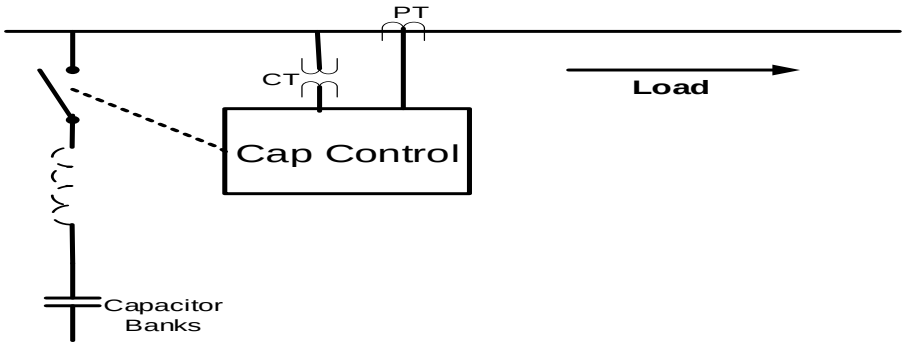

Figure 2.3 Capacitor bank controller with monitored devices

To control the voltage profile and reactive power flow at monitored point/device, the following *algorithm 1* are adopted to CB control as delineated under:

If $V_{i,T}^{mon} < V_{i,T}^{\min}$

CB module is switched ON,

else if, $V_{i,T}^{mon} > V_{i,T}^{\max}$

CB module is switched OFF.

else if, $V_{i,T}^{\min} \le V_{i,T}^{mon} \le V_{i,T}^{\max}$

check the Q limits

if, $Q_{i,T}^{mon} < Q_{i,T}^{\min}$

CB module is switched ON,

else, $Q_{i,T}^{mon} > Q_{i,T}^{\max}$

CB module is switched OFF.

end

end

The specified value of $Q_{i,T}^{\min}$ is 40% of the rating of CBs and $Q_{i,T}^{\max}$ is 60% of the rating of CBs in reverse direction.

2.3.3 Power Flow Algorithm

Conventional load flow methods such as Gauss-Seidel and Newton-Raphson are not suitable for distribution network because of most of the distribution feeders are radial with unbalanced loading pattern and untransposed lines. Due to fast convergence, the

iterative ladder technique is widely used in the radial distribution network. Ladder iterative algorithm uses forward/backward sweeping technique [18]. To determine the corresponding voltage and current backward sweep is applied to equations (1.1) and (1.5) while the forward sweep uses equation (1.4) to find the voltages in a distribution feeder. The sweeping process is repeated until the difference between the defined and the calculated source voltage is below the predefined tolerance limit [113].

2.4 Assessment of CVR Effect Under Different Load Models

This section discussed the analysis of the CVR effect with different load models. The effect of CVR on energy consumption can be described by Joule's law, the power P, voltage V and current I in a resistive circuit satisfying P = VI with the assumption that there is no need of reactive power for consumer's devices. Lowering the voltage level reduces the power when the load consists of pure resistors with constant resistance R, followed by the ohm's low $V = IR$ and $P = V^2/R$. From various CVR tests, it is observed that the CVR effect is highly influenced by the consumer's load type. In this work following types of load models have been used to analyze the CVR effect.

- Constant PQ Model
- Constant Impedance (Z) Model
- Constant Current (I) Model
- Constant ZIP Model
- Nominal Linear P, Quadratic Q Model

2.4.1 Case Study

VVC mode of operation

- *Non CVR mode:* In this mode, effect of both AVR and CBs are considered in power flow analysis. The settings of regulators and CBs are the same, as mentioned in [114]. AVR1 and AVR2 have secondary voltage level 122V, 124V respectively.

- *CVR mode:* This mode includes the effect of both voltage regulators and CBs in power flow analysis. The voltage level of regulators has been reduced, and their modified values are 120V, 120V respectively.

2.4.2 Test System and Description

For analysis of CVR effect IEEE 34-bus, 24.9 kV distribution feeder model has been considered in this study. The distribution model consists of 34 nodes, two voltage regulators, capacitor banks and different load models [114]. Modelling and power flow analysis of the distribution system has been carried out in OpenDSS platform developed by EPRI [113]. A similar load type has been considered at each node of the distribution feeder bus to analysis the CVR effect with the individual load model.

2.4.3 Simulations and Result Discussion

This section presents CVR test simulation results with different load models. Power flow simulations have been done in *SNAP* mode with *STATIC* control mode in OpenDSS. The VVC operation has been carried out at peak demand hour with maximum loading condition (i.e.1 p.u). Various simulation results are analyzed below:

2.4.3.1 Constant PQ Load:

This type of load model increases the energy consumption with the reduction of voltage level because of an increase in line losses due to more current is drawn by the loads. Constant PQ load is defined as *model 1* or constant P+jQ load in OpenDSS platform. Assuming all loads connected in the test system are constant PQ type. From Figure 2.4 and Figure 2.5, it can be seen that power demand and losses are increased in CVR mode in compare to non CVR mode. Hence, CVR operation is not beneficial for constant power load models.

2.4.3.2 Constant Impedance (Z) Load:

Assuming all loads connected in the test system are constant impedance load type. Simulations have been carried out with both with constant Z load for both the mode of operation. From simulation results, as can be seen from Figure 2.4 and Figure 2.5, it is observed that there is a reduction in power demand and losses with CVR mode operation. Significant energy savings can be achieved with CVR mode operation.

2.4.3.3 Constant Current (I) Load Model:

Assuming all loads connected in the considered test system are the constant current load type. Simulation results with Constant I load have shown in Figure 2.4 and Figure 2.5, and it is observed that energy saving is slightly improved with CVR mode. The reduction of energy consumption is less than in comparison to the constant Z load model.

2.4.3.4 Constant ZIP Load Model:

Assuming all loads connected in the test system is a combination of constant impedance (Z), constant current (I) & constant power (P), or constant ZIP load type. The equations of the ZIP load have been shown in (1.17) - (1.20). Figure 2.4 and Figure 2.5 also shows the simulation results with constant ZIP load. From simulation results, it is observed that real power demand is reduced with the CVR effect. There is a slight reduction in real power losses has also been reported. Thus, it is observed that saving achieved in CVR mode in the presence of ZIP type load model is highly depends upon its coefficients. Moreover, ZIP coefficients represent the part of each load type. Generally, savings are influenced by the dominant value of the ZIP coefficient.

2.4.3.5 Nominal Linear P, Quadratic Q Load:

Nominal Linear P, Quadratic Q Load, is defined as model 4 in the OpenDSS platform. The representation of this model looks like exponential type loads. Instead of exponents, this model usages the $CVR_{f(kW)}$ and $CVR_{f(kVAR)}$ as shown in equations (1.21-1.22)

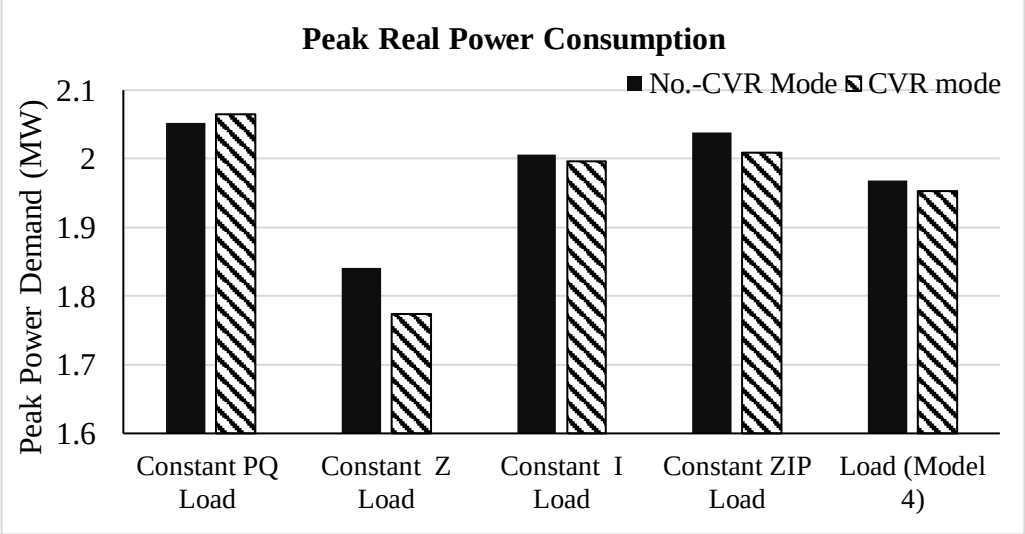

Figure 2.4 Peak real power consumption with and without CVR for different loads

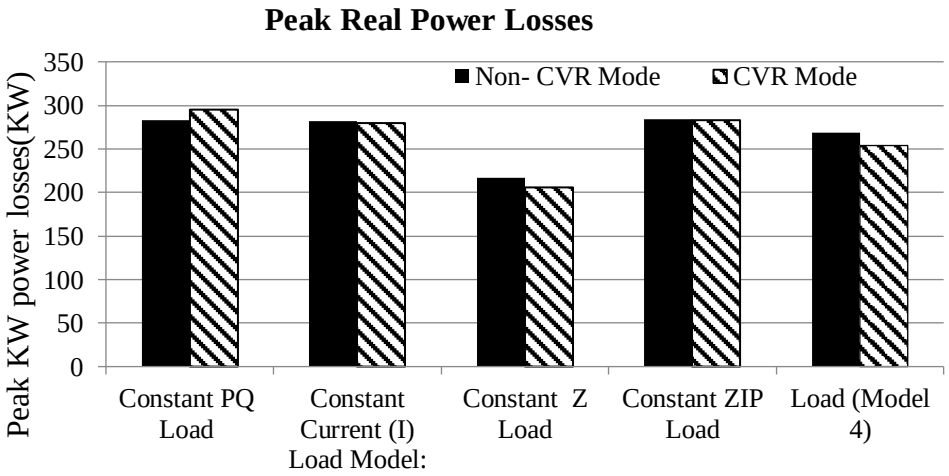

Figure 2.5 Peak real power losses with and without CVR for different load models

respectively. In this study, the simulations with model 4, the value of $CVR_{f(kW)}$ and $CVR_{f(kVAR)}$ is 0.8 and 2.0 is considered respectively. From results, it can be observed that operating in CVR mode, power demand and power losses reduced in comparison to non-CVR mode operation. Considerable energy savings can be achieved with CVR operation.

From the analysis of all simulation results, it can be concluded that a significant amount of energy savings can be obtained with CVR operation. The impact of different load models highly influences the CVR operation, and violation of voltage limits is also a matter of concern.

2.4.4 Observation and key findings

- The proposed smart grid-enabled CVR algorithm is more beneficial in comparison to traditional CVR.
- The highest energy savings can be achieved with constant impedance (Z) loading in the contest to other load models.
- Generally, loads are mixed types such as ZIP model; in such cases, a considerable energy saving can also be achieved.
- While applying CVR schemes, system losses may increase or decrease.
- CVR operation shows the adverse effect during the presence of constant power loads
- During deeper voltage reduction, voltage violation cases may occur in some parts of the distribution network.

Therefore, an additional reactive power source is required to lower the losses and maintain the voltage profile throughout the feeder end.

2.5 Assessment of CVR effect with additional Reactive Power Support

The effect of end-users loading patterns in CVR operation plays a crucial role. Thus, an accurate load model is required to check the effectiveness of CVR operation. Moreover, during the execution of CVR under a deeper voltage reduction range, voltage violations may occur in some parts of the distribution network or near to load to voltage-sensitive nodes. In this context, the CVR study has been carried out with different voltage reduction levels considering the voltage dependent load models. Besides, additional reactive power support has been injected through optimally placed capacitor banks during the deeper voltage reduction to maintain voltage profile within limits.

2.5.1 Methodology

In order to maximize the energy savings and peak demand reduction, VVC operation is carried out with CVR. The VVC problem has been formulated in two parts; the first is the implementation of Voltage and VAR controllers and second is an optimal allocation of reactive power support devices for loss minimization during the CVR operation. The modeling of voltage control devices such as AVR/OLTC and CBs have already discussed in the previous *chapter 1 in section 1.4*.

2.5.1.1 Volt/ VAR Controllers

In CVR operation, regulator controllers of AVR are used known as reg control and capacitor banks are controlled through cap control. These controllers are inbuilt in OpenDSS. Figure 2.6 demonstrates the CVR operation using the VVC algorithm.

2.5.1.2 Power Loss Minimization

The distribution network has high power loses in comparison to another part of the power system. As consequences of large distribution power losses raise the peak power demand, poor voltage profile and generation cost. Therefore, the loss minimization problem is very crucial for the optimal operation of the distribution feeder.

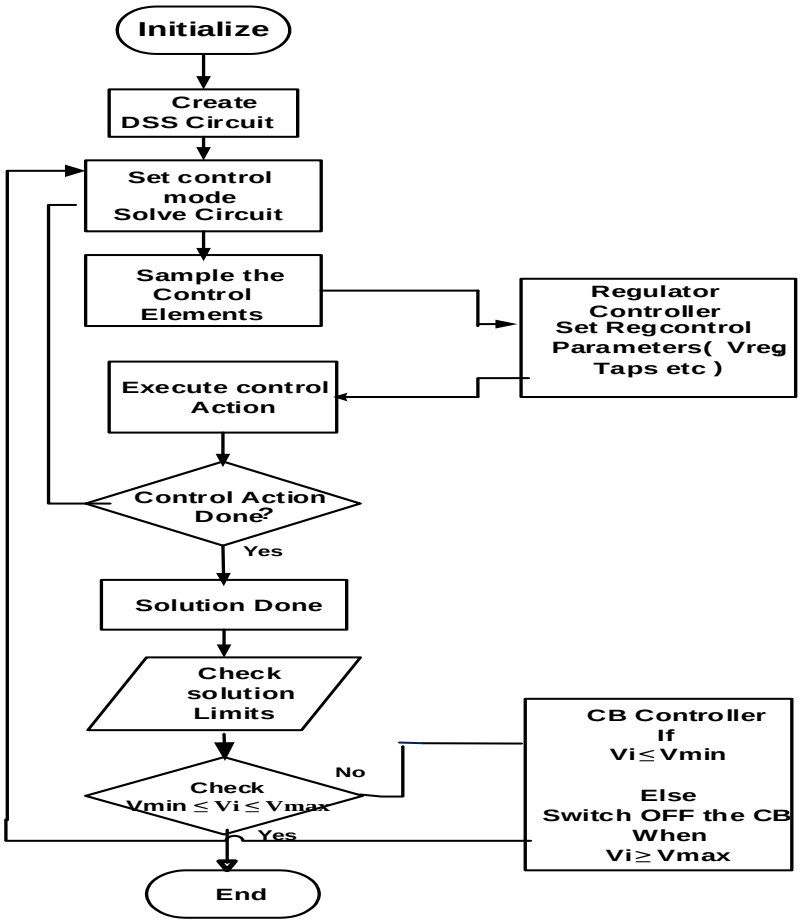

Figure 2.6 Flowchart of VVC operation for CVR mode

The optimization problem in distribution network look like something as shown in the below equation (2.12) [88]

$$\min_{\underline{y}} f(\underline{x}, \underline{y}) = P_{Loss} \tag{2.12}$$

$$s.t. \quad \underline{g}(\underline{x}, \underline{y}) = 0 \tag{2.13}$$

$$V_{\min} \le V_i \le V_{\max} \tag{2.14}$$

Where $\underline{g}(\underline{x}, \underline{y}) = 0$ is the distribution power flow equation. V_i is the voltage at the ith bus.

In order to minimize the system losses, the equation (2.12) find out the required reactive power injection support per node while satisfying the voltage its tolerance limit. Many optimization techniques are available to solve the problem discussed in the above equation (2.12).

In this work, a search technique inbuilt in OpenDSS has been utilized for optimal placement of CBs to find the optimal solutions. Moreover, OpenDSS has an internal Autoadd mode for the minimization of losses. OpenDSS uses ladder iterative method to determine the unknown voltages and currents. So Autoadd mode takes advantage of direct access to the compensation current array in the solution [28], [113]. In order to move a capacitor from node to node, it only needs alternation in the compensation current array. In this technique, solution convergence speed also increased because the admittance matrix remains unchanged and there is no need to re-factorized the admittance matrix. Generally, it takes 2-4 iterations in every solution and produces outputs in percentage per node. Percentage improvement shows the next best location to supply reactive power. Figure 2.7 shows Autoadd optimization technique for loss minimization.

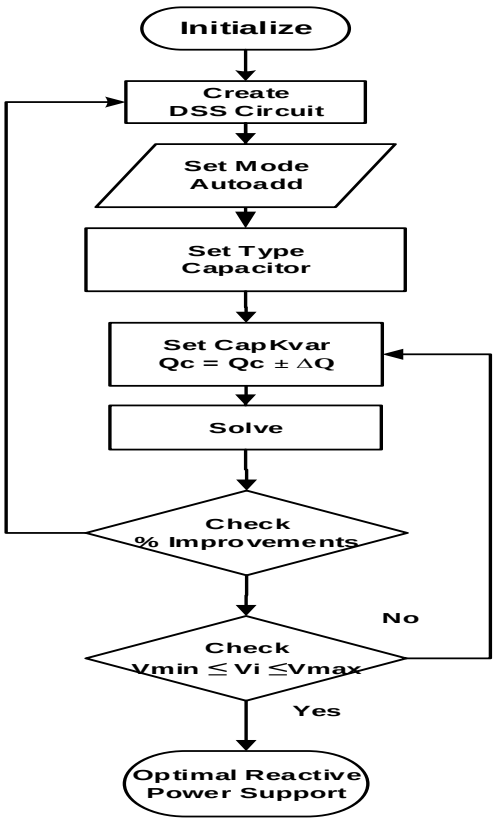

Figure 2.7. Flow chart for optimization Using Autoadd

2.5.2 Simulations and Result Discussion

2.5.2.1 Test System and Descriptions

For assessment of CVR effect, an IEEE, 13 node distribution test feeder with voltage-dependent loads has been considered. The distribution model consists of 13 nodes, one voltage regulators, two capacitor banks and different load models [114]. Modeling and power flow analysis of the distribution system has been carried out in OpenDSS platform developed by EPRI [113]. Before performing simulation of the test system some assumptions are considered such as (i) DMS and communication system is working well and its delay effect not considered during the execution of CVR operation (ii) Same load models are considered throughout the distribution network with and without CVR operation considering load allocation factor 1 in OpenDSS inbuilt load allocation algorithm. (iii) Effect is neglect during the operation of switched shunt capacitor banks.

2.5.2.2 VVC modes of operation

Test feeder has been simulated in three different modes considering constant ZIP and Nominal Linear P, Quadratic Q (feeder mix) type load models (the detail explanation can be seen *chapter* 1 under subsection *1.4.2.4*) with different voltage reduction (VR) level as discussed under:

- *No- CVR Mode:* IEEE 13 node test system is simulated with VVC devices in normal operation with a regulated voltage of 125V with no voltage reduction.
- *Base CVR Mode:* In this mode, IEEE 13 node test system is simulated with VVC devices in CVR operation through LDC setting with the regulated voltage at 122V, 119V, 118 V, or reduction of the voltage level at 2.4%, 4.8%, and 5.6% respectively. No additional reactive power injected to minimize the system losses.
- *CVR with Reactive Power Support (RPS) Mode:* In this mode, additional reactive power support is provided during the deeper CVR operation to minimize the losses and

maintain the feeder voltage limits. Capacitor banks are used here as an additional reactive power support source.

2.5.2.3 Case Study

- *Case-I. Effect of Constant ZIP Load model:* Analysis of voltage reduction with voltage-dependent constant ZIP type load model has been discussed in this case. ZIP coefficients used in this model are the mixture of residential, commercial and industrial type loading areas taken from [53]. From Table 2.1, it can be seen that during the base-CVR mode, about 1.12 to 2.33% peak MW load demand reduction is achieved. However, peak kW losses are also increased (0.06 to 0.17%) slightly because of the incremental rise in current in conductors. This small increase in losses is not so effective with the comparison of achieved peak load relief. However, there is a voltage violation case (crosses the minimum voltage limit of 0.95 p.u) that has been observed with the higher voltage reductions (4.8%, 5.6%) during the base-CVR mode.

Table 2.1 Analysis of CVR effect with ZIP (mix) load

Terms	**No-CVR**	**Base-CVR**			**CVR with RPS**	
Voltage Reduction (%)	0.0	2.4	4.8	5.6	4.8	5.6
Minimum Voltage (p.u)	0.9882	0.9619	0.9373	0.9353	0.9534	0.953
Peak MW Demand	3.6146	3.5741	3.5389	3.5301	3.5376	3.524
ΔP_{demand} kW, (%)	---	- 40.5 (-1.12)	-75.7 (-2.09)	-84.50 (-2.33)	-77.0 (-2.13)	-88.6 (-2.45)
Peak kW Losses, (%)	109.83 (3.03)	111.87 (3.09)	114.86 (3.17)	115.87 (3.2)	104.16 (2.89)	104.0 (2.88)
ΔP_{losses} in kW, (%)	--	+2.04 (+0.06)	+5.03 (+0.14)	+6.04 (+0.17)	-5.67 (-0.14)	-5.83 (-0.21)

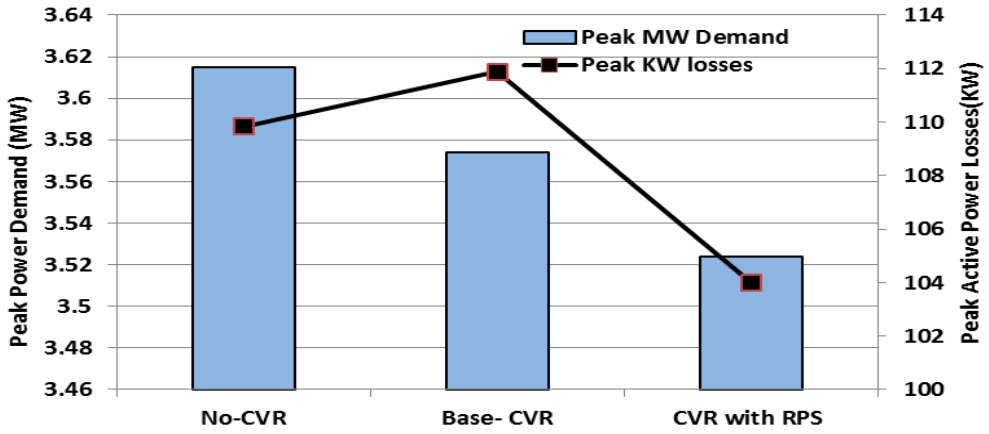

Figure 2.8 Peak demand & peak losses with ZIP load model

This issue has been resolved through CVR with RPS mode. In this mode, the additional, RPS is provided though optimally placed CBs of 100 kVAR and 120 kVAR at each phase of the nodes 611,671,684 for 4.8%, 5.6% of voltage reduction respectively. About 2.45% power demand and 0.21% loss reduction is reported with the operation of CVR with RPS mode. Figure 2.8 clearly shows that peak demand and losses are decreasing during the CVR with RPS mode with improved voltage profile.

- *Case-II Nominal Linear P, Quadratic Q (feeder mix) load:* This feeder mix load model, also known as model 4 in OpenDSS. In model 4 value of CVRwatts and CVR vars are 0.8, 2 considered respectively. Table 2.2 shows the simulation results with the different modes of operation of CVR with different VR levels. In base CVR mode, there is about 1.82 to 4.06 % peak MW load demand reduction is achieved. However, peak load kW losses are also increased slightly with voltage limits violations during the higher voltage reduction level as 5.6%. In order to satisfy voltage limits, simulation is carried out is CVR with RPS mode with the addition of capacitor banks of 100 kVAR at each phase of 611,671, 684 nodes. Figure 2.9 shows the peak demand & peak Losses during CVR operation. From simulation results, it has been observed that both demand (4.3%) and losses (0.2%) are reducing though the enabling of CVR with RPS mode.

A comparative CVR effect with ZIP load model and model 4 have been shown in Figure 2.10 and also observed that power demand is decreasing more in model 4 as compare to ZIP load model with different voltage reduction level.

Table 2.2 Analysis of CVR effects with Model 4

Terms (V&P)	**No CVR**	**Base-CVR**			**CVR with RPS**
VR(%)	0.0	2.4	4.8	5.6	5.6
Min. Volt. (p.u)	0.9936	0.96912	0.9504	0.9348	0.95189
Peak MW Demand	3.6262	3.5603	3.5238	3.4789	3.4727
ΔP_{demand} kW (%)	---	-65.9 (-1.81)	-102.4 (-2.823)	-147.3 (-4.06)	-153.6 (-4.3)
Peak kW Losses, (%)	107.41 (2.962)	107.65 (2.968)	107.82 (2.97)	109.69 (3.02)	100.04 (2.76)
ΔP_{losses} in kW (%)	--	+0.14 (+0.004	+0.41 (+0.008	+2.82 (+0.038	-6.37 (-0.2)

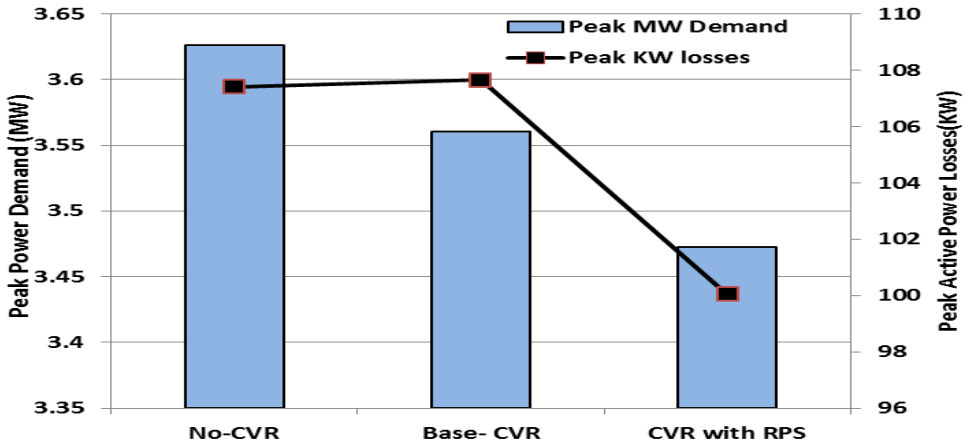

Figure 2.9 Peak demand and peak losses with load model 4

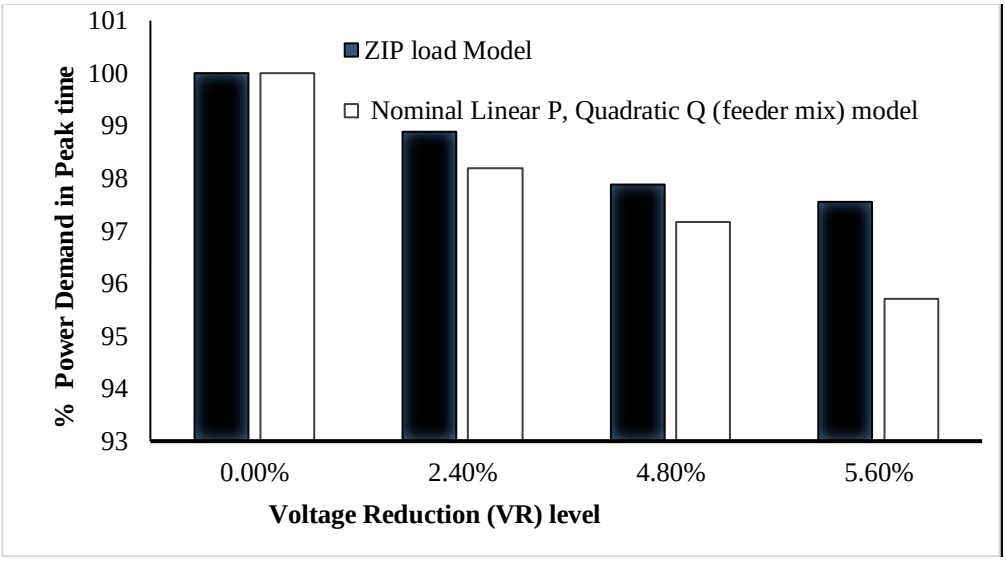

Figure 2.10 Percentage load demand in peak during CVR operation

2.5.3 Important Observations and Findings

- A significant amount of peak load relief is achieved
- CVR is more effective with reactive power support for a higher level of voltage reduction.
- The reactive power support through other sources such as distributed energy resources, distributed energy storage and electric vehicles is also needed to analyze

2.6 Conclusion

This chapter proposed a closed-loop smart grid-enabled CVR methodology for energy conservation in the distribution network. The proposed methodology has been validated under two scenarios (i) analyzing the impact of different load models on CVR and achieved energy savings in power distribution system and (ii) the impact of additional reactive power support through CBs under CVR operations. The effect of loading pattern during CVR operation also carried out, and it is analyzed that the accurate load model and loading pattern also affect the CVR savings. From simulation results, it is observed that a significant amount of peak load relief is achieved with minimum losses. CVR operation

with reactive power support is more effective for reducing the demand for system losses in comparison to without reactive power support. To achieve more savings and demand reduction smart grid-enabled CVR scheme is more beneficial in comparison to tradition CVR. Though reactive power support through capacitor banks is not so much effective solution, but for peak demand and loss reduction, it may be used where constraint cost is not a big issue.

For better controlling and coordination, CVR has to combine with DERs, and smart inverter has to participate in voltage regulation as recommended by the new IEEE 1547 - 2018 standard. In this context, the combined effect of CVR and DERs will be analyzed in the next *chapter 3* including the impact of the smart inverter as a voltage control device.

CHAPTER 3

DISTRIBUTED ENERGY RESOURCES IMPACT ON CVR

3.1 Introduction

The conventional distribution systems are facing numerous operation and control issues since the last few decades due to widespread DER deployment and shift in energy paradigm. To address the control aspects, this chapter has discussed the impact of VVC operation with CVR in the presence of DER which is the third technical barrier, as described in *chapter 1*. In this context, researchers [51], [87] have analyzed the combined impact of CVR and various levels of DG penetration and mitigation of low voltage violation during deeper voltage reduction. In [78], the effect of photovoltaic DER penetrations during CVR is investigated with various cases of VVC, but the ability of PV inverter is not fully utilized. Besides, it lacks the cooperation of the distributed renewable sources due to intermittent behavior and slow operation of traditional Volt/VAR controlling devices. Hence, the impact of PV inverters as VAR support and voltage regulation device has been analyzed in [19], [21], [82], [91],[95]. However, these studies have not analyzed the voltage control through PV inverter during CVR. The combined effect of CVR and PV inverters has been performed in [20], [58], [68], [77]. In [68], a slow and fast time scale based VVC scheme for CVR is proposed with the objective of minimizing total energy consumption. The optimal reactive power support through PV inverter with the objective of minimizing voltage deviation has been presented in [88]. The closed-loop CVR problem has been analyzed through reactive power support from PV inverter in [20]. However, this method has been tested only for a limited voltage reduction range on the simple balanced network considering the impedance load model.

An attempt has been made in this investigation to address the second and third technical barriers for which a smart grid-enabled CVR scheme for VVC has been proposed. In order to control the tap position of OLTC/ AVR, a well-established LDC scheme has been employed. The limits of tap change and CB switching for daily operation have been considered in control algorithms. Besides, CVR in association with PV system has been implemented to achieve a greater saving in peak demand and energy consumption even during deeper voltage reduction. In addition, reactive power compensation has been done through PV inverters to control the lower voltage violation. The desired reactive power has calculated and controlled through Volt/VAR droop control mechanism. The effect of inverter losses due to reactive current generation during reactive power support has also been included. The moving cloud transient effect has been considered while developing the solar PV model. The proposed scheme has been tested on unbalanced radial distribution network with voltage-dependent composite ZIP load models for peak demand hours and whole day operation. The effect of various types of loading such as residential, commercial and industrial are also incorporated in the load model.

3.2 Overview of DER

Distributed energy resources are known as various names as distributed generation, onsite power generation source, etc. DGs are broadly divided into two categories as renewable and non-renewable DERs. Further classification can be inverter type DER which generally operates at unity power factor, and other is synchronous or non-synchronous machine having 0.9 leading power factors [51]. Rapid development in the field of power electronics and control, it is quite possible that renewable DERs can provide not only active power but reactive power support also. Due to global popularity and the potential of fast controlling reactive power with fine-tuned var output, the grid-connected solar PVs

with smart inverter considered as a DER in this chapter. For performing power flow calculations, PV source has been considered as a PQ node with the known value of real and reactive powers with their limits in equations below:

$$P_{DER,Min} \leq P_{DER} \leq P_{DER,Max} \tag{3.1}$$

$$Q_{DER,Min} \leq Q_{DER} \leq Q_{DER,Max} \tag{3.2}$$

$$\left(P_{DER}\right)^2 + \left(Q_{DER}\right)^2 \leq \left(S_{DER}^{rated}\right)^2 \tag{3.3}$$

With the equations of (3.1), (3.2) and (3.3) power facility curve can be defined.

$$\left|Q_{DER}^{Inj}\right| \leq Q_{DER,Max} = \sqrt{\left(S_{DER}^{rated}\right)^2 - \left(P_{DER}\right)^2} \tag{3.4}$$

It is quite possible to develop a variable solar DER VAR source (ΔQ^{Inj}_{DER}) model for voltage regulation. The injected reactive power (Q_{DER}^{Inj}) must satisfy the equation (3.4) and other constraints.

3.3 Voltage regulation through PV Smart Inverter

PV inverter used for the integration of PV panel commonly known as conventional PV inverter. However, PV inverters having advanced functionality such as the ability to participate in VAR support, islanding deduction and power management are refereed as smart inverter. The ability to provide reactive power support and/or performed as VAR compensators enlarge the PV inverters contribution significantly in the improvement of distribution operation, maintain the voltage profile within the acceptable range and minimize the system losses. The detailed description of smart inverter operation has already explained in *chapter 1 subsection 1.4.2.3*. In general, PV smart inverter operates in two quadrants with five modes as shown in Figure 3.1 and explains below [88].

Mode 1- Only active or real power (P), Q=0

Mode 2- Active power, With Inductive Q power

Mode 3- No active power (P=0), Only Inductive Q

Mode 4- Active power (P), Capacitive Q

Mode 5- No active power (P=0), Only Capacitive Q

Modes1, 2, and 4 will operate at day time where solar irradiation is available while mode 3, 5 enabled in the night, or absence of sunlight.

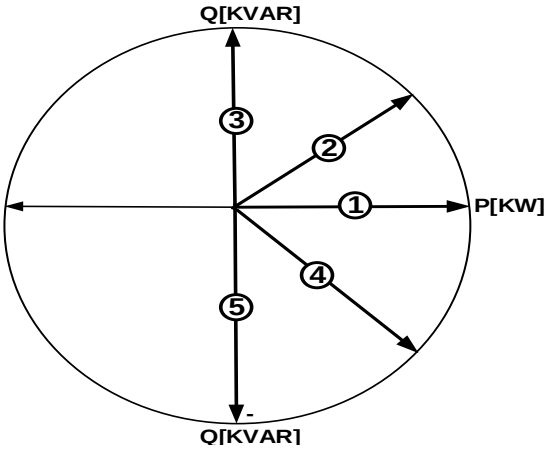

Figure 3.1 PV Inverter P/Q Capability Curve

3.4 Mathematical Formulation and Control Methodology

The basic objective of this investigation is to save energy in ADN. This objective can be fulfilled by reducing the demand of the system by lowering the voltage of the network. Energy savings by reducing the voltage is an advance attribute of the integrated VVC mechanism. Therefore, in this section mathematical formulation and control approach to enable the CVR operation through VVC is delineated as under.

3.4.1 Mathematical Formulation

The power demand at the source substation is the sum of total real power loads and the real power losses on lines/cables ($P_{loss}^{lines/cables}$), transformers ($P_{loss}^{transformers}$) and inverters ($P_{loss}^{inverter}$) as expressed by equations (3.5 - 3.7).

$$P_{Demand} = \sum \left(P_{Load} + P_{Loss} \right) \tag{3.5}$$

where

$$P_{load} = \sum_{\phi \in a,b,c} \sum_{k=1}^{nl} (P_{L,k}(V_k))_{\phi} \tag{3.6}$$

and

$$P_{loss} = \sum \left(P_{loss}^{lines/cables} + P_{loss}^{transformers} + P_{loss}^{inverter} \right) \tag{3.7}$$

From equation (3.6), it can be observed that the real power demand at a node is dependent on its voltage. Transformer core losses depend upon the voltage, whereas transformer winding and line losses mainly depend upon current flow. Inverter losses take place due to electronic circuitry and flow of reactive current when PV inverter absorbs/inject the reactive power. Therefore, total active power losses may decrease or increase with reduced voltage. Moreover, it also depends on several other factors such as network topology, load models, and load types.

- The reduction of voltage is obtained through maneuvering the tap position of OLTC transformer and automatic voltage regulators. Equations (3.8) and (3.9) express the regulated output voltage from OLTC/AVR.

$$V_{tr} = a_{tr} V_P \tag{3.8}$$

$$V_{tr} = \left\{ 1 \pm \left(\frac{\Delta V_{tr}}{100} \right) \times \text{Tap} \right\} V_P \tag{3.9}$$

- Daily tap operation of OLTC/AVR is governed by equation (3.10) to prevent the degradation of the life cycle of voltage regulation devices.

$$\sum_{h=1}^{24} N_{tr,h}^{i} \leq N_{tr,max}^{i} \tag{3.10}$$

- Reactive power supplied by CBs at each switching operation is defined by the equation (1.12) and daily switching operation of CBs should follow the relation (3.11).

$$\sum_{h=1}^{24} N_{sw,h}^{i} \leq N_{sw,max}^{i} \tag{3.11}$$

Reactive power compensation from PV inverter is determined by advanced Volt/VAR droop characteristics as shown in Figure 3.2. This characteristic can further be expressed as relation (3.12) where, $Q_T^{inv,max}$ is governed by equation (1.16).

$$Q_T^{inv}(V) = \begin{cases} Q_T^{inv,max} & V < V_1^{P_1} \\ \dfrac{V - V_1^{P_1}}{V_1^{P_1} - V_2^{P_2}} Q_T^{inv,max}, & V_1^{P_1} \leq V < V_2^{P_2} \\ 0 & V_2^{P_2} \leq V \leq V_3^{P_3} \\ -\dfrac{V - V_3^{P_3}}{V_4^{P_4} - V_3^{P_3}} Q_{T,}^{inv,max} & V_3^{P_3} < V \leq V_4^{P_4} \\ -Q_T^{inv,max} & V > V_4^{P_4} \end{cases} \tag{3.12}$$

- According to ANSI, the node voltage magnitude limit is defined by the following equation.

$$V_{i,T}^{\min} \leq V_{i,T} \leq V_{i,T}^{\max} \text{ or } 0.95\text{pu} \leq V_{i,T} \leq 1.05\text{pu} \tag{3.13}$$

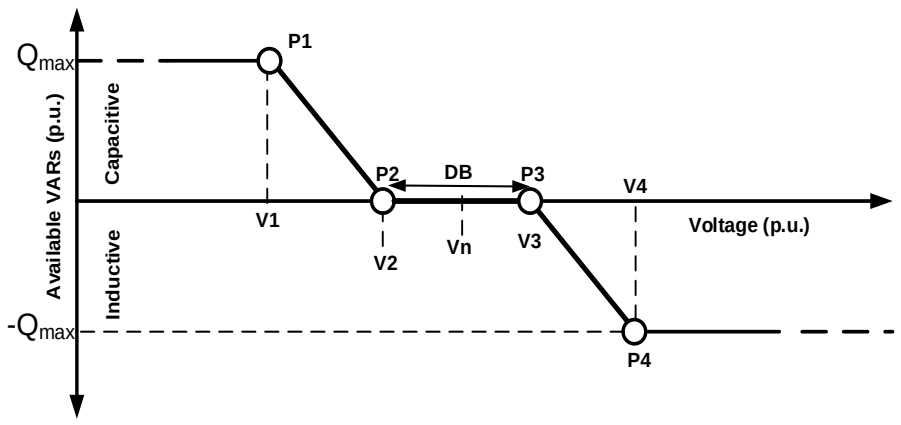

Figure 3.2 Volt/VAR droop characteristics

3.4.2 Control Methodology

Voltage and reactive power flow in the network are governed by controlling of OLTC/regulator, CBs, and smart inverter. The functional control of OLTC/regulator and CB has been already described in *chapter 2,* section 2.3.1 and section 2.3.2. The PV inverter control strategy has been discussed as under.

3.4.2.1 Smart PV inverter control

In this work, inverter control circuitry deals mainly with calculation of the desired reactive power at each time period, T. In order to determine it, a droop characteristics based scheme has been utilized. The Volt/VAR droop characteristics are shown in Figure 3.2. It is piecewise linear to the voltage and also changes dynamically due to its dependency on the $Q_T^{inv,\max}$. The droop characteristics are obtained by defining the four points (P_1, P_2, P_3 & P_4) parameters and dead band (DB). The DB is defined as the width between points P_2 and P_3 in terms of voltage range symmetrical to V_n. In the DB range, inverter neither absorbs nor injected the VAR. Below the point P_2 ($V_2^{P_2}$), the inverter starts injecting reactive power to the grid. However, when a voltage is above point P_3 ($V_3^{P_3}$), the inverter absorbs reactive power from the grid. The amount of reactive power injected/absorbed by the inverter is determined using equation (3.12).

3.5 Implementation of VVC Scheme

The control approach for various controllers is well explained earlier in *section 3.4*. In order to estimate the energy savings and CVR factor, VVC is carried out in three different modes with developed controllers as delineated under:

3.5.1 Mode 1 (Without CVR or Normal Operation)

In this mode, VVC operation is performed within the upper range of the service voltage known as normal, i.e. No- CVR operation. End of line (EOL) / regulated voltages in

regulator control are set between 121-126V with V_{base} of 120V. Shunt capacitors of CB are fixed in nature. Only LTC/regulator controllers are active in this mode.

3.5.2 Mode 2 (Only CVR)

In this mode, VVC operation is carried out with only CVR scheme without any additional power support. CVR scheme is enabled through LDC with the setting of regulated voltages in the lower half range (114V-119V) of the service voltage. CBs are switchable in this mode. Only inverter controller is inactive in this mode. The level of voltage reduction is increased to achieve higher energy savings with only CVR mode. However, this may lead to violation of the minimum voltage limits at some points of the distribution feeder.

3.5.3 Mode 3 (CVR with PV)

In order to achieve higher energy saving through deeper CVR and maintain the minimum allowable voltage throughout the feeder length, an additional power source is required. Therefore, in this mode, CVR is enabled with additional power support from PV system. The required additional active/reactive power is provided through PV system with the advanced functioning of solar PV inverter. The cloud transient effect is considered in PV power output.

The implementation of three modes has been done in three stages as shown in Figure 3.3 and explained as under.

(i) The first stage deals with the development of the network model of considered test system including controllers. After that, the VVC operation mode is selected from the control panel and the required parameters such as EOL/Vreg are set. The controllers for selected mode are enabled.

(ii) The second stage is mainly based on the execution of control actions, power flow analysis and verification of solution limits. Control actions execution for enabled

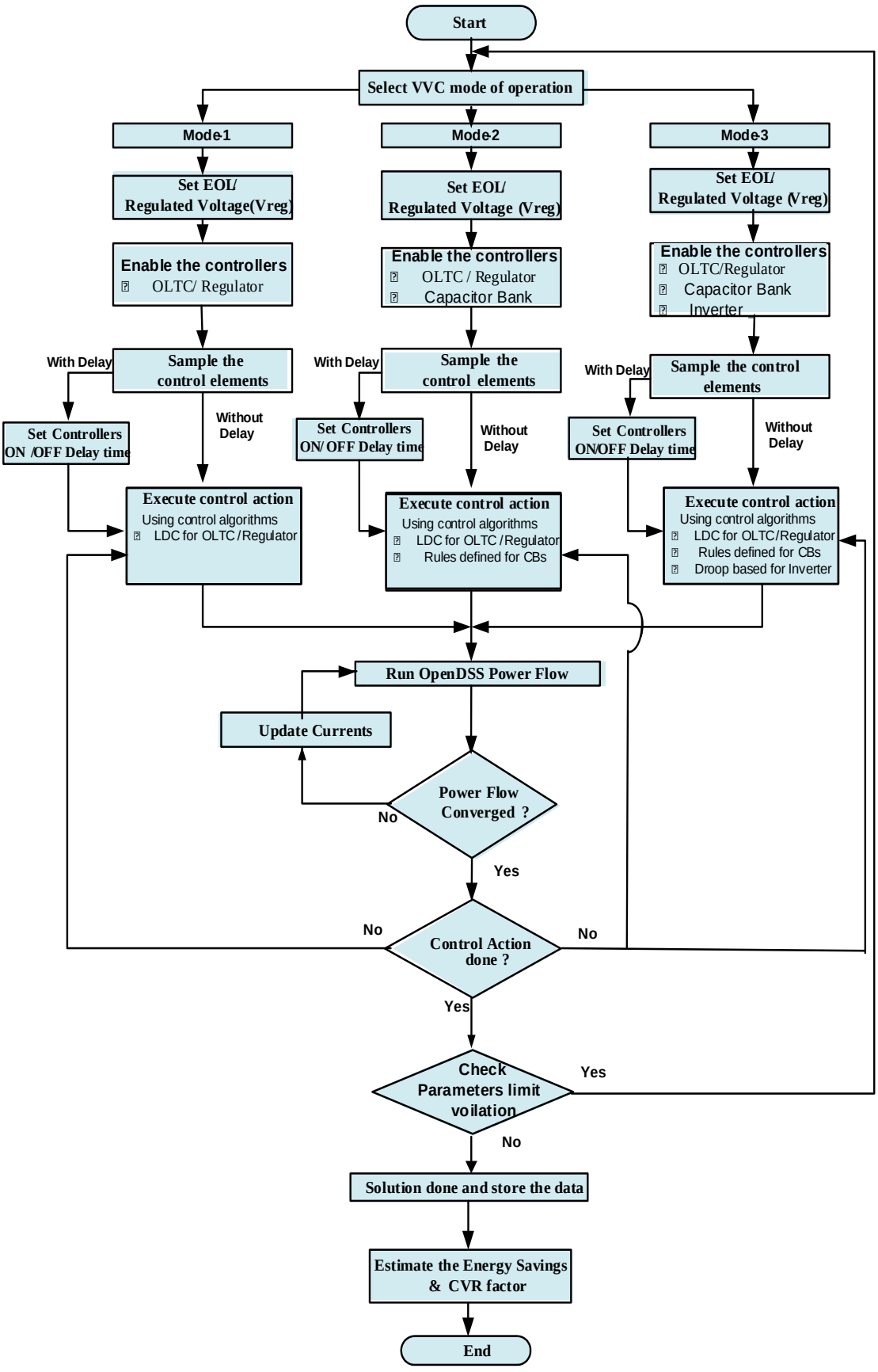

Figure 3.3 Flow chart of VVC mode of operation

controllers can be set either simultaneously or with some delayed action. The stepwise procedure of this stage is delineated under:

- Sample the control elements inputs.
- Set the controllers ON/OFF time delay, if the delay in control queuing is enabled.
- Determine governing VVC parameters using control algorithms.
- Calculate the required tap settings for OLTC/AVR through LDC using equation (2.11).
- Perform ladder iterative method for load flow analysis and obtain the feasible solution.
- Find CB switching step and reactive power support from inverter using equation (1.16) and (3.12) respectively.
- If control action is completed, then verify the violation limits else again execute control action.
- If obtained results are within limits, then accept the solution and store the data, if not, go to the selection of VVC mode of operation.

(iii) In the third stage, estimation of energy savings and CVR factor is performed through data obtained using the equations (2.1) and (2.2) respectively.

3.6 Simulations and Result Discussion

In this section, the simulation results of test cases have been presented and discussed. The proposed smart grid-enabled CVR methodology has been validated in the presence of PV based DER using simulation method.

3.6.1 Test System and Modelling

For the assessment of CVR effect, a modified IEEE 123 node distribution test feeder [114] has been considered as shown in Figure 3.4. Ratings and parameters of VVC devices have been shown in Table 3.1.

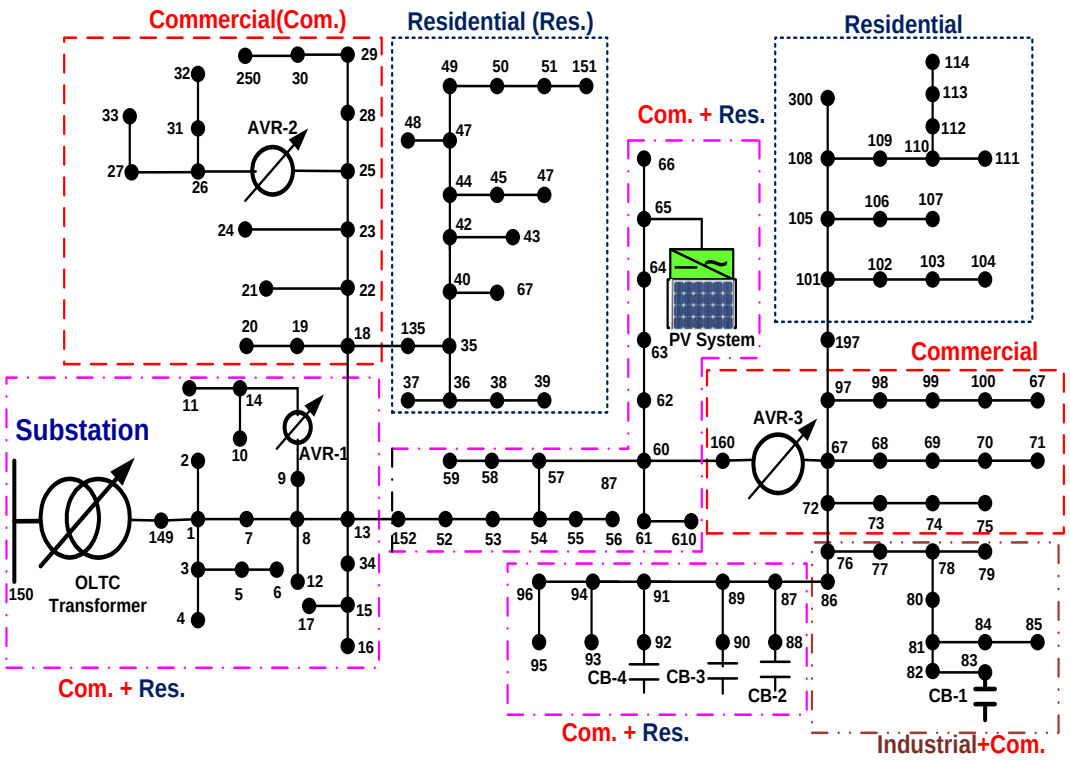

Figure 3.4 Modified IEEE 123 node distribution test feeder

Modeling of the distribution network, controllers, PV system and power flow calculations have been done and simulated on OpenDSS platform[28]. However, the control algorithms have been written in MATLAB and interfaced with OpenDSS model.

Before performing simulations of the test systems, the following assumptions have been incorporated:

- The communication system is working well, and its delay effect has been ignored during the execution of CVR.
- Data up-gradation duration of 15 minutes has been taken for AMI system and field devices.
- ZIP load models are considered throughout the distribution network with and without CVR operation. ZIP coefficients are depicted in Table 3.2. The detailed representation of ZIP load model has been explained in *chapter 1* using equations (1.17) – (1.20) respectively.

- The load allocation factor for distributed load is set to 1 in OpenDSS inbuilt allocation algorithm.
- Load demand profile with active and reactive power demand multipliers for 24 hours with 15 minutes interval of a typical day has been considered, and it is shown in Figure 3.5.
- The switching effect is neglected during the operation of switched shunt capacitor banks. However, switching time has been incorporated, taking a suitable time delay in control queuing.

Table-3.1. Ratings and Parameters of VVC devices

Device		**Phase (Ph) /Connection**	**Location At/Between node/rating**		**Tap range / CB step per phase /Inverter S_{max}**	**Maximum daily tap change/ CB switching operation per phase**
OLTC		3-Phase (a-b-c),Wye	150 - 149		+16 to -16	5
AVR-1		1-Phase, a	9-14		+16 to -16	5
AVR-2		2-Phase, a, c	25-26		+16 to -16	5
AVR-3		3-Phase a,b,c	160-67		+16 to -16	5
CB-1(kVAR)		3- Phase, a,b,c	83	200/Phase	0-4	3
CB-2(kVAR)		1- Phase, a	88	50/ Phase	0-1	3
CB-3(kVAR)		1- Phase, b	90	50/ Phase	0-1	3
CB-4(kVAR)		1- Phase, c	92	50/ Phase	0-1	3
PV Inverter	**KVA**	3- Phase, a-b-c	65	200	200	---
	Efficiency (η_{inv})	0.985, (when it is injecting either P or Q only)				
		0.97, (when it is injecting both P and Q simultaneously).				
Volt/VAR droop characteristics points		Point P1 voltage ($V_1^{P_1}$)= 0.945 p.u., Point P2 voltage ($V_2^{P_2}$) = 0.95 p.u., Point P3 voltage ($V_3^{P_3}$) = 1.05 p.u., Point P4 voltage ($V_4^{P_4}$) = 1.06 p.u., Dead Band (DB) range = Between point P2 and P3, 0.1 p.u.				

Table-3.2. ZIP Load Model Parameters

Loading Type	ZIP Coefficients [53]		Node Number
Residential	Zp = 0.85 Ip= -1.12 Pp =1.27	Zq =10.96 Iq=-18.73 Pq=8.77	2,4,5,6,7,10,12,16,35,37,38,39,41 ,42,43,45,46,4748,4950,51,52,53, 55,56,58,59,60,65,94,95,96,102,1 03,104,106,107,109,111,112,113, 114
Large Commercial	Zp = 0.47 Ip = -0.53 Pp = 1.06	Zq = 5.30 Iq = -8.73 Pq = 4.43	62,63,64, 66,80,82,85
Small Commercial	Zp = 0.43, Ip = -0.06, Pp =0.63	Zq= 4.06, Iq=-6.65, Pq =3.59	1,9,11,17,19,20,22,24,28, 29,30,31,32,33,34,68,69,70,71,73 ,74,75,83,84,87,88, 90,92,98,99,100
Industrial	Zp, Ip = 0, Pp= 1	Zq ,Iq = 0, Pq = 1	76,77,79,86

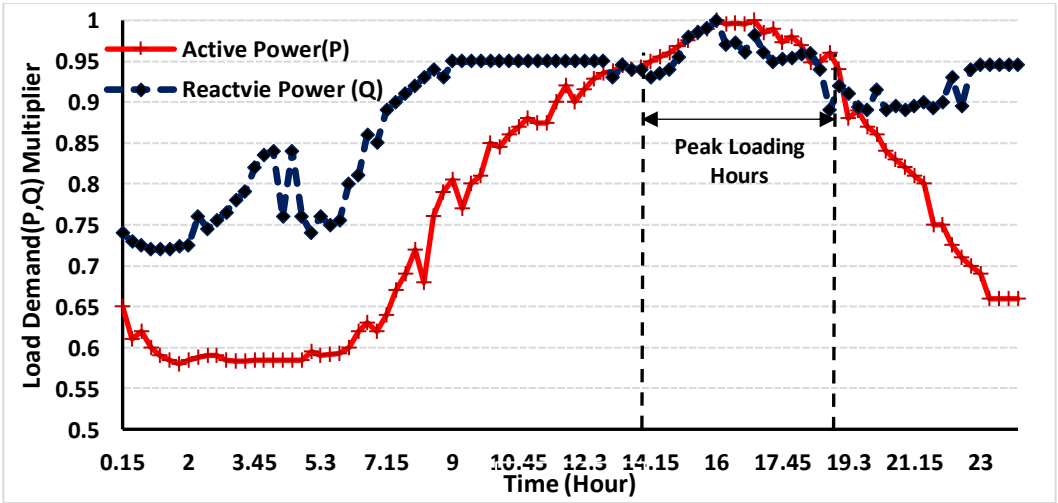

Figure 3.5 Load demand profile for 24 hours

3.6.2 Case Study

The Modified IEEE 123 node test system is simulated for two cases in the above mentioned three modes of VVC operation:

- Case. I- Peak Demand Reduction
- Case. II- Daily Energy Demand Reduction

3.6.2.1 Case. I- Peak Demand Reduction

Peak demand reduction through CVR is investigated in this case study. The demand above 95% of the highest active power demand has been considered as the peak demand hours in the present study. The duration of such load on the test system under consideration spreads from 14:15 to 19:00 hours which approximates to 5 hours. The load profile of a typical day is shown in Figure 3.5 along with peak demand hours. The effect of CVR on peak demand reduction in three modes of VVC operation has been analyzed under this loading condition.

- *Mode 1:* The simulation results for the peak demand duration without CVR (normal operation) have been obtained with the application of VVC to maintain 124V regulated voltage with the help of LDC settings. The results of this mode of operation are shown in the second column of Table 3.3. The active power demand of the system is shown in Figure 3.6 for the considered duration.

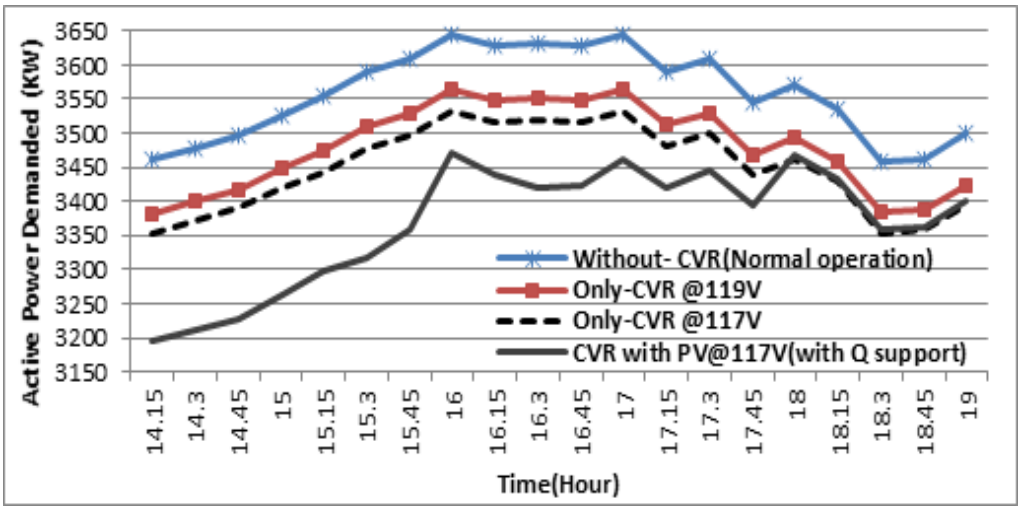

Figure 3.6 Active power demand at feeder head in all modes of operation in Case-I (Peak demand Hours)

- *Mode 2:* The test system, for this mode of operation, has been simulated for two different regulated voltages of 119V and 117V. The results have been given in the third column of Table 3.3. From results, it can be observed that a significant reduction in energy demand about 1.96 % and 2.81% is achieved at 119V and 117V, respectively in comparison to Mode 1. However, the energy losses have been slightly (about 3.2 % for 119V and 4.7 % for117 V) increased. The increased losses are not so significant and can be overlooked because reductions in energy consumption are sufficiently higher than the increased energy losses. From Figure 3.7, it is further observed that there are no violations of minimum voltage limit (below 0.95 p.u.) at 119V. However, during deeper voltage reduction (CVR at 117V regulated voltage) the minimum voltage limits have been violated. The maximum voltage deviation from permissible voltage (0.95p.u.) is 0.006 p.u. The lowest voltage of 0.944 p.u. has been observed at node 65. Figure 3.6 shows the total active power demanded from the substation. The CVR_{fE} is 0.486 and 0.497 for two regulated voltages respectively.

Table-3.3 Simulation results of Case I (Peak Demand Reduction)

Energy (E) Terms	**Mode-1**	**Mode-2**		**Mode-3**	
	Without CVR (124V)	**Only-CVR**		**CVR with PV (117V)**	
		(119V)	**(117V)**	**Without Q support**	**With Q support**
Econsumption (MWh)	17.747	17.400	17.248	16.845	16.842
Energy losses, MWh, (%)	0.446 (2.51)	0.460 (2.59)	0.467 (2.63)	0.449 (2.530)	0.4440 (2.501)
Esaving, kWh, (%)	--	347 (+1.96)	499 (+2.81)	901.7 (+5.08)	904.417 (+5.09)
ΔElosses, kWh, (%)	--	+14 (+03.2)	+21 (+4.7)	-3.244 (+0.72)	+1.840 (-0.41)
Lowest Voltage (p.u.), (Node)	1.00 (65)	0.9634 (65)	0.9441 (65)	0.9464 (65)	0.9500 (63)
CVR_{fE}	--	0.486	0.497	0.900	0.903

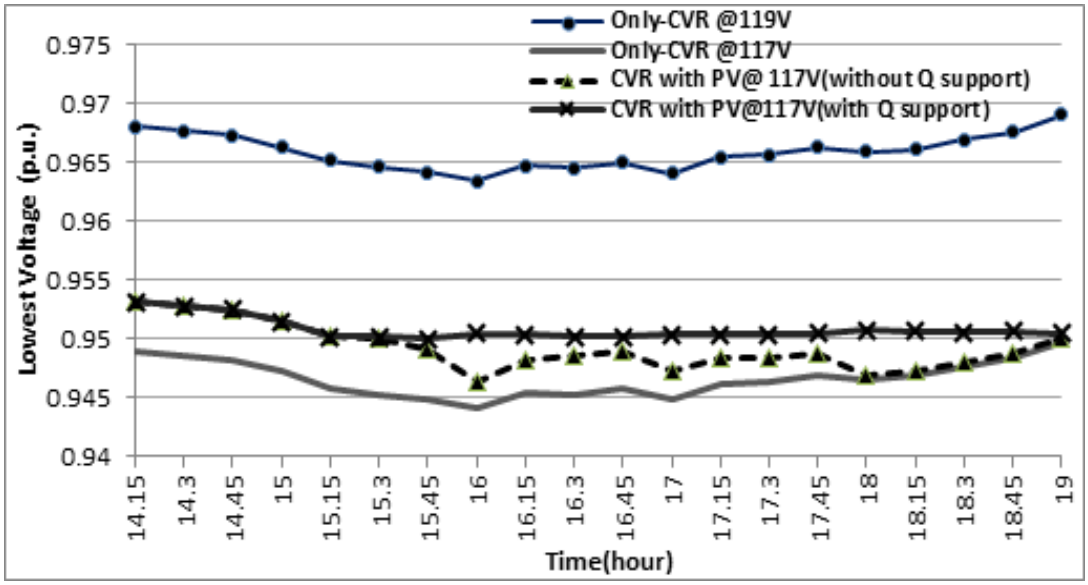

Figure 3.7 Minimum node voltage profile in all modes of operation in Case-I (Peak demand Hours)

- *Mode 3:* In this mode, the test system has been further simulated for two subcases as PV power injection with and without reactive power support from PV inverter. The allocation of PV system in the network has been chosen based on the lowest node voltage profile. The lowest voltage has been observed at node 65 as shown in Table 3.3. Therefore, a residential PV system with 200 KVA rating of the smart inverter has been placed at node 65. The simulated results are depicted in fourth column of Table 3.3. It can be observed from the table that about 5.08% reduction in energy demand is achieved during CVR (with PV without Q support). However, the minimum voltage limit violated during the time span 15:15 to19:00 as shown in Figure 3.7. VVC operation with CVR and PV with Q support mode reported 5.09 % reduced energy demand and 0.41% reduction in energy losses maintaining voltage profile within ANSI range. Figure 3.7 clearly demonstrates the improvement in voltage under this mode of operation. The additional reactive power support is controlled by Volt/VAR droop characteristics as shown in Figure 3.2. The droop characteristics assist in determining the appropriate amount of reactive power to be injected from the inverter to maintain the voltage within the desired

range. In the present case, droop control operation has been carried out in the range prior to point P_3 of droop characteristics. Since the range between point P_2 and P_3 is dead band range, the inverter starts injecting the reactive power prior to point P_2 (i.e., voltage below 0.95 p.u.) until desired reactive power is injected. Figure 3.8 shows the active and reactive power fed by PV system along with its droop control. Active power losses and inverter losses are shown,in Figure 3.9, for this mode. From Figure 3.9, it is observed that inverter losses increased when it injected the reactive power (excluding time span 14:15 to 15:00 because, during this time span, Q support is zero). However, increased inverter losses due to Q support does not affect the net system active power losses. The CVR_{fE} for subcases without and with reactive power support has been found to be 0.900 and 0.903 respectively as shown in Table 3.3. It can be comprehended from the aforesaid results that the maximum peak demand reduction would be achieved by the application of CVR with PV system, extending the reactive power support. The CVR factor estimated in this work measures the effectiveness of deployment of CVR. This factor also indicates that operation in Mode-3 performed better than Mode-2.

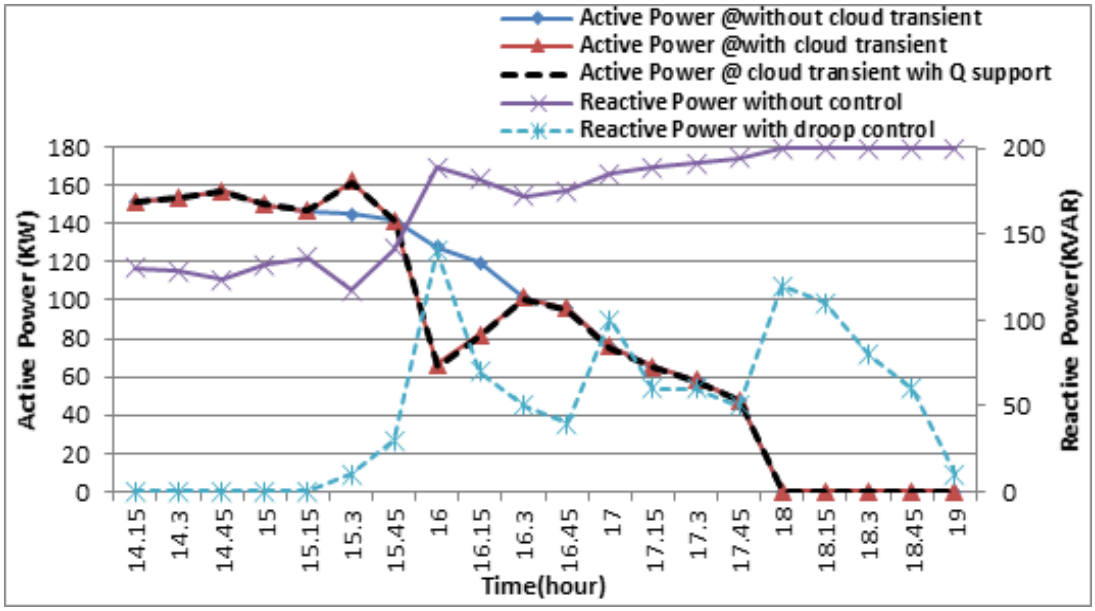

Figure 3.8 Real and reactive power feed by PV system during Mode-3 operation in Case-I (Peak demand Hours)

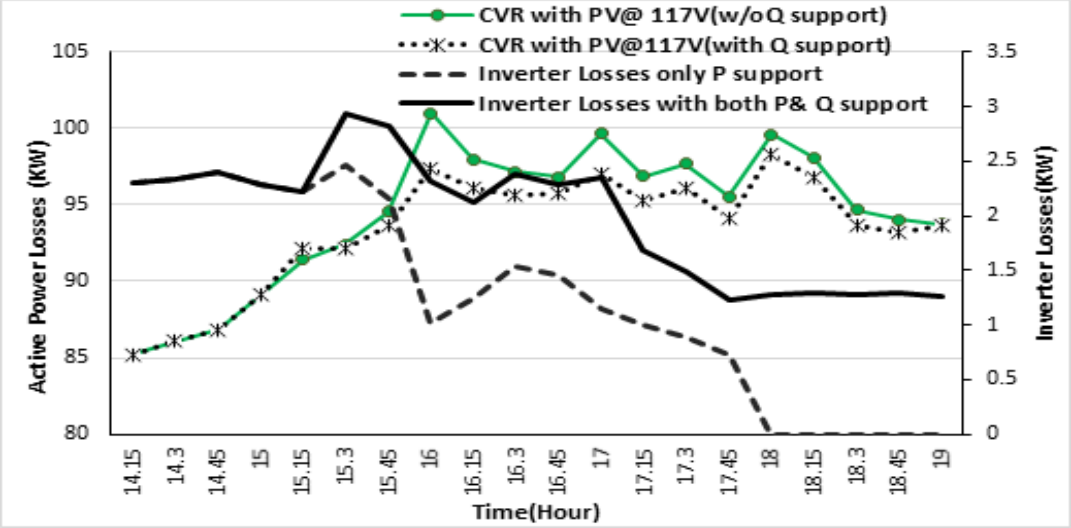

Figure 3.9 Active power losses and inverter losses during Mode-3 operation in Case-I (Peak demand Hours)

3.6.2.2 Case. II- Daily Energy Demand Reduction or Daily Energy Savings

In this case study, CVR scheme is tested with the aim of a reduction in daily energy demand. The proposed scheme is deployed on the same system for a maximum demand day of a week. The entire day's load profile of the day shown in Figure 3.5 has again been used to demonstrate the effect of all the three modes of VVC operation. The simulated results related to energy consumption and losses are shown in Table 3.4. Total active power demand and lowest node voltage profile during whole day operation are shown in Figure 3.10 and Figure 3.11 respectively. The obtained simulation results from each mode are discussed as under:

- *Mode 1:* The simulation results during without CVR operation is obtained with the execution of VVC at 124V regulated voltage. Table 3.4 shows the total active energy demand and active power losses. Figure 3.10 shows the active power demand of the system for the considered duration.
- *Mode 2:* The test system has been simulated for two regulated voltages of 119V and 117V as shown in Table 3.4. From results, it can be demonstrated that during CVR, significant energy savings amounting to 1.9% and 2.83% are achieved. However, the

energy losses have been increased to 2.85 % and 4.08 %, respectively. The increased losses are included in achieved total energy savings. From Figure 3.11, it is observed that the minimum voltage limit is violated at some nodes of the feeder end during CVR operation at 117V. The value of CVR_{fE} is 0.47 and 0.50 respectively for two regulated voltages.

- *Mode 3:* In this mode, the test system is simulated with CVR and PV at 117V regulated voltage with and without reactive power support. The energy savings in this mode is increased to 4.727 % and losses are almost equal to the Mode 1. The feeder voltage profile is maintained within limits with the injection of PV power during CVR operation at 117V as shown in Figure 3.10. The power loss variation throughout the day has been shown in Figure 3.12. The PV power profile during the entire day is shown in Figure 3.13. The calculated CVR_{fE} is 0.89 which is higher than Mode 2.

Table-3.4- Simulation results of Case II (Whole day operation)

Energy (E) Terms*	**Mode-1**	**Mode-2**		**Mode-3**	
	Without-CVR (124V)	**Only-CVR**		**CVR with PV (117V)**	
		(119V)	**(117V)**	**Without Q support**	**With Q support**
Econsumption (MWh)	68.159	66.863	66.232	64.9397	64.9370
Energy losses, MWh, (%)	1.469 (2.15)	1.511 (2.21)	1.5292 (2.24)	1.4783 (2.168)	1.4732 (2.161)
Esaving, MWh, (%)	--	1.30 (+1.90)	1.93 (+2.83)	3.2192 (+4.724)	3.2219 (+4.727)
ΔElosses, kWh, (%)	--	+42 (+2.85)	+60.2 (+4.08)	+9.098 (+0.61)	+4.08 (+0.272)
Lowest Voltage (p.u.), (Node)	1.00 (65)	0.9634 (65)	0.9441 (65)	0.9464 (65)	0.9500 (63)
CVR_{fE}	--	0.47	0.50	0.8366	0.8374

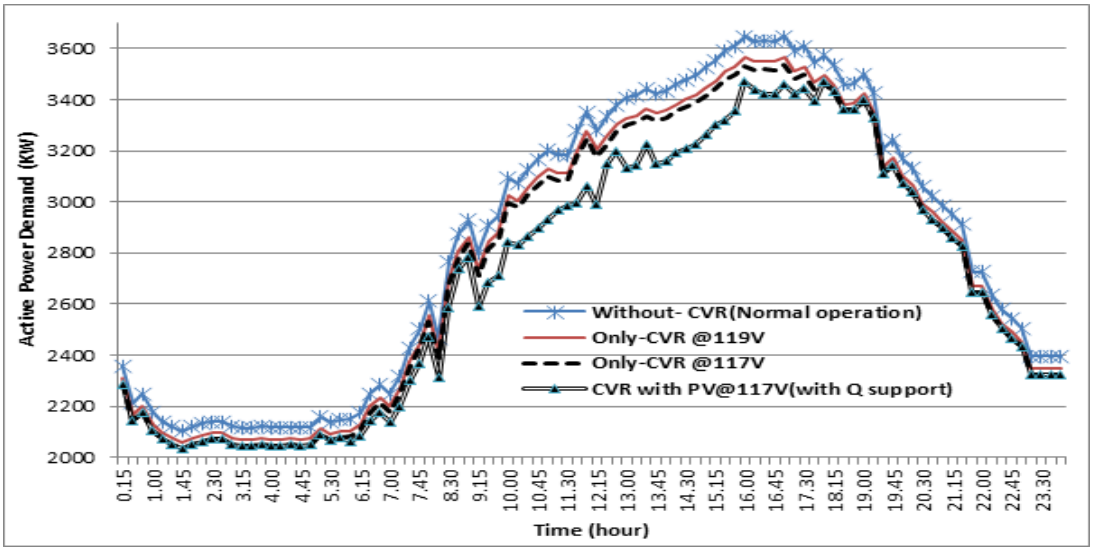

Figure 3.10 Active power demand at feeder head in all modes of operation in Case-II (whole day operation)

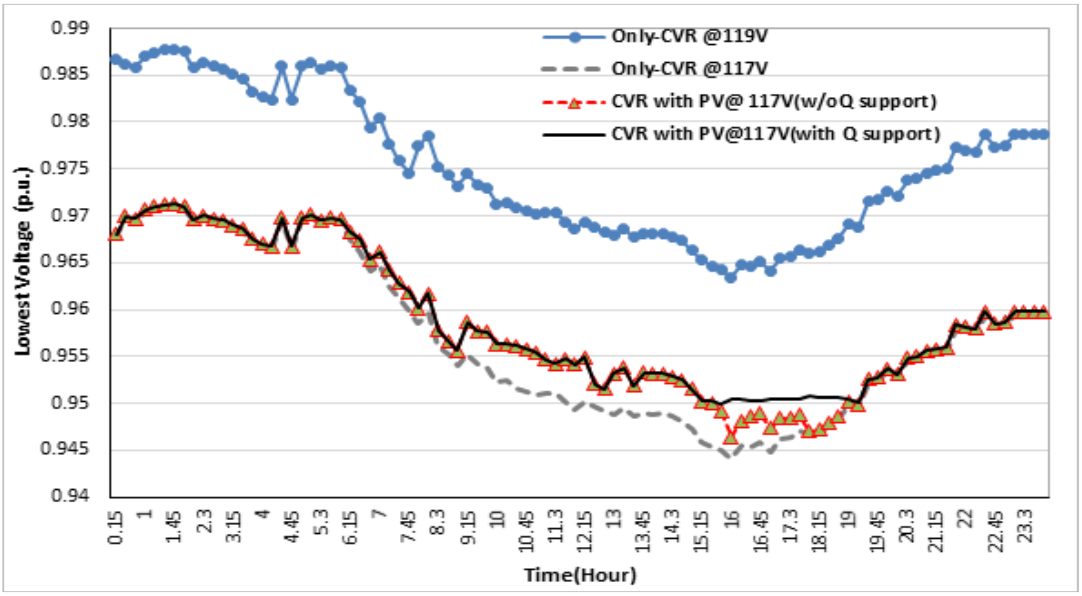

Figure 3.11 Minimum node voltage profile in all modes of operation in Case-II (whole day operation)

Entire day tap positions of OLTC and AVRs are shown in Figure 3.14 – Figure 3.17 respectively. It is observed that tap positions have been reduced with the enabling of CVR. Per phase tap operations for the day for every device are limited to the maximum five times, which are clearly portrayed in Figure 3.14 to Figure 3.17 also. The CB switching operations for the day are also restricted up to three times per phase and it has been shown in Table 3.5.

From the above-discussed case studies, it is demonstrated that considerable energy consumptions and peak power demand can be reduced with CVR operation. To achieve higher energy savings through deeper CVR operation is not a secure way. Therefore, deployment of CVR scheme with PV system is advisable.

Table-3.5 CBs switching operation status

Device \ Mode		**Mode-1**	**Mode-2**				**Mode-3**	
		With out CVR	**Only- CVR (119V)**		**Only- CVR (119V)**		**CVR with PV (117V)**	
Time Duration		00:24	00.15: 6.00	6.15: 24.00	00.15: 6.00	6.15: 24.00	00.15: 6.00	6.15: 24.00
CB-1	**Phase-a**	4	2	3	2	3	2	3
	Phase-b	4	2	2	2	2	2	2
	Phase-c	4	2	3	2	3	2	3
CB-2		1	0	1	0	1	0	1
CB-3		1	0	1	0	1	0	1
CB-4		1	0	1	0	1	0	1

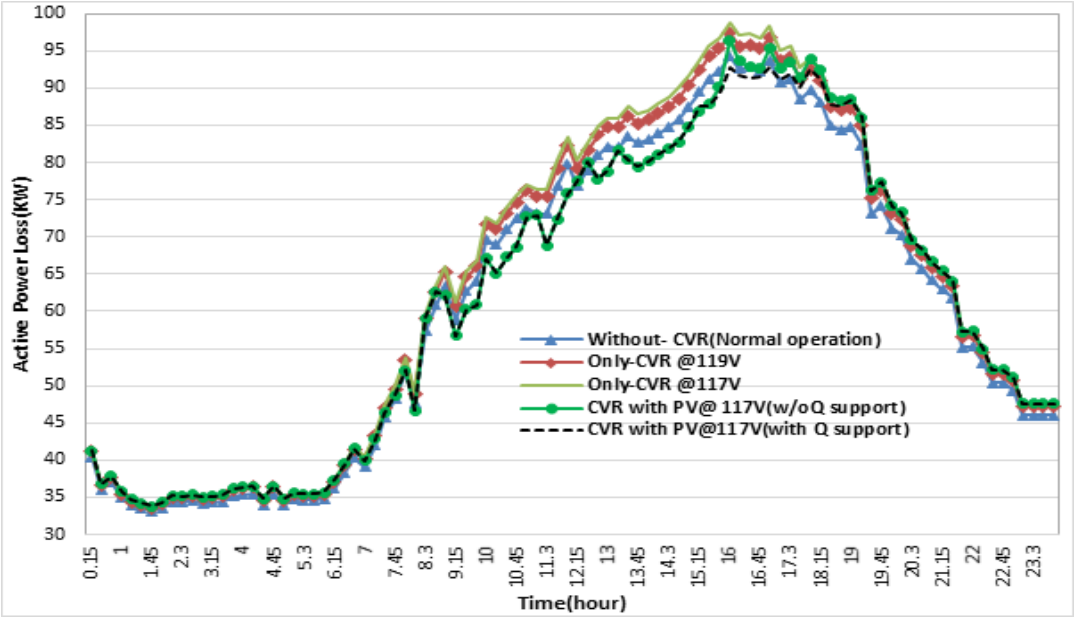

Figure 3.12 Active power losses during Mode-3 operation in Case-II (whole day operation)

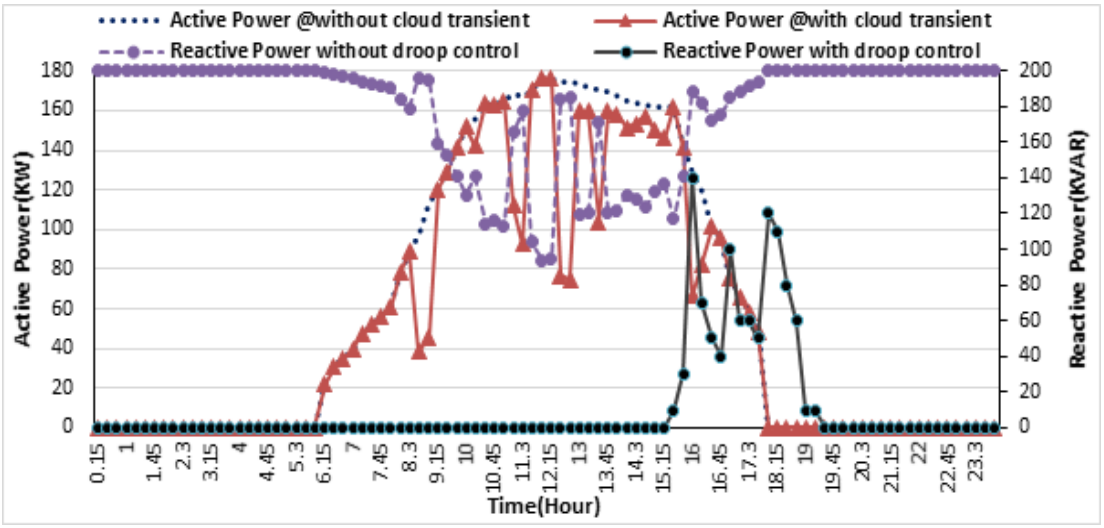

Figure 3.13 Active and reactive power feed by PV system during Mode-3 operation Case-II (whole day operation)

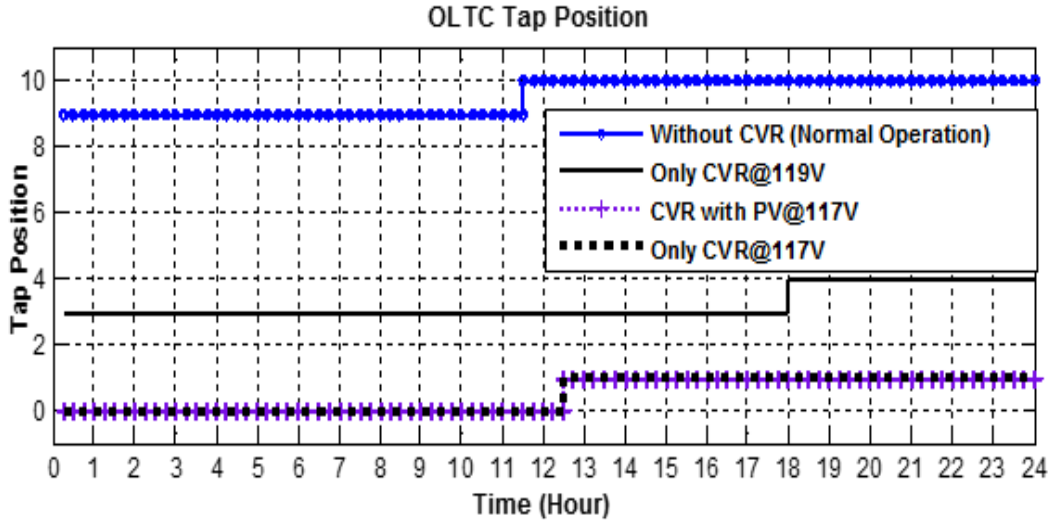

Figure 3.14 Tap Position of OLTC transformer in Case II for whole day operation

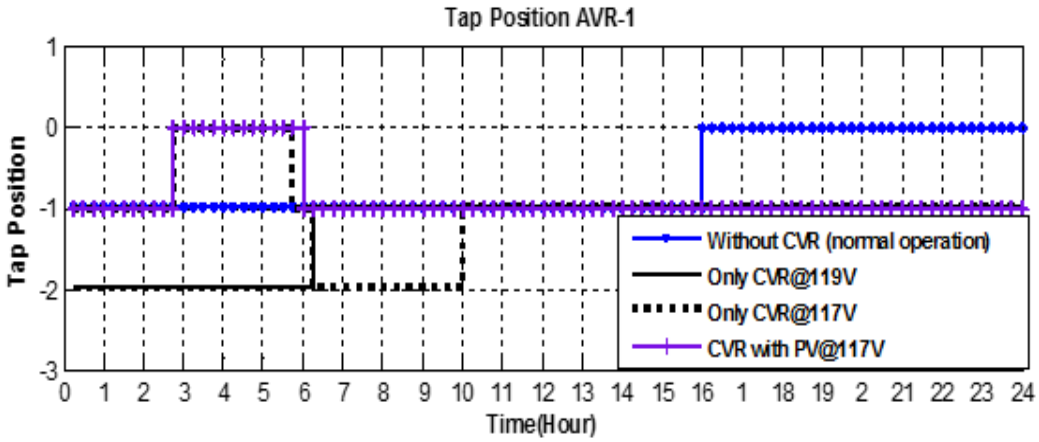

Figure 3.15 Tap Positions of AVR-1 in Case II for whole day operation

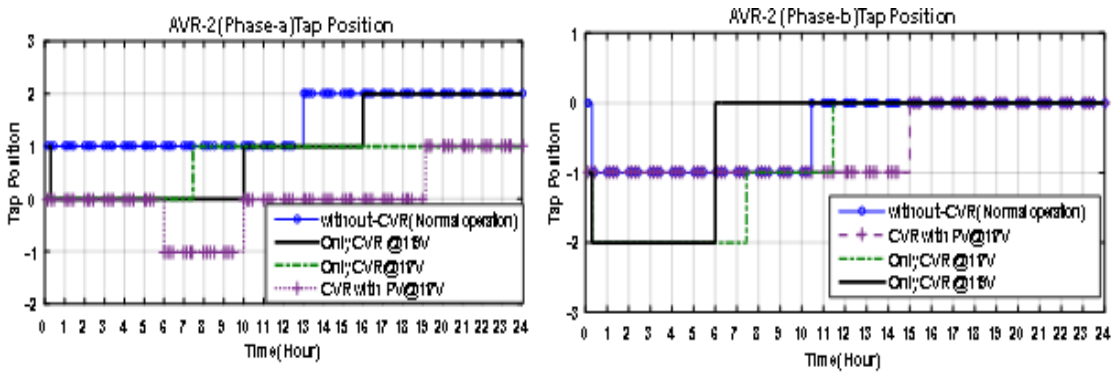

Figure 3.16 Tap Positions of AVR-2 (in Case II for whole day operation)

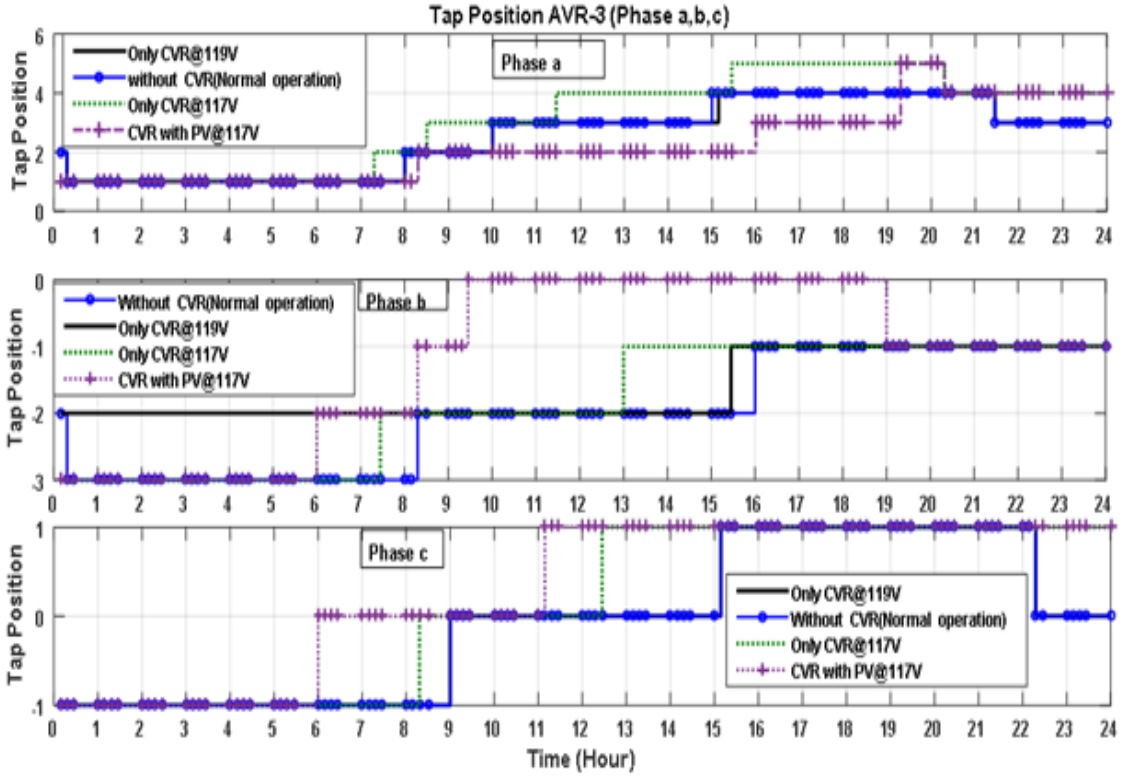

Figure 3.17 Tap Positions of AVR-3 in Case II for whole day operation

3.6.3 Moving Cloud Effect

The partial clouds affect the output of the PV system. The effect of partial cloudy day on the power output of PV system under Mode 3 operation has also been studied in both the cases. Figure 3.8 and Figure 3.12 exhibit the active & reactive power supplied by the system in Case 1 and Case 2 respectively. It can clearly be noticed from these figures that power output is fluctuating in nature because of movement of clouds on PV arrays. The

sudden fall in PV power output followed by a rise in power output indicate the interventions of cloud and its disappearance. Consequently, the voltage rise/fall and reversible power flow problem may occur during PV penetrations.

3.6 Conclusion

The effect of smart grid-enabled CVR with the cooperation of solar PV inverter on energy demand has been studied in this chapter. VVC operation has been carried out without and with a smart grid-enabled CVR to estimate the energy savings. Findings of this investigation are as under:

- Significant energy savings and peak loading relief have been achieved with only CVR.
- The higher energy savings have been achieved with CVR and solar PV systems during deeper level voltage reduction within voltage regulatory range.
- The PV inverter injects the droop controlled reactive power within limits during lower voltage limit violation.
- The effect of inverter losses during reactive power support has also been analyzed.
- Moving clouds effect on PV power output has been analyzed.

It can be concluded that the CVR operation with PV system yields a higher reduction in energy consumptions, peak load demand, and system losses in comparison to only-CVR. Overvoltage can be mitigated if the PV system operates in association with CVR. Lower level PV penetrations are the best solution for handling the fluctuation in PV power output; otherwise, PV system need to be equipped with energy storage. Though implementation of CVR through traditional LDC scheme help to reduce the peak power demand but it does not fully utilize the benefits of CVR and PV technology. Therefore, efficient and optimal coordination among the VVC device is required. In the next *chapter 4*, these issues have been taken care of through optimal CVR operation in the presence of DER and distributed energy storage via VVO method.

CHAPTER 4

OPTIMAL CVR: CENTRALIZED VOLT/VAR OPTIMIZATION

4.1 Introduction

The VVO is one of the featured functions of ADMS that have drawn more attention to utilities for optimal utilization of network control and assets in the distribution grid. It can perform various tasks such as CVR, loss reduction, voltage flattening and power factor correction [63],[13]. For peak load reduction, CVR approach is quite useful; therefore, DNOs are also preferring this method. Though, implementation of CVR with /or without DER through open-loop VVC schemes is an easier way but possesses certain inherent limitations of its adoption when changes occur in network configuration, power generation and demands [32]. On the other side, the closed-loop VVO schemes provide the superior action of VVC with higher energy savings through optimal operations of network assets and control setpoints. In literature, Various optimization algorithms have been used to solve the VVO problem, as explained in earlier *chapter 1* in the literature review section. Other researchers also have studied VVO related works such as an investigation on the loss of life estimation of distribution transformer through VVO method reported in [19], and a bi-level VVO approach has been introduced in [20] to coordinate the smart inverter dispatch and VVC devices simultaneously.

On the other hand, distributed energy storage (DES), especially Community Energy Storage (CES) is also drawing attention due to its inherent benefits such as peak load management, demand balancing and voltage regulation in distribution network operations [6], [115]–[120]. Moreover, the need of balancing the electricity consumption and energy system has also paved the way for CES installation tremendously [117]. The role of CES for shifting the load demand and energy surplus in real-time framework has

been investigated in [121]. The performance and cost benefits analysis with CES has been carried out in [118] considering the time shift impact of solar PV power generations. Optimal allocation and design of multiple CES system in ADN for economic assessment has been done in [122], [123]. The problem of rise in neutral voltage due to the unbalanced allocation of solar power and loads has been mitigated with CES as discussed in [124]. A coordinated control scheme for voltage regulation in distribution network via DES system has been studied in [125] . However, the above studies have not been explored the impact of CVR with DES. The study reported in [126], [127] reveals that the significant power saving can be achieved in the presence of CES in VVO solution. The studies reveal that lack of coordination between the network control such as CVR and asset controls at the energy storage can lead to detrimental effects for grid operations. In order to address this issue, a properly coordinated control scheme is required to integrate both CVR and CES operations simultaneously. Besides, the limited work has been reported in the literature to utilize the CES for maximizing the CVR benefits.

Therefore, this chapter introduces a centralized VVO driven optimal CVR methodology considering the impact of CES for ADNs.

4.2 Centralized Volt/VAR Optimization

A closed-loop framework for smart grid-enabled CVR has been shown in Figure 4.1. The main components of this framework are smart VVO engine located at the control center, VVC field devices (Distribution Transformer with OLTC, AVR, VAR inverters and CB), loads and measurement devices and AMI system. The framework is called closed-loop because it regularly monitors the measurements and sends the control signals to field devices through SCADA with the advanced communication system.

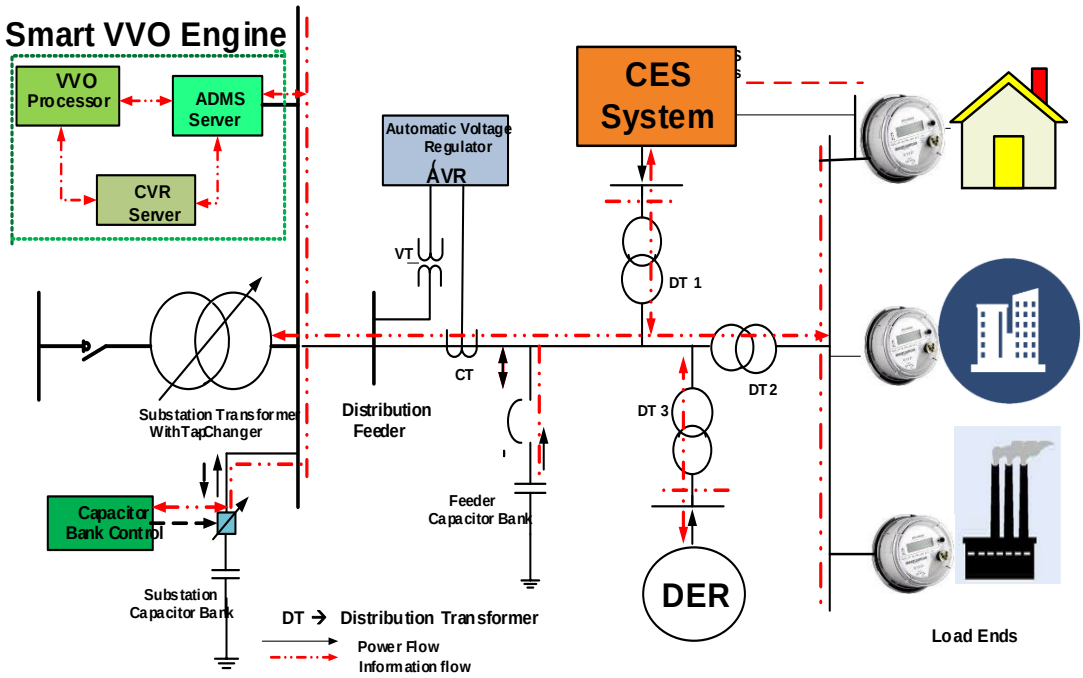

Figure 4.1: Proposed closed-loop VVO based smart grid-enabled CVR

4.2.1 VVO based CVR

In this work, a VVO driven CVR method has been proposed for smart grid operations. It consists of a VVO processor and CVR server assisted through ADMS as shown in Figure 4.1. The main task of VVO processor is to provide the optimal control set points according to desired objectives. The role of CVR server is to provide the CVR settings (such as voltage and time duration) to VVO processor. The control center operator has flexibility to choose different tasks such as loss reduction, voltage flattening, network reconfiguration and CVR. The numerous works have been reported in the literature with the objective of losses reduction, voltage flattening, and network reconfiguration. In this study, the main objective of VVO engine is to enable the CVR. In order to achieve this, the CVR server helps the VVO processor to determine the optimal VVC device settings. The minimization of the total power consumption satisfying the system constraints has been considered as an objective function. In order to achieve this objective, VVO

processor optimizes the voltage and VAR settings of VVC devices in such a manner that the feeder voltage profile remains within the regulatory range.

4.2.2 Estimation of CVR savings

Generally, CVR savings are estimated in terms of technical and economic value. The power and energy saved to add the technical value and cost savings referred as economic gain. Therefore, the employed CVR scheme has been assessed in terms of reduction in the amount of peak power, saving in energy, cost and CVR factors.

4.2.2.1 Estimation of Power, Energy and Cost Saving:

The total peak active power demand reduction, ΔP_{demand}, energy savings, ΔE_{saving}, and cost savings, ΔC_{saving} have been estimated using equations (4.1)- (4.3) respectively.

$$\Delta P_{demand} = P_{demand}^{No-CVR} - P_{demand}^{CVR},\ \%\Delta P_{demand} = \left(\frac{\Delta P_{demand}}{P_{demand}^{No-CVR}}\right)\times 100 \tag{4.1}$$

$$\Delta E_{saving} = E_{demand}^{No-CVR} - E_{demand}^{CVR},\ \%\Delta E_{saving} = \left(\frac{\Delta E_{saving}}{E_{demand}^{No-CVR}}\right)\times 100 \tag{4.2}$$

$$\Delta C_{saving} = C_{\cos t}^{No-CVR} - C_{\cos t}^{CVR},\ \%\Delta C_{saving} = \left(\frac{\Delta C_{saving}}{C_{\cos t}^{No-CVR}}\right)\times 100 \tag{4.3}$$

where P_{demand}^{No-CVR} E_{demand}^{No-CVR} and $C_{\cos t}^{No-CVR}$ are the active power demand, energy demand and cost of power purchase (*Cpp*) respectively during No-CVR operation. However P_{demand}^{CVR}, E_{demand}^{CVR} and C_{cost}^{CVR} are the active power demand, energy demand and cost of power purchase respectively during CVR operation.

The cost of power purchased has been determined using the cost of energy and it has been expressed in equation (4.4) as function ($F_{C_{PP}}$).

$$F_{C_{PP}} = \sum_t^T [C_{Grid}(t) P_{demand}(t)] \tag{4.4}$$

The values of C_{cost}^{No-CVR} and C_{cost}^{CVR} have been determined using equations (4.5) and (4.6) for the time period T, as shown below:

$$C_{cost}^{No-CVR} = \sum_t^T [C_{Grid}(t) P_{demand}^{No-CVR}(t)] \quad (4.5)$$

$$C_{cost}^{CVR} = \sum_t^T [C_{Grid}(t) P_{demand}^{CVR}(t)] \quad (4.6)$$

where $C_{Grid}(t)$ is the grid electricity price at time t and $P_{demand}^{No-CVR}(t)$, $P_{losses}^{No-CVR}(t)$ are the load demand and losses at time t respectively during No-CVR operation. $P_{demand}^{CVR}(t)$ and $P_{losses}^{CVR}(t)$ are the load demand and losses at time t respectively during CVR operation.

4.2.2.2 Estimation of CVR factor

In order to check the effectiveness of CVR in technical terms, CVR factor has been calculated in terms of peak kW power (CVR_{fP}) and kWh energy (CVR_{fE}). From an economic point of view, CVR factor has been calculated in terms of cost savings in purchased power. In this study, CVR factor is estimated in terms of peak active power reduction, energy savings and cost savings with respect to the percentage of voltage reduction as delineated under:

- *CVR factor in terms of active peak power demand (CVR_{fP}):* The CVR_{fP} (kW) is the ratio $\%\Delta P_{demand}$ to percentage voltage reduction (%ΔV).

$$CVR_{fP} = \frac{\%\Delta P_{demand}}{\%\Delta V},\ \%\Delta V = \left(\frac{V_{No\text{-}CVR} - V_{CVR}}{V_{No\text{-}CVR}} \right) \times 100 \quad (4.7)$$

where $V_{No\text{-}CVR}$ and V_{CVR} are node voltage during No-CVR (normal operation) and CVR operation respectively.

- *CVR factor in terms of energy savings (CVR_{fE}):* CVR_{fE} (KWh) is measured as the ratio of $\%\Delta E_{saving}$ to %ΔV.

$$CVR_{fE} = \left(\frac{\%\Delta E_{saving}}{\%\Delta V} \right) \quad (4.8)$$

- CVR factor in terms of economic (CVR_{fC}): CVR_{fC} (K$) is the ratio of %ΔCsaving to %ΔV.

$$CVR_{fC} = \left(\frac{\%\Delta C_{saving}}{\%\Delta V} \right) \tag{4.9}$$

4.3 Distributed Energy Storage

Application of energy storage systems in distribution grid are generally categories as utility-owned and customer-owned storage systems. Placing new storage systems and distributed energy resources near loads offer many potential applications. A customer location-based new storage system is generally referred to as a DES system [116], [119],[128]. One of the most popular examples of DES is a CES system nowadays. CES technologies are being accepted and deployed globally because of their salient benefits, such as active/reactive power support, load-demand balancing, frequency and voltage regulation, and ancillary services [5].

4.3.1 Community Energy Storage

CES is a defined as small DES system in the range of few kW to hundreds of kW that are connected to the secondary of the transformer feeding the power to a few residential /small commercial consumer loads with proper coordination [116], [119], [123]. The rated power capacity of CES units typically varies from 25 kW to 50 kW with the discharge time from one to three hours [5], [18]. The typical CES system and its control have been shown in Figure 4.2. The main components of CES system can be divided into following three main parts:

4.3.2.1 Smart Control and Management System

The three-layered intelligent control approach is best suited for the CES system. The first layer mainly deals with centrally controlling of the energy management system and the

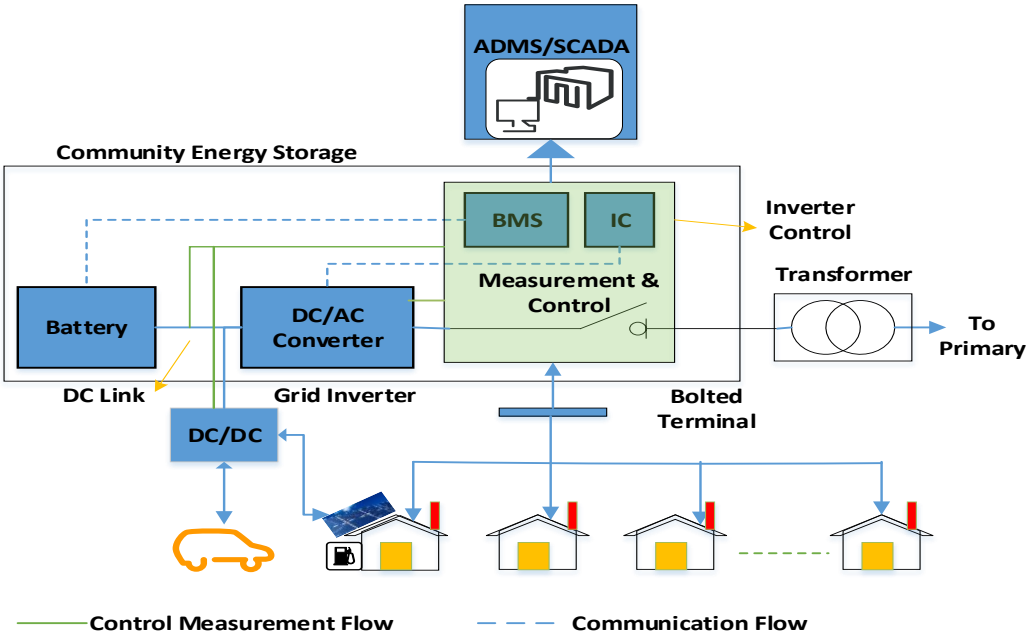

Figure 4.2: Schematic layout of CES system [127]

second is regional control for optimization at the substation transformer level, feeder and for a group of CES units. The third layer operates locally for controlling the CES unit at an individual inverter level at low voltage and islanding mode. CES management system which consists of a battery, inverter control and battery management system (BMS) connected to the Point of Connnection (POC) and ADMS/SCADA system. This POC is connected to the secondary side of the distribution transformer.

4.3.1.2 Power Conversion System (PCS):

The second part is the power conversion system having DC/AC and AC/DC converters through which battery is connected to POC and control blocks. PCS is a main part of the CES system because the whole power conversion process is executed with the help of PCS. The main part of PCS is a smart converter (which converts both AC to DC and DC to AC) combined with a smart inverter controller. Modern smart inverter having the facility to operate in four quadrants in bidirectional mode is deployed in CES system. With the use of these inverters, CES can provide both active and reactive power to the distribution grid or locally.

4.3.1.3 Communication System and Advanced Protection

The third part covers the measurements and communication system which monitors, measures the status of connected devices and sends/receives the control signals to ADMS through the advanced communication system. Generally, distributed energy management interface using a DNP based communication standard is preferred [116], [117]. The CES system is equipped with advanced protection devices such as isolators, DC modules, circuit breakers, Fuse and protection scheme which can clearly differentiate between the islanding conditions and abnormal conditions [116].

4.3.2 CES Control Strategy

The three-layered intelligent control approach is best suited for CES operation. The first layer deals with centrally controlling of the energy management system. Optimal control strategy at substation transformer level, feeder level, and a group of CES units is determined at the second layer and referred as the regional control layer. The local control of CES unit at an individual inverter level is performed at the third layer. Each layer can operate separately and/or combined with other layers. The present investigation focuses mainly on first and second layers for VVC and demand balancing at the substation feeder level. This can be achieved through controlling of CES system.

4.3.2.2 Charging/discharging control strategy of battery management system (BMS):

The control strategy of BMS operates in three states, such as charging, discharging and idle, as shown in Figure 4.3. The strategy begins with identifying the substation loading in three categories such as low, normal and high as recognized by the operator. During the low/off loading, CES system consumes power from the network, i.e. CES units operate in the charging state. Prior to operation in the charging state, it is to be ensured that the kWh stored value ($kWh_{CES,T}^{stored}$) is less than rated kWh capacity (kWh_{CES}^{rated}). Then after, it is to be ensured that the current State of Charge (SOC^T) should be below the upper

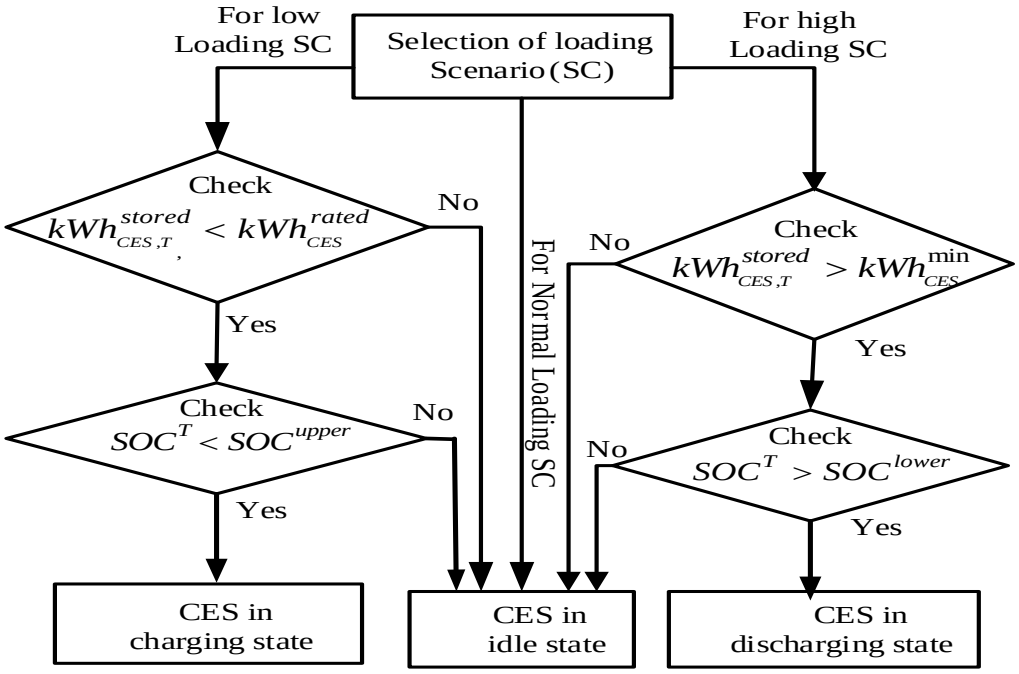

Figure 4.3 Charging /discharging control strategy of BMS

limit of SOC (SOC^{upper}). During the high loading period, CES system operates in the discharge state. However, a higher value of $kWh_{CES,T}^{stored}$ than the minimum specified kWh capacity ($kWh_{CES,T}^{stored}$) of the CES should be ensured before an operation in a discharged state. The (SOC^{T}) should be continuously monitored and it should be maintained above the specified lower limit of SOC (SOC^{lower}). Moreover, during normal loading hours, CES remains in the idle state, i.e., it neither charge nor discharge the CES unit. The SOC of battery at time T is defined by equation (14).

$$SOC^{T} = \left(\frac{kWh_{CES,T}^{stored}}{kWh_{CES}^{rated}} \right) \tag{4.10}$$

4.3.2.3 CES power flow control for Unbalanced Network:

The power flow control strategy at POC of CES has been depicted in Figure 4.4. The unbalance distribution networks have uneven loading in each phase of the feeder. The highest and lowest loading phase at POC of the CES and network is identified before the power flow control is applied.

During charging state, CES system is connected to the lowest loading phase. It consumes power from the grid during the charging state. The CES power output (CES^{Pout}) is equal to CES^{Pout} and it acts as a load. However, during discharging state, CES system is connected to the highest loading phase and it injects the power into the grid. The CES power output is negative and the CES acts as power source. Moreover, in the idle state, CES is disconnected from the network. It is further to be mentioned that the control strategy described in *subsection 4.3.3.2* is applied without any modification.

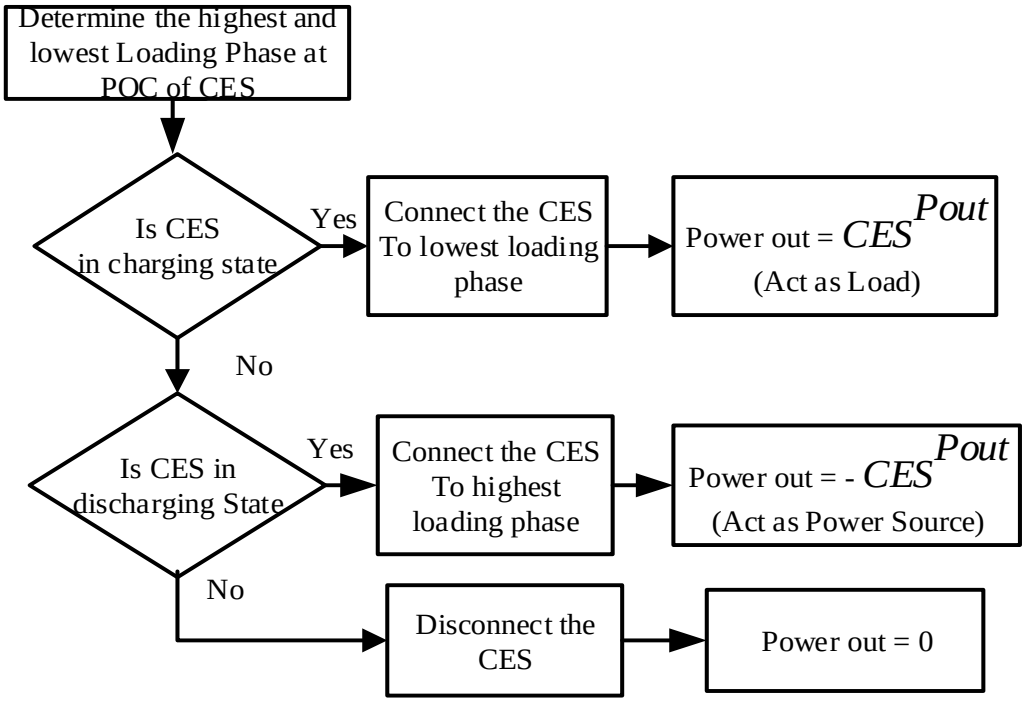

Figure 4.4 CES power flow control

4.4 Problem Formulation and Solution Method

The basic goal of this study is towards, the development of VVO engine for CVR, to achieve higher energy efficiency and peak shaving in the presence of DER and CES. In this section, the problem formulation and solution method for VVO is delineated.

4.4.1 Problem Formulation

In order to deploy the CVR, a VVO engine-based method has been adopted in this work. The VVO engine minimizes the total power demand from the substation allowing

variations in tap positions of OLTC, AVRs and CBs switching. The objective function and constraints are delineated as under.

4.4.1.1 VVO Objective Function:

Total active power demand is the summation of total active power loads ($P_{Total\ Load}$) and active power loss ($P_{Total\ Loss}$) of the active distribution system; thus, the objective function can be written as:

$$Objective\ \ function = \text{minimize}\left(P_{Sub}^{Demand}\right) \tag{4.11}$$

$$P_{Sub}^{Demand} = \sum\left(P_{Total\ Load} + P_{Total\ Loss}\right) \tag{4.12}$$

$$P_{Total\ Load} = \sum_{k=1}^{Nl}\sum_{\phi\in A,B,C} P_{L,k}(V_k)^{\phi} \tag{4.13}$$

$$P_{Total\ Losses} = \sum\left(P_{loss}^{lines} + P_{loss}^{cables} + P_{loss}^{txf} + P_{loss}^{inv,CES}\right) \tag{4.14}$$

here $P_{Total\ Losses}$ is the total active power losses and $P_{Total\ Load}$ is the total active power load of all phases and $P_{L,k}(V_k)$ is the load at *k*th node. Φ represents the phase A,B,C and Nl is the total load node number. $P_{Total\ Losses}$ are the total active power losses on lines (P_{loss}^{lines}), cables (P_{loss}^{cables}),inverter ($P_{loss}^{inv,CES}$) and transformers (P_{loss}^{txf}) as shown in (4.14). From equation (4.13), it can be observed that the real power demand at a node is dependent on its voltage. Further, it reveals that the demand would decrease with a decrease in voltage. Transformer core losses depend upon the voltage, whereas transformer winding and line losses mainly depend upon current flows. Therefore, total active power losses may decrease or increase with reduced voltage.

4.4.1.2 Decision Variable (X)

The taps of OLTC, AVRs and switching steps of capacitor banks are the main decision variables as shown below.

- tap position of OLTC (T_P^{OLTC})
- tap position of AVR (T_P^{AVR})
- CBs reactive power ($Q_{i,cb}^t$)

$$X = \left[T_P^{OLTC}, T_P^{AVR}, Q_{i,cb}^t \right] \tag{4.15}$$

4.4.1.3 System Constraints

The scheduled VVO problem is subjected to the following constraints:

- *Power Balance Constraints:* The constraints dealing with active and reactive power balance constraints are expressed using (4.16) and (4.17) respectively.

$$P_{grid} + P_{DER} \pm P_{CES} - P_{Total\ Load} = V_h \sum V_k (G_{hk} cos\theta_{hk} + B_{hk} \sin\theta_{hk}) \tag{4.16}$$

$$Q_{grid} + Q_{CES} + Q_{cb} + Q_{CES} - Q_{load} = V_h \sum V_h (G_{hk} cos\theta_{hk} - B_{hk} \sin\theta_{hk}) \tag{4.17}$$

where P_{grid} Q_{grid} are the active and reactive power taken from the external grid respectively. P_{CES} , Q_{CES} denotes the active, reactive power of CES and Q_{load} , Q_{cb} are the total reactive power load and reactive power supplied by capacitor banks at time t. G_{hk} , B_{hk} and θ_{hk} represent the conductance, susceptance matrices and phase angle between nodes h and k respectively. The voltage profile at *k*th node is denoted by V_k .

- *Transformer/regulator tap constraints:* The tap range of OLTC transformers/AVR and tap position are given in (4.18) and (4.19) respectively.

$$0.9\text{pu} \le \text{Tap} \le 1.1\text{pu} \tag{4.18}$$

$$\text{Tap} = \left\{ 1 \pm \left(\frac{\Delta V_{tr}}{100} \right) \times T_P \right\} ,\ T_p \in \left\{ T_p^{\min}, ...0.....T_p^{\max} \right\} \tag{4.19}$$

where ΔV_{tr} is increment in voltage at each step and T_p is tap position. $T_p^{\min}$ and $T_p^{\max}$ are the minimum and maximum tap values.

- *CB constraints:* Reactive power supply by CB at each switching operation is determined by equation (1.12) and detailed explained in *chapter 1*.
- *Voltage constraints:* The voltage profile of the distribution feeder should be maintained within limits, as shown in equation (3.13) and explained in *chapter 3*.
- *DER operation Constraints:* The equation (30) shows the active power (PDER) generated by DER is equal to the forecasted value (PfDER). Equation (4.21) represents the reactive power (QDER) generated using power factor angle (_ϕ_{DER}) of DER. Equation (4.22) represents the DER capacity (S_{DER}) constraint.

$$P_{DER} = P_{DER}^{f} \tag{4.20}$$

$$Q_{DER} = P_{DER} \tan \phi_{DER} \tag{4.21}$$

$$S_{DER} \leq \sqrt{\left(P_{DER}\right)^2 + \left(Q_{DER}\right)^2} \tag{4.22}$$

- *CES Constraints:* The operation constraints of CES are shown in equations (4.23) to (4.27).

CES voltage limit:

$$V_{CES}^{\min} \leq V_{CES} \leq V_{CES}^{\max} \tag{4.23}$$

where V_{CES} is the CES terminal voltage and $V_{CES}^{\max}$ $V_{CES}^{\min}$ denotes the maximum and minimum ranges of $V_{CES,}$ respectively.

CES power limit:

Active and reactive power ($P_{CES,T}$ and $Q_{CES,T}$) limit at time T should be less than or equal to its rated value as shown in equations (4.23) and (4.24) respectively. Total power supplied/absorbed by CES system governed by the (4.25).

$$P_{CES,T} \leq P_{CES}^{rated} \tag{4.23}$$

$$Q_{CES,T} \leq Q_{CES}^{rated} \tag{4.24}$$

$$\left(\sqrt{P_{CES,T}^2 + Q_{CES,T}^2}\right) \leq \left|S_{CES,inv}\right| \tag{4.25}$$

where, $P_{CES}^{\max}$ & $P_{CES}^{\min}$ is maximum and minimum value of P_{CES} and $S_{CES,inv}$ is the CES inverter KVA capacity.

CES capacity limit:

$$kWh_{CES}^{\min} < kWh_{CES,T}^{stored} < kWh_{CES}^{rated} \tag{4.26}$$

CES battery SOC limit:

The SOC of CES battery is determined by (4.10) and it should follow the relation (4.27) at T time operation.

$$SOC^{lower} < SOC^{T} < SOC^{upper} \tag{4.27}$$

4.4.2 Proposed VVO Solution using DGSA

The VVO problem has been solved through a Discrete Gravitational Search Algorithm (DGSA) that bears interest in highly complex optimization problems regarding faster convergence and real-time applications [129]. It has been reported to be an efficient method for solving different optimization problems in power systems [130], [131]. The optimization of the static VAR compensator parameters has been achieved through GSA for reactive power compensation in real time application by authors of [132]. Enhanced GSA has been employed for feeder reconfiguration, losses and operational cost minimization in distribution network [130]. In [131], binary GSA has been utilized for optimal cost and observability of wide area measurement Thus, GSA has been found to be suitable method for optimization of parameters of changing operational scenario and real time applications. The present optimization problem deals with discrete control

variables (tap positions and capacitor switching steps). Therefore, the basic concept of GSA has been extended to incorporate discrete search space.

4.4.2.1 Overview of Gravitational Search Algorithm (GSA)

A GSA driven optimization approach is proposed to solve the VVO problem expressed by equations (4.11) through (4.27). Esmat Rashedi et al., [129] introduced a new intelligent search technique called GSA, which is based on gravitational law and concept of mass interactions. In this technique, agents are collection of masses which interact with each other based on the Newton gravitational law and the laws of motion. Consider a system with *n* number of agents with *d* dimensions, in which the position of the i^{th} agent is defined as:

$$X_i = (x_i^1, x_i^2, x_i^3 .....x_i^n) \tag{4.28}$$

At a particular time'*t*,' the force ($F_{ij}^d(t)$) acting on 'i^{th}' mass from 'j^{th}' mass would be,

$$F_{ij}^d(t) = G(t)\frac{M_{pi}(t) \times M_{aj}(t)}{R_{ij}(t) + \xi}(x_j^d(t) - x_i^d(t)) \tag{4.29}$$

At particular time't,' $G(t)$ is the gravitational constant $M_{pi}(t)$ is the passive gravitational mass of i^{th} agent and $M_{aj}(t)$ is the active gravitational mass of j^{th} agent. $R_{ij}(t)$ is the Euclidian distance between the i^{th} and j^{th} agent. ξ is a small constant. The total force ($F_i^d(t)$) acts on an i^{th}agent in d^{th} dimension, and its acceleration ($a_i^d(t)$) from other agents is expressed in (4.30) and (4.31) respectively.

$$F_i^d(t) = \sum_{j=1, j\neq i}^{n} rand_j F_{ij}^d(t) \tag{4.30}$$

$$a_i^d(t) = \frac{F_i^d(t)}{M_{ii}(t)} \tag{4.31}$$

where, *rand* is a random number in the interval [0, 1], M_{ii} is the inertial mass of i^{th} agent.

Velocity ($v_i^d(t)$) and position ($x_i^d(t)$) of the i^{th} agent in the d dimension is updated as follows:

$$v_i^d(t+1) = rand_i \times v_i^d(t) + a_i^d(t) \tag{4.32}$$

$$x_i^d(t+1) = x_i^d(t) + v_i^d(t+1) \tag{4.33}$$

And the masses of each agent are updated by

$$m_i(t) = \frac{fit_i(t) - worst(t)}{best(t) - worst(t)}, \quad M_i(t) = \frac{m_i(t)}{\sum_{j=1}^{n} m_j(t)} \tag{4.34}$$

best = Minimum ($fit_i(t)$) *and worst =Maximum*($fit_i(t)$)

where, *best* and *worst* both depend upon the objective function.

Gravitational constant (G) can be obtained by (4.35):

$$G(t) = G_0 e^{-\alpha \frac{t}{Tr}} \tag{4.35}$$

where G_0, α are the constant parameters and *Tr* is total number of iterations.

4.4.2.2 Discrete GSA

In general, GSA has been mainly used to solve the continuous optimization problems. For solving the discrete optimization problems, the GSA cannot be applied directly due to its internal coding structure. The present VVO problem is an example of the discrete optimization problem. Therefore, following modifications have been done in GSA code before solving the present optimization problem.

- Integer random initialization has been carried out by selecting the nearest integer value of the variables.
- During computation, the new position of the variables is also rounded to the nearest integer value as expressed by equation (4.36).

$$x_i^{d'}(t) = round(x_i^d(t)) \quad (4.36)$$

where, $x_i^{d'}(t)$ is modified d^{th} position value of the i^{th} agent.

4.5 Implementation of VVC Scheme

In this section, the implementation of CVR with traditional method and proposed smart grid enabled CVR through VVO method have been described. The modelling of distribution network, CES system and implementation of CVR methods have been done in OpenDSS and MATLAB platform interfaced through component object model. Figure 4.5 shows the interacting framework of OpenDSS and MATLAB platforms.

4.5.1 Traditional CVR

Traditionally, LDC scheme are deployed for voltage reduction. Figure 4.6 (a) shows the flowchart of the implementation of CVR applying LDC. The regulated /EOL voltage is fixed in the lower half range (120-114V) of the service voltage. The control action is determined through LDC algorithm.

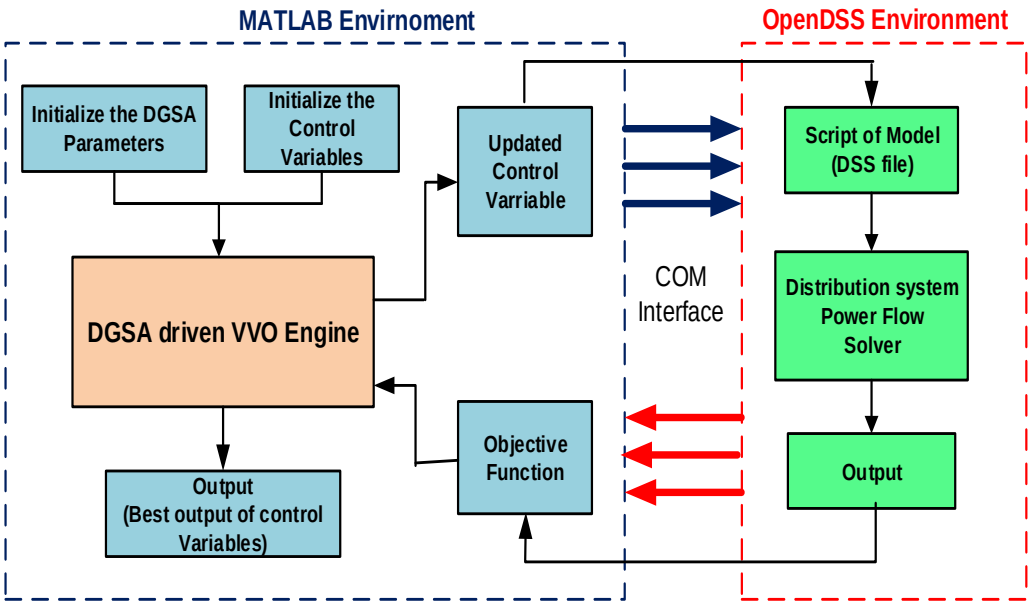

Figure 4.5 Interacting framework of OpenDSS and MATLAB platforms.

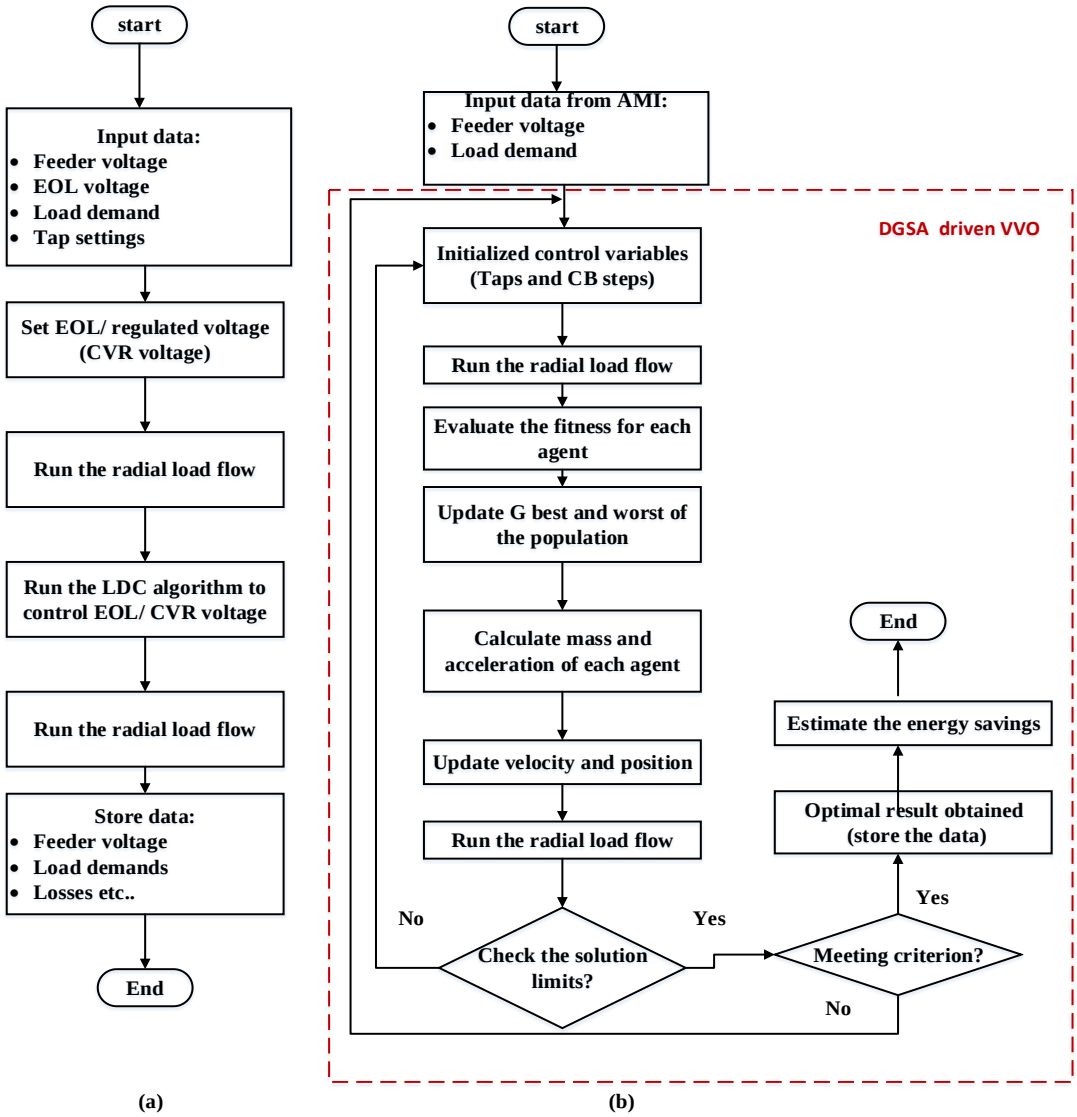

Figure 4.6 Flowchart of CVR methods implementation (a) Traditional CVR Approach (b) SG enabled VVO based CVR

4.5.2 Smart Grid (SG) enabled CVR

The proposed smart grid enabled CVR has been implemented through VVO approach. The DGSA driven VVO has been utilized in this study. The VVO method implementation, estimation of energy savings and CVR factor has been carried out mainly in following two stages:

- In the first stage, deployment and execution of VVO solution is performed. The parameters of VVC devices such as taps, steps of CBs, active & reactive power flows

through CES are obtained through VVO engine. The VVO engine has been developed in MATLAB environment with DGSA driven optimization approach.

- In the second stage, energy savings and CVR factor are estimated using the optimal results obtained in first stage.

The dimension of agents has been divided into various sets such as tap positions of OLTC, AVRs and CB switching. The maximum number of iterations (*Tr*) has been taken as stopping criteria. Step wise procedure of proposed VVO solution is delineated in *algorithm 1* as under:

Algorithm 1 VVC Parameters optimization using DGSA	
1	**Input:** Feed the distribution network data {loads, lines, VVC devices and CES data
2	**Input:** GSA parameters and control varriable limit
3	Set the multiplier of active and reactive power load
4	Enable the CES control stretegy as explained in *subsection 4.3.2* (If CES is present/participating)
5	Divide the dimension of agent among control variables (as tap positions of OLTC, AVRs, and switching steps for CBs & CES)
6	Set the stopping criteria (maximum number of iterations)
7	Initialize population and speed of all the particles in MATLAB and perform load flow analysis in OpenDSS.
8	Evaluate the value of fitness function expressed by equation (4.11) for each agent in MATLAB.
9	Find best and worst among all the agents
10	Calculate force and masses on each agent using equations (4.29) and (4.34) respectively.
11	Calculate acceleration and velocity of each agent using equations (4.31) and (4.32) respectively.
12	Update velocity and position of each agent.
13	Check the stopping criteria if yes then go to *step 14* else move to next iteration.
14	Adopt the settings of VVC devices corresponding best solution
15	**Output:** Estimate energy saving and CVR factor using equations (2.1) and (2.2) respectively.

Implementation of above-described algorithms using OpenDSS and MATLAB has been further explained using a flow chart given in Figure 4.6 (b).

4.6 Case Study

The proposed VVO based CVR Scheme has been validated using in two scenarios as:

- Scenario-1: Demand reduction during fully loading hours
- Scenario-2: Energy saving and demand management during varying load hours

4.6.1 Test System Discription

The proposed CVR method has been validated on modified IEEE 123 node distribution test system as shown in Figure 4.7(a) [114]. It is named modified system due to addition of DER, a CES system and change in load model for demonstration purpose. Voltage dependent constant impedance current power (ZIP) load model has been considered in this study and detailed description can be seen in *chapter 1* under subsection *1.4.3*. The values of ZIP coefficients under various loading types with respect to nodes have been written Table A.2 in Appendix A. The loads in test system contain primary spot and distributed loads at primary. These loads are represented as lumped loads [18]. The model of this system stops at the primary nodes, therefore the secondary distribution system (SDS) configuration connect to CES at POC node has been modelled and shown in Figure 4.7 (b). For example, the kVA of the spot load at 65 is calculated as $\sqrt{(150)^2 + (100)^2}$ = 180 kVA; therefore, this primary node (node 65) can be replaced by a 180-kVA distribution transformer serving a SDS, to match the original spot load. In order to alter the CES connection with different phases during the charging/discharging mode of operation, a switch has been equipped with CES installation systems as shown in Figure 4.7(b).

In this chapter, the DERs are classified as non-renewable and renewable power sources with unity power factor. In context of renewable source, two wind turbine-based power sources located at node 95 and 151 have been considered. The details of wind power modeling can be found in [133]. Ratings and parameters of VVC devices, DERs

and CES have been shown in Table 4.1, Table 4.2 and Table 4.3 respectively. The voltage increments at each step, ΔV_{tr} has been chosen as 0.625.

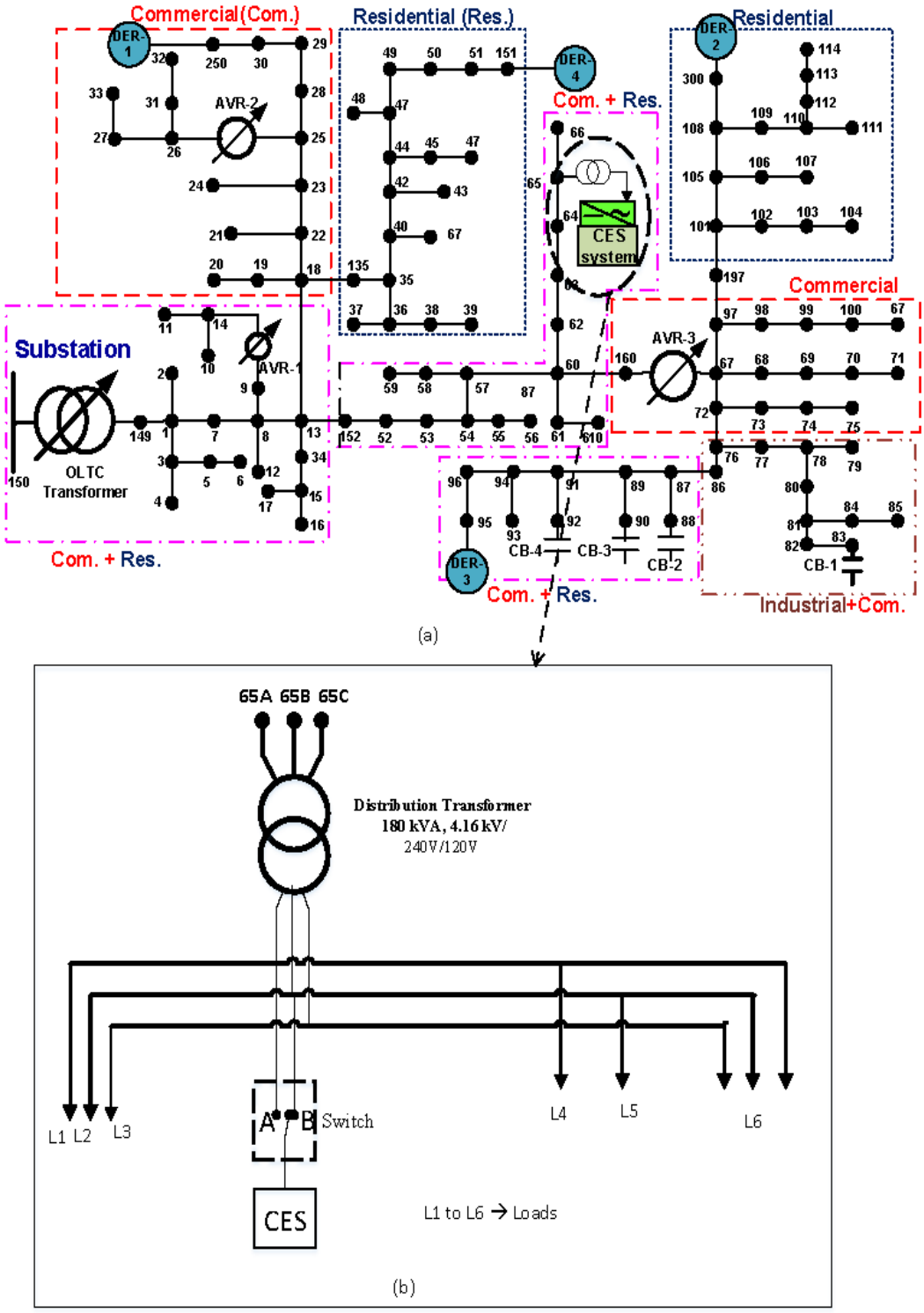

Figure 4.7: (a**)** Modified IEEE 123 node distribution test feeder
(b) Secondary distribution system (SDS) configuration connect to CES at POC node 65

Table-4.1. Ratings and Parameters of VVC devices

Device	**Phase /Connection**	**Location/ rating**		**Tap range / CB step** ($T_p^{\min}$,$T_p^{\max}$, $Sw_{cb}^{p,\max}$)
OLTC	3-Phase, Wye	150 - 149		+16 to -16
AVR-1	1- Phase (A)	9-14		+16 to -16
AVR-2	2- Phase (A, C)	25-26		+16 to -16
AVR-3	3- Phase	160-67		+16 to -16
CB-1(kVAR)	3- Phase	83	200/Phase	0-4
CB-2(kVAR)	1- Phase (A)	88	50/ Phase	0-1
CB-3(kVAR)	1- Phase (B)	90	50/ Phase	0-1
CB-4(kVAR)	1- Phase (C)	92	50/ Phase	0-1

Table 4.2 DERs Rating and Location

Number	**DER Type**	**Rating (kW)**	**Location (node)**
DER -1	Non-Renewable	45	250
DER -2	Non-Renewable	60	60
DER -3	Renewable (wind)	150	95
DER -4	Renewable (wind)	90	151

The hourly load demand profile for an entire year has been taken from [134]. The probability of occurrence of percentage of load demand with respect to peak load demand and cumulative probability of the load demand throughout the year have been shown in Figure 4.8. The fully loaded (100% load) condition is considered as a peak load demand. The wind power output throughout the year during different loading hours has been shown in box plot Figure 4.9.

4.6.2 Simulations and Results Discussion

The communication system is working well, and its delay effect has not been considered during the execution of CVR operation. The performance of proposed method has been

studied for two scenarios under following three different cases of VVC operation on the above-mentioned test system.

Table-4.3. Ratings and Parameters of CES system

Location/ Phase	Node-65/1
Rate kW power (P_{CES}^{rated})	50 kW
Rate kVAr power (Q_{CES}^{rated})	40 kVAr
Rated kWh capacity (kWh_{CES}^{rated})	150 kWh
Reserve kWh capacity ($kWh_{CES}^{\min}$)	20%
CES maximum voltage limit ($V_{CES}^{\max}$)	1.1 p.u.
CES minimum voltage limit ($V_{CES}^{\min}$)	0.9 p.u.
Inverter rating ($S_{CES,inv}$)	100 kVA
SOC range (SOC^{upper} - SOC^{lower})	90% - 20%
Inverter efficiency (η_{inv})	97%
Battery discharge efficiency (η_D)	94%
Battery charge efficiency (η_C)	97%
Charging/ discharging power factor	1/0.85

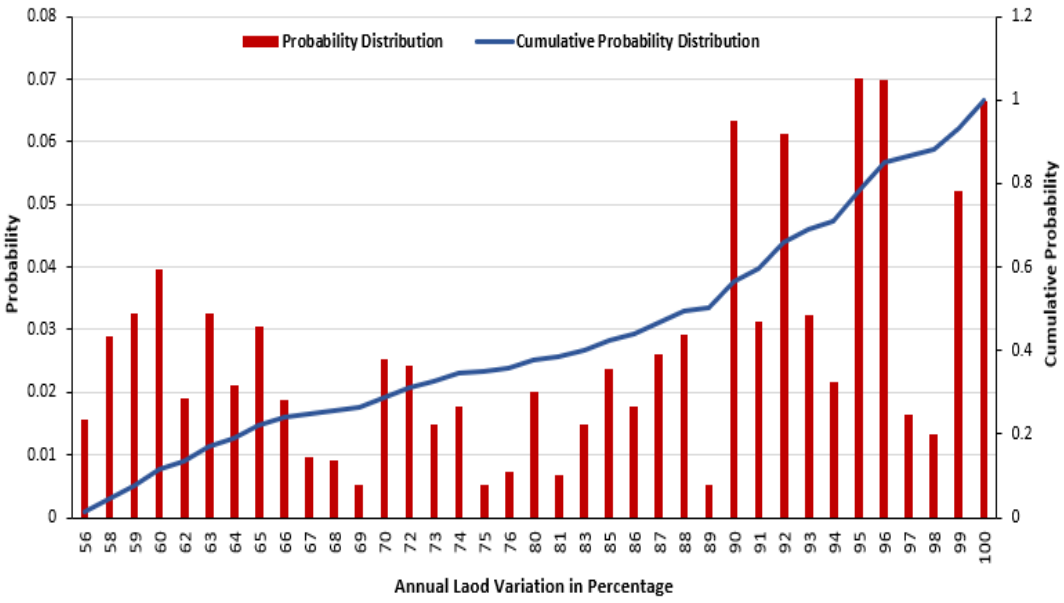

Figure 4.8 Annual load variation in percentage

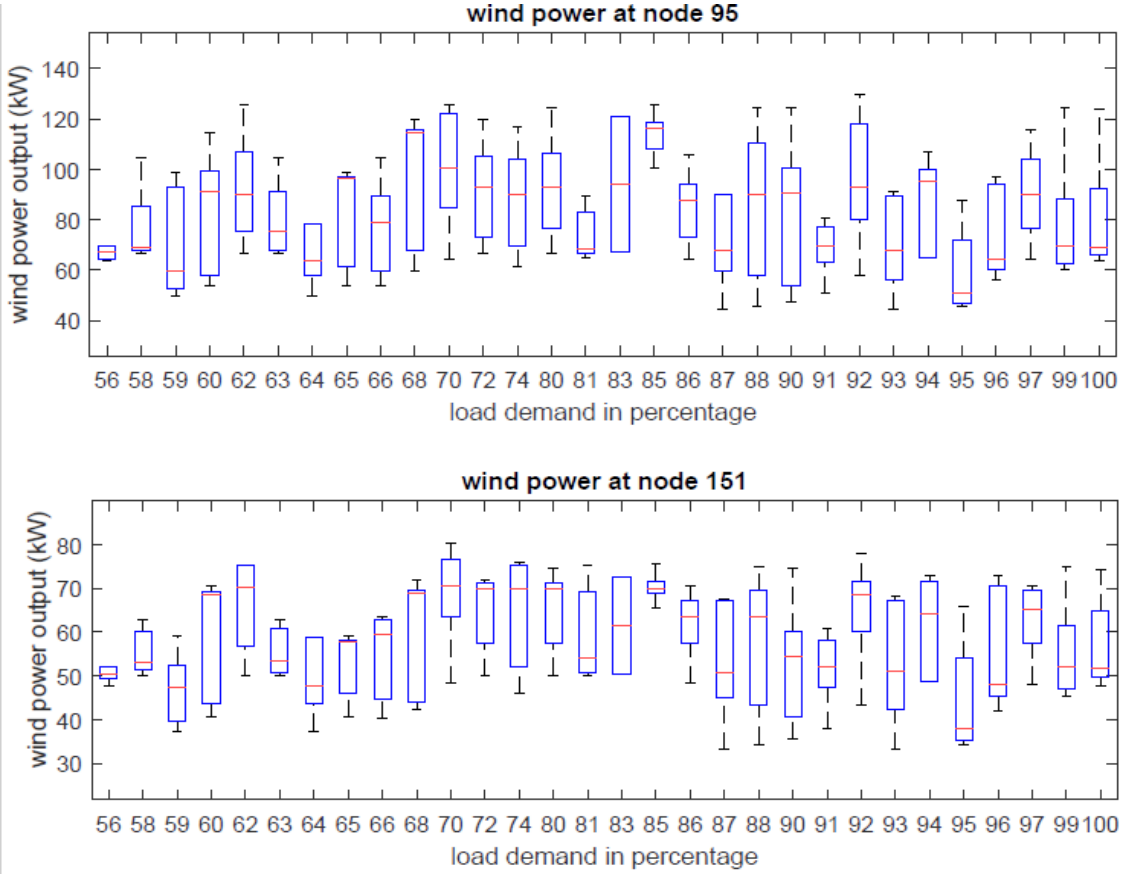

Figure 4.9 Wind power generation at node 95 and node 151 with varying load demand annually

(i) Case 1: Without CVR (Normal Operation)

In this case, the system does not deploy CVR or CES during VVC operation. The execution of VVC has been carried out at 120V regulated voltage with OLTC, AVR-1, AVR-2 and AVR-3 at 124 V. CBs are fixed in nature. The effect of CES has not been included in this case.

(ii) Case 2: With CVR only

In this case, VVC operation has been carried out CVR only taking in two subcases as discussed below.

- *Subcase I- Traditional CVR:* In present implementation of traditional method, the regulation voltage of 118V has been adopted for OLTC, AVR-1, AVR-2 andAVR-3 for enabling CVR. The level of voltage reduction can be increased by controlling the above

devices to achieve higher energy savings. However, continued reduction may lead to violation the minimum voltage limits at some points of the distribution network.

- *Subcase II- VVO based CVR*: The SG enabled CVR has been implemented through optimal VVC operation. The optimal operation has been carried out using proposed VVO method. In this case, impact of CES is not included.

(iii) Case 3: CVR with CES

In this case, the CVR is deployed along with CES device. The CVR is enabled through proposed method considering the presence of CES in the system. The allocation of CES system is based on the minimum node voltage. In this study, minimum voltage was observed at nodes 65 in phase A during normal operation. Therefore, CES unit was placed at node 65. Charging, discharging and power flow of CES have been controlled by proposed scheme as discussed earlier subsection.

4.6.2.1 Scenario-1: Demand reduction during fully loading hours

To evaluate the impact of CVR for peak demand reduction, the simulation has been carried out for above mentioned three cases of the system during fully loading hours of a typical year. Figure 4.10 shows the distributions of peak load hours throughout the year. It can be seen from the figure that peak loading occurs from 11th to 21st hours (excluding 13th; 16th and 17th hour) in daily operation.

- *Case 1:* The simulation results in terms of energy demand and losses, in this case, are shown in the second column of Table 4.4. The aggregated maximum and minimum load node voltage were 1.0451 p.u at node 82A and 0.9751 p.u. at node 65A respectively.
- *Case 2:* In this case, the test system has been simulated for CVR only with two subcases. The simulated results are depicted in Table 4.4. From results, it can be observed that CVR operation with VVO produced about 40.285 MWh, i.e. 2.19 % reduction in energy demand during fully loaded hours annually. Moreover, the reported energy

savings are higher than the traditional CVR method with slightly reduced energy losses. The calculated values of CVR_f are 0.592 and 0.811 for traditional and VVO based CVR respectively. From the simulated results, it is observed that VVO based CVR operation is a better choice for higher peak shavings and CVR factor with proper voltage regulation.

Case 3: The deployment of only CVR operation results in higher energy losses. In order to further reduce the energy losses and achieve higher peak shaving, the VVC operation has been carried out in VVO association with CES. The discharging and power flow controls have been adopted. The CES injects the active and reactive power to phase A in the present case. The simulation results obtained are shown in Table 4.4. The total energy savings of about 67.42 MWh, i.e. 3.0%, have been achieved. The maximum and minimum load node voltages are 1.015 p.u at node 1_B and 0.9532 p.u. at node 104_C respectively. Maximum energy demand reduction is reported in phase A, followed by phase C. About 2.07 % reduction in energy losses with respect to Case 1 has reported in this case. Moreover, the reported losses are lesser than Case 1 and Case 2.

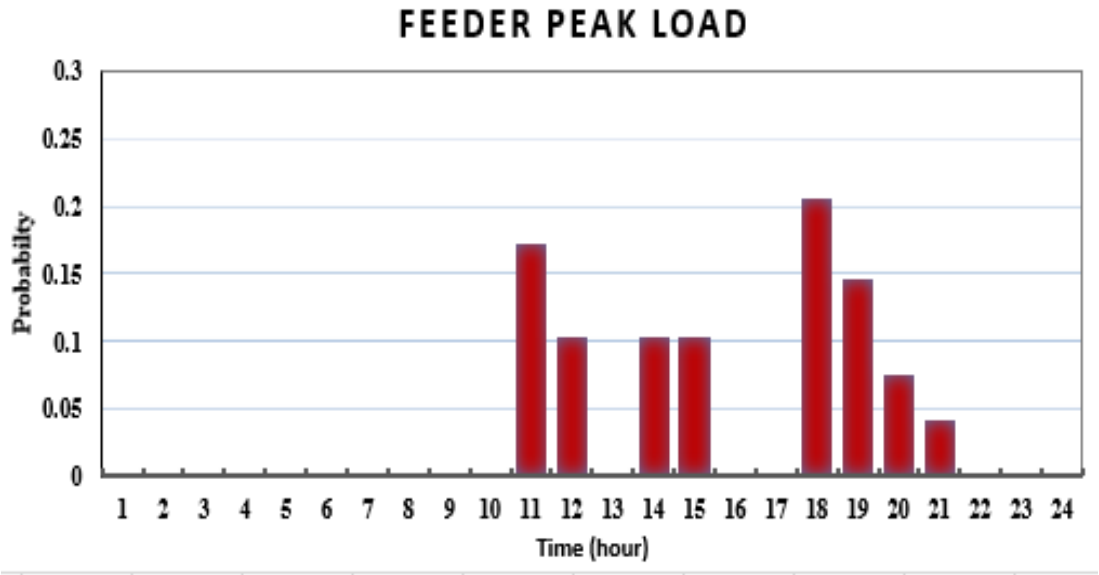

Figure 4.10 Distributions of peak load hours throughout the year.

Table 4.4 Simulation results for scenerio 1

Energy Terms		Case-1 (without CVR)	Case-2 (With CVR Only)		Case-3 (CVR with CES)	MWh Energy Change, (E_{Saving} in %)		
						Case-2		Case-3
			Traditional CVR	VVO based CVR		Traditional CVR	VVO based CVR	
Energy Demand	**Phase A**	852.385	832.922	832.922	805.673	14.0601	19.464	46.712
	Phase B	559.213	548.871	548.871	549.336	8.7155	10.342	9.877
	Phase C	691.158	674.948	674.948	674.657	11.0975	16.21	16.50
	Total	2102.76	2056.74	2056.74	2029.67	33.8771 (+1.611)	46.015 (+2.19%)	73.09 (+3.55%)
Energy Losses (MWh)		56.1827	56.357	57.7514	55.195	-0.1743 (0.31%)	-1.569 (-2.79%)	+0.9877 (+1.79%)
CVR_f		-----	0.592	0.811	0.82	-----	----	

4.6.2.2 Comparative analysis

A comparative study of proposed VVO method and MILP based VVO [12] has been analyzed for peak demand hour in the absence of CES and distributed generation. The simulation results are depicted in Table 4.5. It can be observed from the table that the proposed method yields higher reduction in system losses and power demand at the substation. In addition, the comparison of proposed DGSA and other heuristic optimization-based GA has also been carried out in the absence of DER. The simulations have been performed twenty-five times for both the method. Table 4.6 shows the result of both the methods for Case-2 and Case-3 with respect to the fitness value, standard deviation (STD), convergence (iteration) and CPU time. Figure 4.11 shows the convergence characteristics of both the optimization methods for both cases.

Table 4.5 Simulation results during peak load demand hour

Energy Term/devices		**MILP based VVO** [66]	**Proposed DGSA based VVO**
OLTC taps		[-1]	[+3]
AVR Tap	**AVR-1** **AVR-2** **AVR-3**	Fixed tap ratio (1:1)	[-5] [0, 0] [2, -3, -2]
Cap. steps	**CB-1** **CB-2** **CB-3, CB-4**	[2, 0, 1] [1] [0], [0]	[2, 2, 2] [1] [1], [1]
Losses (kW)		140.4	99.4
Min voltage elsewhere than slack bus		0.9505 p.u (at 66_C)	0.9520 p.u (at 114_A)
Max voltage elsewhere than slack bus (node)		1.0140 p.u. (at 149_B)	1.0188 p.u. (at 149_B)
Total active load (MW)		3.447	3.440
Total reactive load (MVAr)		1.873	1.6123
Active power at slack bus (MW)		3.588	3.540
Reactive power at slack bus (MVAR)		2.026	1.612
Phase wise (A, B, C) power factor at slack bus		0.91, 0.82, 0.87	0.907, 0.90, 0.92

Table 4.6 Comparative analysis of optimization methods

Measuring Parameters		Case-2 (CVR with VVO)		Case-3 (CVR with CES)	
		GA	DGSA	GA	DGSA
Fitness value (kW)	Best	3546.15	3540	3498.61	3493.42
	mean	3556.16	3546.8	3503.71	3497.93
	worst	3563.87	3550.8	3511.78	3505.2
Standard deviation (STD)		6.4949	3.3547	5.14220	4.3643
Required Iter for convergence		48	28	76	27
mean CPU time		216.61	120.05	217.761	120.27

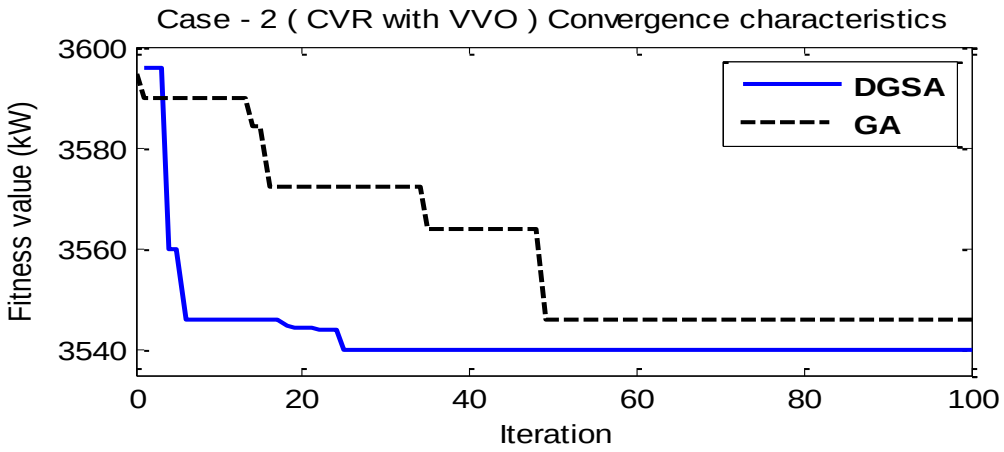

(a)

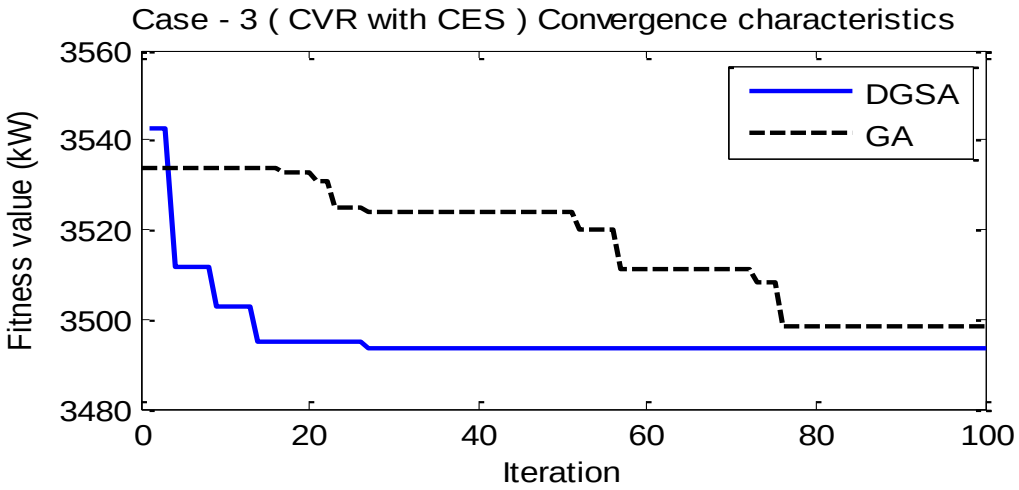

Figure 4.11 Iteration wise convergence characteristics for (a) Case-2 (VVO with CVR) (b) Case-3 (CVR with CES)

It can be observed from the figure and the table that the DGSA method has faster convergence with less computation time. The parameter of DGSA and GA used in this study are depicted in Appendix A, Table A.1.

4.6.2.3 Scenario-2: Energy saving and demand management during varying load hours

To estimate the energy savings and manage the demand through CVR alone and association with CES system, the test system has been simulated for the three cases discussed earlier with different load demand hours for the entire year. The varying load demands with a probability of occurrences have been shown in Figure 4.8 for the entire year. The wind DER power profile for the entire year during different loading has been shown in Figure 4.9. In this study, low loading situation is considered below 67% and high loading is above 94% of peak load demand. The simulated results of each case are discussed as under:

- *Case 1:* The simulation results for this case are depicted in Table 4.7. The aggregated energy demand and energy losses are shown in the second column of Table 4.7. The lowest voltage profile with different percentages of peak load demand for the entire year is shown in Figure 4.12 and it varies from 0.968 p.u. to 0.9978 p.u.
- *Case **2:*** The test system has been simulated for CVR only with the proposed VVO method and obtained results are shown in Table 4.7. From results, it can be observed that in the case of VVO based CVR only, significant aggregated energy savings of about 511.487 MWh, i.e. 2.297%, is achieved annually. Estimated energy savings directly reflect the reduction in energy demand and energy losses at the substation. The calculated aggregated value of CV Rf is 0.795 annually in this case. The lowest voltage profile with different percentages of peak load demand for the entire year is shown in box plot Figure 4.12 in case 2 and it can observe that voltage is above the minimum permissible limit

(0.95p.u.). Figure 4.13 box plot represents the achieved energy savings with respect to load demand and wind DER power output variation for the entire year.

- *Case 3:* In order to manage the peak load management and demand balancing, VVC has been carried out combined with CVR and CES using proposed VVO method. According to the CES power flow control strategy, as depicted in subsection *4.3.3*, node 65, phase A has highest, and phase B has lowest load demand. Therefore, during the discharging state, the CES system is connected in phase A and during the charging state, it is connected to phase B. Generated results are tabulated in Table 4.7. It can be observed from Table 4.7 that aggregated maximum demand reduction of 543.725 MWh is achieved with reduced energy losses. The lowest voltage profile with different percentages of peak load demand for the entire year is shown in box plot Figure 4.12 in case 2, and it can observe that voltage is above the minimum permissible limit (0.95p.u.).

  The CES active and reactive power profile has been shown in Figure 4.13 which indicates that during charging state CES operates on unity power factor consuming the active power of 50 kW. However, during discharging state CES operates with 0.85 power factor feeding 45 kW active power and 27.88 kVAR reactive power into the system. From Figure 4.14, it can be observed that lowest voltage variation in Case 1 is about 2% throughout the entire year. However, Case 2 and Case 3 have approx. 0.6 % voltage variation Figure 4.14 box plot (case 3) represents the achieved energy savings with respect to load demand and wind DER power output variation for the entire year.

Table 4.7 Simulation results for scenario 2

Energy Terms		**Case-1**	**Case-2**	**Case-3**	**MWh Energy/Current Change, (%E_{Saving})**	
		Without CVR	**With CVR (VVO based CVR)**	**CVR With CES**	**Case-2 (VVO based CVR)**	**Case-3 (CVR with CES)**
Energy Demand (MWh)	**Phase A (Φ_A)**	10582.98	10418.4	10302.19	164.58	280.79
	Phase B (Φ_B)	6969.09	6860.774	6963.94	108.316	5.148
	Phase C (Φ_C)	8575.022	8439.938	8439.57	135.084	135.452
	Total	26127.1	25719.1	25705.67	407.98 (+1.56%)	421.39 (+1.61%)
Energy Losses (MWh)		56.1827	603.41	618.39	14.975 (0.057%)	14.975 (0.057%)
CVR factor (CVR_f)		-----	0.637	0.667	--	--
Neutral currents during (A)	**Highest Load (100%)**	180.54 A	174.65 A	156.52 A	5.89A	24.02A
	Lowest Load (56%)	98.317 A	84.215 A	68.39 A	14.10A	29.74A

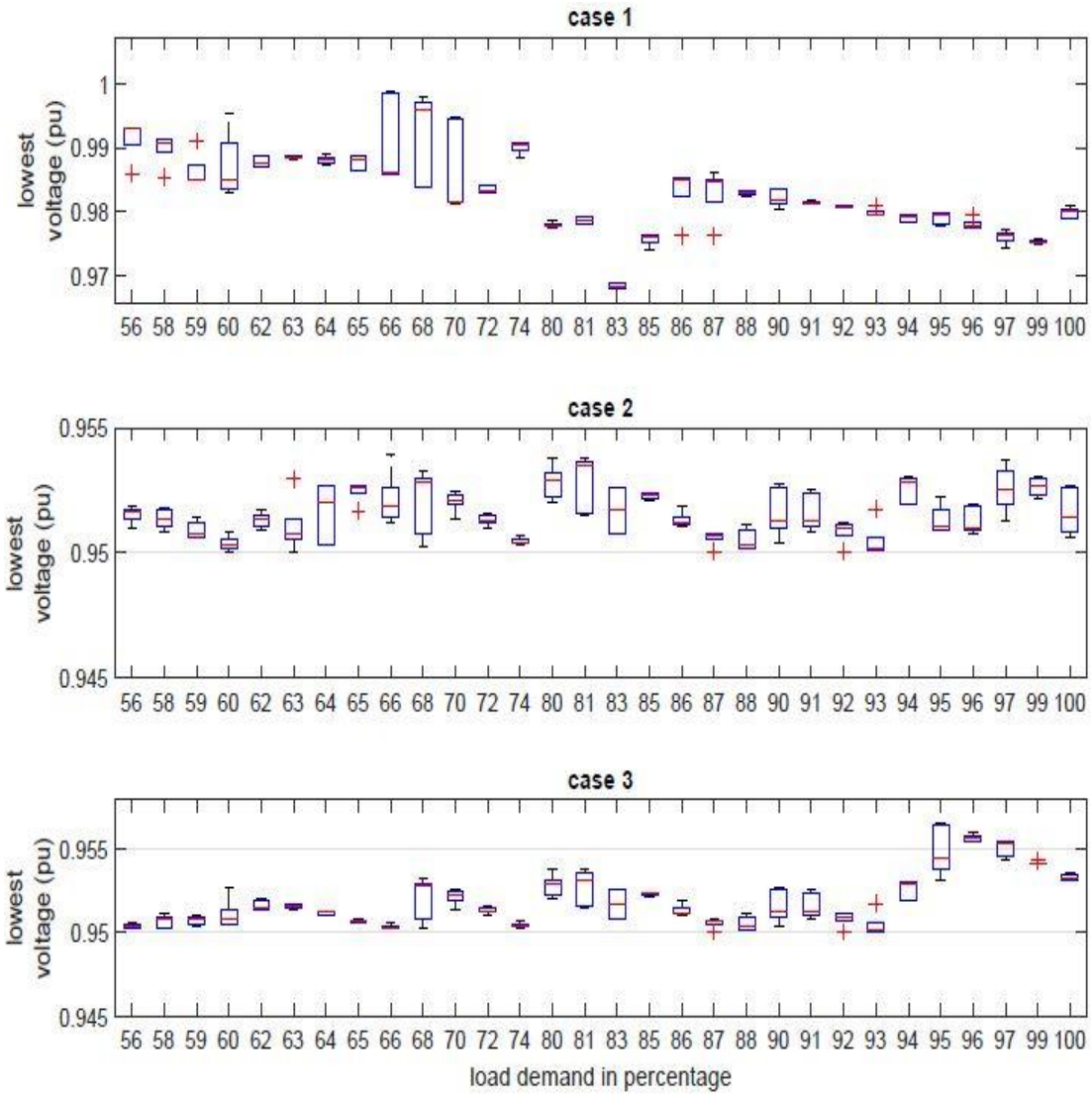

Figure 4.12: Feeder lowest voltage profile in different cases with varying load demand annually (a) *Case 1* (without CVR) (b) *Case 2* (with VVO based CVR) (c) *Case 3* (CVR with CES)

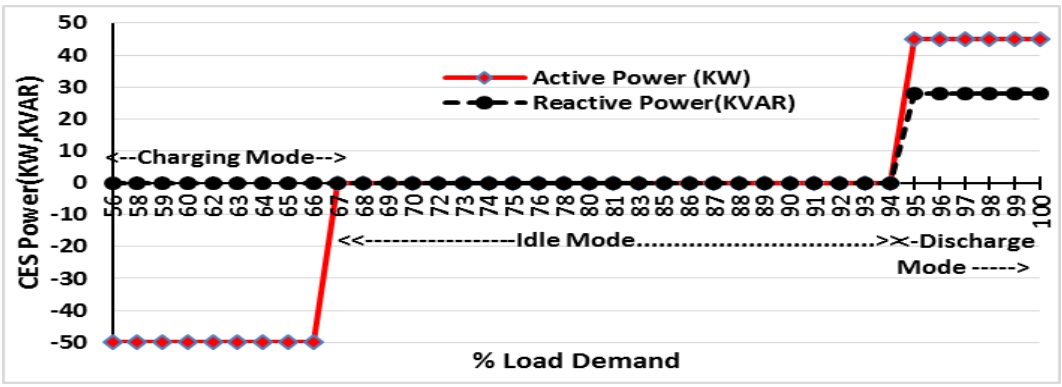

Figure 4.14: CES Active and reactive power profile

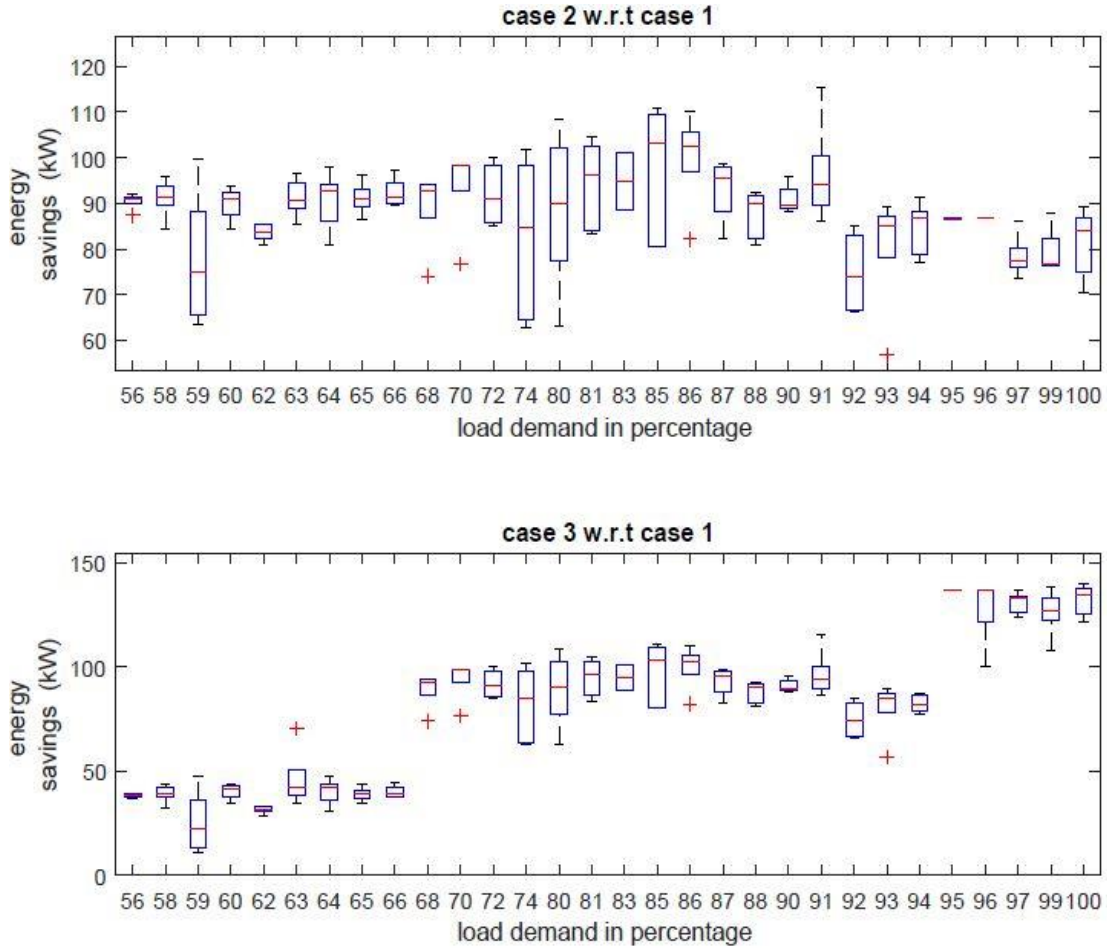

Figure 4.14: Energy savings (kWh) in *Case 2* and *Case 3* with varying load demand annually

4.6.2.4 Demand Balancing

Unbalance loading and imbalanced configuration produces operational issues such as the rise in neutral current and voltage in the distribution system. From the simulation results of Table 4.7, it can be observed that total energy demand is 26127.1 MWh and 25719.1 MWh for Case 1 and 2, respectively. In this, the share of phases A, B, and C are 40.5%, 26.67%, and 32.82%, respectively in both cases. However, in Case 3, the total energy demand shared by phases A, B and C are 40.0%, 27.09% and 32.83%, respectively. Moreover, in this case, there is a slight decrease in demand share of phase A and an increase in demand share of phase B in comparison to Case 1&2. The incremental change in demand share lead towards demand balancing. To elaborate further, the effect on

neutral current has been analyzed with VVO and CES. The magnitude of neutral currents at feeder head transformer during highest and lowest loading has been shown in Table 4.7 and it can be observed that higher reduction in neutral current has been produced with the application of both CVR and CES in comparison to Case1 and Case 2 in both loading scenarios. The decrease in neutral current assists in demand balancing. Hence, it can be concluded that the deployment of CES in association with the VVO engine is a helpful method for mitigation of rise in neutral currents.

4.6.3 Techno-economic Assessment

The performance of CVR scheme is assessed through energy, cost savings and CVR factors. The power and energy savings have been calculated using equations (4.1)- (4.2) for Case 2 and Case 3 operations. For cost savings estimation, equations (4.3) – (4.6) is directly applicable in Case 2 (only CVR) operation. However, cost-saving estimation during Case 3 (CVR with CES), the effect of CES operating and maintenance costs (C_{OMC}^{CES}) also be included in the cost function. The C_{OMC}^{CES} is further divided into two parts as first is the annual fixed CES operating and maintenance costs ($C_{OMC,Fixed}^{CES}$) and second is variable operation and maintenance cost ($C_{OMC,Var}^{CES}$) as defined in the below equations (4.36) and (4.37).

$$C_{OMC}^{CES} = C_{OMC,Fixed}^{CES} + C_{OMC,var}^{CES} \quad (4.36)$$

$$C_{OMC,Fixed}^{CES} = C1 \times Pces \quad (4.37)$$

$$C_{OMC,var}^{CES} = C2 \times \sum_t^T P_{Disch}^{CES}(t) \quad (4.38)$$

After adding the CES operating and maintenance cost the equation (4.6) can be rewritten as equation (4.39),

$$C_{cost}^{CVR\ with\ CES} = \sum_t^T [C_{Grid}(t) P_{demand}^{CVR}(t)] + C_{OMC,Fixed}^{CES} + C_{OMC,Var}^{CES} \quad (4.39)$$

The grid electricity (C_{Grid}) is dynamic changing throughout the year. For simplification, the annual grid electricity price has been split in three range first is 0.02$/KWh for load

demand up-to 75% loading, the second range is considered from 76 % to 94 % and electricity price is 0.3$/KWh. For the third range, i.e., from 94% to 100% load demand, the considered grid electricity price is 0.4$/KWh.

From Table 4.8, it can be observed that the cost savings achieved is about 1.67 % to 1.98 % annually with the deployment of CVR in Case-2(VVO based CVR) and Case-3 respectively. In Case-3, the achieved energy cost savings are much higher than the traditional CVR (LDC based method) and/or VVO based CVR and it can be clearly seen from Table 4.8 in both forms in terms of K$ and percentage. The economic CVR factor (K$) also higher in Case -3 in comparison to Case 2. Table 4.8 results also indicate that reduction in demand cost will directly result in under revenue collection temporarily for a utility point of view. However, this can be rectified later with suitable regulatory schemes such as revenue decoupling mechanism, which recovers revenue shortfall including any inevitable interest. The impact of CVR and CES technology on carbon emission has been studied. The emission rate and emission price have been taken as 0.4 tCo2e/MWh and $6.84/tCo2e, respectively. Table 4.9 shows the carbon emissions of the system in different cases. It can be observed that carbon emissions are reduced by amount 204.59 tCo2e and 217.49 tCo2e in case 2 and case 3 respectively. This is due to the maximum reduction of energy demand.

Table 4.8: Annual cost savings and economic CVR factor in both Case-2 and Case-3

Annual Cost Saving	**With CVR Only (Case -2)**		**CVR with CES (Case-3)**
	Traditional CVR	**VVO Based CVR**	
Saving in K$/year	96.534	134.9263	161.2716
Saving in percentage (%/year)	1.2	1.677228	1.98506
CVR factor in K$	0.491	0.67	0.807

Table 4.9: Annual environmental benefit in Case-2 and Case-3

Parameters	**Case1 (without CVR)**	**Case -2 (With VVO based CVR)**	**Case -3 (CVR with CES)**
Total demand (MWh)	22269.82	21758.33	21726.09
Co2 Emission (tCo2e)	8907.927	8703.332	8690.437
Reduction in Co2 emission (tCo2e)		204.59	217.49
Emission cost ($)	60930.22	59530.79	217.49
Savings in emission cost ($)		1399.428	1487.632

4.7 Conclusion

The VVO is a well-established method for improvement in the operation of distribution networks. The proliferation of CES has paved the way for achieving not only improvement in the system performance but also a reduction in peak load and demand balancing in addition. In order to utilize its benefits in CVR, VVO in association with CES approach has been implemented in this chapter. The investigation reported in present chapter focuses on the combined effect of CVR and CES on smart grid operation. The problem has been expressed as a Volt/VAR optimization problem, which minimizes the total power consumption while meeting the system constraints. The resulting optimization problem has been solved using DGSA driven VVO approach. The proposed methodology is capable of offering optimal coordination of VVO devices and VVO in association with CES in the presence of DER. The case studies on the modified 123 bus unbalanced system demonstrated that the proposed method effectively handled the VVO problem. The obtained results indicate that higher peak shaving, energy efficiency, peak load management, and reduced system losses are achieved when both CVR and CES are applied as compared to only CVR deployment. Besides, the cost-benefit analysis

authenticates the findings. Therefore, utility, prosumers and consumers would be benefitted under combined operation of VVO and CES for CVR technology.

Though the proposed single centralized VVO works well for fixed time step and constant power generation sources, but it lacks coordination with VVC devices under a sudden change in network behaviours such as variable power outputs from renewable DERs due to cloud transients' and other reasons. In this regard, next *chapter 5* presents a multi-stage multi-objective VVO methodology that takes care of both centralized as well as local VVC controls.

CHAPTER 5

MULTI-STAGE-MULTI-OBJECTIVE VOLT/VAR CONTROL AND OPTIMIZATION

5.1 Introduction

Widespread installations of DERs in low and medium distribution systems have enhanced the energy efficiency of the system and also helped to maximize the CVR utilization. However, large number of installations of DERs also resulting in some operational and control issues such as under/over voltage, reversible power flow, etc. Though, the centralized VVO can solve these issues to some extent but suffers from its adoption when sudden changes in the network behavior and lacks proper coordination during the intermittent behavior of PVs output. To resolve this issue, the authors of [19], [21], [77], [88], [91] have proposed PV smart inverter-driven control scheme to achieve a faster response of VVC. Besides, the VAR support through PV inverter using two-time scale VVC scheme has been introduced in [19]. The multi time-scaled CVR deployments using linear least square method has also been suggested in [20] incorporating PV inverter impact. However, this scheme needs efficient reactive power dispatch methodology in different timescales. Though in [19], [20] such schemes have been suggested, but the effect of system and inverter losses has not been addressed. Moreover, these issues are a matter of concern from the economic point of view as well.

On the other side, implementation of CVR does not guaranty the reduction in system losses, which may depend upon several other factors such as network topology, load models, and load types. Therefore, this chapter introduces a multi-objective VVO formulation operating in a multi time scale in the presence of multiple PV power plants.

Besides, multi-objective centralized VVO along with smart inverter-based local control algorithm has been proposed to address these issues during sudden changes and limited voltage reduction issues. The contribution of this chapter includes :i) A Multi-Stage Multi-Objective VVC (MSMO-VVC) algorithm for slow and fast time scale using Discrete Multi-objective PSO (DOMPSO) and droop characteristics scheme; ii) Demonstration of algorithm in the presence of PV system with different levels of penetrations and voltage reduction in distribution network; iii) Analysis of intermittent behavior of PV system output, application of PV inverter for faster response and effect of inverter losses; iv) Assessment of the proposed method in respect of technical and economic aspects.

5.2 MSMO-VVC Strategy

In this investigation, a multi-stage, multi-objective VVC strategy for smart grid-enabled CVR operation coordinated with multiple VVC devices in centralized as well local domain has been presented. The proposed MSMO-VVC aims to enable the CVR operation and meanwhile retaining the voltage profile within allowable range under uncertain behavior of PV power generation and variations in load demand profile. A closed-loop framework for smart grid-enabled CVR has been illustrated in Figure 5.1. It is the combination of VVO processor and CVR server assisted through ADMS. The ADMS is fed back by advance metering infrastructure, which updates the field monitored measurements at regular intervals. The fundamental task of VVO processor is to optimize the settings of VVC devices according to CVR server. The range of CVR duration and CVR voltage are set by control center operator in CVR server block according to requirement. Stage wise description of proposed control strategy has been delineated as under:

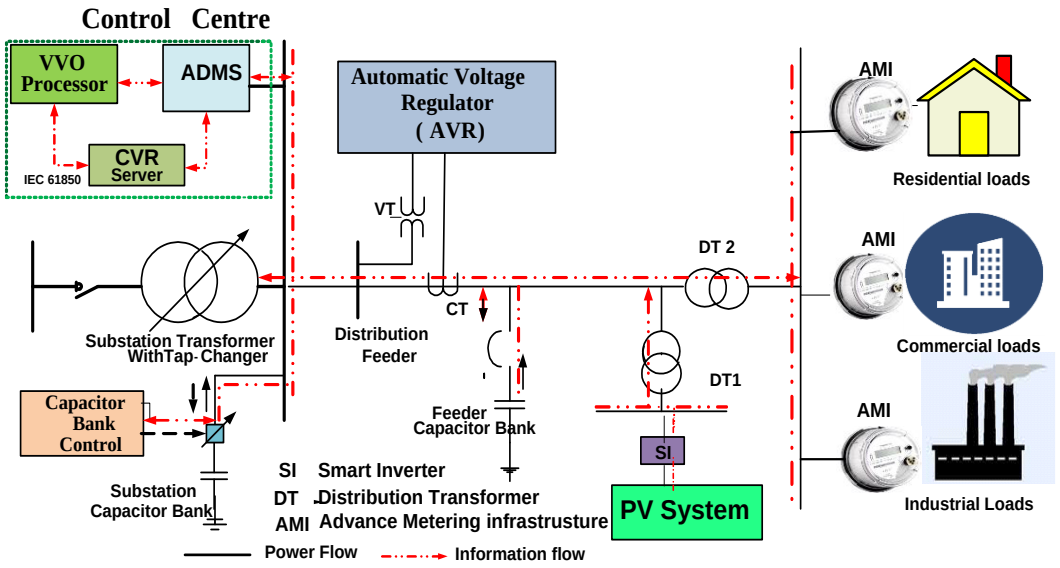

Figure 5.1 Proposed Substation Based closed-loop CVR

5.2.1 First Stage: Slow Time Scale Control (STSC)

In this stage, the actions of Volt/VAR regulating devices are optimized over a finite period with the coordination of central controller located at the substation control center. Therefore, this control is alternatively referred as a centralized control scheme. The control center operator fixed the CVR voltage level and sends control signals to the field devices.

The operation of this stage has been performed in two steps. Firstly, the expected CVR voltage and CVR time duration have been set through the CVR server. In the second step, the control parameters of Volt/VAR regulating devices have been optimized through VVO processor with the objectives of minimization of node voltage deviation from expected CVR voltage and system losses. ADMS regularly monitors and evaluates the power and voltage profile throughout the distribution network with the help of AMI.

5.2.2 Second Stage: Fast Time Scale Control (FTSC)

In the slow time scale stage, optimization of parameters of Volt/VAR regulating devices is carried out for a defined time horizon. However, during this time span (set in the first

stage), the deviation in PV active power with respect to forecasted value can be observed due to unexpected situations such as transient cloud movements, solar eclipse, etc. Consequently, it may cause violation of voltage limits. Therefore, the main objective of second stage is to maintain the voltage profile limits during the reduction of PV power output. The provision of decentralized or local domain-based additional reactive power compensation through fast time-scale control of inverter system has been suggested to fulfill.

A scheme using droop control-based principle has been employed to determine the compensating amount of reactive power from PV inverter such that VAR value is sufficient to achieve the desired voltage. In case, the PV output turns back to the forecast value or minimum allowable voltage is within limits, then the inverter output is retained to the optimal value as in the first stage.

5.2.3 Third Stage: Assessment of Proposed Control Method

The objective of third stage is to assess the employed CVR scheme in terms of amount of peak power reduction, energy, cost savings and CVR factors. In order to check the effectiveness of CVR in technical terms, CVR factor has been calculated in terms of peak kW power (CVR_{fP}) and kWh energy (CVR_{fE}). In the economic point of view, CVR factor has been calculated in terms of cost savings in purchased power. The detailed explanations have been already reported in *chapter 4* subsection 4.2.2 using equations (4.1) – (4.9).

5.3 Problem Formulation and Solution

The main objective of the present investigation is to achieve maximum energy demand reduction and peak shaving in a distribution network through CVR without violating the service voltage profile considering the transient behavior of PV power output. In order to

achieve this, the control scheme for CVR implementation has been formulated in two different time scale slow and fast as delineated under:

5.3.1 Optimal Control Action Under Slow Time Scale

Under the slow time scale control of CVR, the optimal settings of various controllers (OLTC/AVRs taps, steps of Q_{CBs} and Q_{PV} inverters) at the desired time have been determined. Mainly, the CVR is implemented by minimizing the node voltage deviation from expected CVR voltage without negotiating with the system regulatory standards. However, it has been observed that while applying CVR in order to reduce the voltage, increase in losses takes place [51], [20] which is an economically undesirable feature. To overcome, the problem has been combined to form a multi-objective formulation consisting of minimization of the voltage deviation and system losses.

Generally, multi objective optimization problem for N objectives formulated by equation (5.1).

$$\text{minimize } f(\vec{x}) = [f_1(\vec{x}), f_2(\vec{x}), f_3(\vec{x}), ... f_N(\vec{x})] \tag{5.1}$$

satisfying m inequality and p equality constraints equations (5.2) and (5.3) respectively.

$$g_i(\vec{x}) \leq 0 \;\; i = 0,1,2,3.....m \tag{5.2}$$

$$h_i(\vec{x}) = 0 \;\; i = 0,1,2,3.....p \tag{5.3}$$

where $\vec{x} = [x_1, x_2, ...x_n]$ is the decision variables vector.

Multi-objective optimization provides a set of optimal solution vectors rather than a unique optimal solution. An optimal solution vector has two possibilities that any solution can dominate other or no one dominates the other solutions. The nondominated solution (NDS) vector in the search space is defined as pareto-optimal solutions. These pareto

optimal solution vector produces near-optimal trade-off fitness values, which are known as the Pareto front surfaces.

5.3.1.1 Multi-Objectives:

The above discussed two objectives can mathematically, in terms of system variables, be expressed as:

- *First Objective Function (f_1):* The first objective function (f_1) has been represented as the minimization of the sum of the square of the deviation of node voltages from the expected CVR voltage in all phases and all nodes except source node at each hour to maximize the energy saving.

$$f_1 = \min\left\{\sum_{a,b,c}\sum_{i}^{N-1}\left(V_{i,h}-V_{CVR,h}\right)_{a,b,c}^{2}\right\} \tag{5.4}$$

where, $V_{i,h}$ is the node voltage (p,u.) at i^{th} bus at hour, h and $V_{CVR,h}$ is the expected CVR voltage (p,u.) at hour, h and N is the number of the nodes with phase notations of *a,b,c* respectively.

- *Second Objective Function (f_2):* Minimization of total system losses for all phases at each hour is the second objective function, f_2, which can be expressed as:

$$f_2 = \min\left\{\sum_{a,b,c}\left(P_{a,b,c}^{loss,h}+Q_{a,b,c}^{loss,h}\right)\right\} \tag{5.5}$$

where, $P_{a,b,c}^{loss,h}$ is the active power losses at hour, h and $Q_{a,b,c}^{loss,h}$ is the reactive power losses at hour, h.

5.3.1.2 System Constraints:

- *Transformer/regulator tap constraints:* The tap range of OLTC transformers/AVR and tap position are given in equations (4.18) and (4.19) respectively.

- *Transformer edging constraints:* In order to prevent the degradation of the life cycle of transformers, the daily tap operation of OLTC/AVR is governed by (3.18). In this study the value of $N^{i}_{tr,max}$ is considered 10 per phase.
- *Capacitor bank constraints:* Reactive power supplied by i^{th} CB (Q^{i}_{CB}) is determined using equation (1.12) and detailed explained in chapter 1 and daily switching operation of CBs should follow the relation shown in equation (3.11).
- *Solar PV Inverter:* Modern PV inverters have the capability to inject or consume the reactive power from the grid and operate as distributed Volt/VAR control devices. The more details can be found in chapter 1 subsection *1.4.2.3*.

The reactive power supplied by k^{th} PV inverter during slow time scale period ($Q^{k}_{PVst,T}$) is determined using equation (5.6).

$$Q^{k}_{PVst,T} = N^{k}_{PV}\ \Delta Q^{k}_{PV} \tag{5.6}$$

where, $N^{k}_{PV} = \{0,1,2....,N^{k,\max}_{PV}\}$, ΔQ^{k}_{PV} and $N^{k,\max}_{PV}$ are the switching step number, variation in reactive power per step and available maximum number of switching steps at k^{th} PV system respectively. The value of $N^{k,\max}_{PV}$ is dependent on at $Q^{inv,max}_{T}$ each time interval T

- *Voltage constraints:* Minimum and maximum voltage (V_{min}, V_{max}) at i^{th} node should remain within limits as shown in equation (3.13).

5.3.1.3 Solution through discrete multi-objective PSO

A multi-objective PSO approach has been employed to solve the desired optimization problem.

- *Overview of PSO:* Eberhart and Kennedy[135] introduced a powerful search-based optimization algorithm inspired by social behavior metaphor known as Particle

Swarm Optimization. The algorithm is initialized with a population array of particles with random velocity and positions in problem space to find the optima. The movement of a particle' position is based on its previous position and current velocity. PSO dynamic employs two main terminologies i.e. personal best (pbest) and global best (gbest). The pbest value of each particle is the best position so far it has achieved and best value among all pbest is called as gbest. The value of gbest at final iteration is the solution of the optimization problem.

- *Multi-Objective PSO(MOPSO):* The multi-objective optimization problem represented by equations (5.4) - (5.5) followed by system constraints has been solved using MOPSO approach. The MOPSO uses the repository to archive the positions of the particles that present nondominated solutions (NDS) so far [136]. The previously archived NDS leads the convergence toward globally NDS solutions. The velocity ($V_m^{K_r}$) and position ($X_m^{K_r}$) of each particle at K_r^{th} iteration is updated by equations (5.7) and (5.8), respectively.

$$V_m^{K_r+1} = wV_m^{K_r} + c_1 r_1 (P_m^{best} - X_m^{K_r}) + c_2 r_2 (P_r^{rep} - X_m^{K_r}) \quad (5.7)$$

$$X_m^{K_r+1} = X_m^{K_r} + V_m^{K_r+1} \quad (5.8)$$

where, w is inertia weight, c_1, c_2 are personal and global learning coefficients, r_1, r_2 are random numbers ranging between 0 and 1, P_m^{best} is the best position of the m^{th} particle and P_r^{rep} is a repository value. The position and velocity of the particles are updated and the value of objective functions calculated repetitively until the desired stopping criteria is not met. Multi-objective optimization provides a set of optimal solution vectors rather than a unique optimal solution. The NDS vector in the search space are defined as Pareto-optimal solutions. These pareto optimal solution vector produces near-optimal trade-off

fitness values, which are known as the pareto front surfaces. In order to determine the single optimal solution vector from various points generated by pareto dominance solutions, a minimum radial distance from the origin has been calculated. To achieve this, the normalization of fitness value concept has been employed using the equation (5.9).

$$\text{norm}(f(z)) = \frac{f(z) - \min(f(z))}{\max(f(z)) - \min(f(z))} \quad z \in \text{optimal pareto solutions} \tag{5.9}$$

- *Discrete MOPSO (DMOPSO):* Since the control variables (tap positions and switching steps) of the present problem are a discrete integer in nature; the MOPSO solution variable needs to be discretized. In order to do so, the solution variables obtained by (5.5) $X_{md}^{K_r+1}$, in the dth dimension are round off to its nearest integer value using the bracket function as shown in equation (5.10) [136]:

$$x_{md}^{K_r+1} = [X_{md}^{K_r+1}],\ d:\ 1 \rightarrow n$$
$$X_{md}^{K_r+1} \in \Re \ \text{and}\ x_{md}^{K_r+1} \in Z. \tag{5.10}$$

5.3.2 Action Under FTSC using Modified Droop Controller

In fast time scale, VVC has been carried out PV inverters only. The voltage regulation executed through inverter-based VAR dispatch. In order to determine desired compensating VAR from PV system, the droop characteristics based scheme has been utilized for PV inverter VAR control. The Volt/VAR droop characteristics for present problem is shown in Figure 5.2. It is piecewise linear to the voltage and changes dynamically due to its dependency on the PV active power . The droop characteristics is obtained by defining the four points (P_1, P_2, P_3 and P_4) parameters.

Determination of droop characteristics parameters are essential requirements because the reactive power compensation from PV inverters heavily depend upon defined values of

droop points and dead band. The settings of droop parameters vary according to the task requirements. The local control operator has flexibility to choose the appropriate setting according to their needs. In the droop control method, the dead band (DB) range plays an important role. Generally, it is defined as the width between points P_2 and P_3 in which inverter neither absorbs nor injects the VAR. In DB range, the compensated reactive power is zero. However, the PV inverter still feeds the reactive power as defined in STSC. Before the point P_2, inverter can inject the additional reactive power to the grid till point P_1 is reached. After point P_1, inverter can inject the available maximum reactive power. However, when the voltage is above point P_3, inverter absorbs aditional reactive power from the grid till point P_4. After point P_4 is reached, inverter absorbs the available maximum reactive power. The compensated reactive power($\Delta Q_{com,t}^{inv}$) at any instant, t is determined using (5.11).

$$\Delta Q_{com,t}^{inv}(V) = \begin{cases} Q_t^{inv,max} & V < V_1^{P_1} \\ \dfrac{V - V_1^{P_1}}{V_1^{P_1} - V_2^{P_2}} Q_t^{inv,max} & V_1^{P_1} \le V < V_2^{P_2} \\ 0 & V_2^{P_2} \le V \le V_3^{P_3} \\ -\dfrac{V - V_3^{P_3}}{V_4^{P_4} - V_3^{P_3}} Q_t^{inv,max} & V_3^{P_3} < V \le V_4^{P_4} \\ -Q_t^{inv,max} & V > V_4^{P_4} \end{cases} \tag{5.11}$$

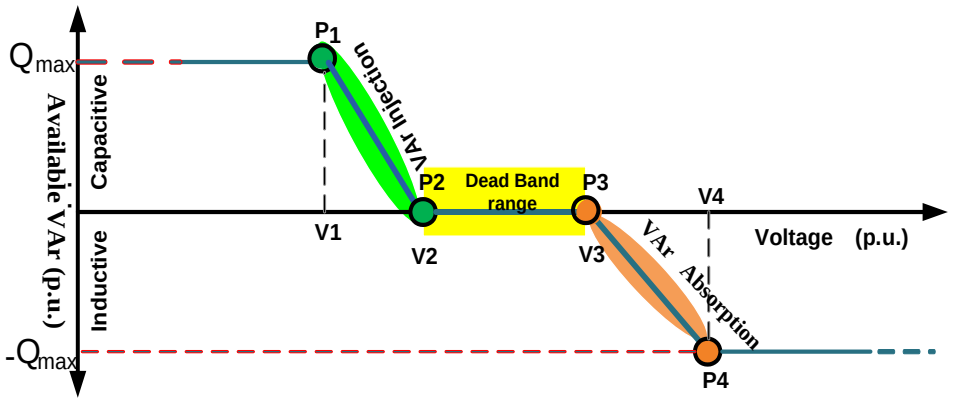

Figure 5.2 Volt/VAR droop characteristics

where, $Q_t^{inv,max}$ is the maximum VAR capacity of the inverter at instant, t, as defined in equation (1.16).

$$Q_{Total,t}^{inv} = Q_{PVst,T}^{k} \pm \Delta Q_{com,t}^{inv} \leq \left| Q_t^{inv,max} \right| \quad (5.12)$$

where $Q_{PVst,T}^{k}$ is the optimal VAR value during first stage.

5.4 Implementation of Proposed MSMO-VVC

Figure 5.3 shows the flowchart of the implementation of the proposed MSMO-VVC method with various stages, as described below.

The stepwise execution procedure of *First Stage* (STSC) has been described done in *algorithm 1* as under:

Algorithm 1 STSC Parameters optimization using DMOPSO	
1	**Input:** Feed the distribution network data {loads, lines, VVC devices and PV plant data (if PV present)}
2	**Input:** PSO parameters and control varriable limit
3	Set the expected CVR voltage and CVR time duration.
4	Divide the particle dimensions among control variables (as tap positions of OLTC, AVRs, and switching steps for CBs & PV inverters)
5	Set the stopping criteria (maximum number of iterations)
6	Initialize the population and speed of all the particles and perform load flow analysis.
7	Evaluate the value of fitness functions expressed using (5.4) and (5.5) for each particle.
8	Find P_{best} and G_{best} of the particles
9	Identify the positions of the particles that represent nondominated vectors and store in the (P^{rep}) repository.
10	Update velocity and position of each particle using (5.7) and (5.8), respectively.
11	Evaluate the position of the particles and update the P^{rep} repository.
12	Check the stopping criteria if yes then go to 13 else go to step 6.
13	Determine the single optimal solution vector using a minimum radial distance from the origin.
14	Prioritize the solution, further assigning the proper weightages to the objective functions.
15	**Output:** Adopt the VVC settings corresponding to top priority objective.

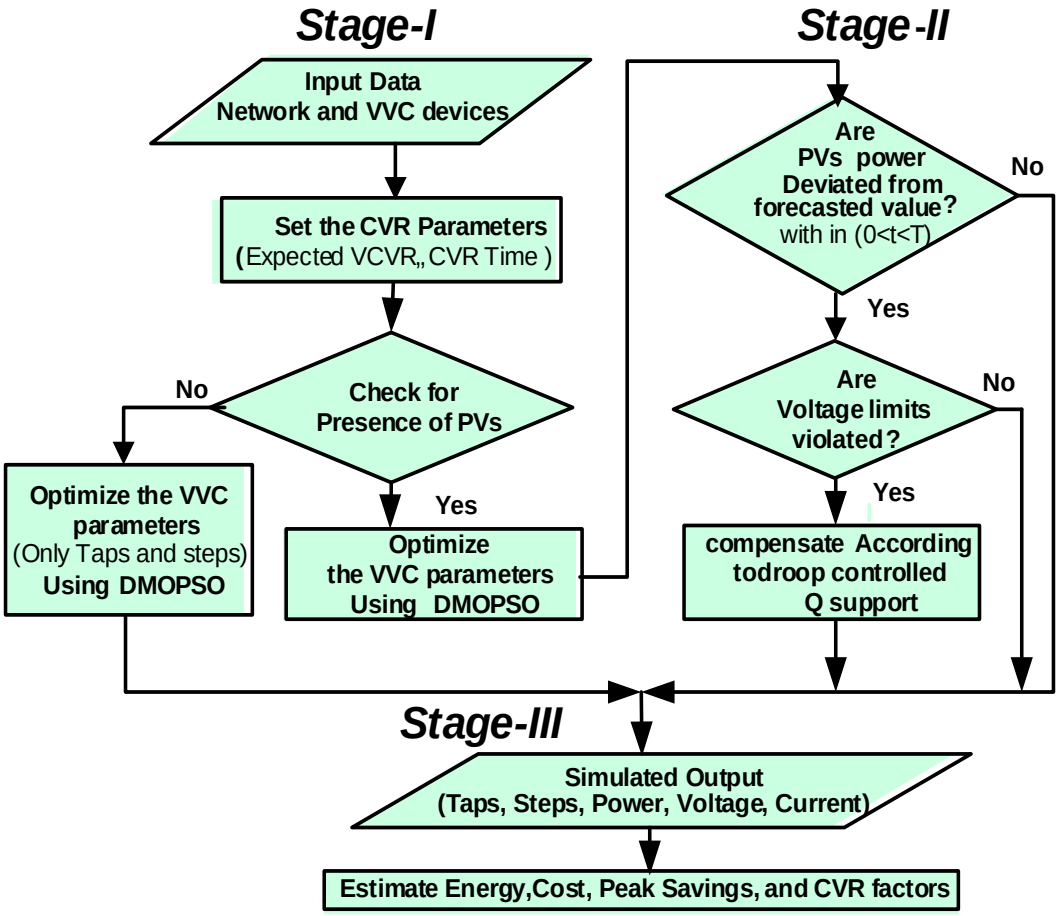

Figure 5.3 Flow chart of implementation of three stages of proposed method

The solution obtained from *Algorithm 1* can directly be implemented for CVR operation for first stage.

- In the *Second Stage* (FTSC) implementation, the DMOPSO solution include the reactive power compensations in case of voltage limit violation due to the deficit in PV system output. The droop control action solution obtained from algorithm 2 directly implemented in stage 2.
- The solutions obtained from *algorithms 1 and 2* can be directly utilized in the *Third Stage* for the estimation of the total active power demand reduction, ΔP_{demand}, energy savings, ΔE_{saving}, cost savings, ΔC_{saving} and CVR factors using equations (4.1) – (4.9). respectively.

Algorithm 2 Droop based controller for FTSC

Input: Feed the optimal VVC parameters for considered CVR duration obtained through Algorithm 1
Input: Feed the droop characterstics parameters (P_1, P_2, P_3 *and* P_4 and dead band)
for time duration 0< t < T (as defined in STSC)
If, PV power output deviates from forecasted value
Then check the voltage limits
Else if voltage profile is in dead band range (between point P2 and P3)
Control action: No action is required.
Else if *lower limit of voltage is violated*
Then droop controller operates in capacitive region (before point P2) as shown in Figure 5.2
Control action: Injects the compensated reactive power determines by equation (5.11) followed by equation (5.12)
Else if *upper limit of voltage is violated*
Then droop controller operates in inductive region (after point P4) as shown in Fig.2
Control action: Absorb the compensated reactive power determines by equation (5.11) followed by equation (5.12)
Else follow the same instruction as suggested by *Algorithm 1*
end
Output: Desired additional reactive power compensation has been achieved

5.5 Simulations and Validation

5.5.1 Test System

The proposed CVR control has been validated on the modified IEEE 123 node distribution test feeder with the composite ZIP load model as shown in Figure 5.4[114]. The values of ZIP coefficients can be found in Appendix A in Table A.2.The optimization and control strategies have been developed in MATLAB, while test system modeled and load flow analysis has been done in the OpenDSS platforms. The test system consists of one OLTC, three AVRs, four switched shunt CBs and three PV systems. The OLTC and AVR transformers have ±16 taps with a per step increment of 0.00625. The OLTC

substation transformer is connected between nodes 150-149. The other three distributed AVRs are connected between nodes 9-14(AVR-1), 25-26(AVR-2), 160-67(AVR-3) respectively. The three-phase CB (Cap-1) is connected to node 83, having 200 kVAR per phase capacity with step variations from 0 to 4. Three single-phase CBs (Cap-2, Cap-3and Cap-4) are connected to node 88_a, 90_b, and 92_c, respectively, having a maximum rating of 50 kVAR. The three PV systems are connected to nodes 65abc (PV_1) 26ac (PV_2), and 104c (PV_3) with the inverter ratings of 1000 kVA, 800 kVA and 400 kVA respectively. Per step, reactive power variation from PV inverter is 50 kVAR for slow time scale. Moreover, the total KVA load demand shared by phase a, b, c is 40.5%, 27% and 32.5% respectively. The hourly load demand and grid electricity price (Indian Energy Exchange–Northern Grid (N2)) for an entirely typical day has been taken from [134] and [137] as shown in Figure 5.5. The controlling parameter used in DMOPSO is depicted in Appendix B in Table B.1

.

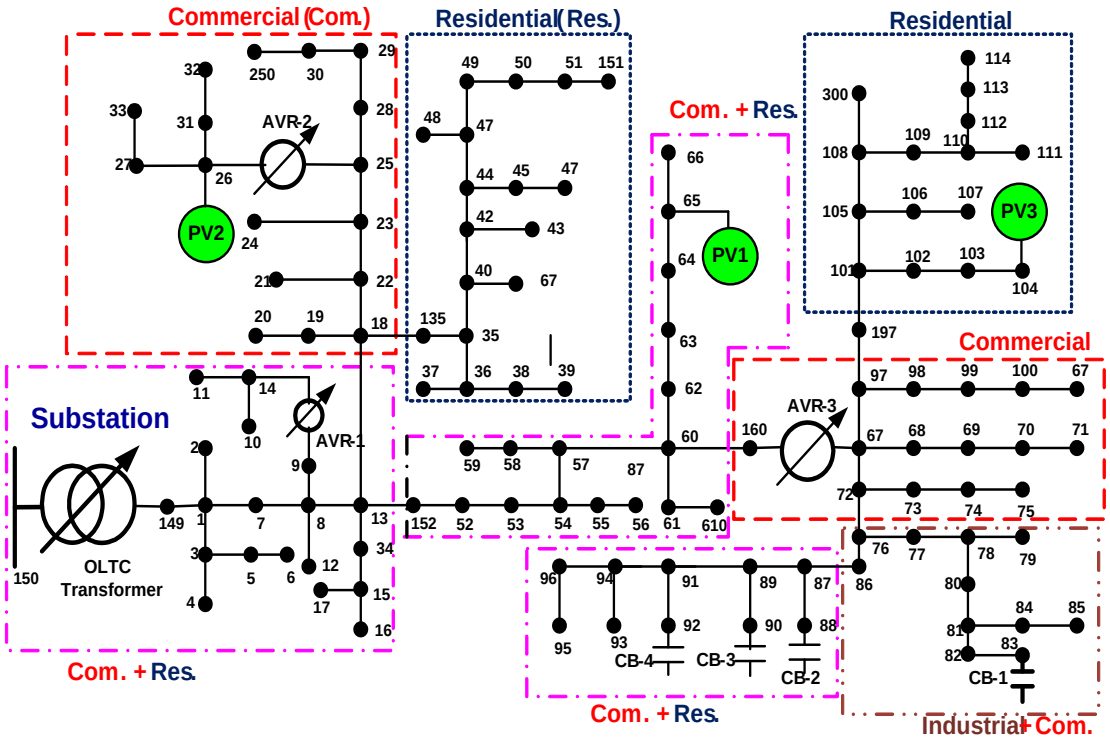

Figure 5.4 Modified IEEE 123 node distribution test feeder

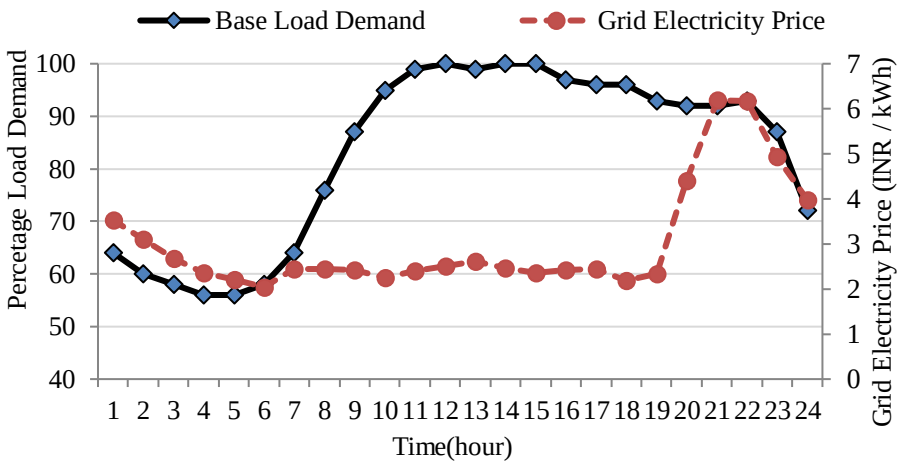

Figure 5.5 Hourly load demand and grid electricity price curve

5.5.2 VVC Modes of Operation

The performance of proposed method has been validated for two different time scale (slow and fast) under the following three different modes of VVC operation.

- *Mode 1: No-CVR (Base or Normal Operation):* In this mode, the system does not deploy CVR for VVC operation. The execution of VVC has been carried out with OLTC, AVR-1, AVR-2 at 120V regulated voltage and AVR-3 at 124 V. The fixed CBs have been used. Impact of PV power has not been considered.
- *Mode 2: Only CVR:* In this mode, the operation of VVC devices is carried out with proposed optimal CVR scheme using DMOPSO. The integration with PV system has not been considered in this mode of operation also.
- *Mode 3: CVR with PV:* In this mode, the proposed CVR scheme deploys with PV system also. The allocation of PV systems has been determined based on minimum node voltage.

5.5.3 Validation Under Slow Time Scale Control

The validation of the proposed method under STSC has been studied for two scenarios; peak shaving and daily energy-saving under the above-mentioned modes of VVC operation.

5.5.3.1 Scenario-I Peak Shaving

Peak shaving through CVR during a typical day has been studied in this scenario. The 14th hour of the daily load curve (as shown in Figure 5.5) is considered as a peak loading hour. The test system has been simulated for three modes of VVC operation at considered peak load hour.

- *Mode 1:* The simulation results of this mode are depicted in the second column of Table 5.1. Total active power demand and losses are 3619.2 kW and 96.7 kW respectively. Vmin and Vmax are 0.9787 and 1.0482 observed at nodes 65a and 83b respectively.
- *Mode 2:* The test system is simulated for only CVR with the proposed method. The NDS at $V_{CVR,h}$ of 0.95 p.u. at peak loading hour of 14th hour has been obtained. The pareto dominance front of these NDS are shown in Figure 5.6(a). In order to figure out the single set of decision variables from obtained NDS, a priority-based scheme has been used for decision making. A weightage of 70% has been assigned to the first objective function. The corresponding weightage factor is multiplied with the normalized fitness value of first objective function while calculating the distance from the origin. The simulated results of corresponding decision variables for this mode are depicted in the third column of Table 5.1. From the above results, it has further been observed that about 85 kW demand (2.35% peak power demand) has reduced with small reduction of 0.3% in system losses within the allowable voltage range. The effect of variation in expected CVR voltage (V_{CVR}) on kW peak demand reduction is shown in Figure 5.7 This figure illustrates that the percentage peak demand reduction increases with a reduction in CVR voltage within the expected range.
- *Mode 3:* In this mode, CVR is applied with PV power penetration in addition to earlier mentioned VVC devices. In order to choose the unique solution from NDS, the

procedure of Mode-2 has been adopted. The study of this mode is carried out for different levels of penetration under three cases. The pareto dominance fronts of these cases are shown in Figure 5.6 (b). The simulation results are depicted in fourth column of Table 5.1.

i) Case-I: CVR with 30% PV Penetrations (Single PV): CVR is deployed with 30% PV penetrations during peak load demand of 14^{th} hour of load duration curve shown in Figure 5.5. Active and reactive power injected by a three-phase PV1 source at node 65abc. Simulation results and other parameters such as PV power supplied, tap positions and CB steps are depicted in fourth column of Table 5.1. From the results, it can be observed that system active and reactive power losses reduced about 37.2% after and 42.9 % respectively. Total peak active power purchase from transmission grid has been reduced to 30%.

ii) Case-II: CVR with 50% PV Penetrations (Two PVs): In this case, CVR is applied along with 50% PV penetrations using three-phase PV1 and two-phase PV2 systems at 65abc and 26ac nodes. The total active & reactive power losses have been reduced to 46.1% and 53.45% respectively. Peak active power has reduced to 50.45 % without affecting customer devices.

iii)Case-III: CVR with 60% PV Penetrations (Three PVs): In this case, CVR is applied along with 60% PV penetrations using three-phase PV1, two-phase PV2 and single-phase PV3 systems at 65abc, 26ac and 104c respectively. The total active and reactive power losses have been reduced to 47.98% and 55.77% respectively. Peak active power has reduced to approx. 60 %. Though, during higher PV penetrations without incorporating

CVR affect results in overvoltage problem. However, this issue can be resolve deploying CVR at higher PV penetration levels.

The effect of different expected CVR voltage on KW peak demand reduction during PV penetrations with and without CVR is shown in Figure 5.8. This figure illustrates that peak shaving is higher in PV with CVR instead off only PV.

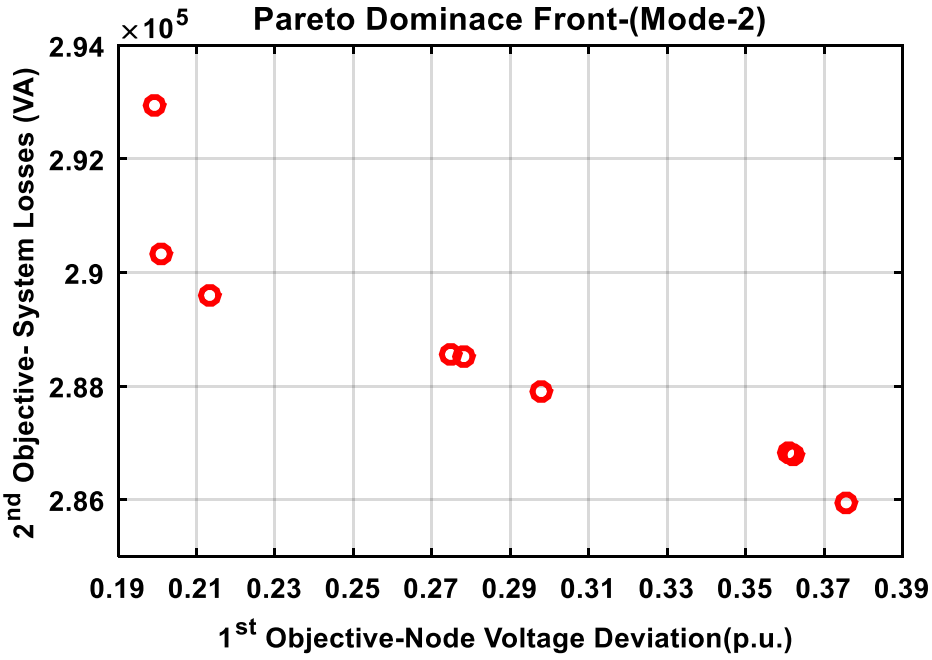

(a)

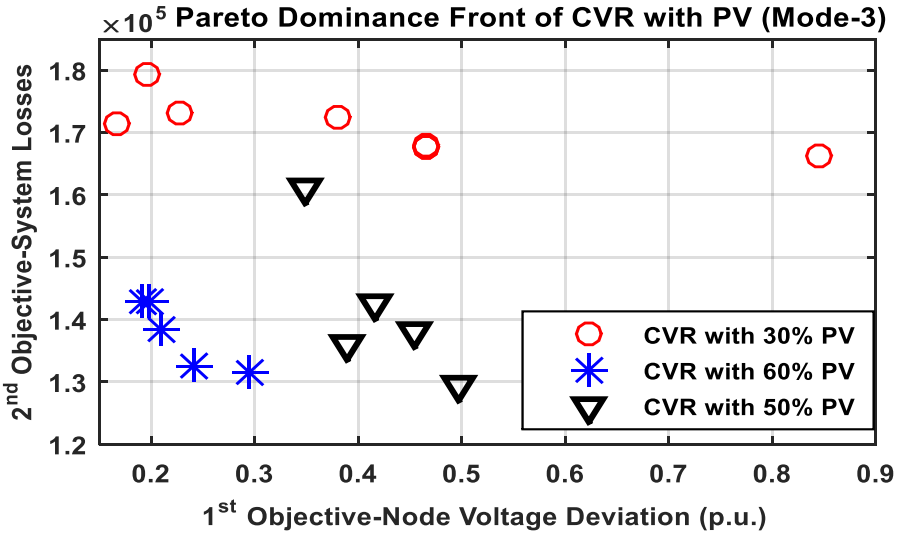

(b)

Figure 5.6 (a) Pareto dominance front for mode-2 (b) Pareto dominance front for CVR with PV

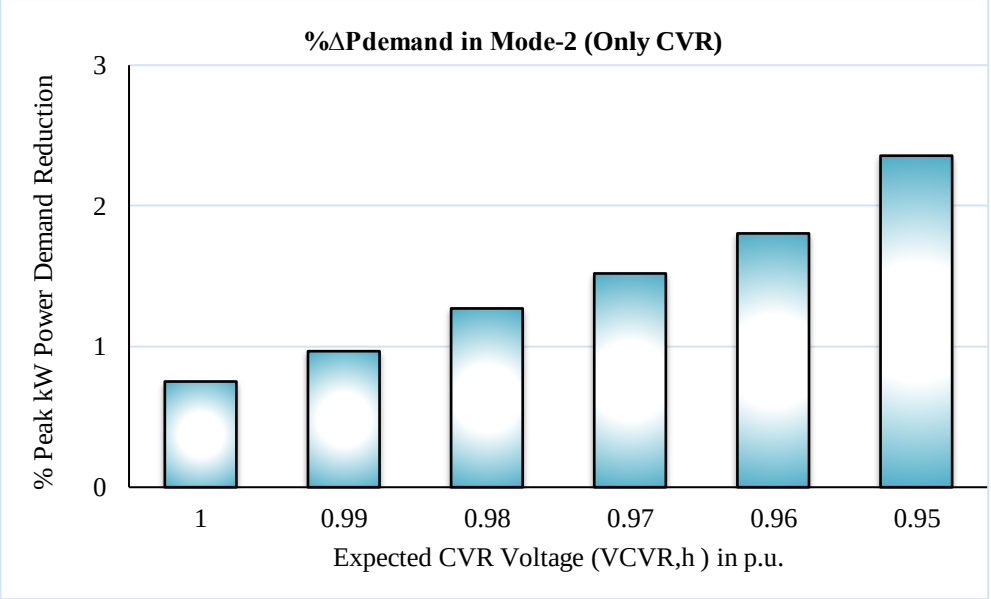

Figure 5.7 Active (kW) power demand reduction with different $\%V_{CVR}$ at peak load during Mode-2 operation

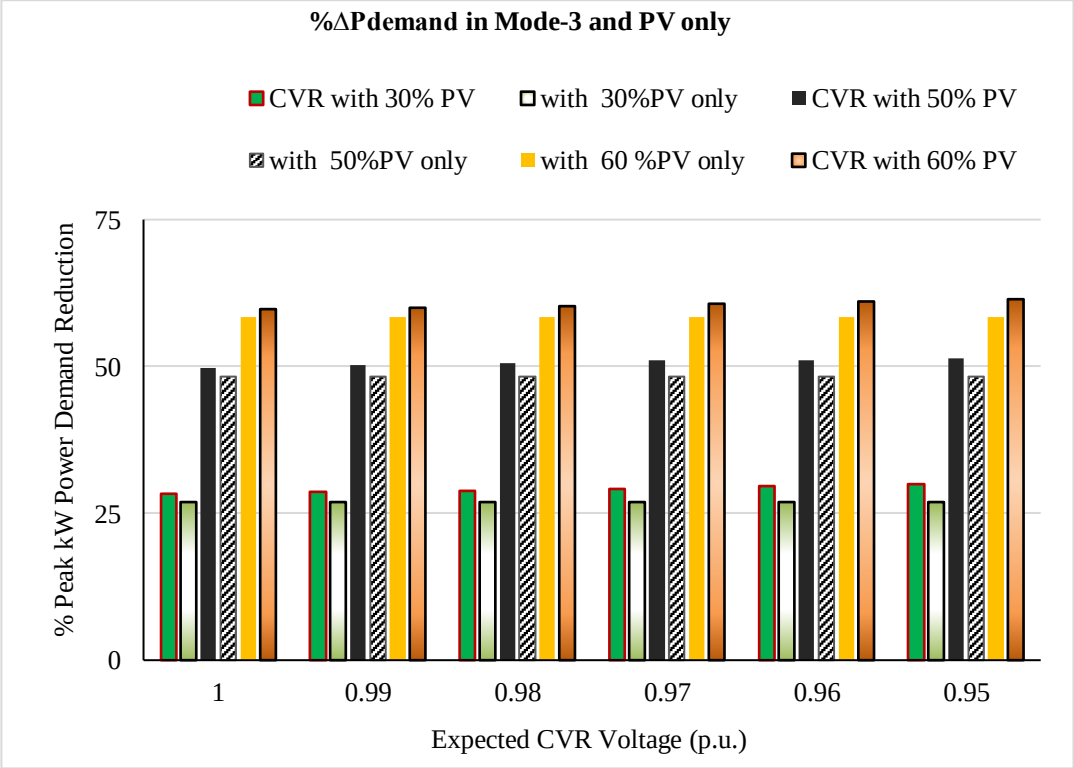

Figure 5.8 Active (kW) power demand reduction with different $\%V_{CVR}$ at peak load during Mode-3 operation and PV only

Table 5.1 Simulation Results of Scenario I

Parameters		**Mode-1 (No-CVR)**	**Mode-2 (CVR Only)**	**Mode -3 (CVR with PV Penetrations)**		
				30% PV	**50%PV**	**60% PV**
P_{demand} (kW)	**Φa**	1467.1	1434.1	1091.1	700.8	707
	Φb	962.5	941.2	615.9	614.6	613.2
	Φc	1189.6	1158.6	829.3	444.6	74.7
	Total	3619.2	2536.2	2536.2	1760.0	1395.0
ΔP_{demand} (kW)	**Φa**	---	33	376	733.3	727.1
	Φb	---	21.3	346.6	347.9	349.3
	Φc	----	31	360.3	745	1114.9
	Total %	----	85 (-2.35)	1082.9 (-29.9)	1826.2 (-50.45)	2119.3 (59.55)
Plosses, kW		96.7	96.46	60.7	50.6	50.3
Qlosses, kVAR		193.8	193.15	110.6	90.2	85.7
ΔPlosses, kW (%)		---	0.284 (-.3)	36 (-37.2)	46.1 (47.63)	46.4 (-47.98)
ΔQlosses, kVAR, (%)		------	-0.63 (-0.32)	83.2 (-42.9)	103.6 (53.45)	108.1 (-55.77)
P(kW), Q(kVAR) injected	**PV1**	--	----	960,200	960,100	960,200
	PV2	---		----	768,000	768,100
	PV3	----		----	---	368,100
Vmin (p.u), At node		0.9787 (65a)	0.9515 (32a)	0.9518 (114a)	0.9517 (114a)	0.9505 (114a)
Vmax (p.u), At node		1.0482 (83b)	1.0121 (150)	0.9994 (150)	1.0195 (150)	1.0334 (26)
Tap Position	**OLTC**	{+6}	{+2}	{0}	{0}	{0}
	AVR-1	{0}	{-3}	{0}	{0}	{0}
	AVR-2	{ +2, 0}	{1, -4}	{5, 4}	{ 5, 4}	{ 5, 4}
	AVR-3	{10,4,6}	{3,-4,2}	{1-2,1}	{1-2,1}	{1-2,1}

5.5.3.2 Scenario-II Daily Energy Savings

In order to reduce the daily energy demand, CVR has been employed for a typical whole day with and without PV penetrations through proposed CVR approach. Daily load demand and grid electricity price profile shown in Figure 5.5 has been considered. In order to demonstrate the effectiveness of the proposed method, the forecasted active power profile of PV systems has been assumed as shown in Figure 5.9. The simulation of the test system has been carried out in all three modes. The simulation results have been depicted in Table 5.2. It can be observed from this table that in Mode-2 operation the daily energy saving of about 1.5 MWh has been achieved with a 0.3 % reduction in energy losses. Thus about 2.1% of energy demand has been reduced without compromising system voltage profile. However, the energy losses it can further be reduced with the penetration of PV power.

CVR operation with different levels of penetration as 30%, 50%, and 60% have been carried out in mode-3 operation. Simulated results depicted in Table 5.2 shows that up to 18.65 to 28% and 21.22 to 31.5% reduction in active (ΔE^{P}_{losses}) and reactive (ΔE^{Q}_{losses},) energy losses respectively have been obtained with various levels of PV penetrations. The optimal reactive power injection has been provided from PV inverters when load demand is above 60% of peak load when higher losses take place. The impact of PV inverter losses has also been considered while calculating total losses. Figure 5.10 shows the optimal reactive power support from PV systems at various levels of penetrations. In case 60% PV penetration is applied without CVR operation, an undesirable event of rise in voltage above the upper threshold (1.054 p.u. at 12:00th hour) has been observed. However, when high-level PV penetration is carried out with CVR, the maximum node voltage has been found to be 1.033 p.u., which is within the permissible range. Even then there is a scope of further increase in PV penetration level

until maximum node voltage up to upper threshold of 1.05 p.u. is observed. Figure 5.11 shows the daily OLTC tap positions.

Table-5.2 Simulation Results of Scenario II

Energy Terms	**Mode-1 (No-CVR)**	**Mode-2 (CVR only)**	**Mode-3 (CVR with PV Penetrations)**		
			30%	**50%**	**60%**
E_{demand} (MWh)	71.967	70.449	62.380	56.001	53.046
ΔEsaving (MWh), %	----	1.518 (2.1)	9.587 (13.32)	15.96 (22.18)	18.92 (26.29)
E^{P}_{losses}, MWh	1.675	1.667	1.3625	1.2430	1.2051
E^{Q}_{losses}, MVARh	3.350	3.326	2.639	2.4019	2.2950
Δ E^{P}_{losses} , kWh (%)	---	8 (-.3)	312.5 (18.7)	432 (25.79)	470 (28.05)
ΔE^{Q}_{losses}, KVARh, (%)	------	24 (0.716)	711 (21.22)	948.1 (28.32)	1055 (31.5)

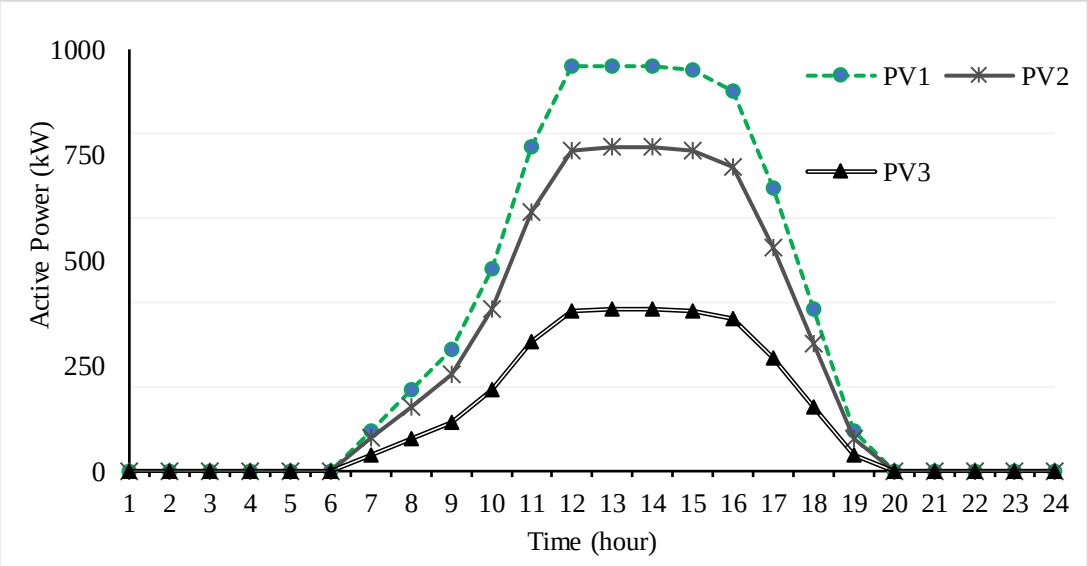

Figure 5.9 Active power profile of PV power systems

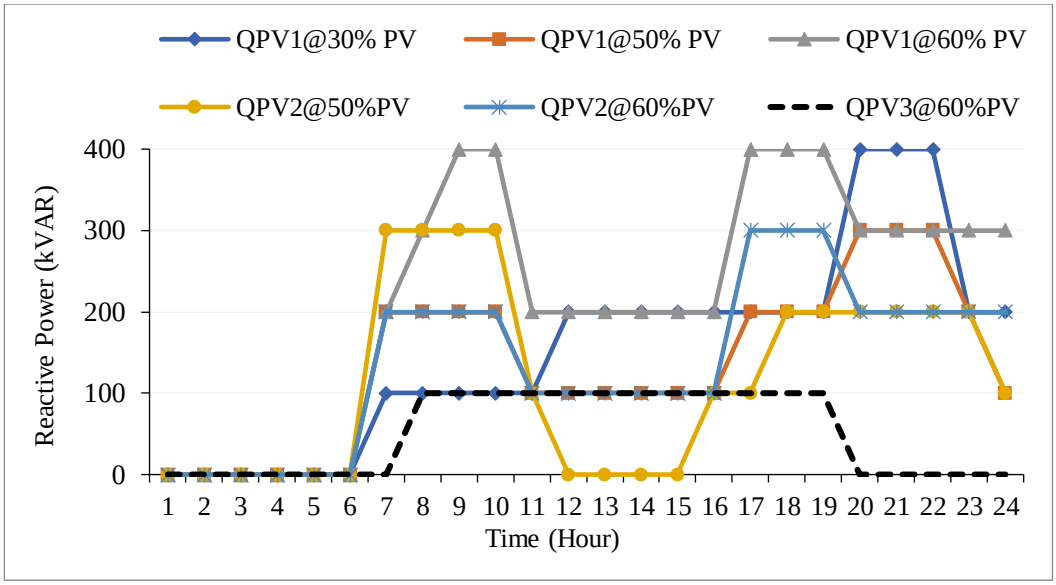

Figure 5.10 Optimal reactive power support from PV inverters

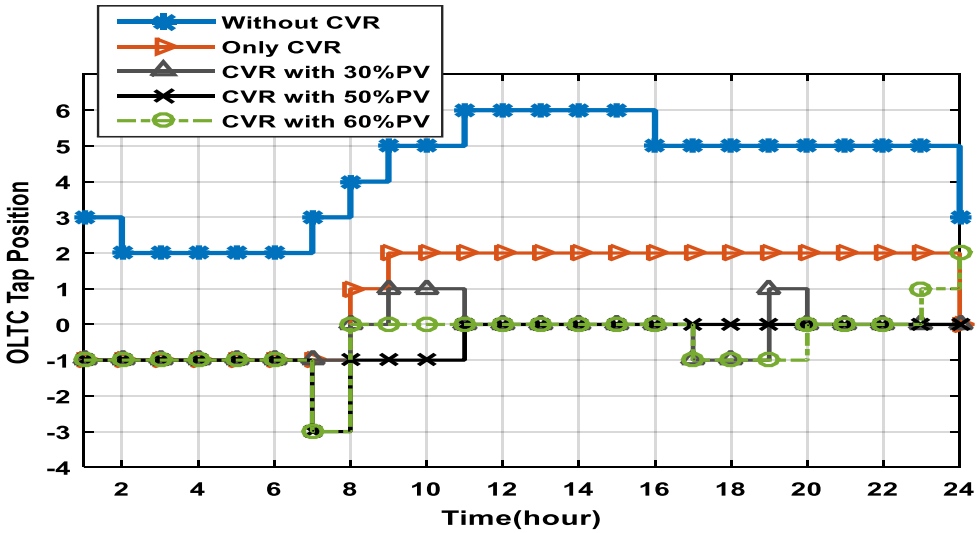

Figure 5.11 OLTC tap position of all modes of operation.

5.5.3.3 Technical and Economical Assessment

The performance of CVR scheme is generally assessed through CVR factor and energy saved. The CVR factors under Mode-2 and Mode-3 operation for both the scenarios has been shown in Figure 5.12. It can be observed from the figure that kW (CVR_{fP}), kWh (CVR_{fE}) and INR (CVR_{fC})) are higher in Mode-3 in comparison to Mode-2. CVR factor in economic terms represents cost savings with respect to voltage reduction.

From Table 5.3, it can be observed that the cost savings achieved is about 2.07 % to 3.31 % with the deployment of CVR in Mode-2 and Mode-3 respectively. While calculating the savings in Mode-3, operational and maintenance cost has been neglected. Table 5.3 presents the reduction in demand cost, loss cost, and total cost also with the enabling of CVR in both Mode-2 and Mode- 3. The reduction in demand cost will directly result in under revenue collection temporarily for a utility point of view. However, this can be rectified later with suitable regulatory schemes such as revenue decoupling mechanism which recovers revenue shortfall including any inevitable interest.

Table 5.3 Demand cost,Loss cost and Total cost saving

Mode		**Demand Cost (kINR)**	**Loss Cost (kINR)**	**Total Cost (kINR)**	**Cost Saving in**		
					kINR	**$***	**%**
Mode-1		215.39	5.148	220.543	-----	---	--
Mode-2		210.85	5.127	215.98	4.53	69.7	2.07
Mode-3	**30%PV**	191.85	4.374	196.228	5.46	84	2.69
	50%PV	176.53	4.086	180.622	5.98	92	3.21
	60%PV	169.44	3.998	173.439	5.93	91.2	3.31

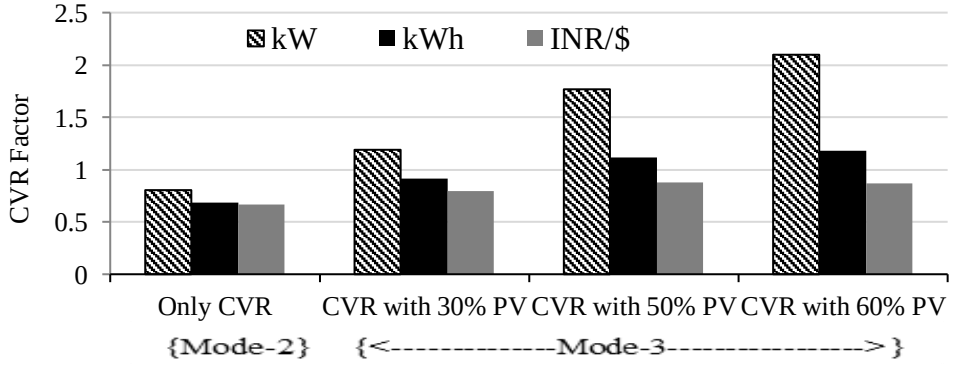

Figure 5.12 CVR factors in terms kW, kWh, INR/$ under Mode-2, and Mode-3

5.5.4 Illustration of Second Stage (FTSC): Local Voltage Control

In order to analyze the effect of fast time scale control, under CVR with 60% PV penetration has been studied. An arbitrary instantaneous point between time intervals from 15:00 to 16:00 has been selected. The load demand is 97% of peak demand at this point and forecasted solar irradiation is 94% of the peak. During this time span, the lowest voltage profile at node 114a becomes vulnerable to any reduction in kW power. Status of Volt/VAR regulation devices OLTC, AVRs, and CBs remain same as in the first stage determined by *algorithm 1*. The fast time scale control has been applied and illustrated for two cases. The droop parameter used in this study is depicted in Appendix B in Table B.2.

5.5.4.1 Case 1 : Single PV power output reduction

In this case, the droop control scheme has been studied when active power for only one PV (PV1) has been varied. The output of other PV systems (PV2 and PV3) remains unchanged. The resulting variation in voltage profile of node 114a with respect to percentage reduction in PV power output has been shown in Figure 5.13. It can be seen that up to 30% reduction in PV1 power output, the lowest voltage remained within minimum allowable voltage limit. Thereafter, the lowest voltage limit violated as the reduction in PV1 power output increases. In order to mitigate the voltage violation, the droop controlled compensating reactive power support has been provided through PV1 inverter. The variation in reactive power support from PV1 inverter has been shown in Figure 5.13. It can be seen from this figure that up to 30% PV power reduction, the injection of compensated reactive power is zero because of lowest voltage profile is within dead-band range. Afterward, the droop controller injects the desired compensating reactive power to meet the lowest voltage profile within the allowable range even when PV1 active power is fully reduced. The effect on active power losses due to the injection

of reactive power from PV inverter has been shown in Figure 5.14. The figure illustrates that total active power losses have also been slightly reducing with droop control action, though the inverter losses are increasing with the control action of droop controller. It happens due to the regeneration of reactive currents in inverter circuitry. Generally, inverter losses due to reactive power compensation are 1-2% of injected/absorbed power. Moreover, the relation $P_t^{inv} = P_t - P_{t,loss}^{inv}$ shows that inverter losses are accommodated P_t unless the value P_t is not zero or not sufficient. From Figure 5.13, at the point when PV1 power is reduced 100 %, the inverter takes power from the grid to bear the inverter losses. In this condition, a slight increase in total active power losses take place as seen in Figure 5.14.

5.5.4.2 Case 2 : Multiple PVs power output reduction

The mutual interference effect has been studied in this case when simultaneously reduction in active power output from more than one PVs is applied. The droop control scheme has been examined by reducing the active power output of both inverters PV1 and PV2 simultaneously. The minimum allowable voltage profile has been observed up to at 29% reduction in power output from both PVs. Further reduction in output would cause a minimum voltage profile violation. In order to mitigate the further reduction in voltage, the compensated droop controlled reactive power support has been enabled through PV1 inverter only. The resulting effect shown in Figure 5.13 indicates that reactive power from PV1 inverter alone is capable of mitigating the voltage violations. The effect on active power losses due to the injection of reactive power from PV inverter has been shown in Figure 5.15. The figure shows that there is a small reduction in total active power losses with droop control action. However, when the reduction in active power output of both the PVs reached above 89%, the total active power losses have been increased slightly. Further, analyzing a case where the active power output reduction in

all PVs sources takes place. The lowest voltage follows the same pattern as the output of both PV1and PV2 was reduced.

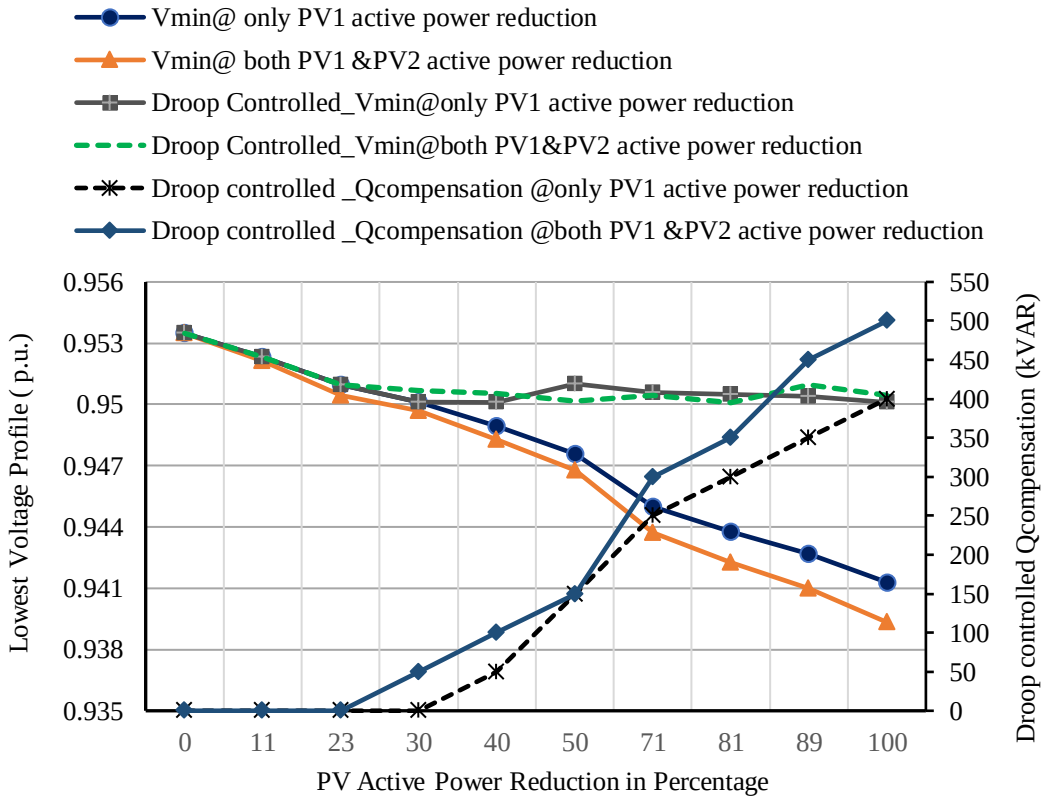

Figure 5.13 Lowest voltage profile at node 114a and compensated Qsupport

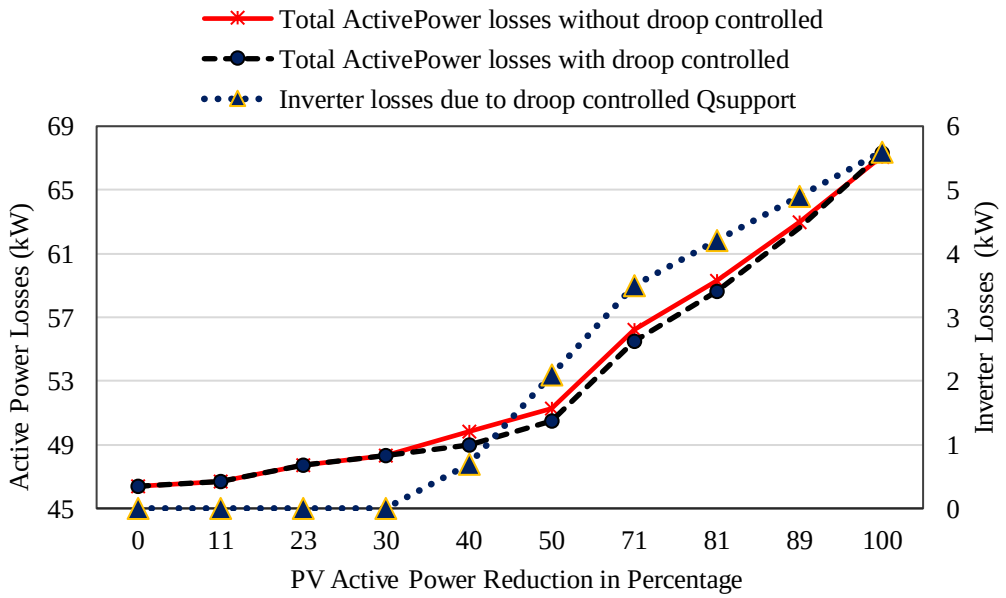

Figure 5.14 Active power losses and inverter losses profile due to PV1 active power reduction.

Considering the condition, where alone PV1 inverter droop controller is not capable of maintaining the voltage profile within the dead-band range. Under such conditions, the local operator may ask to central operators to switch on other PV's droop controllers. While doing so, the coordination among droop controllers would be desired. In case all PV inverters have exhausted compensation limits, the local operator has to ask central operator for compensation from other VVC devices.

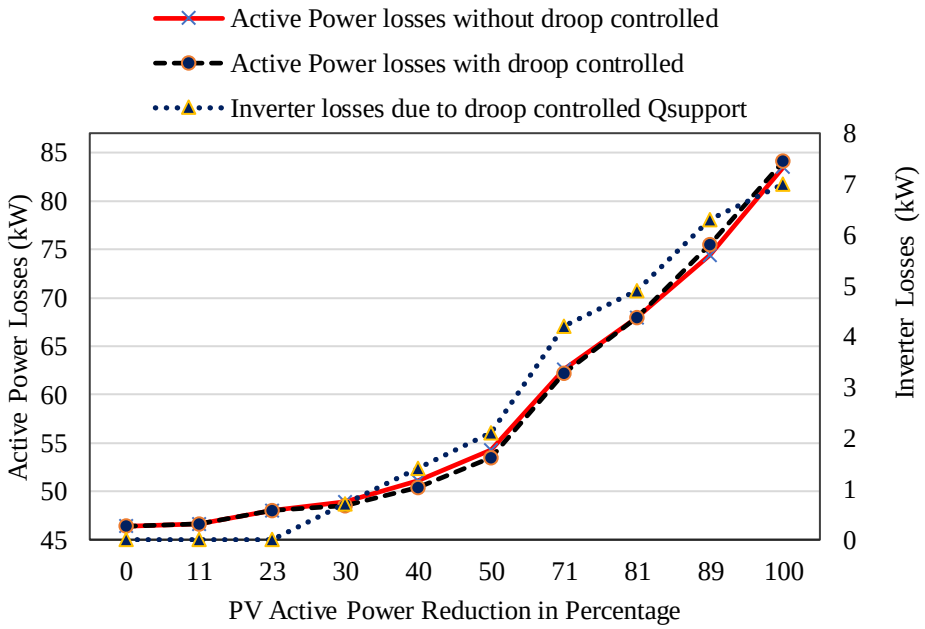

Figure 5.15 Active power losses and inverter losses profile due to PV1and PV2 both active power reduction.

5.5.5 Justification

5.5.5.1 Traditional control Vs Proposed Multi-Stage Control

Implementation of CVR through conventional VVC method has certain limitations regarding voltage reduction range and voltage limit violations during higher demand reduction. The line drop compensation method is widely accepted traditional VVC scheme for CVR deployment. In such studies, the regulated voltages have been is normally fixed at 118V to 120 V and LDC control action is executed in order to enable the CVR operation. The lower voltage limit may violated below the 118V regulated

voltage. Table 5.4 shows the comparative results of Mode -2 operation between traditional and proposed methods. It can be observed that proposed method yields better results in terms of energy demand reduction, loss reduction, and increased CVR factor in comparison to the traditional method with the least variation in lowest voltage profile for a typical day.

5.5.5.2 Centralized Single Stage Control (SSC) Vs Proposed Multi-Stage Control

In centralized SSC, the operation is executed by the control center operator for a fixed time interval ranging from hours to minutes. The settings of VVC devices are tuned according to the defined period.

Table 5.4 Simulation Results in Traditional Method and Proposed Method

Energy Terms	**Mode-1 No-CVR**	**Mode-2 (CVR only)**		**Mode-3 (CVR with PV)**	
		With Traditional Method	**With Proposed Method**	**With Traditional Method**	**With Proposed Method**
Edemand (MWh)	71.967	70.860	70.449	70.860	53.046
∆Esaving (MWh), (%)	---	+1.107 (+1.51)	+1.518 (+2.1)	+1.107 (+1.51)	18.92 (+26.29)
Elosses, MWh	1.675	1.680	1.667	1.680	1.205
∆Elosses, KWh, (%)	---	05 (0.29)	08 (-.3)	05 (0.29)	470 (28.05)
CVR factor (kWh)		0.502	0.642	0.502	1.175
Lowest voltage variations in %	1.1461	1.7025	0.9375	1.7025	1.04

The SSC lacks cooperation when the sudden change in network and intermittent behavior of the PV power output takes place. In that duration, there is a chance of violation in voltage limits. Therefore, the voltage violation ratio remains high. If the optimization and control duration is reduced, say below one hour or 15 minutes, the large data from smart meters and monitoring devices will increase the computational burden. Apart from that, there is a possibility of mishandling or false operations. Moreover, frequent variations in taps of OLTC, AVRs, and switching of CBs will degrade the life cycle of the devices. In order to overcome these issues, the proposed method operates in multi-stages with different time scales. In the first stage, as centralized controlling has been done with the duration of one hour that produces the optimal settings of VVC devices. Moreover, the second stage deals with local control action using a fast response droop controlled based PV inverter in order to handle the voltage fluctuation when any sudden variations in PV power output take place. In conclusion, it can be said that proposed method is beneficial for controlling the operation in centralized as well as in local domains with the less computational burden.

5.6 Conclusion

This chapter has investigated the combined impact of CVR and PV with time-scaled control in various levels of voltage reduction and PV penetrations in the smart grid environment. A discrete multi-objective PSO technique has been used to obtain the optimal setting of controllers. Droop control method has been utilized for fast time scale control to mitigate the voltage drop issue during a sudden fall in PVs active power. The energy and cost savings have been estimated through the proposed method. The findings of this chapter are as under:

- Significant reduction in peak load demand, system losses and daily energy demand have been achieved with only CVR.

- The higher energy and peak savings have been achieved with the deployment of CVR and PV systems. The combined operation of CVR and PV does not result in voltage rise or drop issues even in higher PV penetrations and deeper voltage reduction.
- The economic aspect of CVR deployment has also been analyzed

Thus, it can be concluded that the enabling of CVR control using proposed MSMO-VVC maximizes the CVR benefits in terms of increased voltage reduction range, higher energy and cost savings. In addition, CVR with PV is more beneficial in comparison to CVR or PV alone. Though the proposed methodology works well for CVR implementation, it lacks under transient conditions and presence of intermittency in PV power generations and loads. Hence, there is a need for inclusion of uncertainties (in power generation and loads) impact in VVO model. Moreover, modern ADN demands also fast changing due to the inclusion of flexible loads such as EVs. In this context, next *chapter 6*, analyze EV and uncertainty impact in VVO formulations through model predictive approach.

CHAPTER 6

TIME HORIZON-BASED MODEL PREDICTIVE VVO IN PRESENCE OF ELECTRIC VEHICLE CHARGING LOADS

6.1 Introduction

The rapid increase in the installation of DERs and higher integration of flexible loads [electric vehicles (EVs)] in distribution grid are the major opportunities and challenges for utility operators. The existing electric power infrastructure is not yet ready to adopt the large change in topologies and such integrations. Although enabling CVR in the presence of PV provides significant savings, the system performance is profoundly affected by uncertainties and intermittency associated with PV power generation and load demand. Previous efforts [30], [138] have included the impact of uncertainty in their VVO formulation; however, they have not analyzed its impact on the CVR savings. Moreover, their methodology enables control action only in a centralized manner. A centralized manner works well for a fixed time horizon interval, but it might be inflexible for fast-response events such as PV intermittency. Hence, a multi-time horizon Volt/VAR regulation has introduced in [84], [139]. However, these studies do not analyzed the CVR impact under flexible EV loads.

In the present scenario, EV penetration is one of the fastest growing advanced components of modern distribution systems worldwide. Therefore, DNOs and distribution network planners have the challenge to determine the new control algorithms that coordinate with other components of a network for efficient and optimal operation. In this context, a recent study [140] has presented the agent-based approach for EV charging load modelling, including the aggregated behavior of vehicles and human nature. Besides, the impact of

PHEVs charging on the distribution system and electrified transportation system has also been explored in [141]. Investigations for optimal EV charging scheduling with distributed renewable power and distributed energy management system for Vehicle-to-Grid (V2G) operation has been carried out in [142], [143]. Apart from the use of smart inverter in the solar PV system, the EV charging stations inverter can also play a key role to act as a mobile storage to feed and consume the active and reactive power from and to the distribution grid. In [144]-[146] the various centralized and local control strategies for reactive power compensation through EV charging station in low and medium voltage distribution system has been studied. Though, the authors of [145], [146] have included the impact of EVs on their VVO methodology. However, very few have [147] examined the impact of EVs in the presence of CVR. Though, in [145], [146], authors have analyzed the impact of EV loads penetration while obtaining the optimal VVC devices set points through smart grid VVO engine assessing the optimal V2G impact on power losses and switching cost. However, this study does not include effect of DER and CVR in their VVO formulation in presence of EV loads. Moreover, the method also focused on only centralized control in slow time scale operation.

In this chapter, a multi-time horizon-based model predictive VVO (MP-VVO) engine along with autonomous Volt/VAR droop (VVD) controls has been introduced in the real-time framework. The main objective of proposed VVO is to minimize the CVR cost, network losses cost, and VVO devices operating cost. In addition, provision of VAR support from V2G has also been assessed under centralized VVO operation and voltage control in the local domain due to sudden change in DER power output. The proposed MP-VVO methodology is beneficial for optimal CVR execution, scheduling the VVC devices [both

traditional and power electronics (PE) based], and maintaining the feeder voltage profile even in the presence of EV charging loads. Moreover, the autonomous VVD controller is very useful to handle the smart inverter's (both PV and EV) VAR dispatch under the cloud transients on PV-based DER power output to control the local voltage during the real-time operation. In addition, the proposed control algorithms also tolerate the uncertainties and forecast error present in network loads and DER outputs.

6.2 Time Horizon based Control

Electric power system operation and control are executed in different time horizons and different time scales. In distribution grid, there are mainly two categories of VVO devices, which are traditional and PE-based devices. OLTC, AVR and CBs are traditional VVO that are controlled in slow time scale (from hour to minutes). The PE-based voltage regulation devices, such as smart inverters that can be controlled in slow as well as fast time scale (within few seconds) both. The switched traditional controllers are rescheduled only a few times in a day due to limited cycles operation constraints and the slow variation in load demand. Therefore, control action of these devices in slow time scale is enough for VVC execution. However, during a sudden change in network behaviour and DERs, power output fluctuation may generate the detrimental impact on grid operation. Hence, there is a need of fast-acting distributed control devices, such as smart inverter, that can respond quickly during the fast time scale operation to avoid the undesirable issues. Therefore, in this chapter, a time horizon-based model predictive control methodology has been introduced that can work under both slow and fast time scales. To do so, the entire time horizon (T) is divided into prediction time horizon (Tp) slots. The prediction time horizon (Tp) is further sectionalized into q subslots having control time horizon (Tc) with a sampling time step (dt) as shown in

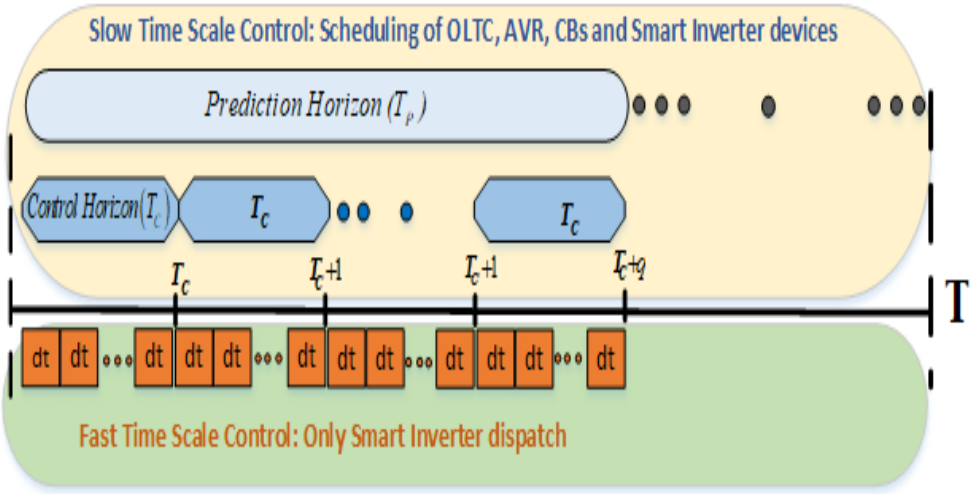

Figure 6.1 Time horizon-based model predictive control

Figure 6.1. For instance, the value of T is 24 h followed by each *Tp* of 1 h. If the value of *q* is four then *Tc* would be 15-min interval with dt time step. A detailed discussion on both timescales is given as follows.

6.2.1 *STSC: Centralized Approach*

In STSC, the aggregated control algorithms have been applied to coordinate and dispatch the control set points over a finite period at the substation level. Therefore, this control is alternatively referred to as a centralized control scheme. In STSC, VVO devices can be scheduled in different prediction and control horizons (Tp and Tc), having time intervals minutes to hour. In present study, Tp of 1 h and Tc of 15-min interval have been taken to reschedule the set points/dispatches of OLTC/AVR, CBs, and smart inverters in optimal manner under STSC operation, as shown in Figure 6.1.

6.2.2 FTSC: Local Control

In STSC, the VVO devices are scheduled for a defined time horizon. During this time span. (set in STSC), however, the deviation in PV power output with respect to the forecasted value can be observed because of unexpected situations, such as transient cloud movements or a solar eclipse. Consequently, it might cause a violation of voltage limits. Therefore, fast control action is needed to maintain the voltage profile limits during the reduction of PV power output. The smart inverters have the ability to respond quickly [89] and they can absorb and inject reactive power. An autonomous approach is used to control the inverter dispatch in a real-time framework. In this study, the dt simulation time step (within the Tc range) is considered to control the only smart inverter dispatch in fast time scale, as shown in Figure 6.1.

6.3 Model Predictive VVO

Generally, the model predictive approach is used to handle the defined finite horizon control problem in optimal manner over the prediction horizon (*Tp*), as shown in Figure 6.2.

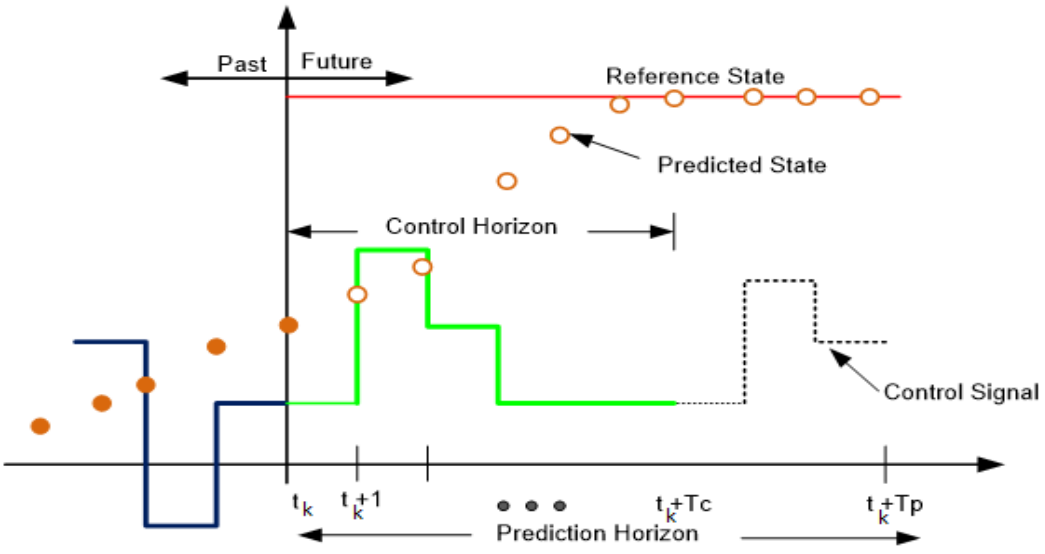

Figure 6.2. Illustration of model predictive control

The achieved control set points are sent to the system to execute the control action over the control horizon Tc ($Tc \leq Tp$). In order to obtain the sequence of control sets, the optimal control problem has been solved based on forecasted data considering the uncertainty and forecasting error. The control variables that lie within the range of $tk + T_c$ (control region) have been implemented for the execution of the system operation and the rest have been discarded. The above-mentioned procedure is repeated using updated observations at $t_k + 1$. Details of uncertainty modeling of loads and DER have been described as under.

6.3.1 Load Prediction Uncertainty

The probability density function is commonly used for representing the load forecast uncertainty of the forecasted load. The information available in literature reveals that normal distribution is an effective method to generate uncertainty in forecasted load consumptions [138]. The forecasted load is defined as the mean value of the normal distribution, and 2% of the expected load is set as the standard deviation.

6.3.2 PV Irradiance Uncertainty Prediction

Solar irradiance is a vital and determinant parameter on which the solar power generated from the PV module depends. Therefore, the highest amount of uncertainty in PV power generation is exhibited by irradiance itself. In order to model the irradiance uncertainty, the beta distribution is considered in this study [138]. The mean of the beta distribution has been defined as Id_{norm}, which represents the value of current irradiance prediction in a time horizon. The standard deviation is a function of the mean value. The variable mean, and standard deviation depend on *A* and *B* parameters. For a predicted irradiance (Id_{norm}), *A* and *B* are the parameters used for defining beta function as follows:

$$F_{Idnorm_{j,t}}(I) = I^{(A-1)}(1-I)^{(B-1)} \tag{6.1}$$

The above-mentioned beta function models the occurrence of irradiance values I when a certain prediction value Id_{norm} has been forecasted. The connection of *A* and *B* with mean and variance for each time instant of the prediction interval have been expressed as follows:

$$Mean(\mu) = \frac{Id_{norm_{j,t}}}{Id_{base}} = \frac{A_{j,t}}{A_{j,t} + B_{j,t}} \tag{6.2}$$

$$Variance(\sigma^2) = \frac{A_{j,t}B_{j,t}}{(\mathrm{A}_{j,t} + B_{j,t})^2(\mathrm{A}_{j,t} + B_{j,t} + 1)} \tag{6.3}$$

The value of *A* and *B* and can be determined using equations (6.2) and (6.3) with the uncertainty produced by equation (6.1).

6.4 EV loads and Charging Stations

The impact of EVs at various consumption levels and different places, such as workplaces, houses, and shopping malls has directed a significant change in daily demand of the network [11]. With the emergence of the smart inverter, EV charging stations have a powerful feature to provide the reactive power support to the grid. Enabling of EVs with this feature leads to the increase in network capacity, reduction in system losses, and enhancing the voltage profile [145], [146]. But these benefits are subjected to system constraints, such as load rise, uncertainty in loads, and DER power generations. In order to achieve the above-mentioned benefits from EV, the role of EV inverter is very crucial. The EV charging stations equipped with smart inverters have the ability to work in different operating modes [146] (shown in Figure 6.3), given as follows.

- *Mode 1*: On the border between Quadrants I and IV (P > 0, Q = 0)
- *Mode 2:* Quadrants I (P > 0, Q > 0)
- *Mode 3*: On the border between Quadrants I and II (P = 0, Q > 0)

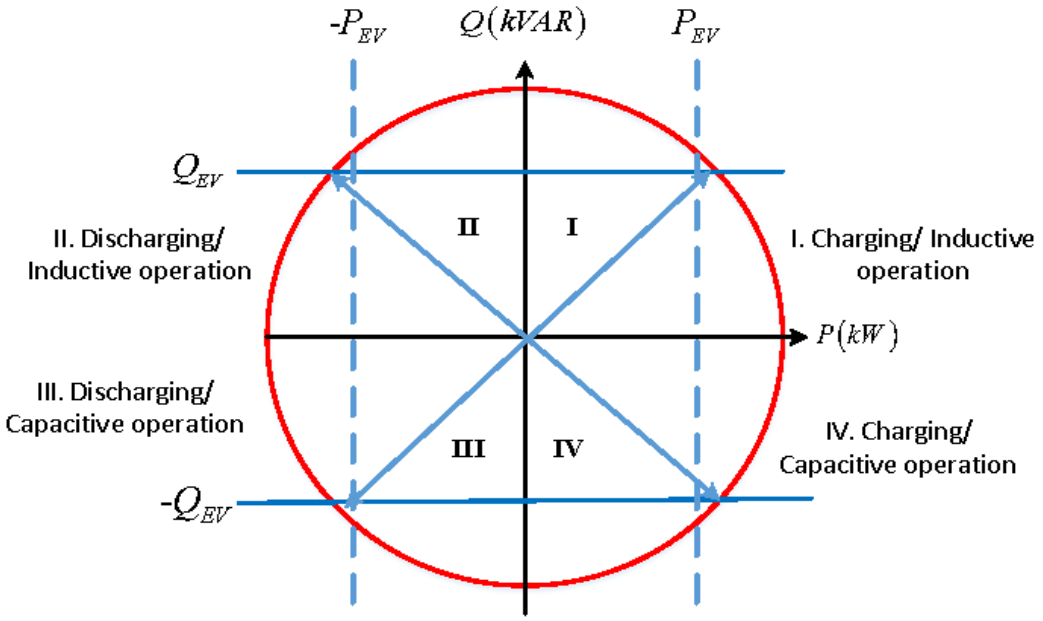

Figure 6.3 Active and reactive power capability of EV inverter

- *Mode 4*: Quadrants II (P < 0, Q > 0)
- *Mode 5*: On the border between Quadrants II and III (P < 0, Q = 0).
- *Mode 6:* Quadrants III (P < 0, Q < 0).
- *Mode 7:* On the border between Quadrants III and IV (P =0, Q < 0). 238
- *Mode 8*: Quadrants IV (P > 0, Q < 0).

Generally, EV operates in P > 0, Q = 0 *Mode 1* (i.e., unity power factor), which exhibits that EV consumes only the real power from the grid. Another possible operating *Mode 8* for EV charging station inverter is to inject the VAR into the grid, while consuming real power for EV battery charging. Apart from the above-mentioned operating Mode 7, there is an operation scenario in which charging station can inject the reactive power to the grid when there is no EV connected to the charging station. Thus, in near future, charging station may be a possible candidate for reactive power support.

6.5 Problem Formulation: Stochastic Optimization

In the present scenario, energy efficiency and demand reduction are the major concerns of DNO. In order to achieve this, an advanced way of CVR operation has been incorporated into VVO models, where multiple voltages regulating devices, such as OLTC, CBs, and smart inverter of PV/EV are coordinated optimally without violating the system constraints. In the slow timescale, enabling CVR and total operating cost are the main objectives. In the fast timescale, the goal is to control the voltage locally.

6.5.1 Optimization Model

In this optimization model, the MP- VVO tries to minimize the CVR cost, network losses cost, and VVO devices operating cost, simultaneously. The proposed MP-VVO objective function can be formulated, as shown in the following:

$$f = \min \sum_{t=t_k}^{t_k+T_P} \left[C_{CVR}^t + C_{loss}^t + C_{VR}^t + C_{OLTC}^t + C_{CB}^t + C_{SI,Qpv}^{t,} + C_{SI,Q_{EV}}^t \right] \quad (6.4)$$

Where,

$$C_{CVR}^t = \alpha \sum_{i \in \Omega_{bus}} C_{cvr,t} \times \frac{1}{\Delta E_{i,t}} \quad 6.5)$$

$$C_{loss}^t = \beta \sum_{br \in \Omega_{br}} C_{loss,t} \times P_{br,loss}^t \quad (6.6)$$

$$C_{VR}^t = \gamma \sum_{vr \in \Omega_{vr}} C_{vr,t} \times X_{vr}^t \quad (6.7)$$

$$C_{OLTC}^t = \gamma \sum_{l \in \Omega_{oltc}} C_{l,t} \times X_{l,oltc}^t \quad (6.8)$$

$$C_{CB}^{t} = \gamma \sum_{cb \in \Omega_{CB}} C_{cb,t} \times Q_{i,cb}^{t} \tag{6.9}$$

$$C_{SI,Qpv}^{t} = \pi \sum_{i \in \Omega_{pv}} C_{grid,t} \times Q_{i,pv}^{t,inv} \tag{6.10}$$

$$C_{SI,QEV}^{t} = \pi \sum_{i \in \Omega_{EV}} C_{grid,t} \times Q_{i,EV}^{t,inv} \tag{6.11}$$

In equation (6.4), $C_{CVR}^{t}, C_{loss}^{t}, C_{VR}^{t}, C_{OLTC}^{t}$, and C_{CB}^{t} represents the CVR cost, power losses cost, operating cost of voltage regulator, OLTC, and CBs respectively. $C_{SI,Qpv}^{t}$ and $C_{SI,QEV}^{t}$ represents smart inverter reactive compensation cost of PV and EV respectively. Similarly, symbols of Ω_{bus}, Ω_{br}, Ω_{vr}, Ω_{oltc}, Ω_{CB}, Ω_{pv} and Ω_{EV} represents the set of all buses, branches, branches with VRs, OLTCs, buses with CB, PV and EV respectively. α, β, γ and π are the weighting factors and their summation should be equal to 1.

6.5.2 Control Variables

The following control variables are considered in the optimization problem.

- Tap position of OLTC/AVR (T_P^t)
- CBs reactive power ($Q_{i,cb}^{t}$).
- PV reactive power dispatch ($Q_{i,pv}^{t,inv}$).
- EV charging station reactive power dispatch ($Q_{i,EV}^{t,inv}$)

The output of the present optimization is the control set points of OLTC/AVR, CBs, and smart inverter in such a way that to achieve the aforementioned goal, the problem has been formulated in slow and FTSC objectives.

6.5.3 System Constraints

Equation (6.4) is subjected to the following system operating constraints

- *Transformer/regulator tap constraints:* The tap range of OLTC transformers/AVR and tap position are given in (6.12) and (6.13) respectively.

$$0.90\,\text{p.u.} \le \text{Tap} \le 1.1\,\text{p.u.} \tag{6.12}$$

$$\text{Tap} = \left\{1 \pm \left(\frac{\Delta V_{tr}}{100}\right) \times T_P^t\right\} \tag{6.13}$$

where $T_P^t \in \{-16,....0.....16\}$, ΔV_{tr} is 0.625 increments in voltage at each step and T_P^t is tap position.

- *Voltage constraints:* Minimum and maximum voltage (*Vmin*, *Vmax*) at *i*th node should remain within limits as expressed in the following:

$$V_{\min} \le V_i^t \le V_{\max},\ V_i^t \in [0.95 - 1.05]\,\text{p.u.} \tag{6.14}$$

- *Capacitor bank constraints:* Reactive power supplied by *i*th CB ($Q_{i,cb}^t$) is determined using equation (6.15)

$$Q_{i,cb}^t = Sw_{i,cb}^t \times \Delta Q_{i,cb}^t ;\ \forall i \in \Omega_{CB} \tag{6.15}$$

where, $Sw_{i,cb}^t = \{0,1,2,3.....,Sw_{i,cb}^{\max}\}$, $Sw_{i,cb}^t$ $\Delta Q_{i,cb}^t$ and $Sw_{i,cb}^{\max}$ are the switching step number, variation in reactive power per step and available maximum number of switching steps at *i*th CB, respectively.

- *PV smart inverter constraints:* The reactive power supplied by *i*th PV inverter ($Q_{i,pv}^{t,inv,stsc}$) during slow time scale period (t) is determined using the following

$$Q_{i,pv}^{t,inv,stsc} = N_{i,pv} \times \Delta Q_{i,\mathrm{pv}}^{t,inv};\ \forall i \in \Omega_{pv} \tag{6.16}$$

where, $N_{i,\mathrm{pv}} = \left\{0,1,2,3.....,\mathrm{N}_{i,\mathrm{pv}}^{\max}\right\}$, $N_{i,\mathrm{pv}}$, $\Delta Q_{i,\mathrm{pv}}^{t,inv}$ and $\mathrm{N}_{i,\mathrm{pv}}^{\max}$ are the switching step number, variation in reactive power per step and available maximum number of switching steps at *i*th PV system.

The available ($Q_{i,pv}^{t,inv,\max}$) is dependent upon the real power generation for a time instance t ($P_{i,pv}^{t,inv}$) which is governed by the following

$$Q_{i,pv}^{t,inv,\max} = \sqrt{\left(S_{i,pv}^{inv,\max}\right)^2 - \left(P_{i,pv}^{t,inv}\right)^2}\ \forall i \in \Omega_{pv} \tag{6.17}$$

On the basis of $P_{i,pv}^{t,inv}$ and $S_{i,pv}^{inv,\max}$, $Q_{i,pv}^{t,inv,\max}$ is recalculated at every time period (t).

- *EV constraints:* Minimum and maximum limits of voltage, active and reactive power of EV as follows

$$V_{i,\mathrm{EV}}^{\min} \le V_{i,\mathrm{EV}}^{t} \le V_{i,\mathrm{EV}}^{\max} \tag{6.18}$$

$$0 \le P_{i,\mathrm{EV}}^{t,inv} \le P_{i,\mathrm{EV}}^{t,inv,\max} \tag{6.19}$$

$$0 \le Q_{i,\mathrm{EV}}^{t,inv} \le -Q_{i,\mathrm{EV}}^{t,inv,\max} \tag{6.20}$$

The reactive power supplied by *i*th EV inverter during slow time scale period (t) is determined using the following:

$$Q_{i,\mathrm{EV}}^{t,inv,stsc} = N_{i,\mathrm{EV}} \times \Delta Q_{i,\mathrm{EV}}^{t,inv};\ \forall i \in \Omega_{\mathrm{EV}} \tag{6.21}$$

where, $N_{i,\mathrm{EV}} = \left\{0,1,2,3.....,\mathrm{N}_{i,\mathrm{EV}}^{\max}\right\}$, $N_{i,\mathrm{EV}}$, $\Delta Q_{i,\mathrm{EV}}^{t,inv}$ and $\mathrm{N}_{i,\mathrm{EV}}^{\max}$ are the switching step

number, variation in reactive power per step and available maximum number of switching steps at *i*th EV system.

The available ($Q_{i,\mathrm{EV}}^{t,inv,\max}$) is dependent upon the real power charging load for a time instance t ($P_{i,\mathrm{EV}}^{t,inv}$) which is governed by the following

$$Q_{i,\mathrm{EV}}^{t,inv,\max} = \sqrt{\left(S_{i,\mathrm{EV}}^{inv,\max}\right)^2 - \left(P_{i,\mathrm{EV}}^{t,inv}\right)^2} \;\forall i \in \Omega_{\mathrm{EV}} \tag{6.22}$$

On the basis of $P_{i,\mathrm{EV}}^{t,inv}$ and $S_{i,\mathrm{EV}}^{inv,\max}$, $Q_{i,\mathrm{EV}}^{t,inv,\max}$ is recalculated at every time period (t).

6.6 Solution method and Procedure

6.6.1 Prediction Error and Scenario Generation

In this work, the PV power generation has been considered as DER. It is well known that the prediction models are always prone to errors. The beta distribution is used to represent solar irradiance prediction errors, as discussed in subsection 6.3.1. Based on uncertain prediction errors and forecasted power, the monte-carlo simulation has been utilized to generate scenarios (N) for solar irradiance and load consumptions. Various distributions and their parameter settings can be varied depending upon the information available regarding the system.

6.6.2 Scenario Reduction and Aggregation

The larger number of scenarios make improvement in the uncertainty model. However, it creates higher computation complexity and enhances computational time. Therefore, in this study, K-means clustering based scenario reduction technique is employed in order to reduce the number of scenarios (N'). While reducing the number of scenarios, a good amount of approximation of the system uncertainty should be maintained. In this method, the data is

clustered based on minimum distance from the centroid of each cluster. After generating N (N=500) scenarios, they have been reduced to N' (15) scenarios using K-means clustering [148] and getting 15 probability of occurrence of each scenario. After implementing the scenario reduction technique, the probability of the achieved scenarios is normalized as follows:

$$\rho_s^{norm} = \frac{\text{(Probability of occurance of one of reduced scenario)}}{\text{(Sum of porbability of occurance of reduced scenarios)}} \tag{6.23}$$

The number of scenarios N reduces to N' by deploying the above procedures. Hence, the problem defined in (6.4) could be rewritten as a stochastic optimization problem with reduced scenarios as given (6.24)

$$\min\left[\sum_{s=1}^{N'} \rho_s^{norm} \times f_s\right] \tag{6.24}$$

The VVO problem redefined in (6.24) is solved by discrete DPSO followed by the system constraints from equations (6.4) – (6.24). PSO is a population-based heuristic optimization technique [149]. The controlling parameters of DPSO used in this study are depicted in appendix C, Table C.1. The achieved optimal control set points from the above formulation are dispatched to the VVO devices for the current prediction horizon based on predicted DER outputs to minimize operating cost of VVO (in this study CVR) implementation. This procedure is repeated when different observations come at t_k + 1. Figure 6.4 shows the flowchart of the implementation of the proposed scheme.

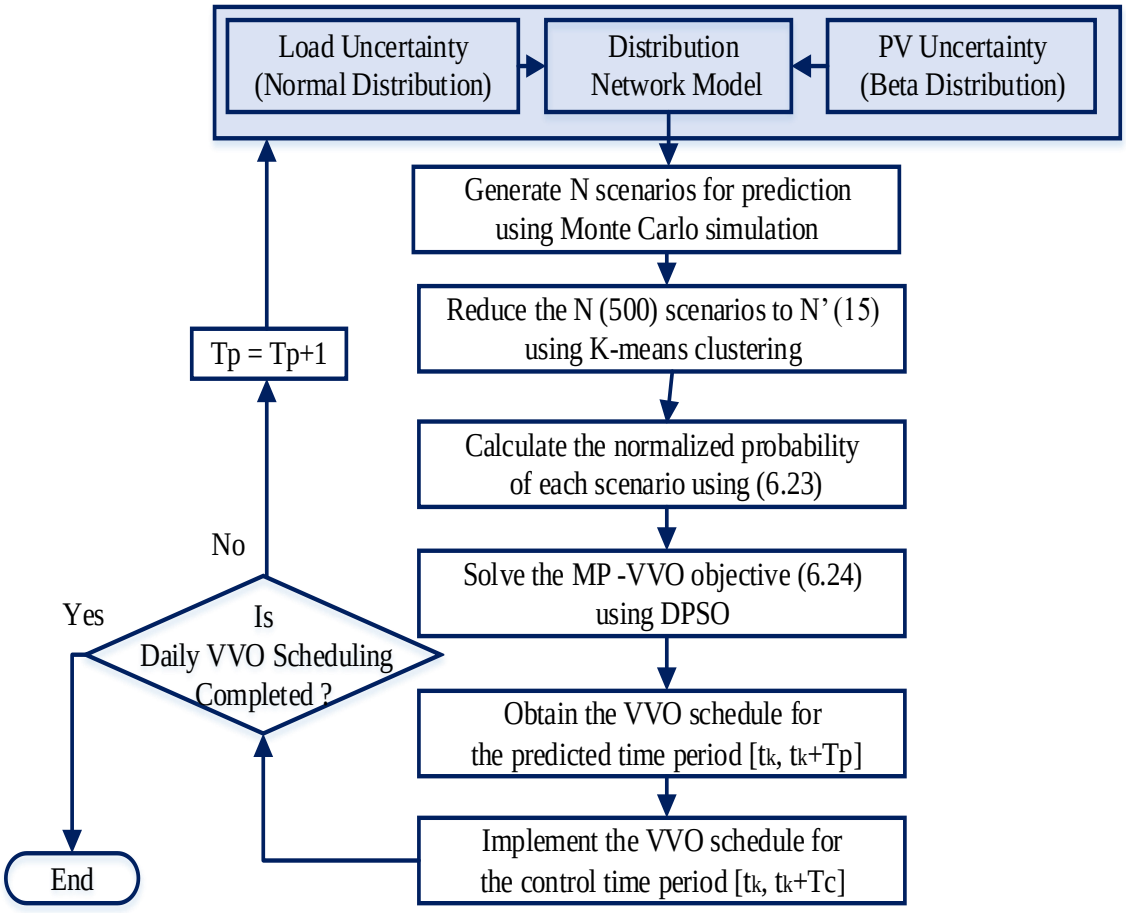

Figure 6.4 Flowchart of MP-VVO execution in STSC

6.6.3 Droop Controller for Smart Inverter

The control set points obtained from model predictive VVO can directly be implemented for CVR under STSC. However, under FTSC, the autonomous approach has been suggested. A droop-based control scheme has been deployed to enable the autonomous operation of the smart inverter to compensate the additional reactive power support. The detailed description can be seen chapter 5. The compensated reactive power ($\Delta Q_{i,PV/EV}^{t,inv,com}$) at any instant, t can be determined using equation (6.25).

$$\Delta Q_{i,\text{PV/EV}}^{t,\text{inv,com}} = \begin{cases} Q_{i,\text{PV/EV}}^{t,\text{inv,av max}} & V < V_1^{P_1} \\ \dfrac{V - V_1^{P_1}}{V_1^{P_1} - V_2^{P_2}} Q_{i,\text{PV/EV}}^{t,\text{inv,av max}} & V_1^{P_1} \le V < V_2^{P_2} \\ 0 & V_2^{P_2} \le V \le V_3^{P_3} \\ -\dfrac{V - V_3^{P_3}}{V_4^{P_4} - V_3^{P_3}} Q_{i,\text{PV/EV}}^{t,\text{inv,av max}} & V_3^{P_3} < V \le V_4^{P_4} \\ -Q_{i,\text{PV/EV}}^{t,\text{inv,av max}} & V > V_4^{P_4} \end{cases} \quad (6.25)$$

where $Q_{i,\text{PV/EV}}^{t,\text{inv,av max}}$ is the maximum available VAR capacity of smart inverter of PV/EV for droop controller at an instant t that is determined by the following:

$$Q_{i,\text{PV/EV}}^{t,\text{inv,av max}} = Q_{i,\text{PV/EV}}^{t,\text{inv,max}} - Q_{i,\text{PV/EV}}^{t,\text{inv,stsc}} \quad (6.26)$$

The total VAR support with droop controller ($Q_{i,\text{PV/EV}}^{t,\text{inv}}$) at an instant t is determined by the following

$$Q_{i,\text{PV/EV}}^{t,\text{inv}} = Q_{i,\text{PV/EV}}^{t,\text{inv,stsc}} + \Delta Q_{i,\text{PV/EV}}^{t,\text{inv,com}} \quad (6.27)$$

6.6.4 Implementation of proposed coordinated scheme

In this subsection, the coordinated operation of STSC and FTSC devices have been implemented using aggregated and autonomous approach as shown in Figure 6.5. This figure demonstrated that in centralized control, MP-VVO executes every 15 minutes interval and generate the optimal set points for STSC devices. However, in local control, droop controller runs autonomously and generates desired set points for FTSC devices in near real time operation.

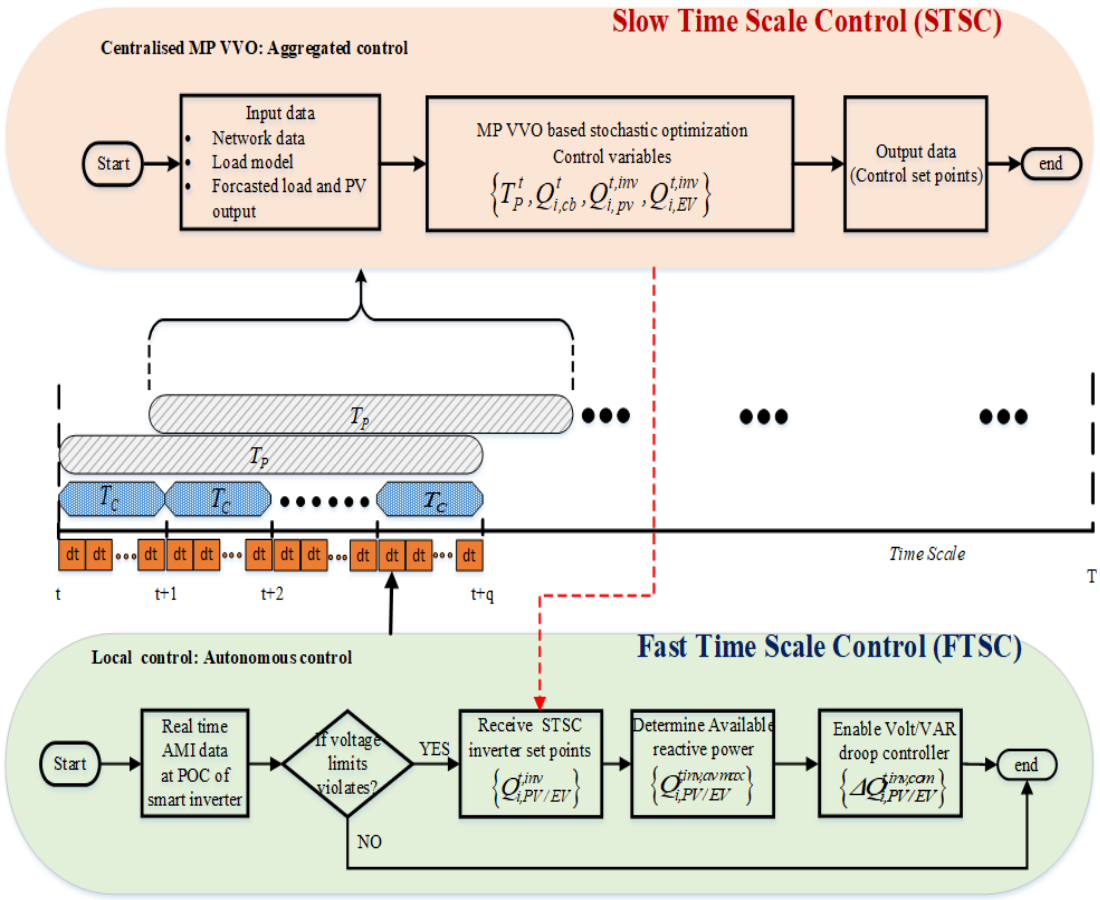

Figure 6.5 Implementation of the proposed coordinated scheme

6.7 Case Study and Simulations

6.7.1 Test system description

In order to validate the proposed VVO methodology, a modified IEEE-34 node test feeder[114] has been considered as shown in Figure 6.6. The slack bus is at the primary side of the 2.5 MVA D–Y substation transformer with 69/24.9 kV voltage rating with a fixed ratio equal to 2.56. There are two automatic voltage regulators connected between nodes 814 - 850 (AVR-1) and 852-832 (AVR-2) and each one has 16 tap increments of 0.625% at the secondary side. Two three-phase CBs are connected to buses 844 and 848 with the ratings of 300 kVAR and 450 kVAR with step variations from 0 to 3 respectively.

The additional three 3 phase PV plants at nodes 848 (PV1), 890 (PV2) and 840 (PV3) having inverter ratings 200kVA, 300kVA and 400kVA respectively. Per step reactive power variation from PV and EV charging station inverter is 10 kVAR and 5kVAR for slow time scale operation respectively. For EV charging mode, the constant power load characteristics with type 1 and type 4 [146] and charging level 2 of 6 kW power rating [142] have been assumed in this study.

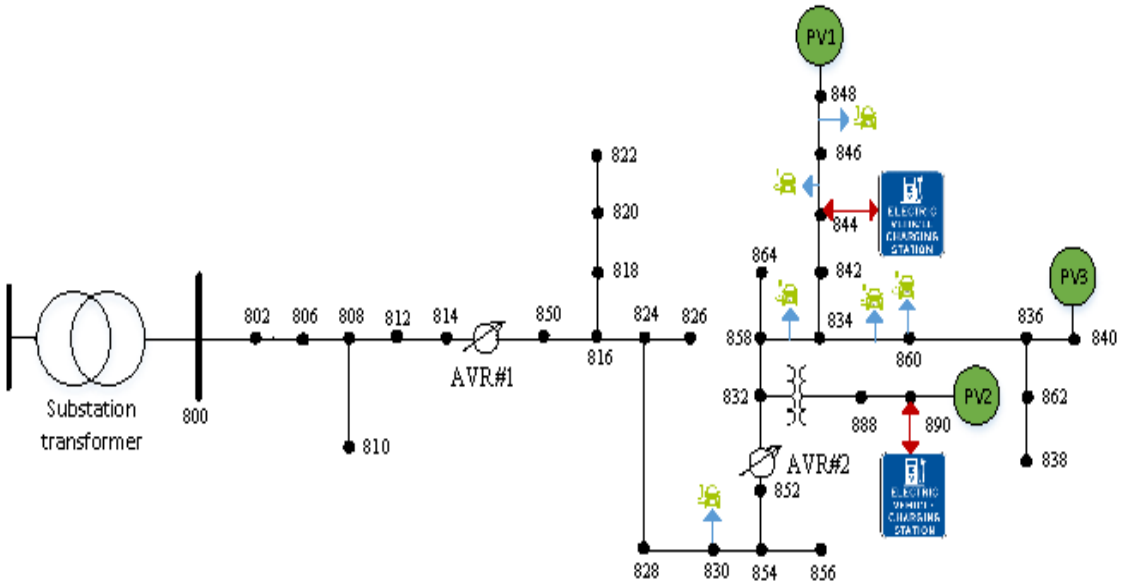

Figure 6.6 Modified IEEE 34 bus distribution system

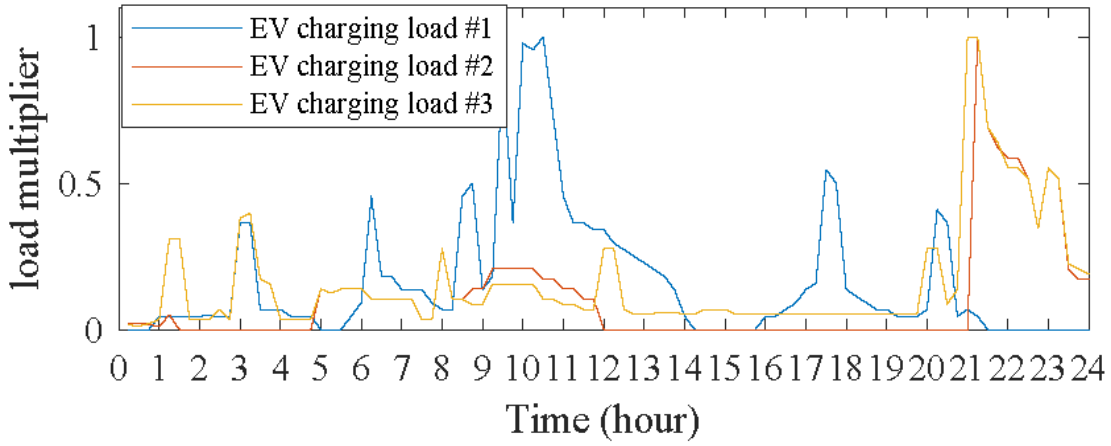

Figure 6.7 EV load profiles

Three different EV charging load profile for a typical day have been used in this study as shown in Figure 6.7. The normal EV penetration range with a maximum of 20% of the system load has been considered. For EV charging outlet and charging stations locations are referred from [141], where the authors have mapped the IEEE 34 bus system to a real-world transportation system and define the EV charging location as shown in Table 6.1. The charging points are divided into two categories. The first type charging outlet which does not participate in VAR support means they are operating in Mode1 (P>0 and Q=0) and second is charging stations that have the ability to inject and absorb the reactive power even when there is no EV is connected (i.e. Mode 7). It is further assumed that EV inverter support's reactive power only if when it has not reached its maximum allowable kW power ratings. Note that charging station 890 and 844 follows the EV charging load profile 1 and EV charging load profile 3 respectively. Rest of the EV charging outlets follow the EV charging load profile 2 as shown in Figure 6.8. The quasi-real-time load and PV profile for a typical day have been shown in Figure 6.9. Similarly, grid price has been shown in Figure 6.9. the cost parameters have been taken from [146].

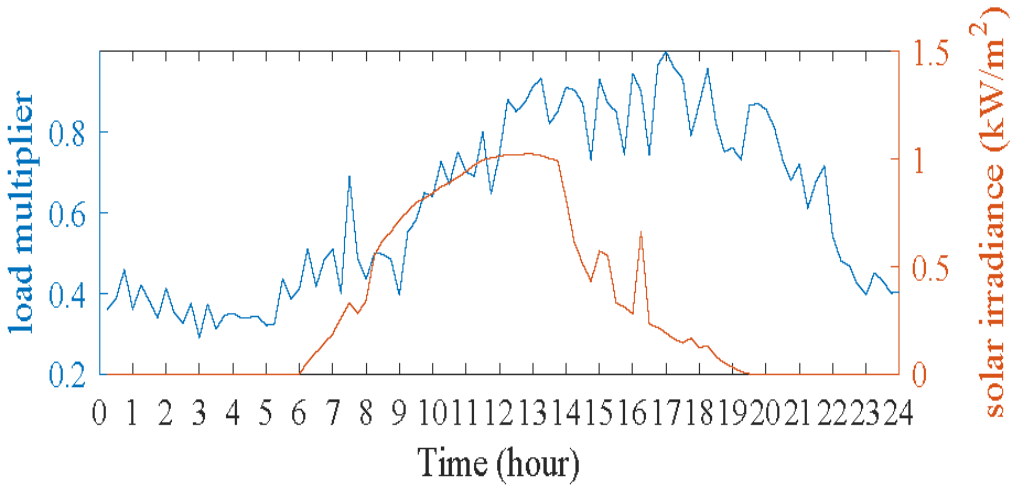

Figure 6.8 Forecasted load and solar irradiance

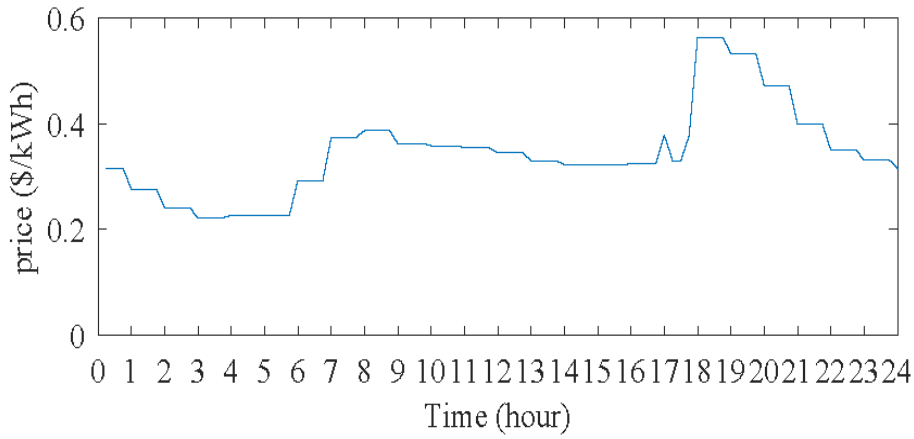

Figure 6.9 Grid price over a day

Table 6.1 EV Charging Location and Ratings

S.no.	**Location / node (a,b,c phase)**	**Maximum Rated Power**	**Charging Point (Outlet/Station)**
1	846_848b	12 kW	Outlet (Only P)
2	844_846b	6 kW	Outlet (Only P)
3	858_834b	6 kW	Outlet (Only P)
4	830c	12 kW	Outlet (Only P)
5	834_860b	6 kW	Outlet (Only P)
6	844	120 kW	Station (P, Q)
7	860	18 kW	Outlet (Only P)
8	890	180 kW	Station (P, Q)
9	834_860a	6 kW	Outlet (Only P)

6.7.2 Simulations and Results Analysis

The proposed VVO methodology has been developed in Python while the test system modeled and load flow analysis has been done in the OpenDSS platforms interfaced through the component object model (COM). The quasi-static time series simulations have been carried out for 24 hours at fifteen minutes interval for the following cases.

- Case 1: ADN without MP-VVO and without EV (Base)
- Case 2: ADN with MP-VVO
- Case 3: ADN in the presence of EV without MP-VVO
- Case 4: ADN with MP-VVO in the presence of EVs as reactive power support

- *Case 1. ADN Without MP-VVO and Without EV (Base)*

In this case the simulation has been carried out without VVO and EV penetration. The CVR has not been performed. The line drop compensation scheme has been used to execute the VVC operation. Simulation results are depicted in the second column of Table 6.2. The energy demand (E^{demand}) and energy losses (E^{losses}) of the system have been observed as 102.37 MWh, and 6.869 MWh respectively. The total operating cost of the distribution system is calculated as $29997.45 for 24 hours.

- *Case 2: ADN with MP-VVO*

In this case, proposed MP-VVO has been implemented aiming to CVR execution. Impact of EV penetrations in ADN has not been considered in this case. The results are depicted in the third column of Table 6.2. From results, it is observed that significant energy demand reduction about 5.024% and 14.383% losses reduction have, respectively, been achieved as compared to case 1. Moreover, the lowest voltage profile has also been improved, which is above the lower voltage limit (0.95 p.u.). The total operating cost of distribution network has also been reduced to $28172.327. The remarkable cost savings of about $1825.123 has been achieved after the inclusion of CVR. Reported savings in terms of energy and cost reveal the effectiveness of proposed VVO methodology for CVR execution.

- *Case 3: ADN in the Presence of EV Without MP-VVO*

This case deals with the simulation of ADN in the presence of EV penetration without involving VVO. The execution of CVR also has not been included. The load flow and VVC have been performed using a line drop compensation method. The obtained results of this case have been portrayed in the fourth column of Table 6.2. The energy demand and energy losses of the system have been observed as 107.396 and 7.625 MWh, respectively. The total operating cost of the distribution system has been calculated to be $34719.54.

Table 6.2 Results of different cases

Parameters	**Without EV**		**With EV**	
	Case 1	***Case 2***	***Case 3***	***Case 4***
E^{demand} **(MWh)**	102.37	97.226	107.396	103.821
ΔE^{demand} **(MWh)**	----	5.144	----	3.575
ΔE^{demand} **savings (%)**	----	5.024	----	3.328
E^{losses} **(MWh)**	6.869	5.881	7.625	6.587
ΔE^{losses} **(%)**	----	14.383	------	13.61
Minimum voltage (pu)	0.9252	0.9501		0.95
Cost of energy purchased from grid ($)	29348.28	27549.81	34022.83	32453.39
Active power loss cost ($)	639.77	550.01	686.16	592.91
PV SI VAR compensation cost ($)	-----	61.08	----	37.67
EV SI VAR compensation cost ($)	----	-----	----	9.404
VR, CBs switching operating cost ($)	9.4	11.2	10.55	11.8
CVR cost ($)	-----	0.227	-----	0.335
Total operating cost ($)	29997.45	28172.327	34719.54	33105.509
Cost of energy savings ($)	-----	1825.123	-----	1614.031

- *Case 4. ADN With MP-VVO in the Presence of EVs as Reactive Power Support:*

In this case, proposed MP-VVO has been utilized in the presence of EV penetration aiming to CVR execution. EV charging stations are participating partially in reactive power support. They can inject about 60% of the maximum EV KVA inverter capability. In this study, only two charging stations at nodes 890 and 844 are providing VAR support with the maximum value of 100 and 50 kVAR, respectively. The simulation results of this case have been shown in the fifth column of Table 6.2. The reported energy demand and losses of the system are 103.821 and 6.587 MWh, respectively. In comparison to Case 3, the significant reduction in energy demand and losses about 3.328% and 13.61% have, respectively, been achieved. Moreover, the total operating cost of distribution network is reduced to $33105.509, as shown in Table 6.2. The remarkable cost savings about $1614.031 have been reported after inclusion of CVR. Reported savings in terms of energy cost reveal that proposed VVO methodology works well in the presence of EV as well.

- *Minimum voltage profile under different cases*

Figure 6.10(a) shows the voltage profile of the node where the voltage is lowest without EV penetration with and without VVO impact. From this figure, it can be seen that in Case 1, the lower limit violates at different instances. Moreover, the lowest voltage varies from 1.012 to 0.9242 p.u., which is in a high range. In Case 2 operation, VVO execution with proposed method yield voltage profile improvement with less voltage deviation in the lowest voltage profile. Further, it can be clearly seen that no lower limit violation occurs with the enabling of MP-VVO during the whole operation. On the other hand, Figure 6.10(b) shows the lowest voltage profile of Cases 3 and 4, which includes the EV penetration impact. Similar to Case 1, Case 3 does not include VVO, which also results in lower voltage limit violations.

However, Case 4 operation that enabled with proposed VVO does not result in lower voltage limit violations.

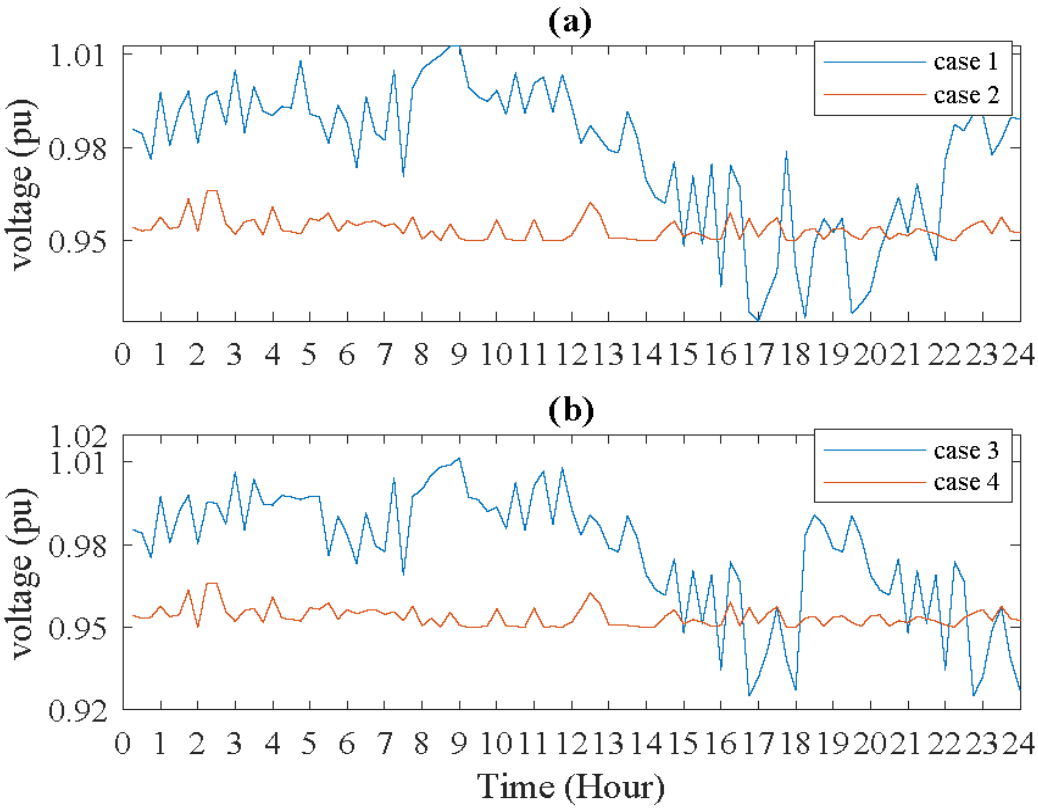

Figure 6.10: Lowest voltage under (a) *case 1* and *case 2* (b) *case 3* and *case 4*

- *Energy demand and dynamic CVR savings under different cases*

The impact of proposed VVO methodology on energy demand and CVR savings has been discussed under different cases. Figure 6.11(a) shows the varying power demand for Case 1 and Case 2, and dynamic CVR saving at each 15-min interval. Figure 6.11 shows that CVR savings are changing dynamically. It can be observed from this figure that most of the time CVR saving is reported on peak loading scenario. On the other hand, in the presence of EV in ADN, the power demand and CVR savings for Cases 3 and 4 have been shown in Figure 6.11(b). From this figure, it can be observed that the proposed VVO method reduces the

energy demand and also coordinates the EV impact in VVO to variation in load demand. At some points, the CVR saving is negative due to the constant power characteristics of EV charging loads. It is a fact that CVR has a negative impact on the constant power load characteristics. Further, in the presence of EV in ADN without VVO, i.e., Case 3, the feeder voltage suffers a higher violation of lower limit. But the execution of VVO in the presence of EV does not result in any voltage violations; it means that it increases the voltage profile of the system. As a consequence, CVR savings may or may not be positive in such conditions.

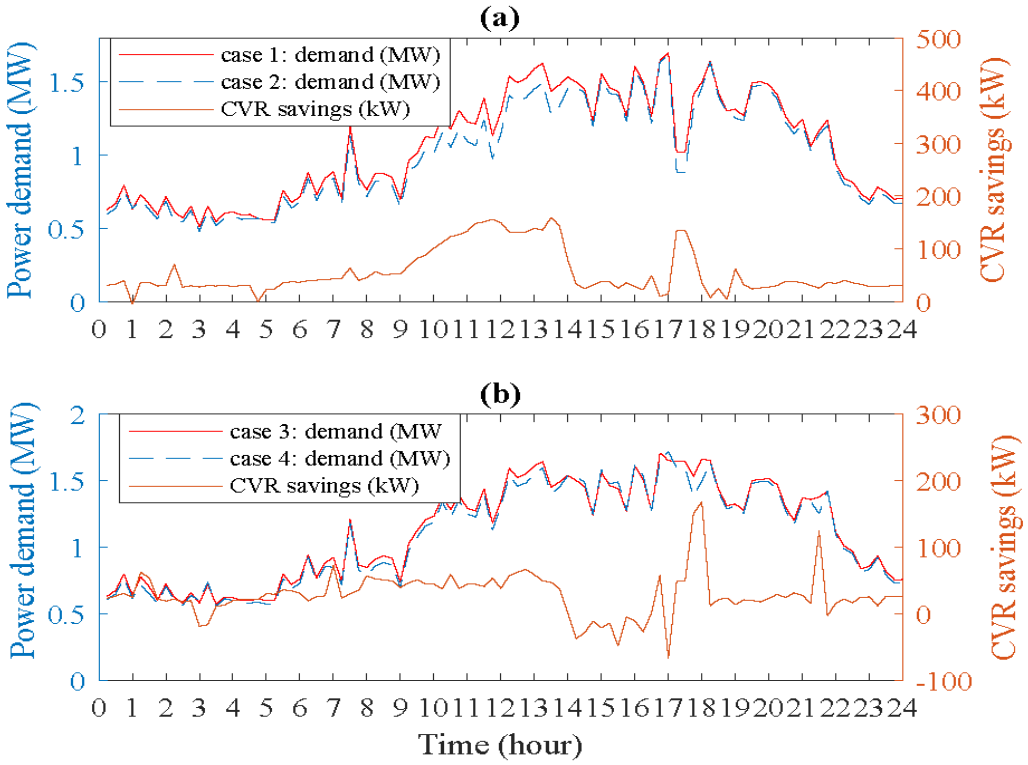

Figure 6.11. Power demand and CVR savings under (a) *case 1* and *case 2*, and (b) *case 3* and *case 4*.

- *Smart inverter reactive power support from PV and EV under different cases*

Figure 6.12 shows the optimal reactive power dispatch from PVs and EV smart inverters. These figures demonstrate that the need for reactive power is much higher in either peak

loads when there 653 is no PV power or higher penetration of EVs. The reactive power dispatch from smart inverters reduces the VAR support from capacitors. It can be said that smart inverter (PV and EV) may limit the use of CBs and emerge as a potential future candidate for VAR support in the global and local domain.

- *Illustration under FTSC: local control*

In order to validate the proposed control methodology under FTSC, the effect of cloud transient has been studied. An arbitrary instantaneous point between time intervals from 14:00 to 14:15h has been selected. The load demand is 91% of peak demand at this point and forecasted solar irradiation is 81% of the peak. During this time span, the lowest voltage profile at node 890 becomes vulnerable to any reduction in kW power. Status of VVO devices AVRs and CBs remain the same, as determined in STSC, as shown in Table 6.3. The FTSC has been applied and illustrated for two cases. The droop parameters used in this study have been shown in Appendix C in Table C.2.

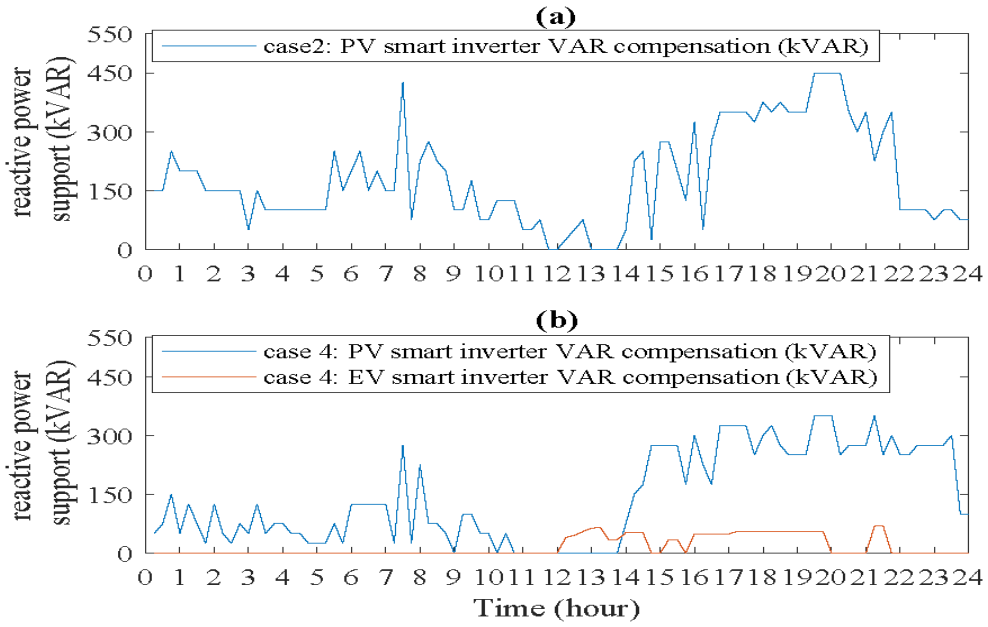

Figure 6.12. Reactive power support from PV/EV smart inverter under (a) *case 2* and (b) *case 4.*

Table 6.3: STSC set point at 14:00 h to 14:15 h

Tap position (T_P^t)	AVR-1 {1, -5, -2}; AVR-2 {5,6,6}
CBs reactive power ($Q_{i,cb}^t$).	CB_{844}{200}; CB_{848}{150}
PV reactive power dispatch ($Q_{i,pv}^{t,inv}$).	PV1 {0}; PV2{100}; PV3{0}
EV charging station reactive power dispatch ($Q_{i,EV}^{t,inv}$)	EV#1{40}; EV#2{10}

(i) *Case I. Effect of Cloud Transient in the Absence of EV:*

In this case, the sudden drop in solar irradiation from 0.81 to 0.4 kW/m^2 is observed due to the cloud movement. Accordingly, the reduction in active power from the PVs plant is reported. Hence, there is a voltage drop occurs due to such incidents. Figure 6.13 shows the drop in the lowest voltage profile with respect to fall in solar irradiation and total VAR support from PV inverters.

(ii) *Case II. Effect of Cloud Transient in the Presence of EV:*

In this case, the sudden drop in solar irradiation from 0.81 to 0.3 kW/m^2 is observed due to cloud movement in the presence of EV in ADN. Figure 6.14 shows the drop in the lowest voltage profile with respect to fall in solar irradiation. Figure 6.14 clearly demonstrates the droop control-based approach for local control that helps to mitigate the lower voltage limit violation by providing additional reactive power compensation from PV inverters up to 0.4 kW/m^2 reduction in solar irradiation. However, after further reduction, PV inverters alone are not capable of maintaining the lower voltage limit. This happens because PV inverters have already reached their maximum allowable reactive power capacity. In such conditions, EV inverters from the charging station equipped with droop control feed the additional VAR support. Figure 6.14 clearly shows that after injecting the VAR from EV inverters, the lower

voltage violations have been mitigated. It is to be noted that the limit of reactive power compensation from EV inverter should also meet their maximum allowable range. If both PV and EV inverters fail to maintain the lower feeder voltage limit, in such conditions, the operator has to reschedule the VVO set points using centralized control approach.

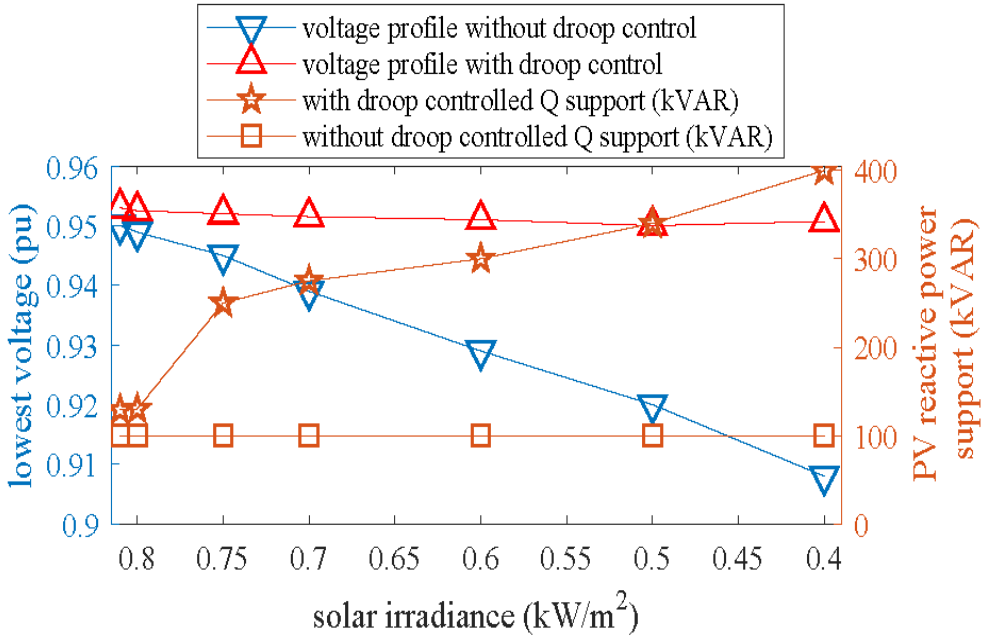

Figure 6.13 Lowest voltage profile and compensated VAR support from PV inverters

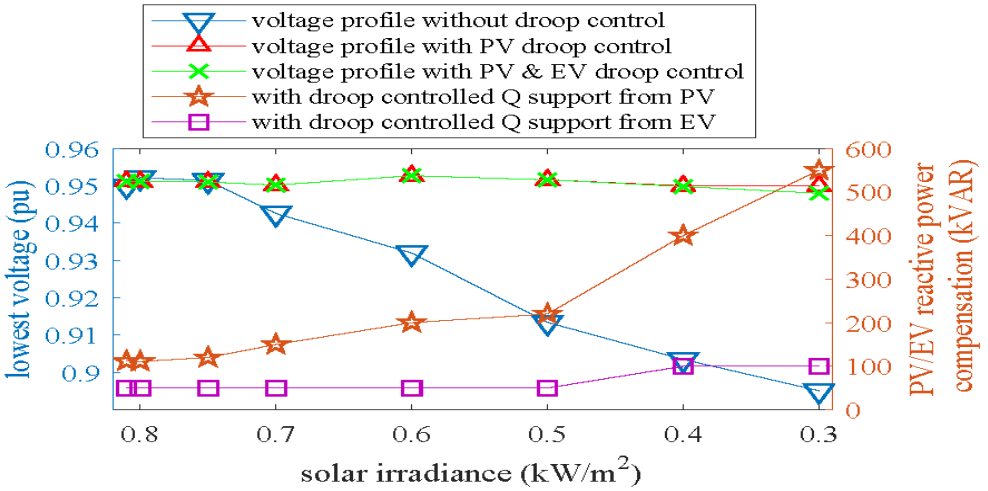

Figure 6.14. Lowest voltage profile and compensated VAR support from PV and EV inverters

6.7.3 Validation of Droop Controls in the Real-Time Simulation Platform

The droop controllers operate autonomously for local control actions in real-time. Therefore, in this study, the proposed droop control actions have been validated in a real-time simulation platform using a real-time digital simulator (RTDS).

6.7.3.1 Real-Time Simulation using RTDS

This thesis intended to use the RTDS in order to perform the real-time simulation. It has its own internal clock, unlike pure computer-based simulations. The RTDS will never stop its real-time simulations; either it does not receive the external command from other simulation platforms timely or waits for such command [150], [151]. Therefore, simulations in RTDS reflects the actual behavior of the grid operations. RTDS can be functionally divided into two main parts as software and hardware. A dedicated software named RSCAD is used to model the network and hardware is used for run time [152]. Apart from normal or Power System simulation mode (50 microsecond time step), RTDS simulator (Version 5.0 or after that) also offering a special mode of operation named as Distribution Mode with time step range of 100-200 microsecond to simulate large-scale distribution feeders in real Distribution Mode with time step range of 100-200 microsecond to simulate large-scale distribution feeders in real-time and can perform various studies and validate their controllers related to distribution system [152], [153]. Therefore, this work intends to use the *Distribution Mode* simulation to test the developed control algorithms in a large-scale test system. A schematic of RTDS Novacor, interacting with RSCAD (version 5.007)/ run time, has been shown in Figure 6.15. The simulation has been carried out in distribution mode with simulation time step (*dt*) of 120 μs. The modeling of DERs and EV loads are built using average models [153].

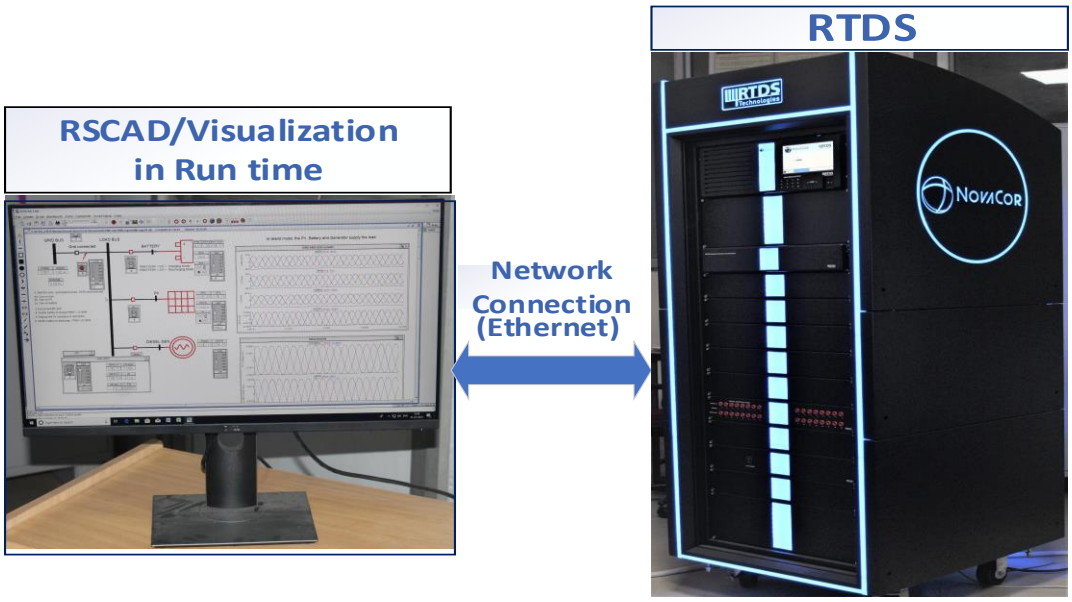

Figure 6.15: Schematic of RTDS (both software and hardware)

6.7.3.2 Real-time implementation under FTSC

In order to validate the droop control action in real-time, the instantaneous point at time period (14:00 to 14:15 h) and set point parameters as depicted in Table 6.3 have been used. The load demand is 91% of peak demand at this point and forecasted solar irradiation is 81% of the peak. During this time span, the lowest voltage profile at node 890 becomes vulnerable to any further reduction in kW power. The FTSC under cloud transient has been applied and illustrated without and with EV load penetrations as given in the following.

- *Case I. Cloud Transient Impact in the absence of EV Loads*

The sudden fall in solar irradiation from 0.81 to 0.4 kW/m^2 has been considered to analyze the cloud movement impact. Accordingly, the active power from the PVs plant has been reduced. As a result, drop in voltage occurs due to sudden fall in PV power output. This resulted in lower voltage limit violation, as seen from Figure 6.16, with red color line. Under the circumstances, the droop controller is enabled in order to rescue from voltage droop below the prescribed lower limit (as set in droop controller). The enabled droop controller

injects the additional VAR support to compensate the voltage deviation. It can be clearly seen from Figure 6.16 that droop control action is able to control the voltage profile locally. The node 890 is most vulnerable node for voltage deviation. Hence, the PV2 inverter reactive power dispatch is critical for droop operation. The reactive power (Q) support by PV2 inverter with and without droop controller has been shown in Figure 6.17. The reactive power dispatch with droop controller indicates the reactive power that is additive to centralized PV2 reactive power dispatch.

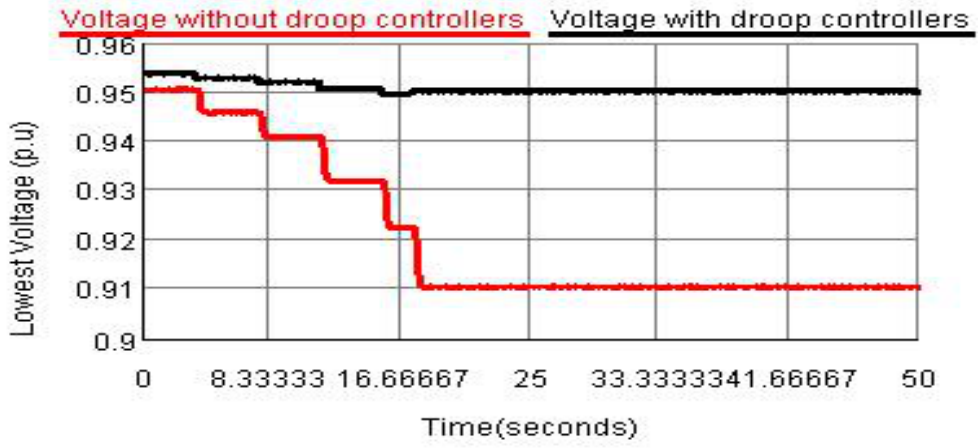

Figure 6.16 Lowest voltage profile without and with droop controllers

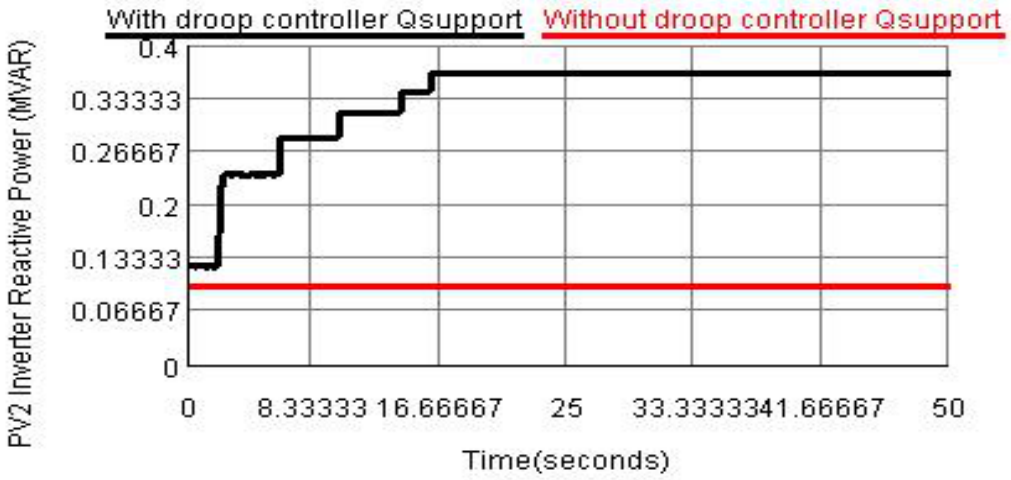

Figure 6.17 PV inverter reactive power compensation without and with droop controls

- *Case II. Cloud Transient Impact in Presence of EV Loads*

In this case, the sudden drop in solar irradiation from 0.81 to 0.3 kW/m^2 is observed due to the cloud movement. Figure 6.18 shows the lowest voltage profile. In both scenarios, when only PV inverters and combined PV and EV inverters are providing the droop-based VAR support. Figure 6.18 clearly shows that up to 0.4 kW/m^2 reduction in solar irradiation, VAR compensation from PV inverters, is alone proficient to maintain the lower voltage limit. However, after further reduction, PV inverters alone are not capable of maintaining the lower voltage limit. This is due to PV2 inverter having already reached its maximum allowable reactive power capacity. In such conditions, EV inverters from the charging station equipped with droop control feed the additional VAR support. Figure 6.18 clearly shows that after injecting the VAR from EV inverters, the lower voltage violation has been mitigated. Figure 6.19 shows the compensated VAR support from PV2 and EV inverter at node 890.

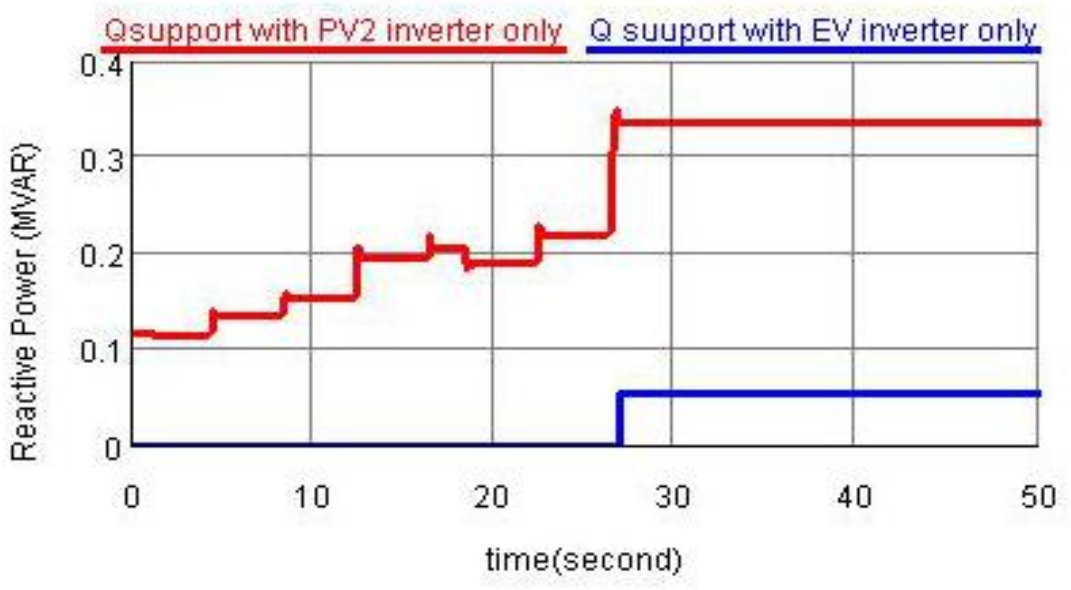

Figure 6.18. Lowest voltage profile with PV and EV inverters VAR support

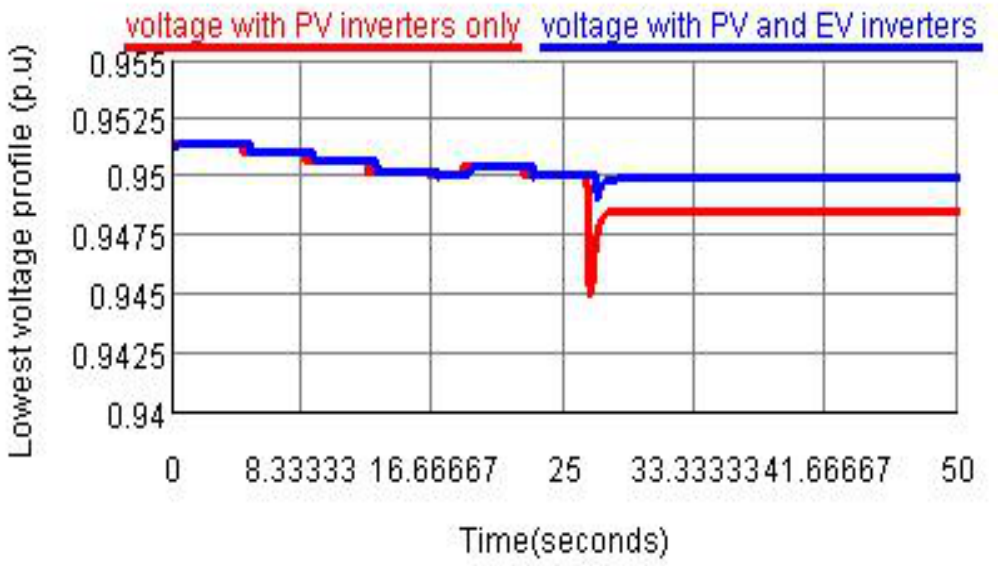

Figure 6.19. Compensated VAR support from PV2 and EV inverter at node 890

6.8 Conclusion

An investigation on CVR energy savings and impact of EV penetration in ADN has been carried out. A time horizon-based model predictive control method has been employed to handle the uncertainties in the system. The impact of different charging levels has been included in VVO formulation. Apart from PV inverters, the provision of reactive power support through EV charging station has been examined during centralized as well as local control. Most of the current EVs exhibit the constant power load characteristics; hence, CVR saving would reduce as EV penetration increases. Besides, the dynamic voltage control using VVD controller has been implemented on RTDS platform. The major findings of the present investigations are as follows.

- Significant reduction in energy demand, system losses, and saving in operating costs have been achieved with MP-VVO based CVR.

- The developed control method is capable of handling uncertainty and intermittency, such as cloud transient, without violating the feeder voltage profile.
- Reactive power compensation through EV charging stations may be a potential candidate for VAR support in the future.
- The simulation results show that EV charging load characteristics also influence the energy savings achieved by CVR.

The implementation of a real-time droop controller validates the proposed dynamic voltage control scheme. Thus, it can be concluded that enabling the CVR through proposed MP-VVO method yields better performance in terms of energy savings, cost savings, and voltage profile improvement even in the presence of EV charging loads.

CHAPTER 7

EVENT-DRIVEN REAL-TIME PREDICTIVE VOLT/VAR OPTIMIZATION AND CONTROL

7.1 Introduction

Growth in installations of DERs is bringing unique opportunities and challenges to DNOs around the world. Therefore, advanced coordination and integration are essential for the efficient and reliable operation of future distribution systems. New technologies, such as AMI, ADMS include a suite of applications designed to monitor and control the entire distribution network in real-time [63], [97]. The integration of AMI on a large scale is enhancing the observability of ADN for real-time operations. The revised IEEE 1547 (2018) [89], also states that every DER must have reactive power support capability when requested by power system operators. Therefore, PV systems are increasingly being paired with smart inverters that can inject and absorb reactive power. Moreover, *the Smart Inverter Working Group Phase 3* has recommended eight functions to be included in *California Rule 21* as mandatory or optional for all inverter-based DER systems [90]. In order to do this, there is need of efficient fast real time controllers that can handle the undesirable issues smoothly. In this context, optimal Volt/VAR curve selection using a heuristics approach for VVC droop controller has been suggested in [7] and a gradient-based decentralized VVO approach under high DER penetration has been introduced in [8]. Though, real-time voltage and VAR regulation have been carried out in [64], [95], [100], [146], but few have analyzed CVR impact with VVC droop controllers.

This chapter presents an event-driven predictive control framework along with the local controller for CVR to maximize its benefits in terms of voltage reduction range and energy savings. In addition, the strategy addresses CVR adoption during sudden changes and limited voltage reduction issues. For local control, an autonomous VVC based droop controller is well known [21], [68], [77], [92], [111]. However, except [92] others has used the conventional droop method with predefined droop parameters. Under changing circumstances, the conventional VVC droop method may not be able to adopt the changes. Therefore, adaptive droop control has been introduced in this work. Moreover, event-driven co-simulation frameworks are suitable for real-time system operations as suggested in [154]–[159], hence this methodology has been adopted in this investigation for validation purpose. The contribution of the chapter includes:

- Event-driven predictive approach for real-time implementation of a multi-time scale, multi-objective VVC (MTMO-VVC) for aggregated and autonomous controls for ADN
- A coordinated three-layer hierarchical dispatching structure for the proposed event-driven predictive framework
- A communication free two-level adaptive droop based local controller for autonomous PV smart inverter operation
- The Development and validation of the proposed methodology in the real-time framework using the RTDS in distribution mode through co-simulation with models based on Python and OpenDSS models.

7.2 MTMO-Volt/VAR Control

A coordinated MTMO-VVC strategy for CVR, including multiple voltage control devices and the impact on the network devices and assets under different time scale, is presented in

this study. The detail description of the methodology is delineated in the below subsections.

7.2.1 Multi-Timescale Operation

The modern distribution system needs an operation in different time horizons under slow and fast timescales control. In daily operations, because of limited cycles and operational constraints, switched controls—such as OLTC, AVR, and capacitor banks—are rescheduled only a few times during the day. hence, slow-timescale control is sufficient for voltage support. However, a sudden change in the system and DER output might have detrimental effects on grid operations; hence, fast-response capabilities from inverters will play a vital role in handling the undesirable issues. Therefore, the proposed control strategy considers controls on both timescales (slow and fast). To do so, the entire time period is divided into Z slots for each day. For instance, if the value of Z is 24, then the duration of each slot of Z is 1 hour. Each slot is further sectionalized into *q* subslots indexed in minutes, with *dt* simulation time step in real-time, as shown in Figure 7.1. A detailed description of both timescales' operations is as follows.

7.2.1.1 STSC using Aggregated Approach

In order to coordinate and dispatch the VVO controller's set points for a finite period at feeder level, the aggregated control algorithm is adopted under STSC operation. VVO devices are scheduled in two sub-time intervals of i) minutes to hours and ii) minutes to seconds, as shown in Figure 7.1.

- *OLTC and Capacitor Banks: (Minutes to Hours):*

The OLTC and capacitor banks respond slowly. Moreover, limited cycles of operation and switching effects restrict the frequent operation of these devices. In practice, their operating range can usually vary from a few minutes to multiple hours; hence, in this study, the OLTC

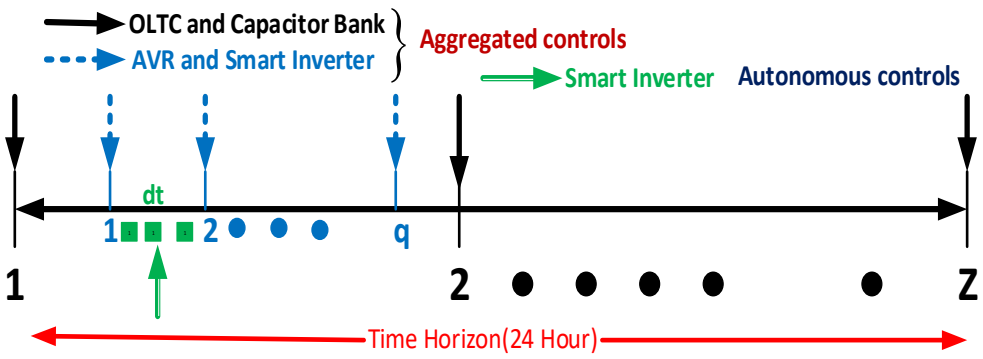

Figure 7.1. Multi-timescale horizon

and capacitor banks are scheduled for every 1-hour duration (as shown in Figure 7.1) during the entire day.

- *AVR and Smart Inverter: (Minutes to Seconds):*

Generally, voltage controllers such as AVR and smart inverters are scheduled for the duration of minutes to seconds. In this model, every 15 minutes, the setpoints of AVR and smart inverters are rescheduled; hence, shown in Figure 7.1, the value of q is set to 4 with the slot duration of 15 minutes.

7.2.1.2 FTSC using Autonomous Approach

In STSC operation, the VVO controllers are scheduled for a given time period. Under this time horizon (as set in STSC), however, there can be a deviation in DER output (such as PV active power) with respect to the forecasted value experienced. This happens due to intermittence behavior of solar PV power generations. Consequently, it might cause a detrimental impact on grid operations through violation of system limits such as voltage and power profile. Therefore, in this context, the fast-adaptive real-time control action is required to avoid such voltage limit violations. In order to do so, the fast-acting devices like smart inverters having the ability to respond quickly, and can absorb and inject reactive power are

utilized in this study. For this, an autonomous approach with adaptive two-level droop control has been proposed to regulate the inverter dispatch in a real-time framework.

7.2.2 Multi-Objective Control

In this study, multiple objectives are considered according to their timescale of operation. In the slow timescale, enabling of CVR through aggregated predictive VVO is the main objective. However, in the fast timescale, the goal is to control the voltage locally in real-time operation. To fulfill both objectives, the problem is combined to form a multi-objective control adopting the aggregated and autonomous approach simultaneously.

7.3 Event-Driven Predictive Framework

7.3.1 Overview of Event-Driven Predictive Approach

Figure 7.2 shows an overview of the event-driven predictive framework. This architecture has two data sources. The first has both forecasted data and historical event data from finished process instances.

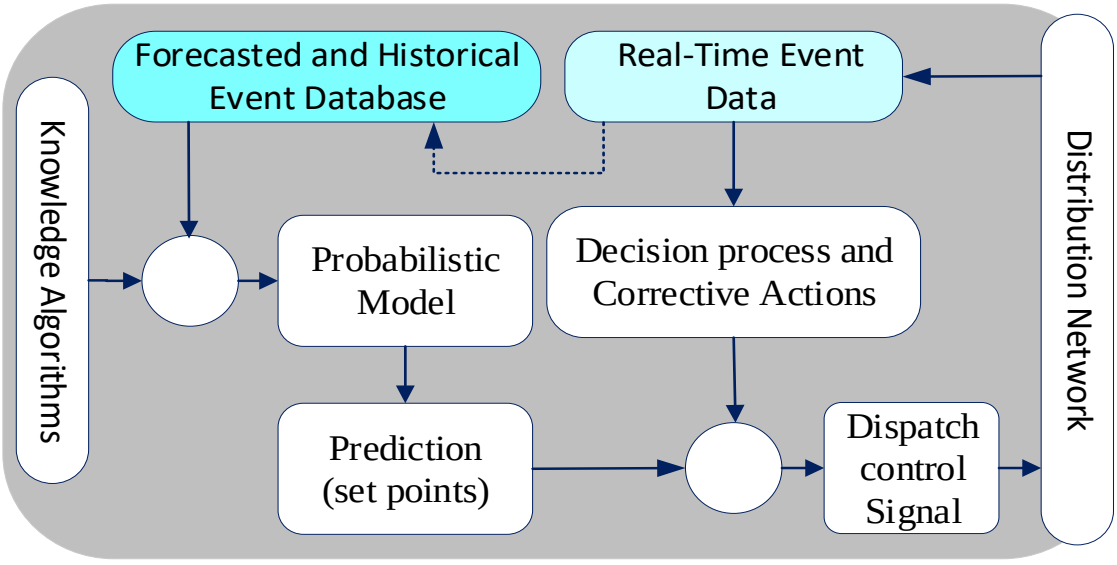

Figure 7.2. Schematic of an event-driven predictive framework

The real-time data from running process instances is another data source. After completion of the running process instance, the current event sequence added to the historical data. This study adopted a simple event log data format such as event log $Y = \{y^{(1)}, \dots, y^{(C)}\}$ having C as a sequence of events. Each event sequence $y^{(C)}$ is a tuple $\left(y_1^{(C)}, \dots, y_{t_c}^{(C)}\right)$ of t_c events where t_c is the length of event sequence $y^{(c)}$ [159]. Each event exclusively fits to an event type $y_t \in \{1 \dots . . E\}$ where E is the type of events. Approach commences with the selection of the suitable forecasted data (in this study loads and solar irradiation) subset for a given time scale. Afterward, the probabilistic model is fitted through a knowledge algorithm [159]. The solution obtained through a knowledge algorithm is used to generate the predictions (in this study controller's set points) and fed to the dispatch block where the control signal will be sent to the distribution network controllers. Afterward, real-time event data from the distribution network must be fed into the framework. A decision process block analyzes the measured sequence of events and sends corrective action to the dispatch block if required.

7.2.2 Probabilistic Model and Knowledge Algorithm

The probabilistic model-driven approach is a favorable scheme for handling the event-based predictive control problem in an optimal manner for a given prediction time horizon (Tp). In this context, probabilistic modeling powered by the knowledge algorithm has been adopted to achieve the sequence of optimal control setpoints and sent to the system to execute the control action during the control horizon 'Tc' ($Tc \leq Tp$). The main purpose of modeling the forecasted data probabilistically is to find a suitable representation that postulates the data into a probability distribution function over a given time framework. The present study considers the forecast data for load and solar PV power. To deal with the forecasting error, the proposed event-driven predictive methodology includes probabilistic modeling of the

uncertainty in the load and the solar PV irradiance predictions. The normal distribution method is used to generate uncertainty in the forecasted load data. On the other hand, the beta distribution is considered to model the PV irradiance uncertainty [30], [138].

Forecasted data of loads and solar irradiance for a given period have been fitted in normal and beta probabilistic distribution functions respectively, detailed explanations can be seen in previous *chapter 6*. A knowledge algorithm driven by monte-carlo sampling and simulation is used to generate number of scenarios (N) for solar irradiance and load consumption. A higher number of generated scenarios increases computation complexity and computational time. Hence, this study employed a K-means [148] clustering-based scenario reduction technique to reduce the number of scenarios (N') such that an accurate approximation of the system uncertainty should be maintained. After implementing the scenario reduction technique, the probability of the achieved scenarios is normalized (Ω_s^{norm}) as follows [138]

$$\Omega_{\mathrm{s}}^{\mathrm{norm}} = \frac{\text{Probability of occurance of one of reduced scenario}}{\text{Sum of the probability of occurrence of reduced scenarios}} \tag{7.1}$$

7.3.2.1 Objective Function: Stochastic Optimization

To maximize the energy savings, CVR has been formulated as a stochastic optimization problem with the objective of minimizing the sum of the square of the deviation of node voltages from the expected CVR voltage in all phases and all nodes except the source node for given *Tp* under slow time scale operation as shown in equation (7.2)

$$f = min \sum_{s=1}^{N'} \Omega_s^{norm} \sum_{t=\, t_k}^{t_k+\, T_p} \left[\left\{ \sum_{a,b,c} \sum_{i}^{l-1} \left(V_{i,h} - \, V_{CVR,h} \right)_{a,b,c}^{2} \right\} \right] \tag{7.2}$$

where $V_{i,h}$ is the node voltage (p.u.) at i^{th} bus at hour h; $V_{CVR,h}$ is the expected CVR voltage (p.u.) at hour h; *l* is the number of the nodes; and *a,b,c* are the phase notations.

7.3.2.2 Control Variables:

The taps of OLTC and AVR, reactive power dispatch of capacitor banks and smart inverters are the main decision control variables.

7.3.2.3 System Constraints:

The following operating constraints are subjected to equation (7.2)

- *Voltage Constraints:* Service voltage at the i^{th} load node must follow the relation as shown in equation (7.3):

$$0.95 \leq V_i \leq 1.05\ p.u. \quad (7.3)$$

- *Tap Constraint:* Tap of z^{th} OLTC/AVR (Tap_z) is given as

$$0.90 \leq Tap_z \leq 1.1\ p.u. \quad (7.4)$$

- *CB Constraints:* Reactive power supplied by j^{th} capacitor bank (Q_{CB}^{j}) is determined using equation (7.5):

$$Q_{CB}^{j} = W_{CB}^{j} \times \Delta q_{CB}^{j}, W_{CB}^{j} = \{0,1,2 \dots W_{CB}^{j,max}\} \quad (7.5)$$

where W_{CB}^{j}, Δq_{CB}^{j} and $W_{CB}^{j,max}$ are the number of switching steps, per step-change in Q_{CB}^{j} and available maximum number of switching steps at the j^{th} capacitor banks, respectively.

- *PV Smart Inverter (SI):* The reactive power dispatch of k^{th} PV inverter the in slow-timescale ($Q_{PV}^{k,stsc}$) is calculated by equation (7.6):

$$Q_{PV}^{k,stsc} = N_{PV}^{k} \times \Delta q_{PV}^{k}, N_{PV}^{k} = \{0,1,2 \dots N_{Pv}^{k,max}\} \quad (7.6)$$

where N_{PV}^{k}, Δq_{PV}^{k} and $N_{Pv}^{k,max}$ are the number of switching steps, per step-change in $Q_{PV}^{k,stsc}$, and available maximum number of switching steps at the k^{th} PV system, respectively. The maximum PV inverter reactive power $Q_{i,t}^{inv,max}$ is governed by the equation (7.7) where

$S_{PV_{inv}}^{k,max}$ and $P_{PV,t}^{k}$ are the PV inverter capacity and real power generation at instant t respectively.

$$\left|Q_{i,t}^{inv,max}\right| = \sqrt{\left(S_{PV_{inv}}^{k,max}\right)^2 + \left(P_{PV,t}^{k}\right)^2} \quad (7.7)$$

- *Voltage-Led Load Model:* The voltage-led composite ZIP (impedance current power) load model is considered for the study. The constant ZIP load model is shown in equations (1.17) -(1.20) respectively, as explained in *chapter 1*. This study uses the value of ZIP coefficients 0.36, 0.20, and 0.44 for both the active and reactive powers, respectively [160].

7.3.2.4 Solution Method:

The optimization problem defined in equation (7.2) is solved by DPSO followed by the system constraints. PSO is a population-based heuristic optimization technique [149]. It shares many similarities with evolutionary computation techniques. The particle dimensions are divided among decision variables. The optimization problem has been solved for the current prediction time horizon (T_P) based on predicted PV outputs and load demands, including forecasting errors. The achieved optimal day-ahead scheduling of control setpoints is dispatched to the VVO devices for the control horizon (T_C). The entire procedure is repeated when different observations come at t+1 for a complete day.

7.3.3 Decision Process and Online Corrective Action

After retrieving the real-time grid measurements both globally and locally, data is processed for event detections and take the corresponding decision for online corrective actions. The two-time scale window i.e. STSC in near real-time and FTSC in real-time has been intended to use for online operation. In near real-time, the corrective actions have been scheduled based on every fifteen minutes measured data set. Based on these global measures, the

decision has been processed weather the online corrective actions in current dispatches $X^o = \left[Tap_z, Q_{CB}^j, Q_{PV}^{k,stsc}\right]$ are required or not. In this context, Six sigma deployment based methodology has been adopted that comprises of five phases: define, measure, analyze, improve, and control (DMAIC) [161] for online process analytics and to determine the required corrective actions ($\Delta X^{corrective}$). The updated dispatches ($X^{updated}$) is calculated by equation (7.8)

$$X^{updated} = X^o \mp \Delta X^{corrective} \tag{7.8}$$

The detailed description regarding real-time control in fast time scale has been delineated below subsection.

7.3.4 Autonomous Approach for Real-Time Local Control

In a FTSC, the autonomous approach is best suited for controlling operation through smart inverter dispatches locally. The local controller dispatch reactive power based on local measurements to control the voltage fluctuations. For example, if $V_k(t)$ is voltage measurement at instant t, then corrective action is defined with relation (7.9)[156].

$$Q_k(t+1) = Ki\ (V_k(t)) \tag{7.9}$$

where $Q_k(t+1)$ is updated inverter Q dispatch for next *t+1* instant and *Ki*(.) is the local controller coefficient. To determine the appropriate value of $Q_k(t+1)$ in changing scenarios, the role of *Ki* is very important. Therefore, an adaptive droop-based local controller is deployed to enable the autonomous operation of the smart inverter to compensate the additional reactive power support. This additional VAR compensation would be additive to the optimal reactive power fed by PV inverters under aggregated STSC.

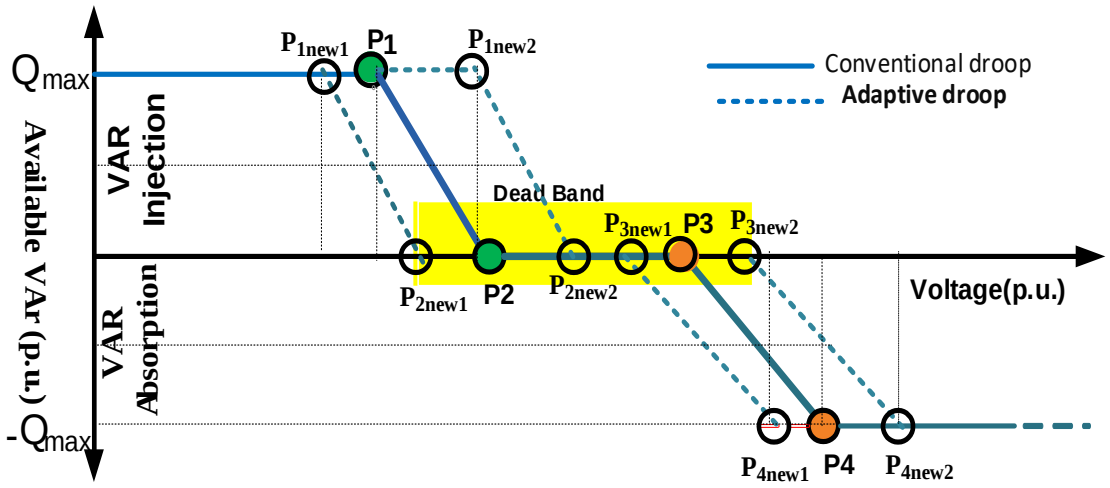

Figure 7.3. Adaptive Volt/VAR droop characteristics

7.3.4.1 Adaptive droop controller under FTSC

To determine the desired compensating reactive power from the PV system, the Volt/VAR droop characteristics are used for PV inverter VAR control. The adaptive Volt/VAR droop characteristics for the present problem are shown in Figure 7.3. The droop characteristic is obtained by defining the four-point (P1, P2, P3, and P4) parameters, also referred to as control/droop parameters. In conventional droop method, these parameters are constant or remain unchanged during the operation. However, these settings may or may not result the targeted output during changing operating conditions and external disturbance. Therefore, in this study adaptive droop controller has been introduced in which droop parameters are adopted according to the operating scenario. It can be seen from Figure 7.3 that the new droop parameters (P_{1new1}, P_{1new2}, P_{2new2}, P_{3new1}, P_{3new2}, P_{4new1} and P_{4new2}) are flexible and adaptive in nature using proposed control strategy. In order to do so, the two-level control approach has been utilized. In the first level, the droop controller uses pre-defined parameters and dispatches the control actions accordingly. Afterward, a correction factor (K_d) $= V_{specified} - V_{measured}$. based on local measurements has been calculated in order to check the voltage

limits and verify whether the correction in droop parameters is essential. If the K_d is outside the tolerance range, modification in the droop parameters is required. The second level deals with the selection of appropriate parameters utilizing K_d and steady-state error. The more details regarding steady state error and parameter selection can be found in [92]. The default droop parameters used in this study are depicted in Appendix C in Table C.3.

7.4 Real-time Co-Simulations Platform

The co-simulation platform has been made to examine the effect of different components, network assets and utility management applications involved in the operation and control of distribution grids. In order to do so; this study used the RTDS based co-simulation platform to check the effectiveness of the developed control algorithms including communication network delays.

7.4.1 Co- Simulations using RTDS -Python- OpenDSS

In this chapter, RTDS and OpenDSS have been utilized through Python in order to perform the real-time co-simulations. The generalized framework of the co-simulation platform has been shown in Figure 7.4. The detailed description regarding basic of RTDS has already been explained in *chapter 6* in subsection *6.7.3.1*.

To check the effectiveness of the developed control algorithms, a real-time a co-simulation platform is developed. In this context, a co-simulations framework through RTDS and OpenDSS with the help of external agents (such as Python for this study) has been introduced. This study uses RTDS Novacor, RSCAD 5.007 in *Distribution Mode* with simulation time step (dt) of 120 microseconds to test the developed control algorithms in a large-scale active distribution test system [150], [153]. The average models of PV DERs have been used.

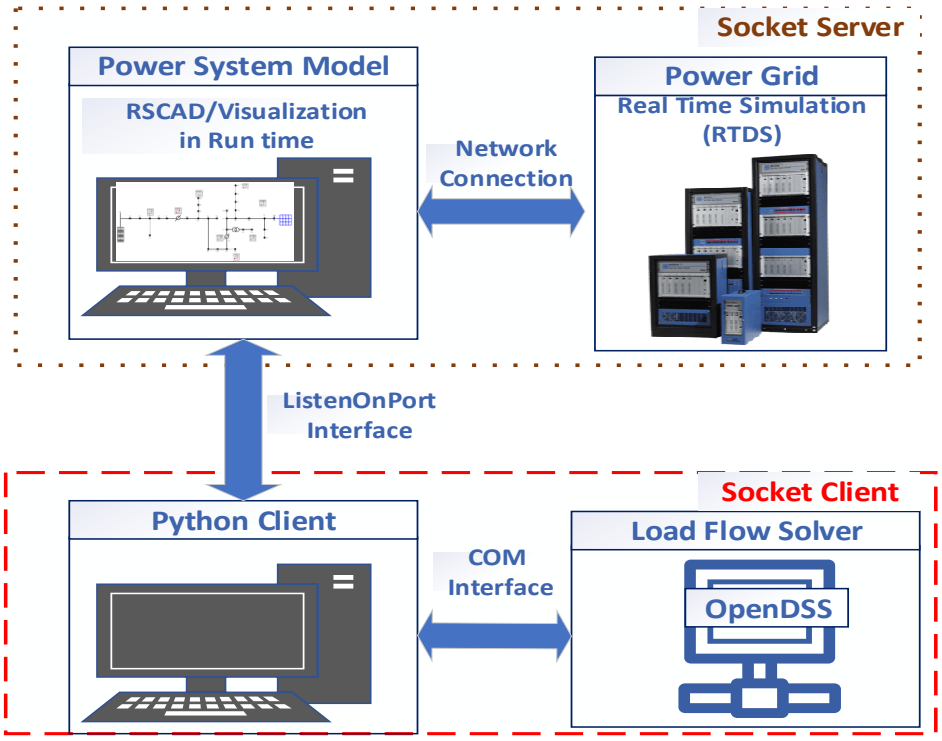

Figure 7.4 Framework of real-time co-simulation platform

The interaction during the real-time simulation in RTDS is implemented through '*ListenOnPort'* [150] command by external application, where the control algorithm was developed with the help of the OpenDSS platform.

7.4.2 Communication Interface

In order to interact with the simulation to external controllers or hardware, sometimes, the real-time simulation requires a standard communication protocol such as IEC-61850 and DNP 3 etc. In general, the specifications of these communication protocols are designed for a particular application. Besides, it is very hard to be modified frequently for the use of different purposes. Such specific use of communication protocols is also associated with the burden of the significant development in cost and effort. Moreover, some users who want to

send out the small set of control commands to the simulation and retrieve the corresponding measurements with lower interaction speed (usually in the range of hundreds of milliseconds) from external applications such as Python/ MATLAB [151]. Such needs can be fulfilled by a specific communication capability in RSCAD/Runtime through the scripting-based interface. The RTDS offer such a script-based '*ListenOnPort()*' command to enable the Transmission Control Protocol/Internet Protocol (TCP/IP) socket communication between RSCAD/Runtime and the applications running in the same network [150], [162]. The visualization of RTDS' output can be seen in its run time screen and it is in the same machine in which the RSCAD is installed, as shown in Figure 7.4. Once the connection established by execution of script commands the RSCAD/Runtime becomes a socket server and external application act as a socket client. This communication interface is generally known as socket communication.

7.4.3 Simulation Set up and Procedure

The interaction during real-time simulation in RTDS has intended through using '*ListenOnPort*' command by Python application where the control algorithm has been developed with the help of the OpenDSS platform as shown in Figure 7.4. The stepwise simulation procedure to interact with the RSCAD/Runtime server can be concise as follows [162].

- Once the '*ListenOnPort*' command is executed by the Runtime script reading engine, the RSCAD/Runtime becomes a specified port number.
- The external application, such as Python, executes the script and commences the essential client socket connection.

- The client application interacts with the Runtime TCP server port. Now, the socket communication is established.
- The socket communication is directed to the use of IP and TCP for address (AF INET) allocation and data streaming (SOCK STREAM) respectively.
- With the specifying of socket IP address and port number, the connection to the Runtime server is established. Now, the client (external application) can send commands to the run time simulations. These commands read as script commands by Runtime server.
- In order to ensure the synchronism between the Runtime and the external application Python (in this case) and also for bidirectional communications (i.e., from Runtime to the external application), a script command called '*ListenOnPortHandshake()*' can be used, It usage exchange of token string for synchronism acknowledgment. Meanwhile, that token string is also read the system measurements from RTDS simulation. A user-defined port is opened with TCP socket server.

7.5 Implementation of proposed methodology

The event-driven predictive control framework has been implemented using the developed real-time co-simulation framework as shown in Figure 7.4. A coordinated hierarchical dispatching structure [158] has been utilized for the execution of proposed methodology as described below subsection:

7.5.1 Coordinated three-layer hierarchical dispatching structure

The structure includes three layers for different timescales, such as scheduling, dispatching, and real-time control layer as shown in Figure 7.5. The control action is carried out in two modes of operation, as aggregated and autonomous controls, with different timescales. The scheduling layer works on a day-ahead hourly basis using a predictive control scheme to

obtain the VVO dispatches offline and stored in the sequence table. Besides, to limit the excessive tap excursion, a control strategy is adopted, as described in *Algorithm 1*. In the dispatching layer, if real-time measurements are violating the limits due to forecasting events error and inconsistency, the sequence table needs to be readjusted online based on current states. A control strategy as stated in *Algorithm 2*, is used to readjust the VVO dispatches and take online corrective action. The real-time control layer handles unpredictable violation events such as feeder voltage profile due to cloud transients and sudden change in network configuration and takes emergency action to eliminate such events immediately. In this context, a two-level adaptive droop-based autonomous real-time control for PV inverters are executed locally. A detailed procedure of the droop controller action is depicted in *Algorithm 3*. The overall implementation flowchart of the proposed methodology has been shown in Figure 7.6.

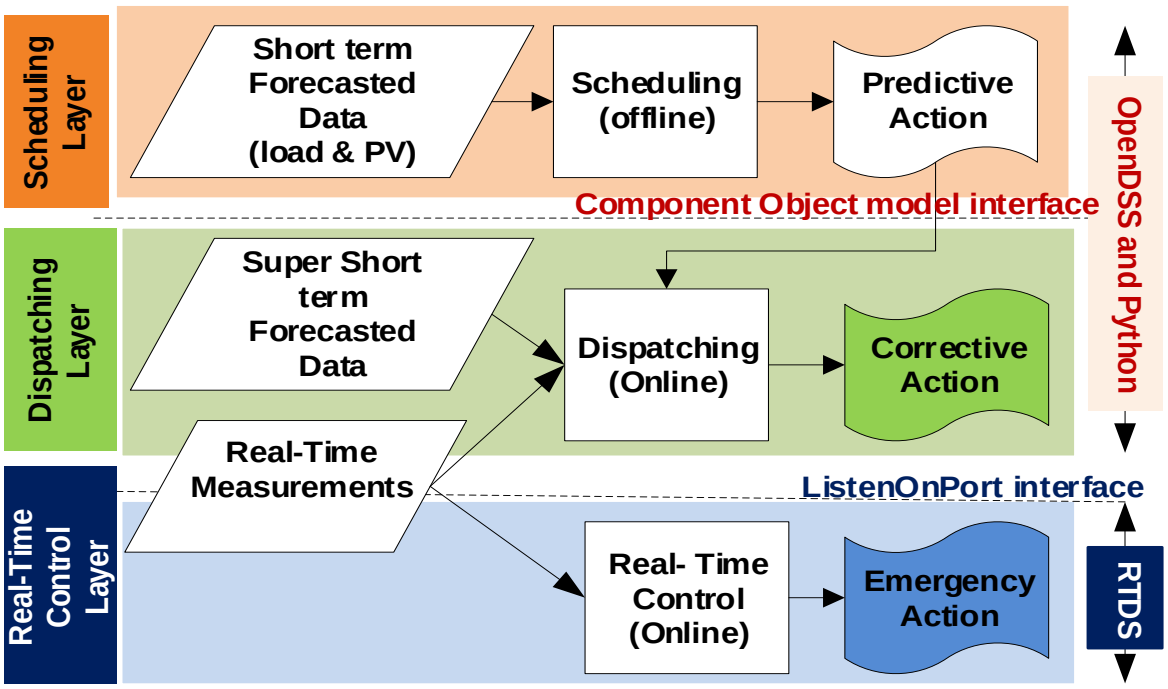

Figure 7.5 Coordinated three-layer hierarchical dispatching structure

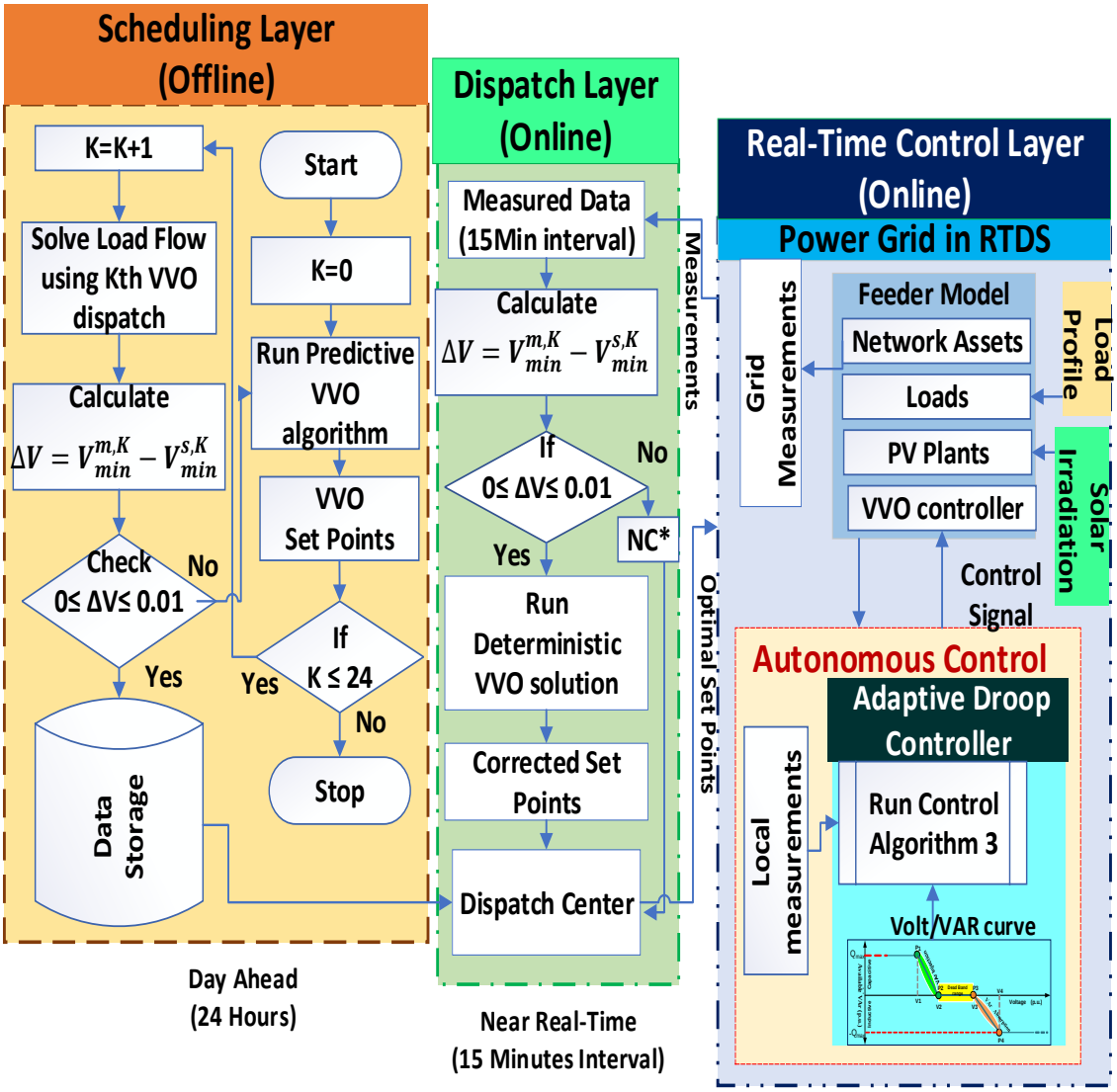

Figure 7.6. Implementation flowchart of the proposed methodology in real-time

(*NC – No change required. Already at optimal state, $V_{min}^{m,K}$, $V_{min}^{s,K}$ are the minimum measured and specified voltage, respectively)

The following special events type such as load and generation forecasting error event, voltage violation event, economic event (high power loss and CVR) and unpredicted events (cloud transients) have been considered to apply the proposed event-driven framework.

Algorithm 1: Predictive-driven day-ahead VVO scheduling layer (offline)

1 **Input:** Feed the required data of network assets and controllers
2 Initialize the counter K = 0
3 Run the predictive VVO algorithm using equation (7.2) subject to system constraints equations (7.3) -(7.8)
4 Obtain the current state VVO dispatch and stored in the sequence table
5 ***If*** K reaches its maximum limit (number of stages i.e. 96),
6 Then, stop the time series simulation
7 ***Else,*** set the counter K = K+1
8 ***Do*** the power flow using OpenDSS with previous K^{th} state
9 Then calculate: $\Delta V\ (p.u.) = V_{min}^{measured,K} - V_{min}^{specified,K}$
10 ***If*** $0 > \Delta V > 0.01$
11 Go to Step 3
12 ***Else,*** store the VVO dispatch in data storage
13 Repeat the entire process for the whole day
14 ***End***

Algorithm 2: Dispatching layer near real-time online control

1 **Input:** Feed the required load and PV solar irradiation data in the feeder model in a real-time digital simulator (RTDS)
2 Get the VVO schedule in the dispatch center from the scheduling layer
3 Send the setpoint commands to the real-time simulation
4 Collect the real-time measurements in each 15-minute interval
5 Calculate the correction factor
$\Delta V\ (p.u.) = V_{min}^{measured,K} - V_{min}^{specified,K}$
6 ***If*** $0 > \Delta V > 0.01$
7 Solve the deterministic VVO problem (7.2), subject to system constraints using Python- and OpenDSS-based co-simulations
8 Obtain the corrected dispatches, modify the sequence table
9 Send the corrected set points through the dispatch center
10 ***Else,*** no change is required; already in the optimal sate
11 ***End***

Algorithm 3: Two-level adaptive droop-based controller for Autonomous Controls operating in real-time control layer

Input: Feed the optimal VVC parameters for considered CVR duration obtained through *Algorithm 1*

Input: Feed the pre-defined droop characteristic parameters (P1, P2, P3, and P4 and deadband)

for time duration 0< t < T (as defined in STSC)

    If PV power output deviates from the forecasted value,

        check the voltage limits

        Else, if voltage profile is in the dead band range

            Control action: No action is required.

        Else, if voltage limit is violated

First Level control:

        Droop controller operates with pre-defined parameters

        Control action: Injects/absorb the compensated Q power

Second Level control:

            Calculate the correction factor (K_d)

            If , K_d is within tolerance range, no further action is required

            Else, calculate the new droop parameters using K_d

            Control action: Set the new droop parameters and injects/absorb the compensated Q power accordingly

        End

    End

End

Output: Desired additional reactive power compensation achieved.

7.6 Case study

7.6.1 Test System Description

To validate the proposed methodology, a modified IEEE 123-feeder test is considered, as shown in Figure 7.6 [24]. The total nominal load is 3.524 + j1.940 MVA, and the maximum

PV active power generation is 2.2 MW, with approximate 63% penetration. The three PV systems are connected to nodes 66abc (PV1), 26ac (PV2), and 104c (PV3) with the inverter ratings of 1,000 KVA, 800 KVA, and 400 KVA, respectively. Per-step reactive power variation from the PV inverter is 10 kVAR for the slow timescale. The OLTC and AVR transformers have ±16 taps with a per-step increment of 0.00625. The three-phase capacitor bank (CB 1) is connected to Node 83 having 200 kVAR per phase capacity with step variations from 0 to 4. Three single-phase capacitor banks (CB-2, CB-3, and CB-4) are connected to nodes 88a, 90b, and 92c, respectively, having a maximum rating of 50 kVAR. The hourly forecasted and real-time load demand and solar irradiation are shown in Figure 7.8 and Figure 7.9 for an entire typical day were taken from NREL's SMART-DS project. The controlling parameter used in the DPSO is depicted in Appendix C in Table C.1.

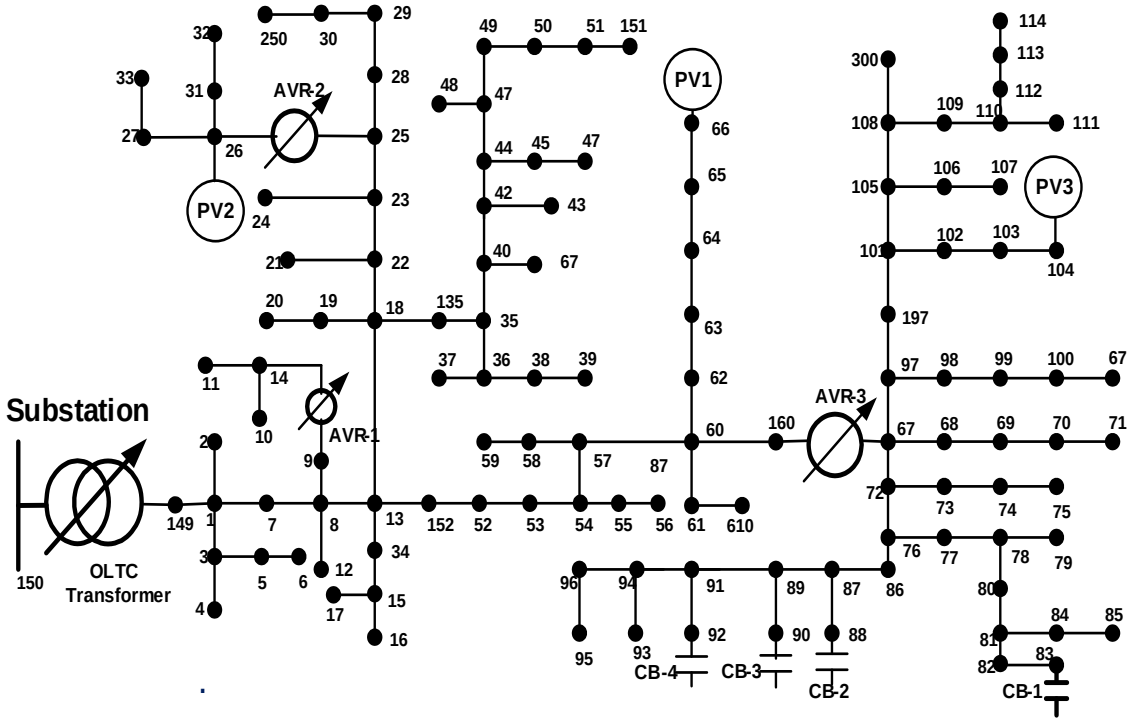

Figure 7.7 Modified IEEE 123-node distribution test feeder

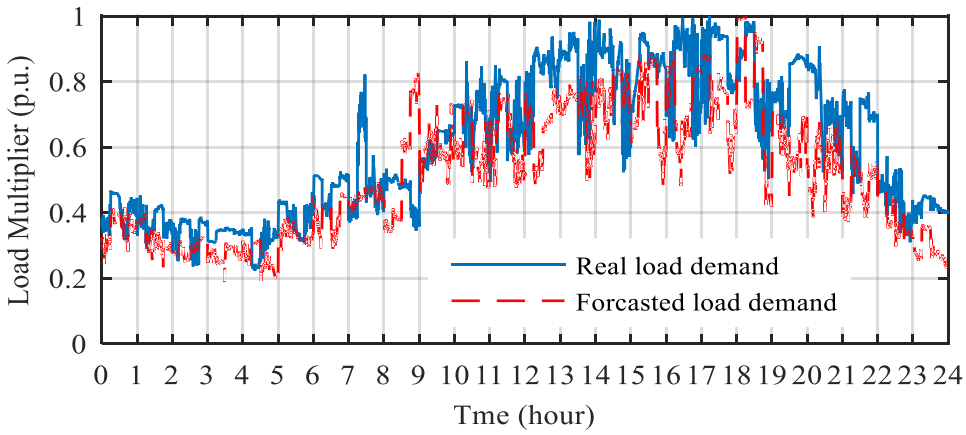

Figure 7.8. Real and forecasted load demand profile for a day

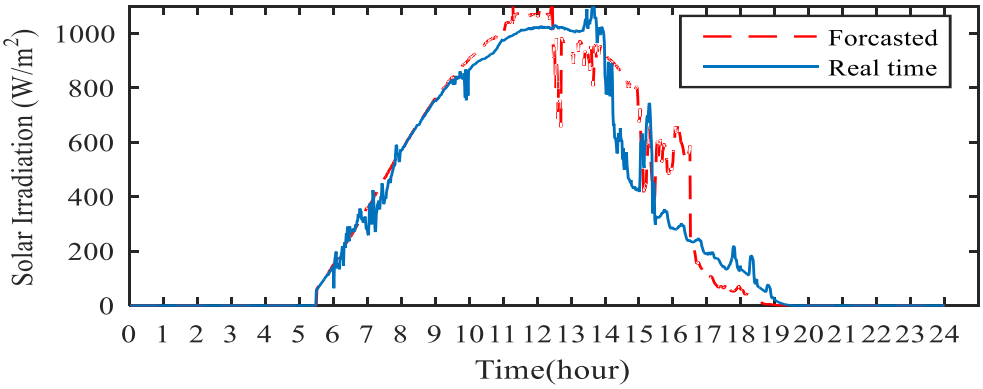

Figure 7.9. Real and forecasted solar irradiation profile for a day

7.6.2 Modes of VVC operation

The performance of the proposed method is validated for two different timescales (slow and fast) under the following three modes of VVC operation:

- *Mode 1: No CVR (Normal Operation):* In this mode, the system does not deploy CVR for VVC operation. The execution of VVC is carried out with OLTC, AVR-1, and AVR-2 at 120-V regulated voltage and AVR-3 at 124 V. Fixed CBs are used.
- *Mode 2: Traditional CVR:* In this mode, the LDC scheme is deployed for voltage reduction. The regulated voltages/end of the line are fixed in the lower half range (120 V–114 V) of

the service voltage. The control action is determined through the LDC algorithm. A detailed discussion of the LDC control mechanism is described in previous *chapter 2*. In the traditional method, the regulation voltage 118 V for OLTC, AVR-1, AVR-2, and AVR-3 is adopted to enable CVR. The level of voltage reduction can be increased to achieve increased energy savings; however, this might violate the minimum voltage limits at some points of the ADN.

- *Mode 3: Event-Driven Predictive VVO-Based CVR:* In this mode, the test system is simulated with the proposed event-driven predictive VVO-based CVR operation. The simulated results are described in Table 7.1. The event-driven predictive VVO predicts the solar PV irradiance and load demand for the next 1 hour in each 15-minute interval. Afterward, it determines and executes the control decisions for every 15-minute interval. Monte Carlo simulations are used to generate the 500 scenarios (N = 500) that signify the forecasted error in the prediction horizon. After that, the generated 500 scenarios are reduced to 15 scenarios (N' = 15). The stochastic VVO problem defined in equation (7.2) is solved every prediction horizon (1 h) using the DPSO technique.

7.6.3 Daily Energy Scheduling layer (offline simulations): Predictive Action

The proposed aggregated control *algorithm 1* is validated for the day-ahead scheduling in offline mode, considering the uncertainty in the network model. The test system is simulated for the modes, as mentioned. Table 7.1 shows the simulation results of all modes of operation. The Mode 1 (No CVR) operation results are depicted in the second column of Table 7.1. In Mode 2, CVR operation uses the traditional method, and results are portrayed in the third column of Table 7.1. Results show that around 3.96% of energy demand and 2.410% of energy losses are reduced during Mode 2 operation. Moreover, about 2.206% peak power

demand and 1.33% peak power loss are also decreased. Although sufficient energy savings and demand reduction can be achieved with traditional CVR (Mode 2), this scheme does not cooperate when any uncertainty is encountered in the network model. Moreover, system constraints are violated during deeper voltage reduction with improper VAR management. On the other hand, the proposed Mode 3 operation is capable of handling the network uncertainty, such as forecasting errors in load and generation, with proper coordination among multiple voltage regulation devices and network assets. Results shown in the fourth column of Table 7.1 indicate a reduction of about 5.039% daily energy demand and a decrease of about 4.337% kWh energy losses. AS shown by the simulation results depicted in Table 7.1, Mode 3 operation exhibits much more energy and power savings than Mode 1 and Mode 2 operations.

Table 7.1. Simulation results for the day-ahead Energy Scheduling

Energy (E)Terms	**Mode 1 (No CVR)**	**Mode 2 (Traditional CVR)**	**Mode 3 (Event-Driven Predictive-VVO-Based CVR)**
E_{demand} (MWh)	37.3005	35.8338	35.4210
ΔE_{saving} in MWh, (%)	----	1.4667, (3.96)	1.8796, (5.039)
E^{p}_{losses}, MWh	0.8055	0.7861	0.77061
ΔE^{p}_{losses} in kWh, (%)	----	19.420, (2.410)	34.937, (4.337)
Peak kW Demand	3166.60	3083.203	3044.55
ΔP_{saving} in kW, (%)	----	83.39381, (2.206)	122.0464, (3.85)
P_{losses}, kW	73.3667	72.5353	71.15977
ΔP_{losses} in kW, (%)	----	0.8315, (1.333)	2.2069, (3.08)

7.6.4 Online Real-Time Validation In RTDS

In this section, the proposed control algorithm is validated in the developed real-time co-simulation platform in online, as described in subsection 7.4. The 1-hour time duration from 14:00 to 15:00 is considered for the simulation period. The corresponding real-time load and solar irradiations are shown in Figure 7.8 and Figure 7 .9. The developed control *algorithms (2 and 3)* are tested in the STSC and FTSC scenarios, respectively.

7.6.4.1 Validation under STSC: Corrective Action:

The STSC operates in both hourly and 15-minute time intervals, as discussed in section 7.2. A near-real-time aggregated control scheme is best suited for this horizon, with the corrective action in each 15-minute interval, as shown in the flowchart in Figure 7.6 under the dispatching layer. The time-series simulations are carried out according to *Algorithm 2* for the considered time period using the developed co-simulation platform. The megawatt power demand without CVR and with proposed predictive VVO-based CVR and CVR saving is shown in Figure 7.10 and indicates that a significant amount of power demand reduction can be achieved with model predictive VVO-based CVR. Moreover, event-driven predictive VVO-based CVR reduces energy demand by about 5.39% during a 1-hour CVR duration. In addition, Table 7.2 shows the change in VVO set points during the CVR operation. Table 7.2 also shows that the action required from the OLTC and capacitor banks are in an hourly duration. On the other hand, AVR and smart inverter execute an optimal control action in a 15-minute interval according to the correction factor. If the correction factor is within limits, then no change is required. The setpoints are already at an optimal state. If not, calculate the corrected set points and corresponding required the number of changes, as shown in Table 7.2.

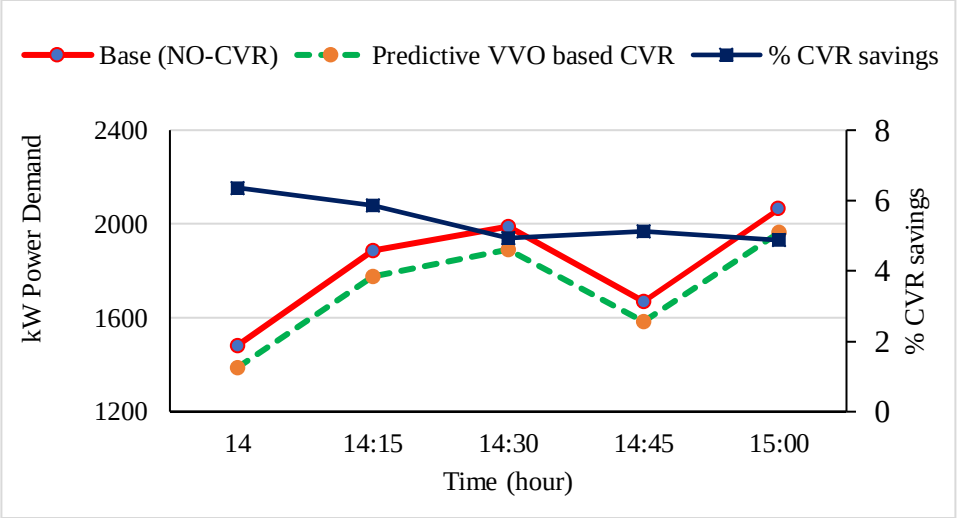

Figure 7.10 Active power demand and percentage CVR power savings

Table 7.2 VVO Set Points Change

Device/Time	14:00–14:15	14:15–14:30	14:30–14:45	14:45–15:00
OLTC	*NC, (Hourly)			
CB	NC, (Hourly)			
AVRs	NC	1	2	NC
SI Q step	NC	NC	1	NC

*NC – No change required, already at the optimal state

7.6.4.2 *Illustration under FTSC: Emergency Action*

During the occurrence of unpredicted events in fast timescale, the emergency action is executed in a real-time control layer by a local adaptive droop controller autonomously. To illustrate the effect of the developed adaptive control *algorithm 3*, two subcases of local droop control with unpredicted external disturbances have been examined as under.

- *Sudden cloud transient Appearance*

An arbitrary instantaneous point between time intervals from 14:00 to 14:15 is selected. The load demand is 1.0 p.u., and solar irradiation is 0.81 kW/m^2 at this instant. During this time span, the lowest voltage profile at Node 114a becomes vulnerable to any reduction in kilowatt power. The status of the volt/VAR regulation devices—OLTC, AVRs, and capacitor banks—remains the same as in the STSC determined by *Algorithm 2*. The solar irradiation reduces from 0.81 to 0.1 kW/m^2 because of the sudden appearance of cloud transients. Accordingly, the reduction in PV power production is reported. The decrease in active PV power injection results in a decrease in the voltage profile and system and might violate the lowest feeder voltage limit. In this study, a similar scenario is observed. The lower voltage limit (0.95 p.u.) is violated as the sudden drop in solar irradiation is reported. Figure 7.11 shows the lowest voltage profile at Node 114a without control, with conventional droop control and adaptive drop control in real-time. This figure shows that the violation of the lower voltage limit occurs when the PV inverters do not have autonomous control and even during the operation of conventional drop controller. This study employs autonomous control using the adaptive droop-based controller in real-time. Figure 7.11 also shows that there no lower voltage limit violation is reported locally when enabling autonomous controls using the proposed two-level adaptive droop controller for better visual comparison. Figure 7.12 shows the additional reactive power compensated by the adaptive droop controllers of PV inverters.

- *Sudden cloud transient Disappearance:*

An arbitrary instantaneous point between time intervals 15:00 to 15:15 is selected. The load demand is 0.40 p.u., and solar irradiation is 0.41 kW/m^2 at this instant due to cloudy weather. The sudden cloud disappearance and solar irradiation vary from 0.41 to 0.8 kW/m^2.

Accordingly, an increase in PV power production is reported. The PV3 power plant located at 104c is most affected and it violates the maximum voltage limit (1.02 p.u) at point of connection. Other PV power plant voltage remains within range. Figure 7.13 shows the comparative analysis of voltage profiles.

Figure 7.11. Lowest feeder voltage profile at Node 114a without control, conventional droop controller, and adaptive droop controllers.

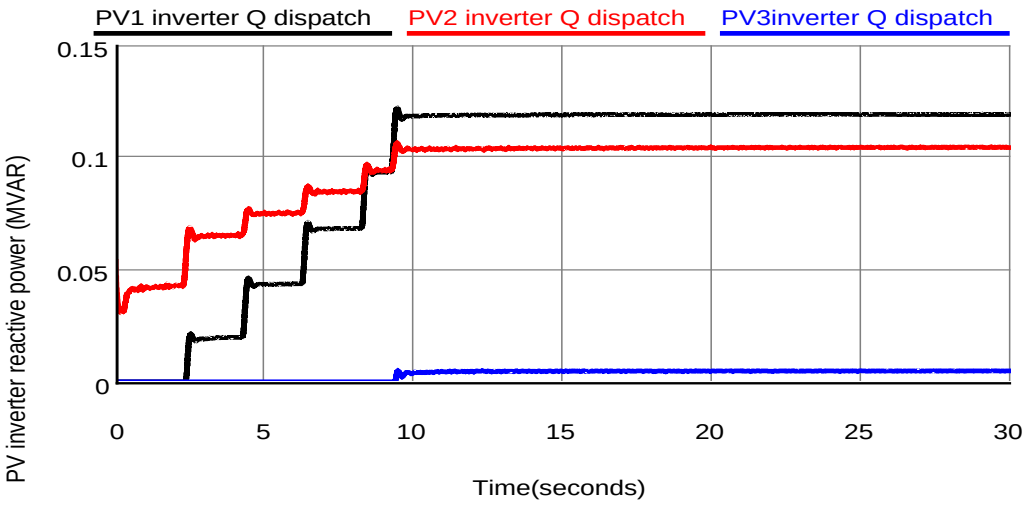

Figure 7.12 Per phase additional reactive power compensation from PV inverters

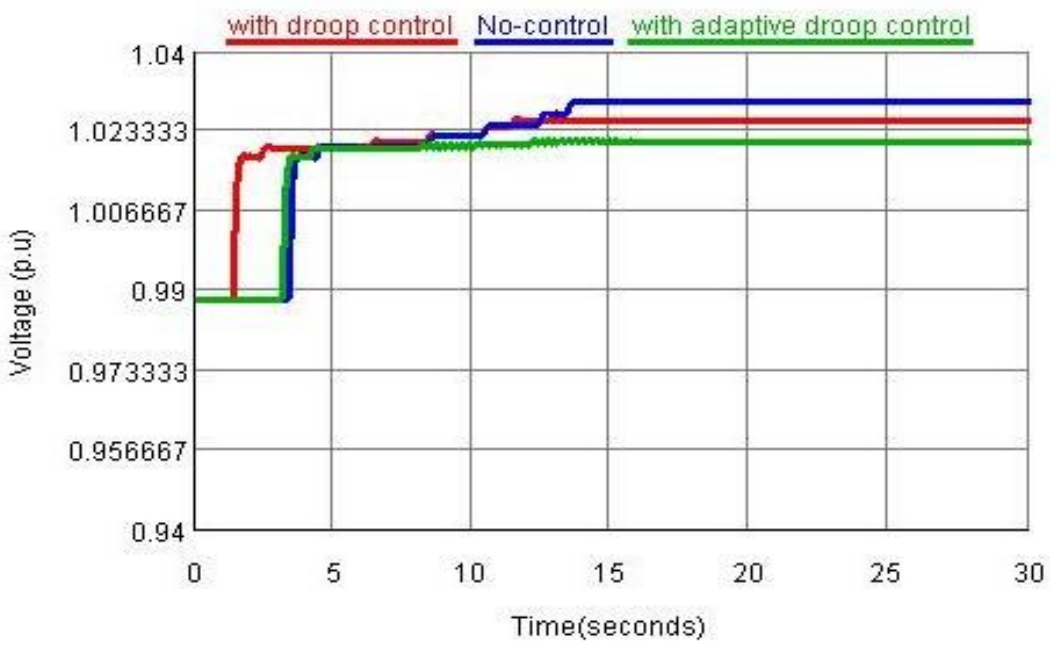

Figure 7.13 Voltage at PV3 node No control,with the conventional droop and with adaptive droop control

7.7 Conclusion

This chapter investigated the impact of CVR on energy savings in the presence of high penetrations of PV with multiple timescale control operation. An event-driven predictive control has been employed to handle the uncertainties and disturbances in PV power generation and loads under aggregated as well as the autonomous control mode. The adaptive droop control method has been used for autonomous control to mitigate the local voltage drop/rise issue during cloud transients' effect in PV active power. The simulation results reveal that the proposed event-driven predictive control method yields better performance than the LDC in terms of voltage fluctuation control and energy savings during CVR operation, even when intermittency occurs in PV power output. Moreover, the developed real-time co-simulation platform validates the effectiveness of the proposed control algorithms. The findings of this investigation are as follows:

- A significant reduction in peak load demand and daily energy demand have been achieved with the proposed method.
- The developed control methodology is proficiently capable of handling the disturbances (uncertainty and intermittency) of the active networks.
- The developed real-time co-simulation platform using the RTDS (distribution mode) could be useful for the study of large-scale practical distribution systems.

CHAPTER 8

CONCLUSIONS AND FUTURE WORK

This chapter summarized the main contributions of the thesis and discussed the salient benefits of the proposed methodologies. Finally, suggestions for future work to improve the developed schemes conclude this chapter.

8.1 Conclusions

Energy conservation in active distribution networks through advance smart VVC schemes such as CVR emerged as a viable solution for distribution operation and control. In this context, a closed-loop smart grid-enabled CVR framework has been developed in this thesis. Besides, AMI data and SCADA driven systems have been used for better monitoring and controllability of the distribution networks. The effect of different load models on CVR savings has been analyzed. Besides, voltage and VAR regulation through smart inverters have been attempted. The optimal CVR operation in the presence of DERs through VVO algorithms has also been investigated in this thesis. Besides, a multi-objective VVO framework for the multi-time-scale operation has been examined during centralized as well as local control. Further, a stochastic optimization has been employed in model predictive VVO formulation to handle the uncertainties in the system.

Increasing penetration of EV flexible loads in ADN is one of the major concerns for DNO. Therefore, in this research work, the impact of EV charging loads with different profiles on CVR operation has been analyzed. The noteworthy application of vehicle to grid reactive power dispatch from EVs charging station for voltage regulation has also been demonstrated.

The real-time event-driven predictive framework has been developed to validate the developed VVO methodology in this thesis. Besides, a coordinated three-level hierarchical dispatching structure is used to realize the event-driven predictive framework online. To check the effectiveness of the developed control algorithms and framework, a real-time co-simulation platform using RTDS in distribution mode through co-simulation with Python and OpenDSS models has been developed. In addition, a Volt/VAR curve based dynamic real-time droop controller for smart inverter's operations (both PV and EV) has been established in this research work. Real-time validation demonstrates that the proposed VVO methodology works well in centralized as well as in local domains in the presence of CVR. Further, it is also capable of controlling the voltage fluctuations during a sudden change in network behavior and the occurrence of unpredictive events.

Finally, the simulation results demonstrate that significant energy savings can be achieved through the proposed VVO algorithms without violating the network constraints. Further, it has been noticed that the proposed CVR algorithm controls the voltages closer to minimum permissible voltage limit; hence, the peak and annual energy savings could increase significantly, compared to primary substation voltage control.

The major findings of the thesis can be summarized as under:

- Proposed Smart-Grid enabled CVR could be accepted as an advance application for peak demand and energy consumption reduction
- Optimal CVR operation under high PV penetrations may solve the overvoltage and reversible power issues.
- The combined effect of VVO and distributed energy storage maximizes the benefits of both the technology

- Multi-time scale multi-objective VVC scheme comprising centralized as well as local control is suitable for voltage regulation.
- Time-horizon based model predictive VVO along with droop controller works well under aggregated and autonomous controls.
- The developed control methods are capable to handle uncertainty and intermittence such as cloud transient in PV power production without violating the feeder voltage profile.
- Reactive power compensation through EV charging station may be a potential candidate for VAR support in the future.
- The EV charging loads characteristics also influence the energy savings achieved by CVR.
- The implementation of a real-time co-simulation framework validates the developed controllers for multi time scale operations.

The concluding remark of the present thesis reveals that the reduction in load demand through developed CVR algorithms directly or indirectly reduces the power generation requirement from fossil fuel-based power plants. Hence, the decrease in carbon emission could be achieved as value addition in terms of cost and carbon footprint reduction.

8.2 Suggestions for Future Work

The present work can be further extended towards the following aspects:

(i) Various forecasting methods based on artificial intelligence and machine learning can be used in order to forecast the CVR factor accurately.

(ii) Analyze the combined effect of CVR and other ADMS functions such as network reconfiguration and demand response in the large practical distribution system.

(iii) The proposed CVR methodology can be scalable for Micro-Grid applications in both islanded and networked connected modes.

(iv) The developed real-time VVO methodology can be validated under cyber-attack and communication delay effects and develop the possible solutions for handling the malicious attacks.

(v) Analyze the impact of CVR on integrated transmission and distribution operations to assess the various parameters such as available transfer capability (ATC), voltage stability and congestion management in the transmission system.

REFERENCES

[1] V. C. Gungor *et al.*, "A Survey on smart grid potential applications and communication requirements," *IEEE Trans. Ind. Informatics*, vol. 9, no. 1, pp. 28–42, 2013.

[2] H. Farhangi, "A Road Map to Integration: Perspectives on Smart Grid Development," *IEEE Power Energy Mag.*, vol. 12, no. june, pp. 52–66, 2014.

[3] [Online].Available:http://www.mnre.gov.in/solar-mission/jnnsm/introduction 2/2Accessed 24-August-%0A2017.

[4] Tom Kenning, "Indian solar facing first curtailments in Tamil Nadu," *16 July*, 2016. [Online].Available,https://www.pv-tech.org/news/indian-solar-facing-first curtailments-in-tamil-nadu, accessed 24-August-2017

[5] "How California Grid Operators Managed the Eclipse," *IEEE spectrum*. [Online].Available http://spectrum.ieee.org/energywise/green-tech/solar/how-california-grid-operatorsmanaged-the-eclipse, Accessed 24-August-2017.

[6] C. J. Hanley, G. H. Peek, and J. D. Boyes, "Solar Energy Grid Integration Systems – Energy Storage (SEGIS-ES)," no. July, 2008.

[7] M. N. Rao, "Energy Conservation Opportunities In Power Distribution Systems - a paper presentation at PMI workshop."2004.

[8] "Intergovernmental Panel on Climate Change - IPCC,"Climate Change 2014: Mitigation of Climate Change," 2014,"." online available https://www.ipcc.ch/report/ar5/wg2/

[9] International Energy Agency (IEA), "Electricity Information 2017,",2018. https://webstore.iea.org/electricity-information

[10] O. P. M. Abdelhay and A. Sallam, *Electric Distribution Systems*. Wiley-IEEE Press, 2011.

[11] R. W. Uluski, "VVC in the Smart Grid Era .," *IEEE PES Gen. Meet.*, pp. 1–7, 2010.

[12] V. D. P. Eng *et al.*, "BC Hydro's Experience on Voltage VAR Optimization in Distribution System," *IEEE PES T&D 2010*, pp. 1–7, 2010.

[13] V. Dabic, "Voltage Var Optimization Real Time Closed Loop Deployment - BC Hydro Challenges and Opportunities," *2015 IEEE Power Energy Soc. Gen. Meet.*, pp. 1–5, 2015.

[14] H. Ahmadi, J. R. Martí, and H. W. Dommel, "A Framework for Volt-VAR Optimization in Distribution Systems," *IEEE Trans. Smart Grid*, vol. 6, no. 3, pp. 1473–1483, 2015.

[15] S. Rahimi, S. Massucco, and F. Silvestro, "Coordinated Closed-Loop Voltage Control by using a Real-time Volt / VAR Optimization Function for MV Distribution Networks," *2015 IEEE 15th Int. Conf. Environ. Electr. Eng.*, vol. 2, no. 1, pp. 1222–1228, 2015.

[16] S. Rahimi, M. Marinelli, and F. Silvestro, “Evaluation of requirements for Volt / Var Control and Optimization function in Distribution Management Systems,” *2012 IEEE Int. Energy Conf. Exhib.*, pp. 331–336, 2012.

[17] Renewables 2017: Global Status Report, “Renewable Energy Policy Network for the 21st Century,” 2017.

[18] W. H. William, *Distribution System System Modeling and Analysis, Third Edition*, CRC press, 2012.

[19] M. Farivar, C. R. Clarke, S. H. Low, and K. M. Chandy, “Inverter VAR Control for Distribution Systems with Renewables,” *2011 IEEE Int. Conf. Smart Grid Commun.*, pp. 457–462.

[20] T. Van Dao, S. Chaitusaney, and H. T. N. Nguyen, “Linear least-squares method for conservation voltage reduction in distribution systems with photovoltaic inverters,” *IEEE Trans. Smart Grid*, vol. 8, no. 3, pp. 1252–1263, 2017.

[21] P. Jahangiri, S. Member, D. C. Aliprantis, and S. Member, “Distributed Volt / VAr Control by PV Inverters,” *IEEE Trans. Power Syst.*, vol. 28, no. 3, pp. 3429–3439, 2013.

[22] Price, W. W., et al. "Load representation for dynamic performance analysis,” vol. 8, no. 2, pp. 472–482, 1993.

[23] K. P. Schneider, and J. C. Fuller,“Detailed End Use Load Modeling for Distribution System Analysis,” *IEEE PES Gen. Meet.*, pp. 1–7, 2010.

[24] B. Shah, A. Bose, and A. Srivastava, “Load Modeling and Voltage Optimization Using Smart Meter Infrastructure,” *2013 IEEE PES Innov. Smart Grid Technol. Conf.*, pp. 1–6, 2013.

[25] K. P. Schneider, S. Member, J. C. Fuller, D. P. Chassin, and S. Member, “Multi-State Load Models for Distribution System Analysis,” *IEEE Trans. Power Syst.*, vol. 26, no. 4, pp. 2425–2433, 2011.

[26] A. Arif *et al.*, “Load Modeling — A Review,” *IEEE Trans. Smart Grid*, vol. 9, no. 6, pp. 5986–5999, 2018.

[27] Forsten, K, “Green Circuit: Distribution Efficiency Case Studies,” *Electric Power Research Institute (EPRI)*, Technical Report, *Palo Alto*, 2011.

[28] R. C. Dugan, “Reference Guide the Open Distribution System Simulator (OpenDSS),” no. June, pp. 1–214, 2019.

[29] Y. Hong, F. Lin, , Y. Lin, and F. Hsu, “Chaotic PSO-Based VAR Control Considering Renewables Using Fast Probabilistic Power Flow,” *IEEE Trans. Power Deliv.*, vol. 29, no. 4, pp. 1666–1674, 2014.

[30] Z. Wang *et al.*, “MPC-Based Voltage / Var Optimization for Distribution Circuits With Distributed Generators and Exponential Load Models,” *IEEE Trans. Smart Grid*, vol. 5, no. 5, pp. 2412–2420, 2014.

[31] A. Padilha-feltrin, D. Alexis, Q. Rodezno, J. Roberto, and S. Mantovani, “Volt-VAR Multiobjective Optimization to Peak-Load Relief and Energy Efficiency in Distribution Networks,” *IEEE Trans. Power Deliv*, vol. 30, no. 2, pp. 618–626,

2015.

[32] Z. Wang, J. Wang, and S. Member, “Review on Implementation and Assessment of Conservation Voltage Reduction,” *IEEE Trans. Power Deliv*, vol. 29, no. 3, pp. 1306–1315, 2014.

[33] ANSI C84.1-1995, “American National Standards for Electric Power Systems and Equipment—Voltage Ratings (60 Hz),” 1995.

[34] CAN3-C235-83, “Preferred Voltage Levels for AC Systems,0 to 50 000 V,” 1983.

[35] De Steese, J. G., J. E. Englin, and R. D. Sands. Conservation voltage reduction potential in the Pacific Northwest. No. PNL-SA-17705; CONF-900801-37. Pacific Northwest Lab., Richland, WA (USA), 1990.

[36] D. M. Lauria and P. O. Box, "Conservation voltage reduction (CVR) at Northeast utilities." *IEEE Trans. Power Deliv*, no. 4, pp. 1186–1191, 1987.

[37] D. Kirshner and P. Giorsetto,"Statistical test of energy saving due to voltage reduction." *IEEE Trans on Power App. and Systems*, no. 6, pp. 6–11, 1984.

[38] M. S. Chen, R. Shoults, and J. Fitzer, "The effects of reduced voltages on the efficiency of electric loads." *IEEE Trans. on Power Apparatus and Systems*, no. 7, pp. 2158–2166, 1982.

[39] Erickson, J. C., and S. R. Gilligan. "The effects of voltage reduction on distribution circuit loads." *IEEE Trans. on Power Apparatus and Systems*, no. 7, pp. 2014–2018, 1982.

[40] B. W. Kennedy, and R. H. Fletcher. "Conservation voltage reduction (CVR) at Snohomish County PUD." *IEEE Trans. on Power Systems*," vol. 6, no. 3, pp. 986–998, 1991.

[41] A. Dwyer, R. E. Nielsen, J. Stangl, B. C. Hydro, B. C. V. N. Canada, and N. S. Markushevich, “Load to voltage dependency tests at B.C. Hydro, *IEEE Trans. on,” Power Systems*, vol. 10, no. 2, pp. 709–715, 1995.

[42] M. A. Peskin, P. W. Powell, and E. J. Hall, “Conservation Voltage Reduction with Feedback from Advanced Metering Infrastructure,” *PES T&D 2012*, pp. 1–8, 2012.

[43] B. R. Williams, “Distribution Capacitor Automation Provides Integrated Control of Customer Voltage Levels and Distribution Reactive Power Flow,” *In Proceedings of Power Industry Computer Applications Conference,* pp. 215-220. IEEE, 1995.

[44] J. De Steese, *Assessment of Conservation Voltage Reduction Applicable in the BPA Service Region*. *BPA, PNL 6380, Pacific Northwest Laboratories*. 1987.

[45] K. P. Schneider, “Evaluation of Conservation Voltage Reduction (CVR) on a National Level,” Pacific Northwest National Lab.(PNNL), Richland, WA (United States),July, 2010.

[46] W. Ellens, A. Berry, and S. West, “A Quantification of the Energy Savings by Conservation Voltage Reduction,” *2012 IEEE Int. Conf. Power Syst. Technol.*, pp. 1–6, 2012.

[47] T. Fallon and C. Power, “Conservation Voltage Reduction and Voltage Optimisation On Irish Distribution Networks” vol. 5, pp 264-264, 2012.

[48] P. K. Sen and K. H. Lee, “Conservation Voltage Reduction Technique : An Application Guideline for Smarter Grid,” *IEEE Trans. Ind. Appl.*, vol. 52, no. 3, pp. 2122–2128, 2016.

[49] T. A. Short and R. W. Mee, “Voltage Reduction Field Trials on Distributions Circuits,”in *IEEE PES T&D 2012*, pp. 1–6, 2012.

[50] J. M. Triplett and S. A. Kufel, “Implementing CVR through Voltage Regulator LDC Settings,” *2012 Rural Electr. Power Conf.*, pp. B2-1-B2-5, 2012.

[51] A. Bokhari *et al.*, “Combined Effect of CVR and DG Penetration in the Voltage Profile of Low-Voltage Secondary Distribution Networks,” *IEEE Trans. Power Deliv* vol. 31, no. 1, pp. 286–293, 2016.

[52] R. Anilkumar, G. Devriese, and A. K. Srivastava, “Voltage and Reactive Power Control to Maximize the Energy Savings in Power Distribution System With Wind Energy,” *IEEE Trans. Ind. Appl.*, vol. 54, no. 1, pp. 656–664, 2018.

[53] M. Diaz-aguiló *et al.*, “Field-Validated Load Model for the Analysis of CVR in Distribution Secondary Networks : Energy Conservation,” *IEEE Trans. Power Deliv* ,vol. 28, no. 4, pp. 2428–2436, 2013.

[54] S. Chanda, F. Shariatzadeh, A. Srivastava, E. Lee, W. Stone, and J. Ham, “Implementation of non-intrusive energy saving estimation for Volt / VAr control of smart distribution system,” *Electr. Power Syst. Res.*, vol. 120, pp. 39–46, 2015.

[55] J. Pierre *et al.*, “Energy and Economic Impacts of the Application of CVR in Heavily Meshed Secondary Distribution Networks,” *IEEE Trans. Power Deliv*, vol. 29, no. 4, pp. 1692–1700, 2014.

[56] J. Park, S. Nam, J. Park, and S. Member, “Control of a ULTC Considering the Dispatch Schedule of Capacitors in a Distribution System,” *IEEE Trans. Power Syst*, vol. 22, no. 2, pp. 755–761, 2007.

[57] S. Member, “Capacitor Placement for Conservative Voltage Reduction on Distribution Feeders,” *IEEE Trans. Power Deliv* ,vol. 19, no. 3, pp. 1360–1367, 2004.

[58] S. Emiroglu, Y. Uyaroglu, and G. Ozdemir, “Distributed Reactive Power Control based Conservation Voltage Reduction in Active Distribution Systems,” *Advances in Electrical and Computer Engineering*, vol. 17, no. 4, pp. 99–106, 2017.

[59] C. McCarthy and J. Josken, “Applying capacitors to maximize benefits of conservation voltage reduction,” in *IEEE Rural Electric Power Conference, 2003*, 2003, pp. C4-C4.

[60] J. Zhao, Z. Wang, and J. Wang, “Robust Time-Varying Load Modeling for Conservation Voltage Reduction Assessment,” *IEEE Trans. Smart Grid*, vol. 9, no. 4, pp. 3304–3312, 2018.

[61] D. G. Bell, P. C. S. Utilidata, and D. G. Bell, “"Energy conservation and demand control using distribution automation technologies," in *Rural Electric Power Conference, 2004*, 2004, pp. C4-1-12.

[62] M. Nasri, G., H. Farhangi, A. Palizban, and M. Moallem, “Multi-Agent Control System for Real-time Adaptive VVO / CVR in Smart Substation,” In *2012 IEEE Electrical Power and Energy Conference*, pp. 1–7, 2012.

[63] N. Markushevich, and W. Luan, “Achieving Greater VVO Benefits through AMI Implementation,” In *2011 IEEE Power and Energy Society General Meeting*, pp. 1-7. IEEE, 2011.

[64] M. System, B. Shahabi, H. Farhangi, and A. Palizban, “Real-time adaptive VVO/CVR topology using multi-agent system and IEC 61850-based communication protocol." *IEEE Trans. on Sust. Energy*” vol. 5, no. 2, pp. 587–597, 2014.

[65] I. Roytelman, I. S. Member, J. Medina, and I. S. Member, “Volt / VAR Control and Conservation Voltage Reduction as a Function of Advanced DMS,” *2016 IEEE Power Energy Soc. Innov. Smart Grid Technol. Conf.*, no. Vvc, pp. 1–4, 2016.

[66] A. Borghetti, F. Napolitano, and C. A. Nucci, “Electrical Power and Energy Systems Volt / var optimization of unbalanced distribution feeders via mixed integer linear programming,” *Int. J. Electr. Power Energy Syst.*, vol. 72, pp. 40–47, 2015.

[67] S. Paudyal, S. Member, and C. A. Cañizares, “Optimal Operation of Distribution Feeders in Smart Grids,” *IEEE Trans. on Ind. Elect.*, vol. 58, no. 10, pp. 4495–4503, 2011.

[68] F. Ding, and M. Baggu, “Coordinated Use of Smart Inverters with Legacy Voltage Regulating Devices in Distribution Systems with High Distributed PV Penetration — Increase CVR Energy Savings,” *IEEE Trans. Smart Grid*, vol. PP, no. c, p. 1, 2018.

[69] B. A. De Souza, S. Member, A. Márcio, and F. De Almeida, “Multiobjective Optimization and Fuzzy Logic Applied to Planning of the Volt / Var Problem in Distributions Systems,” *IEEE Trans. Power Syst.*, vol. 25, no. 3, pp. 1274–1281, 2010.

[70] S. Satsangi and G. B. Kumbhar, “Effect of load models on scheduling of VVC devices in a distribution network,” *IET Generation, Trans. & Distr.,* 12.17, 2018, pp: 3993-4001.

[71] D. F. Pires, A. G. Martins, and C. H. Antunes, “A Multiobjective Model for VAR Planning in Radial Distribution Networks Based on Tabu Search,” *IEEE Trans. Power Syst.*, vol. 20, no. 2, pp. 1089–1094, 2005.

[72] V. B. Pamshetti, “Optimal coordination of PV smart inverter and traditional volt - VAR control devices for energy cost savings and voltage regulation,” *Inter. Trans. on Electrical Energy Systems*,2019: e12042, pp. 1–24, 2019.

[73] H. Yoshida, K. Kawata, Y. Fukuyama, S. Takayama, and Y. Nakanishi, “A Particle Swarm Optimization for Reactive Power and Voltage Control Considering Voltage Security,” *IEEE Trans. Power Syst.*, vol. 15, no. 4, pp. 1232–1239, 2000.

[74] A. E. Group, “CVR as an Energy Efficiency Resource,” *IEEE Innovative Smart Grid Technologies Conference*, Washington DC, USA, 2014. 2014.

[75] S. Hossan, S. Member, B. Chowdhury, and S. Member, "Time-Varying Stochastic and Analytical Assesment of CVR in DER Integrated Distribution Feeder." In *2017 North American Power Symposium (NAPS)* (pp. 1-6). IEEE.

[76] D. Ranamuka, A. P. Agalgaonkar, and K. M. Muttaqi, "Electrical Power and Energy Systems Conservation voltage reduction and VAr management considering urban distribution system operation with solar-PV," *Electr. Power Energy Syst.*, vol. 105, no. September 2018, pp. 856–866, 2019.

[77] F. Ding *et al.*, "Application of Autonomous Smart Inverter Volt-VAR Function for Voltage Reduction Energy Savings and Power Quality in Electric Distribution Systems," In *2017 IEEE Power & Energy Society Innovative Smart Grid Technologies Conference (ISGT)*, pp. 1-5. IEEE, 2017.

[78] R. Singh, F. Tuffner, J. Fuller, K. Schneider, and S. Member, "Effects of Distributed Energy Resources on Conservation Voltage Reduction (CVR)," *2011 IEEE Power Energy Soc. Gen. Meet.*, pp. 1–7, 2011.

[79] T. Lawanson, R. Karandeh, V. Cecchi, and A. Kling, "Impacts of Distributed Energy Resources and Load Models on Conservation Voltage Reduction," *2018 Clemson Univ. Power Syst. Conf.*, pp. 1–6.,2018.

[80] G. B. K. Satsangi, Saran, "Integrated volt-VAr optimization with distributed energy sources to minimize substation energy in distribution system," *Electr. Power Components Syst.*, vol. 46, no. 14–15, pp. 1522–1539, 2018.

[81] L. Gutierrez-lagos, G. S. Member, L. F. Ochoa, and S. Member, "OPF-Based CVR Operation in PV-Rich MV – LV Distribution Networks," *IEEE Trans. Power Syst.*, vol. 34, no. 4, pp. 2778–2789, 2019.

[82] M. Farivar, R. Neal, C. Clarke, and S. Low, "Optimal Inverter VAR Control in Distribution Systems with High PV Penetration," *2012 IEEE Power Energy Soc. Gen. Meet.*, pp. 1–7, 2012.

[83] Z. Wang, S. Member, B. Chen, J. Wang, S. Member, and M. M. Begovic, "Stochastic DG Placement for Conservation Voltage Reduction Based on Multiple Replications Procedure," *IEEE Trans. Power Deliv.*, vol. 30, no. 3, pp. 1039–1047, 2015.

[84] R. P. Xu, C. Zhang, Y. Xu, and Z. Y. Dong, "Rolling horizon based multi-objective robust voltage / VAR regulation with conservation voltage reduction in high PV-penetrated distribution networks," pp. 1621–1629, 2019.

[85] D. A. Quijano and A. Padilha-feltrin, "Electrical Power and Energy Systems Optimal integration of distributed generation and conservation voltage reduction in active distribution networks," *Electr. Power Energy Syst.*, vol. 113, no. October 2018, pp. 197–207, 2019.

[86] S. Satsangi and G. B. Kumbhar, "Energy Savings Estimation Considering Volt / VAr Optimization and Distributed Generation," *2019 IEEE 28th Int. Symp. Ind. Electron.*, pp. 87–92, 2019.

[87] D. A. Quijano, "Assessment of Conservation Voltage Reduction Effects in Networks with Distributed Generators," *2015 IEEE PES Innov. Smart Grid Technol. Lat. Am. (ISGT LATAM)*, pp. 393–398, 2015.

[88] H. J. Liu and T. J. Overbye, "Smart-Grid-Enabled Distributed Reactive Power Support with Conservation Voltage Reduction," *2014 Power Energy Conf. Illinois*, pp. 1–5.

[89] "IEEE standard for interconnection and interoperability of distributed energy resources with associated electric power systems interfaces,." in IEEE Std 1547-2018 (Revision of IEEE Std 1547-2003), vol., no., pp.1-138, 6 April 2018

[90] IWG Phase 3 DER Functions:, "Recommendations to the CPUC for Rule 21, Phase 3 Function Key Requirements, and Additional Discus sion Issues." March 31, 2017.

[91] H. V. Padullaparti, N. Ganta, and S. Santoso, "Grid, Voltage regulation at edge: Tuning of pv smart inverter control," in *in Proc. IEEE/PES Transmis Distrib. Conf. Expo., 2*.

[92] A. Singhal, V. Ajjarapu, J. Fuller, and J. Hansen, "Real-Time Local Volt / Var Control Under External Disturbances With High PV Penetration," *IEEE Trans. Smart Grid*, vol. 10, no. 4, pp. 3849–3859, 2019.

[93] M. Jafari, and T. O. Olowu,, "Optimal Smart Inverters Volt-VAR Curve Selection with a Multi-Objective Volt- VAR Optimization using Evolutionary Algorithm Approach," *2018 North Am. Power Symp.*, no. September, pp. 1–6, 2018.

[94] Y. Shi and M. Baran, "Distribution Systems with High DER Penetration," *2019 IEEE PES GTD Gd. Int. Conf. Expo. Asia (GTD Asia)*, no. 2, pp. 649–654, 2019.

[95] L. Wang, S. Member, F. Bai, and R. Yan, "Real - Time Coordinated Voltage Control of PV Inverters and Energy Storage for Weak Networks with High PV Penetration." *IEEE Trans. Power Systems* vol. 33,no. 3, no. 4, pp. 3849–3859, 2019.

[96] H. Farhangi *et al.*, "Real-time co-simulated platform for novel Volt-VAR Optimization of smart distribution network using AMI data," In *2015 IEEE International Conference on Smart Energy Grid Engineering (SEGE)*, pp. 1-7. IEEE, 2015

[97] A. Pratt *et al.*, "Test Bed to Evaluate Advanced Distribution Management Systems for Modern Power Systems Preprint Test Bed to Evaluate Advanced Distribution Management Systems for Modern Power Systems Preprint,"National Renewable Energy Laboratory (NREL), USA no. July, 2019.

[98] B. Panajotovic, M. Jankovic, and B. Odadzic, "ICT and Smart Grid," *2011 10th Int. Conf. Telecommun. Mod. Satell. Cable Broadcast. Serv.*, vol. 1, pp. 118–121, 2011.

[99] R. Bottura, A. Borghetti, F. Napolitano, and C. A. Nucci, "lCT -power Co-simulation Platform for the Analysis of Communication-based Volt / Var Optimization in Distribution Feeders," *ISGT 2014*, pp. 1–5, 2014.

[100] H. Farhangi *et al.*, "Real-time communication platform for Smart Grid adaptive Volt-VAR Optimization of distribution networks," *2015 IEEE Int. Conf. Smart Energy Grid Eng.*, pp. 1–7.

[101] A. Electric and P. Service, "Impact of voltage reduction on energy and demand,"

IEEE Trans. on Power Apparatus and Systems, vol. PAS-97, no. 5, pp. 1665-1671, Sept. 1978. vol. 75, no. 5, pp. 1665–1671, 1978.

[102] Daniel Kirshner, "Implementation Of Conservation Voltage Reduction At Commonwealth Edison" *IEEE Trans. on Power Systems*, vol. 5, no. 4, November 1990

[103] C. S. Chen, T. H. Wu, C. C. Lee, and Y. M. Tzeng, "The Application of Load Models of Electric Appliances to Distribution System Analysis," *IEEE Trans. Power Syst.*, vol. 10, no. 3, pp. 1376–1382, 1995.

[104] Northwest Energy Efficiency Alliance, "Distribution Efficiency Initiative Final Report," December 2007.

[105] Global Energy Partners, LLC "Utility Distribution System Efficiency (DEI): Phase 1," Market Progress Evaluation Report ,2008.

[106] S. Lefebvre, G. Gaba, A. Ba, and D. Asber, "Measuring the Efficiency of Voltage Reduction at Hydro-Québec Distribution," In *2008 IEEE Power and Energy Society General Meeting-Conversion and Delivery of Electrical Energy in the 21st Century*, pp. 1–7, 2008.

[107] K. P. Schneider, J. C. Fuller, and D. Chassin, "Evaluating conservation voltage reduction: An application of GridLAB-D: An open source software package," *IEEE Power Energy Soc. Gen. Meet.*, pp. 1–6, 2011.

[108] W. G. Sunderman, "Conservation Voltage Reduction System Modeling, Measurement, and Verification," in *IEEE PES T&D 2012*, pp. 1–4, 2012.

[109] Z. Wang, S. Member, M. Begovic, J. Wang, and S. Member, "Analysis of Conservation Voltage Reduction Effects Based on Multistage SVR and Stochastic Process," *IEEE Trans. Smart Grid*, vol. 5, no. 1, pp. 431–439, 2014.

[110] K. Shim, S. Go, and S. Yun, "Estimation of Conservation Voltage Reduction Factors Using Measurement Data of KEPCO System," *Energies* 10, no. 12,2017 pp.: 2148 .

[111] L. Gutierrez-lagos, "Advanced voltage control for energy conservation in distribution networks A thesis submitted to The University of Manchester for the degree of," no. December 2018, 2019.

[112] T. J. Krupa, "The Detroit Edison Company HaukurAsgeirsson," no. 4, 1987.

[113] R. C. Dugan, T. E. Mcdermott, and S. Member, "An Open Source Platform for Collaborating on Smart Grid Research," *2011 IEEE Power Energy Soc. Gen. Meet.*, pp. 1–7, 2011.

[114] "IEEE PES distribution test feeders'," *IEEE*. [Online]. Available: https://site.ieee.org/pes-testfeeders/resources/.

[115] A. Nourai, S. Member, R. Sastry, and T. Walker, "A Vision & Strategy for Deployment of Energy Storage in Electric Utilities," *2011 IEEE Power Energy Soc. Gen. Meet.*, pp. 1–4, 2010.

[116] American Electric Power,"Functional Specification For Community Energy Storage (CES) Unit."2009

[117] P. R. Thomas, I. T. J. W. Jr, and C. A. Mccarthy, “Demonstration of Community Energy Storage Fleet for Load Leveling , Reactive Power Compensation , and Reliability Improvement,” *2011 IEEE Power Energy Soc. Gen. Meet.*,pp. 1–4, 2012.

[118] D. Parra, M. Gillott, S. A. Norman, and G. S. Walker, “Optimum community energy storage system for PV energy time-shift q,” *Appl. Energy*, vol. 137, no. September 2013, pp. 576–587, 2020.

[119] B. B. P. Roberts and C. Sandberg, “The Role of Energy Storage in Development of Smart Grids,” *Proceedings of the IEEE*, *99*(6), pp.1139-1144, 2011.

[120] J. Sardi and N. Mithulananthan, “Smart Grid : A Review of Technology , Prospect , Challenges and Opportunity,” *2014 4th Int. Conf. Eng. Technol. Technopreneush.*, pp. 125–130, 2014.

[121] D. Parra, S. A. Norman, G. S. Walker, and M. Gillott, “Optimum community energy storage system for demand load shifting,” *Appl. Energy*, vol. 174, pp. 130–143, 2016.

[122] R. Arghandeh, J. Woyak, A. Onen, J. Jung, and R. P. Broadwater, “Economic optimal operation of Community Energy Storage systems in competitive energy markets,” *Appl. Energy*, vol. 135, pp. 71–80, 2014.

[123] S. A. El-batawy and W. G. Morsi, “Optimal Design of Community Battery Energy Storage Systems With Prosumers Owning Electric Vehicles,” *IEEE Trans. Ind. Informatics*, vol. 14, no. 5, pp. 1920–1931, 2018.

[124] M. J. E. Alam, K. M. Muttaqi, S. Member, D. Sutanto, and S. Member, “Community Energy Storage for Neutral Voltage Rise Mitigation in Four-Wire Multigrounded LV Feeders With Unbalanced Solar PV Allocation,” *IEEE Trans. Smart Grid*, vol. 6, no. 6, pp. 2845–2855, 2015.

[125] Y. Wang *et al.*, “Coordinated Control of Distributed Energy- Storage Systems for Voltage Regulation in Distribution Networks,” *IEEE Trans. Power System*, vol. 31, no. 3, pp. 1132–1141, 2016.

[126] Y. Zhang, S. Ren, Z. Y. Dong, Y. Xu, K. Meng, and Y. Zheng, “Optimal placement of battery energy storage in distribution networks considering conservation voltage reduction and stochastic load composition,” *IET Generation, Transmission & Distribution*, vol.,*11*, 15, 2017., pp.3862-3870.

[127] M. Manbachi, H. Farhangi, A. Palizban, and S. Arzanpour, “Community Energy Storage Impacts on Smart Grid Adaptive Volt-VAR Optimization of Distribution Networks,” In *2016 IEEE 7th International Symposium on Power Electronics for Distributed Generation Systems (PEDG)*, pp. 1-8. IEEE, 2016

[128] B. Prasad, E. Van Oost, and H. Van Der Windt, “Community energy storage : A responsible innovation towards a sustainable energy system ?,” *Appl. Energy*, vol. 231, no. June, pp. 570–585, 2018.

[129] E. Rashedi, H. Nezamabadi-pour, and S. Saryazdi, “GSA : A Gravitational Search Algorithm,” *Inf. Sci. (Ny).*, vol. 179, no. 13, pp. 2232–2248, 2009.

[130] M. R. Narimani, A. A. Vahed, R. Azizipanah-abarghooee, and M. Javidshari,

"Enhanced gravitational search algorithm for multi-objective distribution feeder reconfiguration considering reliability , loss and operational cost," *IET Generation, Transmission & Distribution*, vol 8 (1), 2014, pp 55-69.

[131] S. P. Singh and S. P. Singh, "Optimal cost wide area measurement system incorporating communication infrastructure," *IET Generation, Transmission & Distribution*, vol. 11, pp. 2814–2821, 2017.

[132] S. Das, D. Chatterjee, and S. K. Goswami, "A GSA-Based Modified SVC Switching Scheme for Load Balancing and Source Power," *IEEE Trans. Power Deliv.*, vol. 31, no. 5, pp. 2072–2082, 2016.

[133] C. Kamalakannan, L. Padma Suresh, S. S. Dash, and B. K. Panigrahi, "Power Electronics and Renewable Energy Systems: Proceedings of ICPERES 2014," *Lect. Notes Electr. Eng.*, vol. 326, pp. 853–862, 2014.

[134] Grigg, C., Wong, P., Albrecht, P., Allan, R., Bhavaraju, M., Billinton, R.,"Reliability Test System Task Force of the Application of ProbabilityMethods Subcommittee," *IEEE Trans. Power Syst.*, vol. 14, no. 3, pp.1010-1020, Aug 1999

[135] C. Coello, G. Pulido, and M. Lechuga, "Handling multiple objectives with particle swarm optimization," IEEE Trans. Evol. Comput., vol. 8, no. 3, pp. 256–279, Jun. 2004.

[136] Del Valle, Del Valle, Y., Venayagamoorthy, G.K., Mohagheghi, S., Hernandez, J.C. and Harley, R.G.. "Particle swarm optimization: basic concepts, variants and applications in power systems." *IEEE Trans. Evol. Comput.*, vol. 12, no. 2, pp. 171-195, 2008.

[137] "IEX | Indian Energy Exchange Limited | IEX India.". https://www.iexindia.com/marketdata/areaprice.aspx (assess on 01/08/2017)

[138] T. Niknam, M. Zare, and J. Aghaei, "Scenario-based multiobjective volt/var control in distribution networks including renewable energy sources," *IEEE Trans. Power Deliv.*, vol. 27, no. 4, pp. 2004–2019, 2012.

[139] C. Zhang, Y. Xu, Z. Dong, and J. Ravishankar, "Three-Stage Robust Inverter-Based Voltage/Var Control for Distribution Networks with High-Level PV," *IEEE Trans. Smart Grid*, vol. 10, no. 1, pp. 782–793, 2019.

[140] A. Krishnan, S. Member, A. Ukil, and S. Member, "Agent-Based Aggregated Behavior Modeling for," *IEEE Trans. Ind. Informatics*, vol. 15, no. 2, pp. 856–868, 2019.

[141] J. Xiong, S. Member, K. Zhang, Y. Guo, and S. Member, "Investigate the Impacts of PEV Charging Facilities on Integrated Electric Distribution System and Electrified Transportation System," *IEEE Trans. Transp. Electrif.*, vol. 1, no. 2, pp. 178–187, 2015.

[142] B. K. Jha, "Coordinated effect of PHEVs with DGs on distribution network," *Int. Trans. on Electrical Energy Systems, p. e2800.* pp. 1–24, 2019.

[143] Q. I. Han, G. A. O. Xiaojing, G. A. O. Yifang, Z. Hongmei, and L. I. Zhipeng, "Optimization of the Active Distribution Network Operation Considering the V2G

Mode of Electric Vehicles," i*n 2018 International Conference on Power System Technology (POWERCON). IEEE, 2018*, pp. 4488–4493.

[144] N. Leemput, F. Geth, J. Van Roy, J. Büscher, and J. Driesen, "Sustainable Energy , Grids and Networks Reactive power support in residential LV distribution grids through electric vehicle charging," *Sustain. Energy, Grids Networks*, vol. 3, pp. 24–35, 2015.

[145] M. Manbachi, H. Farhangi, A. Palizban, and S. Arzanpour, "A novel Volt-VAR Optimization engine for smart distribution networks utilizing Vehicle to Grid dispatc," *Int. J. Electr. Power Energy Syst.*, vol. 74, pp. 238–251, 2016.

[146] M. Manbachi *et al.*, "Impact of EV penetration on Volt – VAR Optimization of distribution networks using real-time co-simulation monitoring platform," *Appl. Energy*, vol. 169, pp. 28–39, 2016.

[147] N. Bhusal, "The Combined Effect of Photovoltaic and Electric Vehicle Penetration on Conservation Voltage Reduction in Distribution System," no. May, 2018.

[148] L. Wu, L. Jiang, and X. Hao, "Optimal Scenario Generation Algorithm for Multi-objective Optimization Operation of Active Distribution Network," *Control Conference (CCC)*, 2017 36th Chinese. IEEE, 2017.

[149] R. Eberhart and J. Kennedy, "A New Optimizer Using Particle Swarm Theory,"., *Proceedings of the Sixth International Symposium on*. Micro Machine and Human Science, 1995. MHS'95IEEE, 1995. pp. 39–43.

[150] "Connecting RSCAD / Runtime with external applications Using ' ListenOnPort ()' script command."

[151] K. M. Dowling, "Hardware-In-Loop Evaluation of Microgrid Protection Schemes," 2014.

[152] RTDS Technologies,"RSCAD tutorial mannual" 2017

[153] M. Dyck and O. Nzimako, "Real-time simulation of large distribution networks with distributed energy resources," CIRED-*Open Access Proceedings Journal* 2017, no. 1, 2017: pp. 1402–1405.

[154] H. Lin *et al.*, "GECO : Global Event-Driven Co-Simulation Framework for Interconnected Power System and Communication Network," *IEEE Trans. on Smart Grid*, vol. 3, no. 3, pp. 1444–1456, 2012.

[155] F. Kristensen, R. L. Olsen, and J. G. Rasmussen, "Analysis of Information Quality in event triggered Smart Grid Control," *2015 IEEE 81st Veh. Technol. Conf. (VTC Spring)*, pp. 1–5, 2015.

[156] S. Magnusson and C. Fischione, "Optimal Voltage Control Using Event Triggered Communication," In *Proceedings of the Tenth ACM International Conference on Future Energy Systems*, pp. 343-354. ACM, 2019.

[157] B. Schwegmann, M. Matzner, and C. Janiesch, "A Method and Tool for Predictive Event-Driven Process Analytics," In *Wirtschaftsinformatik*, p. 46.2013.

[158] Z. Wang, Y. Chen, G. He, and A. M. O. Model, "Predictive Voltage / VAR Control

Based on Hybrid Frame in Distribution Power Systems," *2009 Int. Conf. Sustain. Power Gener. Supply*, no. Grant 50595411, pp. 1–4.

[159] J. Becker, D. Breuker, P. Delfmann, and M. Matzner, "Designing and Implementing a Framework for Event-based Predictive Modelling of Business Processes," *Enterprise modelling and information systems architectures-EMISA*, 2014 pp. 71–84.

[160] S. Pandey, A. K. Srivastava, P. Markham, and M. Patel, "Online Estimation of Steady-State Load Models Considering Data Anomalies," *IEEE Trans. Ind. Appl.*, vol. 54, no. 1, pp. 712–721, 2018.

[161] Aggogeri, Francesco, and Enzo Gentili. "Six Sigma methodology: an effective tool for quality management." *Int. Journal of Manufacturing Technology and Management* 14, no. 3-4,2008:pp 289-298.

[162] V. Venkataramanan, S. Member, A. Srivastava, and S. Member, "Real-Time Co-Simulation Testbed for Microgrid Cyber-Physical Analysis," *2016 Workshop on Modeling and Simulation of Cyber-Physical Energy Systems*, Vienna, 2016, pp. 1-6. pp. 2–7.

Appendices

Appendix A

Optimization algorithms parameters

Table -A.1 DGSA and GA controlling parameters

DGSA	Value	GA	Value
Number of Agents	50	Population size	50
Initial Gravitation Constant (Go)	100	Mutation probability	0.15
Specified constant (α)	20	Crossover probability	0.8
R(Distance between two particles) Power	1	Length of chromosomes	8 bits
Maximum iterations (Iter)	100	Maximum iterations (Iter)	100

Table -A2. IEEE 123 node feeder test system loading type classification with ZIP coefficients

Loading Type	**ZIP Coefficients [16]**		**Node Number**
Residential	Zp = 0.85 Ip= -1.12 Pp =1.27	Zq =10.96 Iq=-18.73 Pq=8.77	2,4,5,6,7,10,12,16,35,37,38,39,41, 42,43,45,46,4748,4950,51,52,53,5 5,56,58,59,60,65,94,95,96,102,10 3,104,106,107,109,111,112,113,1 14
Large Commercial	Zp = 0.47 Ip = -0.53 Pp = 1.06	Zq = 5.30 Iq = -8.73 Pq = 4.43	62,63,64, 66,80,82,85
Small Commercial	Zp = 0.43, Ip = -0.06, Pp =0.63	Zq= 4.06, Iq=-6.65, Pq =3.59	1,9,11,17,19,20,22,24,28, 29,30,31,32,33,34,68,69,70,71,73, 74,75,83,84,87,88, 90,92,98,99,100
Industrial	Zp = 0, Ip = 0, Pp= 1	Zq=0, Iq = 0, Pq = 1	76,77,79,86

Appendix B

DMOPSO controlling parameters

Table -B.1 DMOPSO controlling parameters

Population Size	100
Repository Size	80
Inertia Weight (w)	1
Mutation rate	0.1
Inertia Weight Damping Rate (wdamp)	0.99
Maximum iterations (Iter)	150
Personal and Global Learning Coefficient (c1, c2)	2, 1.8

VVC droop point parameters

Table B.2 VVC droop point parameters

Point P1 voltage = 0.94 p.u.,	Point P2 voltage = 0.95 p.u.
Point P3 voltage = 1.05 p.u.,	Point P4 voltage = 1.06 p.u.
Dead Band (DB) range = Between point P2 and P3 (0.95 p.u. -1.05 p.u.), 0.1 p.u.	

Appendix C

DPSO optimization parameters

Table -C.1 DPSO controlling parameters

Population Size	100
inertia weight damping rate	0.99
Inertia Weight (w)	1
Mutation rate	0.1
Inertia Weight Damping Rate (wdamp)	0.99
Maximum iterations (Iter)	50
Personal and Global Learning Coefficient (c1, c2)	2, 1.8

PV/EV smart inverter droop parameters

Table C.2 PV/EV droop point parameters

PV Droop Parameters	**EV Droop Parameters**
V^1_{P1} = 0.948, V^2_{P2} = 0.951	V^1_{P1} = 0.946, V^2_{P2} = 0.95
V^3_{P3} =1.05, V^4_{P4} =1.06	V^3_{P3} = 1.05, V^4_{P4} = 1.06

PV Inverter droop point parameters

Table C.3 Predefined droop point parameters

Point P1 voltage = 0.94 p.u.,	Point P2 voltage = 0.97 p.u.,
Point P3 voltage = 1.02 p.u.,	Point P4 voltage= 1.05 p.u.,
Dead band range (between point P2 and P3) = 0.97–1.02 p.u.	

AWARD

- Awarded Prestigious ***POSOCO Power System Award (PPSA-2020)*** under ***Doctoral Category*** for his research work, organized **by *Power System Operation Cooperation (POSOCO) Ltd***. India in association with Fundamental for Innovation Technology Transfer (FITT), Indian Institute of Technology, Delhi.

- Awarded Prestigious ***Bhaskara Advance Solar Energy (BASE) Fellowship-2018*** award supported by the Department of Science and Technology, Govt. of India, and the Indo-U.S. Science and Technology Forum (IUSSTF) for six-month Internship at ***National Renewable Energy Laboratory, (***NREL) Golden, CO, USA.

LIST OF PUBLICATIONS

Journals

1. **Shailendra Singh,** and S. P. Singh, "Energy Saving Estimation in Distribution Network with Smart Grid enabled CVR and Solar PV Inverter." ***IET Generation, Transmission & Distribution****,* Vol. 12, No. 6, pp. 1346-1358, 2018.
2. **Shailendra Singh,** Vijay Babu P, and S. P. Singh, "Time Horizon-based Model Predictive Volt/VAR Optimization for Smart Grid Enabled CVR in Presence of Electric Vehicle Charging Loads", ***IEEE Transactions on Industry Applications***. Vol. 55, No. 6, pp. 5502-5513, Nov.-Dec. 2019.
3. Vijay Babu Pamshetti, **Shailendra Singh,** S. P. Singh. "Combined Impact of Network Reconfiguration and Volt-VAR control devices on Energy Savings in the presence of Distributed Generation". ***IEEE Systems Journal.*** Vol. 14, No. 1, pp.995-1006, 2019.
4. **Shailendra Singh**, Vijay Babu P, A, K, Thakur and S. P. Singh, "Multistage Multiobjective Volt/VAR Control for Smart Grid-Enabled CVR With Solar PV Penetration." ***IEEE Systems Journal, 2020*** (Early Access).
5. **Shailendra Singh,** S. P. Singh, Vijay Babu P., "Energy Efficiency and Peak Load Management via CVR and Distributed Energy Storage in Active Distribution Grid," ***International Transactions on Electrical Energy Systems***, Vol. 30, No. 3, 2020: e12224.
6. Vijay Babu Pamshetti, **Shailendra Singh,** S. P. Singh, "Reduction of Energy Demand via Conservation Voltage Reduction considering Network Reconfiguration and Soft Open Point"**.** ***International Transactions on Electrical Energy Systems***. Vol. 30, No. 1, 2020: e12147.
7. **Shailendra Singh,** Santosh Veda, S. P. Singh, R. Jain and Murali Baggu, **"**Event-Driven Predictive Approach for Real-Time Volt/VAR control with CVR in solar PV rich Active Distribution Network," ***IEEE Transaction on Power System,*** 2019 (**Revise &submit**)
8. **Shailendra Singh,** S. P. Singh, Santosh Veda and Murali Baggu**, "**Energy Conservation in Active Distribution Network via Integrated Volt/VAR Optimization and Demand Response Framework Considering Community Distributed Energy Resources and EV Charging Loads," ***IEEE Transactions on Smart Grid. 2020 (Under Review)***

Conferences

1. **Shailendra Singh,** S. P. Singh, Santosh Veda, and Murali Baggu, "Smart Grid-Enabled CVR: An Advanced Application for Distribution Management Systems," *2018 Power and Energy Society General Meeting,* 5-9 August 2018, *Portland, Oregon U.S.A(Student Poster)*

2. **Shailendra Singh,** S. P. Singh, Santosh Veda, and Murali Baggu, "Maximizing the Benefits of Volt-VAR Optimization in the Presence of Community Energy Storage*" IEEE Power Electronics, Drives and Energy Systems Conference, (PEDES),* at IIT Madras in Chennai, Tamilnadu, India. 18-21 December, 2018.

3. **Shailendra Singh,** Sunil Muwal, Devesh Shukla, and S. P. Singh, "Model Predictive Driven Volt/VAr Control for Smart Grid Enabled CVR in Active Distribution Network," *2018 IEEE 8th Power India International Conference (PIICON),* At NIT Kurukshetra December 9-10, 2018

4. **Shailendra Singh,** S. P. Singh, 'Peak Load Relief in MV/LV Distribution Network Through Smart Grid Enabled CVR With Droop Control EV2G Reactive Power Support', *IEEE International conference on Power, Instrumentation, Computing and Control,* GEC Trichur, India, Jan. 18- 20, 2018.

5. **Shailendra Singh,** Vijay Babu P. and S. P. Singh, "Impact of Combined Operation of CVR and Energy Storage System in Distribution Grid," *20th National Power Systems Conference (NPSC),* at NIT Trichy India, December 14-16, 2018.

6. Vijay Babu P. **Shailendra Singh**, S. P. Singh, "Distributed Generators allocation in Distribution System" *2017 IEEE PES General Meeting, Chicago USA*, July 16-20, 2017.

7. **Shailendra Singh,** A. K. Thakur and S. P. Singh, "Energy Savings in Distribution Network with Smart Grid-enabled CVR and Distributed Generation," *19th 2016 National Power Systems Conference (NPSC),* Bhubaneswar, 2016, pp. 1-6.

8. **Shailendra Singh,** S. P. Singh, "Opportunities and Challenges for Deployment of CVR/VVO Methodology in Indian Smart Energy Distribution System"

International Conference & Exhibition on Smart Grids and Smart Cities, (ISGW 2016), at ISGF India, 15-19 March, 2016

9. **Shailendra Singh,** D. Shukla and S. P. Singh, "Peak Demand Reduction in Distribution Network with Smart Grid-enabled CVR," *2016 IEEE PES Innovative Smart Grid Technologies - Asia (ISGT-Asia), Melbourne, VIC, 2016*, pp. 735-740

10. **Shailendra Singh,** S. P. Singh, "A Smart Volt-Var Optimization Engine for Energy Distribution System" *IEEE International Conference on Emerging Trends in Electrical, Electronics & Sustainable Energy Systems (ICETEESES-16),* at KNIT, Sultanpur India, on March 11-12, 2016